

Abstract

Ovarian cancer (OvCa) is the most lethal gynaecological malignancy worldwide and while less prevalent than other malignancies among women, 5-year survival is low and has remained relatively unchanged over the past 40 years. In recent decades the importance of bioelectric properties, in particular the plasma membrane potential (V_m), have become increasingly recognised as playing central roles in the regulation of numerous biological processes and disease states, including cancer. Recent studies have demonstrated alterations of V_m impact critical properties of cancer hallmarks, namely sustained proliferation and metastasis. Na^+ channels play critical roles in regulating V_m and recent evidence has accrued implicating voltage gated Na^+ channels in metastatic progression of numerous cancers. Limited information however exists for the role of the epithelial Na^+ channel (ENaC) a constitutively open channel ubiquitously expressed across numerous cell types.

The aim of this study was to investigate the involvement of Na^+ and ENaC in modulating the proliferative and migratory potential in OvCa. The contribution of Na^+ to V_m in SKOV-3 and primary cells derived from the ascites of patients with FIGO₃₋₄ cancer OvCa (OvCa_{asc}) cells were assessed by patch clamp studies. V_m values in both cell types were markedly depolarised in physiological solutions (≈ -5 to -10 mV) and hyperpolarised markedly by ≈ 20 to 25 mV ($p < 0.05$) upon removal of extracellular Na. The contribution of ENaC to V_m was assessed using the blocker amiloride. Wash-in induced a mild hyperpolarisation of ≈ 5 mV in SKOV-3 cells.

The contribution of ENaC to the proliferative capacity of SKOV-3 and OVCAR-3 cell lines was assessed using the resazurin reduction assay. Amiloride resulted in a marked reduction in cell proliferation in SKOV-3 and a mild reduction in OVCAR-3 cell lines ($\text{IC}_{50} \approx 60$ and $110 \mu\text{M}$ respectively at 72 hours post-treatment). The faster growing SKOV-3 cell line exhibited a dose dependent increase in apoptosis when treated with amiloride whereas OVCAR-3 cells demonstrated a cytostatic response. Mild increases in $[\text{Na}^+]_e$ up to 30 mM resulted in a significant reduction in the rate of proliferation of SKOV-3 cells. Conversely, elevated $[\text{Na}^+]_e$ resulted in a mild increase ($\approx 20\%$, $p < 0.05$) detectable at 72 hours. Since cell volume (V_{cell}) changes are required in proliferating cells, V_{cell} of amiloride treated SKOV-3 populations were assessed using imaging flow cytometry. Cells incubated in lower doses of amiloride (10 & $50 \mu\text{M}$) yielded no significant change in volume relative to control conditions. Cells cultured in the presence of $100 \mu\text{M}$ amiloride resulted in a significant increase in cell volume. This

however only equates to an $\approx 1\%$ change relative to control and significance is likely attributable to high sensitivity of non-parametric rank tests.

Gene expression studies of ENaC- α and delta were conducted between normal ovarian (NOv), FIGO3-4 primary tumours (FIGO₃₋₄T) & OvCa_{asc} tissue. ENaC- α demonstrated an ≈ 60 -fold up-regulation in FIGO₃₋₄T & OvCa_{asc} groups relative to NOv ($p < 0.05$). Conversely ENaC- δ demonstrated a significant down-regulation between NOv and OvCa_{asc} tissue. Functional expression was confirmed by western blot (WB) and immunofluorescence. Differential expression of ENaC- α was assessed in distinct OvCa_{asc} sub-populations using flow cytometry. Approximately 80% of CD117⁺/CD44⁺ were positive for ENaC- α , whereas only $\approx 50\%$ of EpCam⁺ cells exhibited ENaC- α staining.

The role of ENaC in cell migration in SKOV-3, OVCAR-8 & A2780 cells was next assessed using scratch assays. Amiloride reduced wound closure in all three cell lines, with the maximal effects observed in SKOV-3 cells (3-fold reduction in wound closure relative to control). In a wound-stimulated environment, SKOV-3 cells exhibited a functional up-regulation of ENaC- α (≈ 1.5 -fold increase) as assessed by WB. Since cell deformability is important in cancer migration, the role of ENaC in modulating cell stiffness was assessed using atomic force microscopic (AFM). Amiloride resulted in an ≈ 4 -fold increase in cell stiffness in A2780 cells.

Finally, since long-distance endogenous electric fields (EF) have been implicated in directing metastatic dissemination of cancer, it was assessed whether OvCa cells exhibited galvanotaxis. OvCa_{asc} cells were strongly galvanotactic, exhibiting highly directional migration towards the anode. Amiloride and phenamil (a derivative of amiloride) resulted in a mild reduction in anodal migration, however, cells still exhibited the ability to ‘sense’ an external EF. Depletion of $[\text{Na}^+]_e$ with impermeant replacements abolished the anodal migration in an external EF.

In conclusion this study demonstrated that ENaC may have an important role in contributing to the depolarised phenotype and modulating critical hallmarks in OvCa. ENaC contributes to sustained proliferation, potentially by persistent facilitative depolarisation of V_m . ENaC- α is up-regulated in OvCa progression and potentially contributes to sustained Na^+ influx in OvCa, and stemness. ENaC facilitates OvCa migration and modulates critical cell properties essential for migrating in heterogeneous environments. ENaC and Na-mediated depolarisation seem to be central to controlling the galvanotactic response in OvCa dissemination. The contribution of the galvanotactic cue in OvCa metastasis still needs to be identified. Altered Na^+ homeostasis and subsequent modulation of V_m is thus a promising area for further research in OvCa.

Acknowledgements

This work could not have happened without the incredible support and guidance from my primary supervisor, Prof Khan. She saw my interest and gave me the opportunity to learn to patch during my undergrad after which point I fell into fascination with all things bioelectric and cancer. She encouraged me and allowed me to build and develop galvanotaxis in the lab on what was not really much more than a hunch where other supervisors would not have been so facilitating. Her insight and the critical nuggets of information she has provided me with over the years have guided me through my project.

To my secondary supervisors. Anish Bali let me see first-hand how terrible a disease ovarian cancer is and made it possible to collect primary tissue which has proved invaluable. To Galina for her passion with all things Na^+ and NMR. And to Cyril who as a hardcore biophysicist fed my hunger for trying to understand what Na^+ really does.

To my labmates and now lifetime friends that have kept me sane and provided plenty of craic through the years; Ryan for his continuous encouragement, Artur for the coffee, Sophie for the chats and tea, Will and Ujjal for our discussions (arguments) about ion channels and Ben for a his perspectives. The lab technicians, Ave, Rebecca and Ella have helped me endless times. We are all like a lab family here and I am very grateful for that. Some undergraduate students have contributed a lot to this project; Lyndsay, Vanessa and Kasheir and I am very thankful for their hard work and passion.

Lastly, I thank my family. My parents have always helped me and inspired me to work hard to achieve my goals and helped me retrain in a new discipline which has changed the course of my life and I will be forever grateful. My girlfriend Fed, has always been supportive even when things were tough and I wasn't around much.

Contents

1	Introduction	21
1.1	Introductory remarks	21
1.2	Ovarian cancer	23
1.3	The hallmarks of cancer	23
1.4	The contribution of ion channels to the hallmarks of cancer	25
1.4.1	Metastatic dissemination of OvCa	27
1.4.2	Current and future therapeutic approaches in OvCa	29
1.5	The establishment of V_m	31
1.5.1	Ion channel control of V_m in non-excitabile cells	34
1.5.2	ENaC channels	37
1.5.3	Additional pathways for Na^+ entry in cancer cells	45
1.5.4	ENaC in the hallmarks of cancer	48
1.6	Bioelectric regulation of cell proliferation	49
1.6.1	V_m as a primary modulator of cell fate in healthy cells	49
1.6.2	V_m as an instructive regulator of oncogenesis	51

1.6.3	The importance of Na ⁺ permeability in cancer	55
1.6.4	Cell volume regulation in proliferation and the role of ENaC	60
1.7	Ion channels in cell migration	63
1.7.1	Cell migration	63
1.7.2	The role of cell deformability in motility	64
1.7.3	Roles for ENaC and V _m in cell migration	71
1.8	Galvanotaxis in cancer	72
1.8.1	Characterisation of external endogenous electric fields	73
1.8.2	The physiological EF	73
1.8.3	Galvanotaxis and metastatic disease	76
1.8.4	V _m perturbations in regulation of galvanotaxis	78
1.9	Rationale, hypothesis and aims	82
1.9.1	Hypothesis	83
1.9.2	Aims	83
2	Materials and Methods	85
2.1	Drugs	85
2.2	Cell culture and processing of primary cells from tissue and ascites	85
2.2.1	Cell lines	86
2.2.2	Primary cells from OvCa ascites	90
2.2.3	Normal Ovary (NOv) and OvCa primary tumour processing	93

2.3	Membrane potential recordings using the current clamp I=0 patch clamp method	93
2.4	Scratch wound assays	97
2.5	Wound stimulation experiment	98
2.6	Western blotting	99
2.6.1	Cell lysis and protein extraction	99
2.6.2	Protein determination	100
2.6.3	SDS-PAGE and Immunoblotting	101
2.7	Cell proliferation assays	102
2.8	Effect of Na ⁺ gradient on cell proliferation	104
2.9	Cell cytotoxicity assays	105
2.10	RT-qPCR experiments	106
2.10.1	RNA extraction	106
2.10.2	qPCR	109
2.11	Immunofluorescence	112
2.11.1	Microscopy	112
2.11.2	IF characterisation of OvCa _{asc} primary isolates	114
2.12	Flow cytometry	116
2.12.1	OvCa _{asc} panel	116
2.12.2	Assessment of apoptosis	118
2.12.3	Determination of V _{cell}	120

2.13	Cell stiffness measurements as assessed by atomic force microscopy force spectroscopy	122
2.14	Galvanotaxis	123
2.14.1	Preparation of silver chloride electrodes	123
2.14.2	Preparation of agar salt bridges	124
2.14.3	Media and solution composition	124
2.14.4	Construction of electrotactic chambers	125
2.14.5	Chamber seeding	126
2.14.6	Application of electric fields	126
2.14.7	Image acquisition	129
2.14.8	Image analysis	129
2.14.9	Quantitative parameters of cell migration	130
2.14.10	Assessment of ENaC inhibition and Na ⁺ replacement on galvanotaxis in OvCa _{asc} samples	131
2.15	Statistical analysis	134
2.15.1	Galvanotaxis experiments	134
3	Assessment of Na⁺ and ENaC contribution to V_m in OvCa	137
3.1	Introduction	137
3.2	Results	140
3.2.1	The contribution of persistent Na ⁺ permeability to V _m in OvCa and MCF-7 cells	140

3.2.2	Effect of riluzole on V_m in SKOV-3 and MCF-7 cells	142
3.2.3	The contribution of ENaC to V_m in SKOV-3 cells	144
3.3	Discussion	144
3.3.1	Effects of Na^+ replacement on V_m in OvCa and MCF-7 cells . . .	145
3.3.2	Effects of riluzole on V_m in SKOV-3 and MCF-7 cells	150
3.3.3	Amiloride results in V_m hyperpolarisation in SKOV-3 cells . . .	152
3.4	Conclusions	153
4	The effects of Na^+ flux on proliferation in OvCa cells	155
4.1	Introduction	155
4.2	Results	157
4.2.1	Effects of amiloride on proliferation of OvCa cell lines	157
4.2.2	Effects of phenytoin on proliferation of OvCa cell lines	162
4.2.3	Effects of Na^+ gradient on proliferation	165
4.2.4	Effects of amiloride treatment on V_{cell}	167
4.3	Discussion	169
4.3.1	ENaC inhibition reduces proliferation in OvCa cell lines	169
4.4	Na_V channel inhibition reduces proliferation in OvCa cell lines	176
4.4.1	ENaC does not regulate V_{cell} in proliferation of OvCa cells	178
4.4.2	Conclusion	178
5	Differential regulation of ENaC in OvCa and the role in modulation of migratory properties	179

5.1	Introduction	179
5.2	Results	183
5.2.1	Expression of ENaC subunits in OvCa	183
5.2.2	Expression of Na _V channels in OvCa	187
5.2.3	Flow cytometry of OvCa _{asc}	187
5.2.4	Effect of ENaC inhibition on OvCa migration	190
5.2.5	Effect of ENaC inhibition of cell stiffness	193
5.3	Discussion	194
6	The migration of OvCa cells in an external electric field and the role of ENaC, Na⁺ and V_m	205
6.1	Introduction	205
6.2	Results	208
6.2.1	Investigation of galvanotactic response in OvCa _{asc} isolates	208
6.2.2	Effect of ENaC inhibition on galvanotaxis	212
6.2.3	Effect of Na ⁺ replacement on primary OvCa _{asc} cells	216
6.3	Discussion	218
6.3.1	OvCa _{asc} migrate preferentially in an external EF	219
6.3.2	ENaC and V _m modulate the galvanotactic cue in OvCa _{asc}	221
7	Final overall discussion	231
7.0.1	Future work	236

A	Limitations of patch clamp and sharp microelectrode methods to measure V_m	241
B	Optimisation and validation of cell viability assays	245
	B.1 Seeding density optimisation	245
	B.2 Validation of cell doubling time	245
C	Primary OvCa ascites (OvCa_{asc}) sample characterisation	247
D	Matlab code for quantifying cosine values	251

List of Figures

1-1	The factors effecting V_m in non-excitabile cells.	35
1-2	Structure of ENaC	38
1-3	V_m as a marker of proliferative capacity.	52
1-4	Cartoon showing potential mechanisms by which ENaC activity may modulate migration.	72
2-1	Experimental setup and model circuit used in galvanotaxis experiments	128
2-2	Schematic depicting the quantitative parameters of cell migration used in galvotaxis studies	132
2-3	Schematic depicting the criterion boundary for cells migrating in an external electric field	132
3-1	The contribution of Na^+ to V_m in SKOV-3 cells	141
3-2	The contribution of Na^+ to V_m in MCF-7 cells	141
3-3	The contribution of Na^+ to V_m in OvCa _{asc} cells	142
3-4	The effect of riluzole on V_m in MCF-7 and SKOV-3 cells.	143
3-5	The effect of amiloride on V_m in SKOV-3 cells.	144

4-1	Cell proliferation of SKOV-3 and OVCAR-3 cell lines 72 hours after treatment with amiloride.	158
4-2	Cytotoxicity of SKOV-3 and OVCAR-3 cell lines 72 hours after treatment with amiloride.	160
4-3	Assessment of apoptosis by flow cytometry in SKOV-3 cells following treatment with amiloride.	161
4-4	Cell proliferation of SKOV-3 and OVCAR-3 cell over 72 hours following treatment with phenytoin.	163
4-5	Summary of cell proliferation parameters in SKOV-3 and OVCAR-3 cell lines following treatment with phenytoin	164
4-6	Cytotoxicity of SKOV-3 and OVCAR-3 cell lines 72 hours after treatment with phenytoin.	164
4-7	Effect of an increase of extracellular Na^+ on growth rate of SKOV-3 and OVCAR-3 cells.	166
4-8	Effect of ENaC on regulating V_{cell} in proliferating SKOV-3 cells	168
5-1	Expression of ENaC- α in SKOV-3 and OVCAR-3 cell lines.	184
5-2	Alterations in mRNA expression of ENaC subunits in NOv, FIGO ₃₋₄ T primary tumours and OvCa _{asc} from samples of malignant ascites. . . .	185
5-3	Expression of ENaC- α in normal ovary and high grade OvCa	186
5-4	Alterations in mRNA expression of NaV1.5- α subunits in normal ovarian tissue (NOv) and FIGO ₃₋₄ T primary tumours.	187

5-5	Gating strategy to identify OvCa cell populations of differing tumorigenic potential and assessment of differential ENaC ⁺ populations. . . .	188
5-6	Fraction of ENaC- α ⁺ cell populations in OvCa ascites cells of differing tumorigenic potential as assessed by flow cytometry.	190
5-7	Effect of amiloride on cell migration in OvCa cell lines.	192
5-8	Alterations in expression of ENaC- α in SKOV-3 cells during migration stimulated conditions.	192
5-9	Effect of amiloride treatment on cell stiffness of A2780 cells.	194
6-1	Representative time-lapse photographs of cells from a primary derived OvCa _{asc} sample migrating in the absence and presence of an external electric field	209
6-2	Composite trajectories of OM8, OM11 and OM12 OvCa _{asc} cell lines migrating in the absence and presence of an external EF.	210
6-3	The grouped effects of an applied external EF on the galvanotactic properties of primary OvCa _{asc} cell lines in an external EF of 5V/cm.	211
6-4	The effects of pharmacological inhibition of ENaC on the galvanotactic properties of primary OvCa cell isolates.	213
6-5	Percentage of primary OvCa cell isolates crossing a criterion boundary following treatment with amiloride or phenamil.	215
6-6	The effects of Na ⁺ replacement on the galvanotaxis of primary OvCa _{asc} cell isolates.	217

6-7	The effects of Na ⁺ replacement on the galvanotactic parameters of primary OvCa cell isolates in an external EF of 5V/cm.	218
A-1	Effect of membrane shunt resistance on V _m measurement using the sharp microelectrode method.	242
B-1	Cell seeding density optimisation for resazurin reduction assay.	246
C-1	Reflective images of characterisation of OvCa _{asc} sample OM5 cell surface marker expressed by immunofluorescence	248
C-2	Assessment of percentage contribution of differing cell populations present within primary isolates of malignant OvCa ascites samples.	249

List of Tables

1.1	Involvement of ENaC in cancer.	49
2.1	Properties of OvCa cell lines used in this study	86
2.2	Clinical characteristics of participants from which OvCa _{asc} were collected	91
2.3	Composition of percoll stock solutions for OvCa _{asc} cell purification . . .	92
2.4	Clinical characteristics of participants from which NOv or FIGO ₃₋₄ T samples were collected	94
2.5	Patch clamp solutions used for all experiments.	95
2.6	Primer information of reference and target genes used in this study . .	111
2.7	Primary antibodies used in IF experiments.	113
2.8	Primary conjugated antibodies used in flow cytometric characterisation of OvCa _{asc} populations.	118
4.1	Summary of cell proliferation parameters in SKOV-3 and OVCAR-3 cell lines following treatment with amiloride	159

6.1	Quantitative metrics of cell migration in OvCa _{asc} isolates in the presence and absence of an external EF.	212
6.2	Quantitative metrics of amiloride and phenamil treatment on OvCa _{asc} .	214
6.3	Quantitative metrics of external Na ⁺ replacement on OvCa _{asc}	216

Abbreviations

$[\text{ion}]_e$	extracellular ion concentration
$[\text{ion}]_i$	intracellular ion concentration
ASIC	Acid-sensitive ion channel
BME	β -Mercaptoethanol
CGM	complete growth medium
Cl^-	Chloride ion
Dis_{ACC}	Accumulated distance
Dis_{EUC}	Euclidean distance
DMEM	Dulbecco's modified eagles medium
EDTA	Ethylenediaminetetraacetic acid
ENaC	Epithelial Na^+ channel
ENaC- α	Epithelial Na^+ channel α subunit
ENaC- β	Epithelial Na^+ channel β subunit
FBS	Foetal bovine serum
HBSS	Hanks' balanced salt solution
K^+	Potassium ion
K_{ir}	Inwardly rectifying K^+ channel
K_V	Voltage-gated K^+ channel
Na^+	Sodium ion

$\text{Na}_V1.x$	Voltage-gated Na^+ channel of genesubfamily 1 and channel isoform .x
NOv	Normal ovaries
OSE	ovarian surface epithelium
OvCa	Ovarian cancer
P_{Cl^-}	Ionic permeability to Cl^-
P_{K^+}	Ionic permeability to K^+
P_{Na^+}	Ionic permeability to Na^+
P/S	Penicillin / streptomycin
RPMI	1640 RPMI medium
RT	Room temperature
V_m	Plasma membrane potential

Chapter 1

Introduction

1.1 Introductory remarks

Bioelectricity is a field of physiology whose first observations of relevance were described by the ancient Egyptians and Greeks, long before the discovery of the first enzymes, which are considered to explain so much of biology (Armstrong, 1933). However, excluding the field of neuroscience, bioelectric phenomena have garnered limited appreciation within the general scientific community, despite its readiness to accept, for instance, that the calcium ion (Ca^{2+}) is a ubiquitous second messenger, and that ion transport in the nephron maintains circulatory fluid and ion balance. In the past 20-30 years however, bioelectrical considerations have yielded stark insights into the mechanism by which certain physiological processes involving ion pump and channel activity are regulated. Examples of this can be found in wound healing, embryological development and cancer, to name but a few (Zhao, 2009; Levin, 2011; Yang, Charles, Hummler, Baines and Isseroff, 2013).

In the field of cancer, critical differences in a specific bioelectric signal, the plasma

membrane potential (V_m), have emerged to play a key role in the regulation of proliferation, differentiation, apoptosis and migration; all of which are centrally dysregulated ‘hallmarks’ in the progression of the disease. Indeed, it has been demonstrated that a depolarised V_m *in vivo* occurs early in cancer, and may even allow for detection of tumours. Moreover, seminal work undertaken by field pioneers such as Michael Levin and others has shown that forced hyperpolarisation of V_m via differing mechanisms prevents said cells from forming tumours. These observations have been critical in progressing our understanding of bioelectric events in cancer, suggesting that V_m depolarisation in cancer is not merely an observed phenotype, but likely serves as a functionally instructive cue. That being said however, bioelectricity is a field that is still poorly understood, necessitating further research to provide insights and potential novel targets for bioengineering approaches to cancer.

With a background as an electronic engineer, I became fascinated with the concept of bioelectricity during my second degree in biomedical science, and I have spent the last 4 years trying to understand the role of Na^+ , the Epithelial Na^+ channel (ENaC) in particular, in modulating V_m in ovarian cancer (OvCa). To that end, since V_m changes are associated with multiple properties or hallmarks of cancer, the following body of work takes a systematic approach, first assessing the contribution of Na^+ to V_m in OvCa, then assessing the regulatory role in proliferation and migration. Finally, it assesses whether endogenous long distance bioelectric fields may play a role OvCa dissemination, and whether Na^+ conductances facilitate this response. The following sections outline the role of V_m in modulating the hallmarks of cancer and present the potential mechanisms and evidence by which Na^+ , and specifically ENaC, are implicated in ovarian cancer.

1.2 Ovarian cancer

Ovarian cancer (OvCa) is the most fatal type of all gynaecological malignancies and the fifth most common cancer among women (Prat et al., 2015; WHO, 2012). In England, the incidence of disease has remained fairly stable over the last two decades. Although mortality rates have fallen by approximately 20% over the same time-period, the overall prognosis for women diagnosed with OvCa is poor, with a 5-year survival of less than 45% (*Ovarian cancer statistics | Cancer Research UK*, 2019). The high mortality rate of ovarian cancer is largely attributable to the diagnosis of disease at a late stage. Symptoms characteristic at presentation are bloating, abdominal discomfort, gas, nausea and urinary urgency; these are not disease specific and as such they are often attributed to gastrointestinal origin. Indeed, greater than 70% of ovarian cancer patients have metastases at the time of diagnosis. In contrast, if the disease is detected at an early stage where it is confined to a single or both ovaries, conventional approaches encompassing cytoreductive surgery and chemotherapy have a high chance of achieving cure.

Approximately 90% of all OvCa derives from epithelial origin. OvCa is classified into five main subtypes; high-grade serous, low-grade serous, endometrioid, clear cell and mucinous (Jayson et al., 2014). The most common subtype is high-grade serous (HGS), which is characterised by mutations in the tumour suppressor gene p53 and genomic instability (Cancer Genome Atlas Research Network, 2011).

1.3 The hallmarks of cancer

In a seminal review by Hanahan and Weinberg, critical ‘hallmarks’ of cancer were proposed, which confer the cancer cell with biological capabilities to facilitate the multi-

step development of tumours (Hanahan and Weinberg, 2011). They include: sustaining proliferative signalling, insensitivity to anti-growth signals, evasion of programmed cell death, limitless replicative potential, persistent angiogenesis and tissue invasion and metastasis (Hanahan and Weinberg, 2000).

Of all the hallmarks, perhaps the most fundamental trait of cancer cells is their ability to sustain persistent proliferation. Healthy or normal cells require mitogenic growth signals to transition from a quiescent state to one of active proliferation (Lemmon and Schlessinger, 2010). However, cancer cells are not fundamentally dependent on external cues, since they acquire the capability to grow independently (Witsch, Sela and Yarden, 2010), producing and secreting mitogenic cues or mitogens which act in an autocrine or paracrine manner. One mechanism through which this is achieved, is by alteration of expression or properties of cell surface receptors or ion channels that receive growth signals and transduce them to downstream targets (Sever and Brugge, 2015). Further deregulation of intracellular pathways that target gene expression is also required (Sever and Brugge, 2015).

In the progression of the disease towards a disseminated state, another critical acquired property of cancer cells is their ability to invade and metastasise to distant sites. Metastasis is characterised by local invasion into surrounding tissues, intravasation into vasculature, lymphatics or, as is often the case in OvCa, transcoelomic spread into ascitic fluid in the peritoneum. Invasion occurs due to extrinsic cues present in the tumour microenvironment that attract cells to migrate into local tissue. Multiple cues in the microenvironment can promote local invasion. Components of the extracellular matrix can promote migration of cells across the basement-membrane; collagen type 1 secreted by mesothelial cells increases the invasion of OvCa across the mesothelium

(Burlison, Hansen and Skubitz, 2005).

The second instalment proposed by Hanahan and Weinberg added some hallmarks to the first, the most notable being the tumor microenvironment as a contributor to progression (Hanahan and Weinberg, 2011). Despite this, changes driving cancer cell behaviour through modified ion channel activity and V_m , although not currently recognised as ‘hallmarks’, clearly underlie key transformations driving oncogenesis such as proliferation and events in the metastatic cascade (Prevarskaya, Skryma and Shuba, 2010). The role of ion channels in driving the hallmarks of cancer will be discussed in the next section.

1.4 The contribution of ion channels to the hallmarks of cancer

Within the last two decades, the facilitative role of ion channels in conferring cancer cells with properties central to tumour hallmarks has become increasingly recognised. The first associations between aberrant functions of ion channels and cancers became apparent in the observations that ion channels are often differentially expressed in cancer tissues, in comparison to untransformed tissue of the same origin.

Several observations have been made implicating the dysregulation of ion channels in driving one central hallmark: sustaining proliferative signalling. Regulation of ion channel dynamics have long been known to impact on two biophysical properties important in progression through the cell cycle; cell volume (V_{cell}) and V_m (the interaction between ion channels on V_{cell} and V_m are discussed in detail in sections 1.6 and 1.6.4 respectively). V_{cell} changes are an integral property governing cell cycle progression, and numerous ion channels exhibit altered function in cancer. For example, a premitotic cell

shrinkage is required in astrocytic glioma cells undergoing cell division (Habela, Olsen and Sontheimer, 2008). This shrinkage is predominantly facilitated by chloride (Cl^-) efflux via ClC3 , a member of the ClC voltage-gated Cl^- channel family (Habela, Olsen and Sontheimer, 2008). Targeted approaches to inhibit ClC channels in glioma have manifested in the form of phase 1/2 clinical trials using the small molecule neurotoxin, chlorotoxin (Mamelak and Jacoby, 2007).

Properties conferring cells with increased proliferative potential have also been attributed to members of the two-pore domain K^+ (K_{2P}) channels. TASK-3 , a member of (K_{2P}), is overexpressed in breast and lung cancers, and the presence of an increased K^+ conductance has been shown to confer cancer cells with increased oncogenic potential (Plummer et al., 2004; Pei et al., 2003). Another (K_{2P}) channel, TREK-1 , was found to have a role in the proliferation of prostate cancer (Voloshyna et al., 2008).

Recent investigations have also implicated altered ion fluxes in the evasion of apoptotic pathways and resistance to chemotherapy. Sustained activity of K^+ and Cl^- channels is required for apoptotic cell shrinkage; an early event in apoptosis (Elmore, 2007). Interestingly, certain members of the voltage-gated potassium (K_V) channel family are downregulated in cancers. $\text{K}_V1.3$ is downregulated in pancreatic carcinomas when compared to normal tissue (Brevet et al., 2009). Similarly, $\text{K}_V1.3$ shows lower expression in breast cancer tissue when compared to normal tissue (Brevet et al., 2008). Thus, targeting of K^+ channels in cancer via ion channel activators or pathways that result in increased ion channel expression may prove beneficial in restoring apoptotic sensitivity. The K^+ channel modulatory protein KChAP , when overexpressed in the LNCaP prostate cancer cell line, resulted in increased K^+ efflux, with concomitant reduction in mean V_{cell} and an increase in the fraction of cells undergoing apoptosis

(Wible et al., 2002). Similarly, in DU-2145 xenograft models, KChAP overexpression also resulted in increased levels of apoptosis (Wible et al., 2002).

Evidence is growing that enhanced metastatic capacity correlates with the appearance of ion channels that are characteristic of excitable cells; those which participate in the generation and transduction of the action potential. One channel family strongly implicated in metastatic progression is the voltage-gated Na^+ (Na_V) channel family. In prostate, cervical, breast and ovarian metastatic tumour biopsies and in highly metastatic tumour derived cell lines, increased expression of Na_V channels has been detected (Diss et al., 2001; Diaz et al., 2007; Fraser et al., 2005; Gao et al., 2010). Furthermore, the expression of a specific Na_V channel isoform does not seem to be critical in conferring metastatic capacity; in breast cancer $\text{Na}_V1.5$ is ≈ 1000 -fold overexpressed, whereas in prostate cancer $\text{Na}_V1.7$ is the most altered (≈ 20 -fold) (Brackenbury et al., 2007; Diss et al., 2001). In multiple non-small-cell lung cancer cell lines, expression of Na_V channels alone is not sufficient to convey metastatic properties. Indeed the presence of a functional Na^+ current is required to furnish the cell with an invasive phenotype, as evidenced by pharmacological treatment with tetrodotoxin, a specific blocker of Na_V channels (Roger et al., 2007). Taken together, this implicates increased Na^+ conductance in metastatic cancer cells as central to their metastatic potential.

Thus, there is strong evidence implicating aberrant expression and function of ion channels in driving the hallmarks of cancer.

1.4.1 Metastatic dissemination of OvCa

Initial metastatic spread of OvCa is similar to other epithelial tumours; it is characterised by the direct extension into local organs adjacent to the ovary, primarily the fallopian tubes, uterus and adnexal spaces and less frequently the rectum, bladder and

pelvic sidewall (Tan, Agarwal and Kaye, 2006). However, the pattern of metastatic dissemination to more distant sites is quite different to those observed in numerous other epithelial cancers. OvCa predominantly spreads through the transcoelomic route, which is characterised by extensive seeding of the peritoneal cavity. Indeed, 70% of patients are found to have peritoneal metastases at the time of staging laparotomy. Further evidence is lent to this hypothesis by the observations that patients subjected to peritoneovenous shunts to ameliorate symptoms of the disease infuse billions of cancer cells into the systemic circulation, yet metastases are almost always confined to the peritoneum (Tarin et al., 1984). However, emerging evidence implicates a potential role for hematogenous spread to distant sites within the peritoneum.

The mode through which OvCa cells metastasise from the primary tumour is considered to be ‘passive’ (Lengyel, 2010; Naora and Montell, 2005). Detachment of OvCa cells from the primary tumour into peritoneal fluid (known as malignant ascites) and subsequent transport to the peritoneum and omentum are associated with the direction of peritoneal fluid flow (Pannu and Oliphant, 2015). The net flow of peritoneal fluid is from the pelvis, along the intestinal mesentery to the right hemidiaphragm, which facilitates the seeding of lesions at more distant sites (Avraham-Chakim et al., 2013). It is of note that in the absence of significant ascites, disease is often limited to local sites of invasion. Thus the presence of ascites is correlated with morbidity, and most likely plays a central role in the progression of disease.

The ascitic microenvironment is characterised by the accumulation of a malignant cell population present in the ascitic fluid. It typically includes a relatively large number of leukocytes, and in some cases, a significant population of mesothelial cells (Runyon, 1994; Feki et al., 2009; Bansal, Kaur and Bansal, 1998). This is instigated by tumour

cells from the primary site losing cell to cell contacts, which makes them susceptible to exfoliation during mechanical movements of adjacent intra-peritoneal organs and peritoneal fluid flow. Adherent epithelial cells generally undergo anoiksis (programmed cell death upon the loss of adherence to a substratum) in the absence of attachment to a substrate; this is one of the primary barriers to passive dissemination that OvCa cells must overcome (Cai, Yan and Xu, 2015). OvCa cells may aggregate to form spheroids or remain as single dissociated cells (Ahmed and Stenvers, 2013). Spheroids often contain cancer-associated fibroblasts, which can contribute to the aggressive phenotype (Gao et al., 2019). Successful metastasis then requires the OvCa cells in suspension to adhere to the lining of the peritoneal cavity (known as the mesothelium) and subsequently gain access to the extracellular matrix (ECM) beneath it (Yeung et al., 2015).

1.4.2 Current and future therapeutic approaches in OvCa

Primary treatment for OvCa involves surgical intervention for histological diagnosis, staging, and optimal debulking. Since most cases of OvCa present at an advanced stage, the surgical approach to determine the extent and stage of disease (in accordance with the International Federation of Gynecology and Obstetrics (FIGO) classification) is usually an open laparotomy procedure.

Adjuvant chemotherapy usually follows surgery for women with stage II-IV disease. The most common chemotherapeutic regime involves platinum based chemotherapy: 3-weekly paclitaxel and carboplatin, for 6 cycles. Although trials suggest that the addition of Bevacizumab (a vascular endothelial growth factor inhibitor) may improve outcomes in recurrent disease, it is not currently recommended by NICE for treatment of primary ovarian cancer; in part due to a significant risk of side effects (Rossi et al., 2017).

While the aetiology of epithelial OvCa is still poorly understood, a subset of cases are strongly associated with mutations in genes involved in homologous recombination (HR); an important DNA repair mechanism in mammalian cells (Hodgson and Turashvili, 2020). Proper repair of double strand breaks (DSBs) is essential for the maintenance of genomic integrity; if they remain unrepaired, DSBs are often lethal and can result in apoptosis (Hoeijmakers, 2001). Homologous recombination (HR) is one such DSB pathway. Cells with defective/mutated BRCA proteins are deficient in HR mechanisms and must rely on other pathways to repair DNA damage (Hoeijmakers, 2001). One such pathway is the poly(ADP-ribose) polymerase (PARP) pathway that is involved in the detection and repair of single strand DNA breaks. In cells deficient in HR mechanisms, the inhibition of the PARP pathway leads to cell death from gross genetic disarray; a term coined ‘synthetic lethality’ (Slade, 2020). Olaparib is the first approved PARP inhibitor for HGS OvCa (Ledermann, 2016). Indeed 60% of patients receiving olaparib have had no progression after 3 years, in comparison to $\approx 20\%$ in the placebo group (Washington, Richardson and Moore, 2019). A Cochrane database review found that PARP inhibitors improve progression free-survival in women with recurrent, platinum-sensitive disease. Olaparib is also approved for BRCA-mutated patients after first line chemotherapy (Washington, Richardson and Moore, 2019).

Recent developments in the last number of years in the field of immune therapies have led to a dramatic increase in number of ongoing trials. One area of particular interest is the use of immune checkpoint inhibitors (ICPIs) in OvCa. ICPIs reduce the capacity of the tumour to activate checkpoint proteins expressed on the surface of T cells. This has been shown to prevent the cancer immune evasion which subsequently allows the generation of an antitumour immune response. The best characterised im-

immune checkpoint inhibitors are involved in the programmed death receptor-1 (PD1) PD1/PD-L1 and CTLA-4 (cytotoxic lymphocyte-associated antigen 4) pathways. PD-1 is involved in the regulation of previously activated T cells in the immune response and modulates apoptosis of regulatory T cells. CTLA-4 evades autoreactive T cells residing in lymph nodes. Numerous early-phase trials are currently running to assess ICPIs in OvCa. The JAVELIN Solid Tumour trial of avelumab, (anti-PD-L1) found that treatment was safe in 125 patients with recurrent or refractory OvCa. However, data on activity showed that overall response rate was 9.6% (Disis et al., 2019). A similar modest response was found for pembrolizumab, with an overall response rate of 8.6% in 376 patients (Matulonis et al., 2019).

1.5 The establishment of V_m

The plasma membrane of mammalian cells consists of approximately 50% lipid molecules, the remainder being comprised predominantly of protein (Harayama and Riezman, 2018). All of the membrane lipid molecules are amphipathic, that is to say they possess a polar or hydrophilic phosphate ‘head’ and a hydrophobic non-polar ‘tail’; this results in their spontaneous assembly into a bilayer structure in an aqueous environment (Goñi, 2014). The primary function of the plasma membrane is to serve as a protective barrier that regulates the passage of ions and larger molecules in and out of the cell, thus establishing an internal environment that is conducive to the sustained existence of the cell (Goñi, 2014).

The plasma membrane potential (V_m) is defined as the charge that exists across the plasma membrane (Koester, Sielgelbaum, 2013). V_m arises as the result of two parameters; firstly, the non-uniform distribution of monovalent and divalent ions across

the membrane, predominantly potassium (K^+), sodium (Na^+) and chloride (Cl^-) and secondly, the differing membrane permeability to the respective ions. The relative dependency of V_m on the permeability and associated ionic gradient was uncovered by seminal work undertaken by Goldman, Hodgkin & Katz in artificial membranes and the squid giant axon (Hodgkin and Katz, 1949; Goldman, 1943). These ground-breaking experiments were the first to directly record the electrical potential that existed across the axon membrane using glass capillary electrodes, an approach that was to become the basis of electrophysiology. The aim of these experiments was to characterise the key properties establishing V_m . The primary cell types investigated were of an excitable nature; neurons, axonal processes and skeletal muscle cells (Hodgkin and Katz, 1949; Goldman, 1943). While the plasma membrane of excitable cells is persistently permeable to K^+ (P_{K^+}) in resting states, during the instigation of bioelectric signalling events such as the action potential, the value of P_{Na^+} changes dramatically. The subsequent establishment of V_m is described by the Goldman-Hodgkin-Katz equation:

$$V_m = \frac{RT}{zF} \ln \left(P_{K^+} \frac{[K^+]_i}{[K^+]_e} + P_{Na^+} \frac{[Na^+]_i}{[Na^+]_e} + P_{Cl^-} \frac{[Cl^-]_e}{[Cl^-]_i} \right) \quad (1.1)$$

where R is the ideal gas constant, z is the valence number of the electron, T is the temperature in Kelvin, F is Faraday's constant, P_{Na^+} , P_{K^+} & P_{Cl^-} are the relative permeability coefficients of the plasma membrane to Na^+ , K^+ & Cl^- respectively. $[ion]_i$ and $[ion]_e$ denote the ion concentration in mM in the intracellular and extracellular compartments respectively.

Since there a persistent outwardly directed K^+ gradient, there will be net diffusion

of K^+ from high $[K^+]_i$ to low $[K^+]_e$. This persistent flow of K^+ ions will result in an outwardly directed current and a negative charge separation within the cell relative to the extra cellular space. As K^+ flows out of the cell down the chemical concentration gradient, the positively charged cation will encounter an attractive electrical force to the negative charge developed on the inner surface of the cell membrane, and be drawn back in. These chemical and charge gradients are in opposition to each other, but at a certain diffusion point a potential develops where they are equal to each other, that is to say, the outward gradient mediated flux of K^+ ion will be directly equal to the inward charge mediated electrical K^+ flux (Sawyer et al., 2017). This is known as the K^+ equilibrium potential (E_K) and is described by the Nernst equation. In a cell predominantly permeable to K^+ , it is the primary determining factor for V_m (Wright, 2004). In fact, in specific cell types such as astrocytes that are almost exclusively permeable to K^+ , E_K can approximate V_m (Ransom and Goldring, 1973).

In normal cell homeostasis, $[K^+]_i$ is higher (120 - 140 mM) than $[K^+]_e$ (5 - 10 mM) and there is an outwardly directed gradient for K^+ (Palmer, 2015). In contrast, $[Na^+]_i$ is lower (≈ 5 mM) than $[Na^+]_e$ (≈ 130 mM) and there is an inward concentration gradient (Palmer, 2015). These substantial concentration gradients are continuously maintained, predominantly by the activity of the electrogenic Na^+ - K^+ -ATPase, a ubiquitously expressed plasma membrane transporter across all mammalian cell types, that transports 3 Na^+ ions out of the cell and imports 2 K^+ ions into the cell (Palmer, 2015). With stoichiometry of 3:2 Na^+ : K^+ , the transporter hydrolyses 1 molecule of adenosine triphosphate (ATP) for each cycle (Jorgensen, Håkansson and Karlsh, 2003). Selective plasma membrane permeability to differing ionic species is established through the ion-selectivity properties of ion channels and the probability that they are ‘open’ (P_{open}) or

conducting at resting states. Classically, potassium channels are predominantly open during resting states and as such, K^+ is the primary membrane permeant ion (Wright, 2004) (see figure 1-1).

In considering non-excitabile cells from which cancer cells predominantly originate, V_m is not adequately described by the persistent permeability to a single ionic species, since Na^+ also contributes significantly. Since the physiological Na^+ gradient is inwardly directed and in opposition to the K^+ gradient, an increased permeability to Na^+ or an increase in $[Na^+]_e$ would establish equilibrium at a more depolarised V_m (Wright, 2004). Non-excitabile cells including cancers perform different physiological roles to excitable cells, and utilise influx / efflux of Na^+ for a wide range of physiological processes (discussed in detail below). As such, the persistent membrane permeability to Na^+ in non-excitabile cells is considerably higher than excitable cells, resulting in a more depolarised phenotype (Binggeli and Weinstein, 1986) (figure 1-1).

1.5.1 Ion channel control of V_m in non-excitabile cells

Ion channels are ubiquitously expressed across all mammalian cell types; they regulate numerous physiological properties including excitability and cell volume (V_{cell}), and facilitate transport of metabolites and secondary signalling cascades, to name a few (Nilius and Droogmans, 1995). A brief overview of Na_V channels is now provided, followed by a detailed consideration of the physiological roles of ENaC.

1.5.1.1 Na^+ channels

Na^+ channels expressed in non-excitabile cells comprise two primary groups: voltage-gated Na^+ channels (Na_V) and the epithelial Na^+ channel family (ENaC). Na_V channels are classically considered to be expressed in excitable cells such as neurons, skeletal and cardiac muscle cells, where they facilitate the voltage-dependent activation of inward

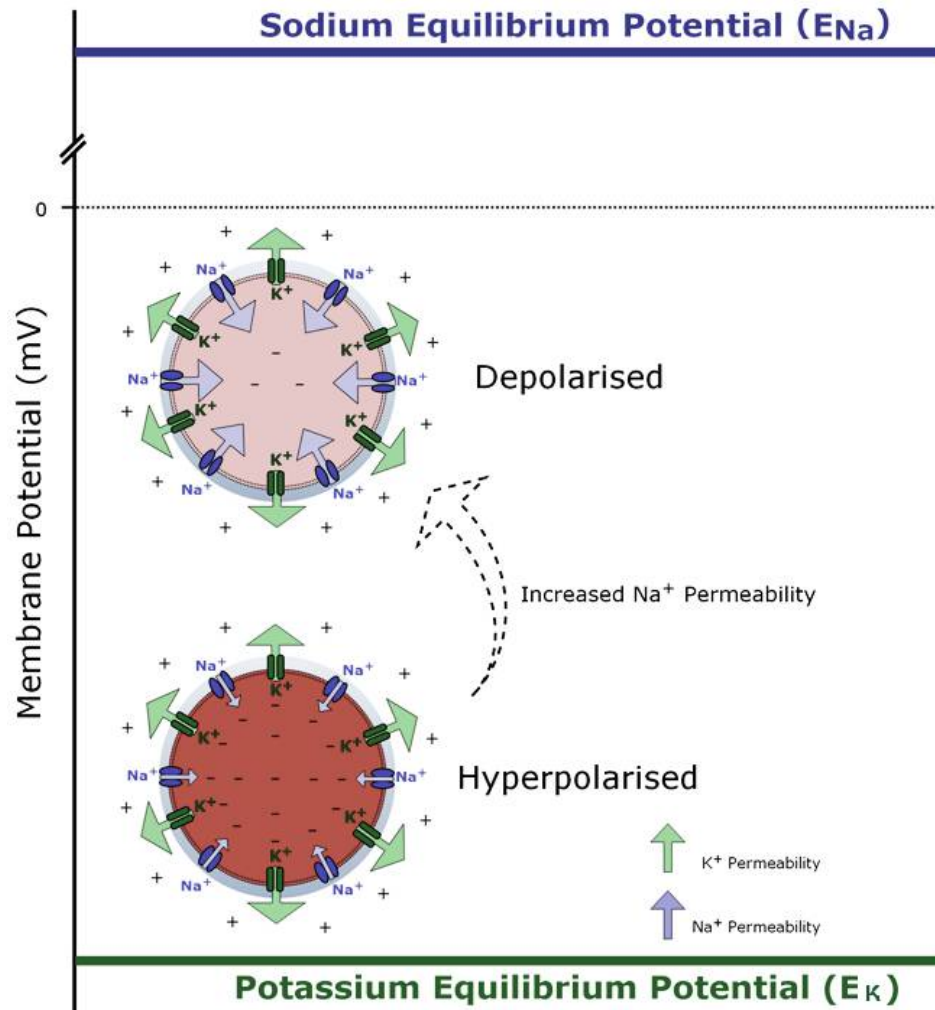


Figure 1-1: The factors regulating V_m in non-excitable cell types. Classically V_m is considered to be established predominantly through the activity of 'background' or 'leak' K^+ channels. Persistent membrane permeability to Na^+ is relatively low due to the low conductance of Na^+ channels at resting potentials. K^+ is considerably higher within the cytosolic compartment than the extracellular space. Diffusion of K^+ down its concentration gradient out of the cell results in the formation of a net negative charge relative to the cytosol, resulting in a hyperpolarised V_m . The flow of K^+ down the chemical concentration gradient will generate a negative electrical charge that is in opposition the chemical gradient and acts to attract K^+ ions back into the cytosolic compartment, such that the net flux of K^+ ions will be 0. This is known as the K^+ equilibrium potential (E_K) and acts as a good approximation of V_m in excitable cells. In numerous non-excitable cells however, Na^+ channels play an important role in cellular homeostasis and as a result they offer a greater net permeability to Na^+ . The physiological Na^+ gradient is in opposition to the K^+ gradient, and as a result additional contribution of Na^+ resting membrane permeability results in the establishment of a more depolarised phenotype.

Na^+ currents and the subsequent depolarisation of the cell membrane. However, they have more recently been found to be expressed in many non-excitabile cell types, including cancer cells (Roger et al., 2015). Na_V channels are classed as fast-inactivating channels, allowing a transient inward current for approximately 1 - 2 ms (Gilly, Gillette and McFarlane, 1997). They comprise a single α pore-forming subunit and two smaller β subunits (Marban, Yamagishi and Tomaselli, 1998). There are nine human genes, *SCN1A*, *SCN2A*, *SCN3A*, *SCN4A*, *SCN5A*, *SCN8A*, *SCN9A*, *SCN10A* & *SCN11A*, which encode for $\text{Na}_V1.1$ – $\text{Na}_V1.9$ respectively (Yu and Catterall, 2003). The α subunits are composed of four domains (DI – DIV), each comprising six transmembrane domains (S1-S6). Transmembrane domains S1-S4 make up the voltage-sensing region, while S5-S6 comprise the pore-forming functional unit (Marban, Yamagishi and Tomaselli, 1998).

While Na_V channels rapidly inactivate after voltage-gated activation, it has been demonstrated that after depolarisation they can remain in a partially-inactivated state and contribute a greatly reduced but persistent basal conductance to Na^+ (Roger et al., 2015). Non-excitabile cells typically exhibit a significantly more depolarised phenotype than excitable cells, and as such it is feasible that Na_V facilitates a persistent contribution of the Na^+ gradient to V_m , though the extent to which this contributes to V_m in the vast array of non-excitabile cells remains poorly understood (Fraser et al., 2005). $\text{Na}_V1.7$ regulates V_m in dendritic cells (Kis-Toth et al., 2011). In non-excitabile contractile cells such as smooth muscle, Na_V channels play a central role in regulation of vascular tone by small modulations of V_m . It has been proposed that this facilitates Ca^{2+} entry into the cytoplasm, potentially via reverse mode of NCX (discussed in further detail in section 1.5.3), thus mediating contractility (Fort et al., 2009). In addition

to their role in establishing V_m , Na_V channels have numerous additional roles in non-excitable cells. In gastric epithelial cells, $Na_V1.5$ mediates cell proliferation, whereas in astrocytes it plays a central role in cell migration (Pappalardo et al., 2014; Wu et al., 2006). $Na_V1.6$ has been shown to be a regulator of phagocytic capacity in macrophages and microglia (Waxman, 2012). These data demonstrate multiple mechanisms through which Na_V channels are implicated in important signalling pathways, either through direct modulation of V_m or otherwise, indicating their central roles in Na^+ homeostasis in non-excitable cells.

1.5.2 ENaC channels

ENaC is expressed on the apical plasma membrane in numerous salt-reabsorbing epithelia, and facilitates Na^+ transport across this membrane as the first stage of the process of transepithelial Na^+ transport (Garty and Palmer, 1997). Ion flow is accomplished via diffusion into the cell down the electrochemical gradient, independently of coupled ion / solute fluxes or metabolic energy input (Kellenberger and Schild, 2002). ENaC is characterised by sensitivity to the K^+ -sparing diuretic amiloride and its derivatives (Garty and Palmer, 1997).

1.5.2.1 Structure and stoichiometry

With successful cloning of ENaC, significant advances have been made in understanding the structure and composition of the channel. ENaC is comprised of 4 similar but distinct subunits: α -, β -, γ - & δ - ENaC, which vary from 85 - 95 kD in length in their unmodified state. Each subunit shares approximately 30 - 40% sequence homology and has two hydrophobic domains M1 and M2 (see figure 1-2), which are predicted to span the membrane twice, separating a large extracellular loop and intracellular N- and C-termini (Canessa, Merillat and Rossier, 1994). While it is accepted that each

of the four subunits may contribute to the formation of a functional channel forming pore, the definitive subunit stoichiometry remains disputed (Kosari et al., 1998). Indeed, ENaC subunits may form a homomeric pore and in particular ENaC- α has been suggested to form channels with significantly different biophysical properties. Further evidence for the heterogeneous assembly of different subunits into a functional channel is provided in the observation that not all Na⁺ absorbing epithelia express all of the discrete subunits (McNicholas and Canessa, 1997). In lung epithelia, some cells express only α and γ subunits, whereas in the colonic epithelium only α subunits are expressed. However, only channels comprised of at least one α or δ subunit can form a functional Na⁺ conducting channel (Lingueglia et al., 1994; Farman et al., 1997; Renard et al., 1995). Recent investigations utilising single-particle cryo-electron microscopy have suggested that ENaC assembles in a ‘heterotrimeric’ structure with a 1:1:1 stoichiometry for α : β : γ in human embryonic kidney HEK293 cells (refer to figure 1-2) (Noreng et al., 2018).

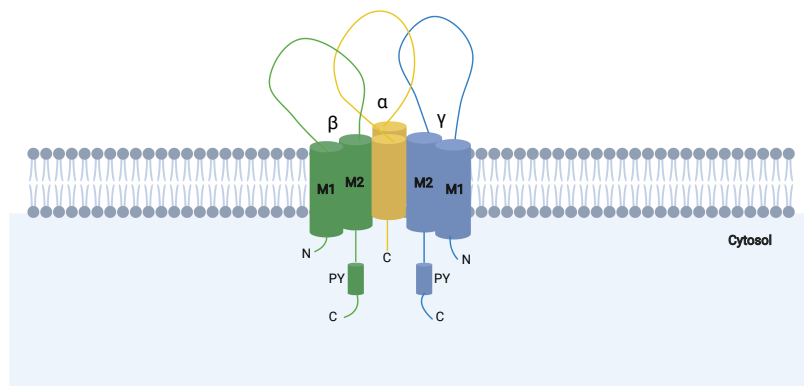


Figure 1-2: The putative structure and stoichiometry of ENaC. ENaC may exist as a heterotrimer comprising a single α , β and γ subunit. Subunits consists of two membrane spanning domains (M1 and M2) and intracellular N- and C-termini. β and γ subunits contain a 'PY' motif located with their C-termini. Figure adapted from Bhalla and Hallows (2008).

1.5.2.2 Physiological Roles of ENaC

As mentioned above, the primary functional role of ENaC in non-excitabile cells is epithelial membrane transport (Qadri, Rooj and Fuller, 2012). One of the most important sites of ENaC activity in mammalian physiology is the urinary tract. Channels are most abundant in the distal nephron and principal cells of the collecting duct, and play a central role in tubular reabsorption of filtered Na^+ (Garty and Palmer, 1997). The majority of H_2O and Na^+ reabsorption ($\approx 85\%$) is accomplished in the proximal tubule, loop of Henle and distal convoluted tubule (Feraille and Dizin, 2016). ENaC located on the apical membrane of principal cells of the collecting duct mediates Na^+ transport across the epithelial layer, a process which is accomplished through the concomitant activity of Na-K-ATPase expressed in the basolateral membrane; thus it has a key role in fine-tuning body volume homeostasis (Schild and Kellenberger, 2001). Since it is a constitutively open channel, the number of channels present in the apical membrane is tightly regulated. For example the steroid hormone aldosterone is a member of the renin-angiotensin-aldosterone system (RAAS), a core hormonal axis which plays a vital role in regulating fluid volume and hence blood pressure. Aldosterone exerts effects on ENaC through binding to the mineralocorticoid receptor (MR); a member of the nuclear receptor family of nuclear transcription factors (Verrey, 1999). Aldosterone-bound MR is then translocated to the nucleus and modulates gene expression and plasma membrane insertion of ENaC subunits (discussed in greater detail in section 1.5.2.3) (Shigaev et al., 2000). Indeed, the importance of ENaC in fluid volume regulation is evidenced in the observation that gain-of-function mutations in ENaC, and deletion of the PY-motif in the β and γ subunits cause Liddle syndrome; whereby excessive ENaC-mediated Na^+ re-uptake at the apical membrane results in severe arterial

hypertension (Lu et al., 2007). Conversely, the rare disease autosomal recessive type I pseudohypoaldosteronism (PHA-1) is characterised by severe salt-wasting; it is caused by a missense mutation in the β subunit and a marked reduction in P_o in assembled channels (Gründer et al., 1997).

ENaC also plays a central role in the regulation of alveolar lining fluid (ALF) volume (Matalon, Bartoszewski and Collawn, 2015). ENaC located on the apical membrane of alveolar epithelial cells facilitates paracellular transepithelial transport down the electrochemical gradient established by the activity of basolateral Na-K-ATPase. In turn, Cl^- ions move into ALF passively via paracellular junctions, or transcellularly through cystic fibrosis transmembrane conductance regulator (CFTR) and transmembrane protein 16a (TMEM16A) channels in order to maintain electro-neutrality (Matalon, Bartoszewski and Collawn, 2015). The opposite vectorial transport of Na^+ and Cl^- thus creates an osmotic gradient, facilitating diffusion of fluid from the air space into the interstitium, and bringing about alveolar fluid clearance (AFC) (Matalon, Bartoszewski and Collawn, 2015). This process is critical for removal of alveolar oedema following alveolar flooding due to increased permeability to plasma proteins. In adult mice, knock-down (KD) of ENaC- α in the lung with (small interfering RNA) siRNA results in marked reduction of AFC rates (Chen et al., 2014). In gene targeting studies involving ENaC- α deficient (ENaC- α^-) mice, deletion of ENaC- α proved lethal in neonates within 40 hours of birth, since mice were not able to clear their lungs of liquid (Hummler et al., 1996). Thus ENaC plays a critical role in adaptation of the neonatal lung to gas exchange.

While the critical roles that spatially localised ENaC plays in salt-reabsorbing epithelia are well established, more roles for ENaC in non-polarised cells are becoming

apparent. Under certain circumstances ENaC can act as a modulator of total Na^+ permeability and subsequently V_m (O'Donnell and Villereal, 1982). In smooth muscle cells mechanoactivation has been shown to increase ENaC conductance, resulting in depolarisation of the cell and subsequent Ca^{2+} influx and contraction (Jernigan and Drummond, 2006). An additional member of the ENaC family which is primarily expressed in neuronal tissue, FMRamide-gated channel (FaNaC), induces a fast excitatory depolarising response upon channel activation, demonstrating the heterogeneous physiological function of the ENaC family (Lingueglia, Deval and Lazdunski, 2006).

1.5.2.3 Regulation of ENaC

Since ENaC activity is critically important in the regulation of salt/water reabsorption and secretion, it is subject to regulation by a variety of intrinsic and extrinsic factors. These mediate channel function via different mechanisms, namely: regulation of channel synthesis / expression, membrane trafficking and by directly altering P_o .

Extrinsic factors include hormonal regulation; as mentioned above, aldosterone binds to MR and the aldosterone-MR complex translocates to the nucleus and binds to the promoter region of numerous genes to increase expression (Verrey, 1999; Shigaev et al., 2000). One such gene is serum and glucocorticoid-regulated kinase (Sgk1), which is upregulated within 30 minutes of aldosterone stimulation, and promotes localisation of ENaC in the plasma membrane (Vuagniaux et al., 2002). Antidiuretic hormone (ADH) (also known as vasopressin) is a hormone central to tonicity homeostasis. It promotes increased water uptake in the distal nephron due to insertion of aquaporins (AQP) into the apical membrane, via stimulation of the second messenger cyclic adenosine monophosphate (cAMP). Chronic ADH exposure (in the order of days) has been shown to upregulate β and γ ENaC subunits (Nicco et al., 2001).

Other extrinsic factors altering ENaC function have been identified. ENaC has long been thought to be mechanosensitive due to its sequence homology with mechanosensitive channels identified in *Caenorhabditis elegans* (*mecs*) (Althaus et al., 2007). However, the mechanism by which ENaC is mechanosensitive; whether it be by membrane stretch due to cell swelling or hydrostatic pressure is disputed. In *in vivo* studies in the rabbit collecting duct, laminar shear fluid flow has been shown to activate ENaC (Satlin et al., 2001). In *Xenopus* ENaC expression models, shear stress increases activity by increasing P_o and is not influenced by membrane trafficking (Satlin et al., 2001). Another critical extrinsic factor modulating ENaC activity is proteolytic cleavage. The large extracellular region of the ENaC subunits contains multiple sites for proteolytic cleavage. It is well established that ENaC activation is modulated by the proteolytic activity of numerous members of the serine protease family (Kleyman, Carattino and Hughey, 2009; Rossier and Stutts, 2009). In microdissected mouse distal nephron and cultured mouse M1 collecting duct cell whole-cell patch clamp experiments, addition of trypsin type I (trypsin I) to the bath solution resulted in a significant increase in amiloride-sensitive whole cell current (Nesterov et al., 2008). In NIH/3T3 mouse fibroblast models transfected to stably express rat α , β & γ ENaC subunits, addition of trypsin I resulted in a significant increase in P_o (Caldwell, Boucher and Stutts, 2004). Other members of the serine protease family such as furin and prostatic, also termed channel-activating protease 1 (CAP1) or Prss8, are also known to activate ENaC (Kleyman, Carattino and Hughey, 2009). In *in vivo* studies of lung fluid balance in mice, prostatic deficiency in airway epithelial cells resulted in a 48% reduction in amiloride-sensitive alveolar fluid clearance (Planes et al., 2010).

Intrinsic factors also regulate ENaC function, the most important of which is perhaps

membrane trafficking (Butterworth, 2010). The majority of ENaC subunits do not reside permanently in the plasma membrane, but are located in intracellular vesicles (Edinger et al., 2012). Stimulation of ENaC by cAMP results in increased insertion in the apical membrane of collecting duct epithelia (Butterworth et al., 2005). As is the case for many membrane-bound proteins, ENaC is subject to endocytosis and internalisation / recycling by ubiquitin-protein ligases, which target it for lysosomal degradation (Staub et al., 2000). The ubiquitin ligase most strongly associated with ENaC is Nedd4-2, which interacts with ENaC via the C-termini PY motifs (Asher, Sinha and Garty, 2003).

In summary, ENaC function is subject to a large number of regulatory factors which serve to markedly alter Na^+ transport across the cell membrane.

1.5.2.4 Pharmacological modulators of ENaC

Due to the importance of ENaC function in modulating Na^+ homeostasis, considerable effort has been invested in the development of small molecule pharmacological targets, many of which are used clinically in the management of systemic blood pressure. Of all current small molecule inhibitors, perhaps the best characterised is amiloride (de la Rosa, Navarro-Gonzalez and Giraldez, 2016). Amiloride is a pyrazinoyl-guanidine derivative that has been demonstrated to act from the external side of the cell and exerts an inhibitory effect by directly occluding the pore of assembled channels, possibly by binding of the amiloride guanidinium moiety to the ENaC selectivity filter (Sheng et al., 2005). Affinity for ENaC has been reported to be in the high nanomolar range ($\text{IC}_{50} \approx 100 \text{ nM}$), however important studies conducted by McNicholas and colleagues demonstrated significant differences in half inhibition constant (K_i) values depending on the subunit composition of functional ENaC channels, using patch clamp meth-

ods in *Xenopus* oocyte expression models (Garty and Palmer, 1997; McNicholas and Canessa, 1997). Channels comprised of $\alpha\beta$ subunits exhibited an ≈ 20 -fold higher K_i of amiloride relative to channels formed of $\alpha\gamma$ subunits, demonstrating the importance of subunit assembly in altering amiloride sensitivity (McNicholas and Canessa, 1997). Importantly, studies assessing the inhibitory effect of amiloride on ENaC in cells derived from origins other than renal tissue, such as neuronal progenitor and glioblastoma multiforme cells, required doses of amiloride of the high micromolar range ($\approx 100 \mu\text{M}$) to elicit a significant amiloride-sensitive Na^+ current; it has been suggested that this is due to the assembly of functional channels comprised predominantly of $\alpha\beta$ subunits or α subunits alone (Petrik et al., 2018; Rooj et al., 2012; Kapoor et al., 2011).

While amiloride has been classically characterised as a selective inhibitor of ENaC, it has also been shown to inhibit sodium-hydrogen exchanger (NHE) antiporters. The values of amiloride reported to inhibit NHE vary widely. In studies conducted in low $[\text{Na}^+]_e$, IC_{50} values for NHE1, the best characterised NHE isoform, are between 5 - 50 μM (Masereel, 2003). However in the presence of normal physiological $[\text{Na}^+]_e$ (140 - 150 mM), IC_{50} values of 1 mM are reported (Teiwes and Toto, 2007). Derivatives of amiloride formed by introducing substitutions into the functional moieties have resulted in the development of more potent ENaC inhibitors, namely phenamil and benzamil (Hirsh et al., 2004). Studies using these inhibitors have reported IC_{50} values of ≈ 10 nM in ENaC channels formed of $\alpha\beta\gamma$ subunits, however in human lung epithelial cells values are 30 and 80 μM for benzamil and phenamil respectively (Hirsh et al., 2004).

Other indirect inhibitors of ENaC which alter membrane trafficking and insertion into the plasma membrane have been reported and characterised (de la Rosa, Navarro-Gonzalez and Giraldez, 2016). For example spironolactone is a competitive antagonist

of the MR receptor and diminishes ENaC activity in principal collecting duct cells and is in clinical use (Ochs et al., 1978).

As such, amiloride and its analogues present a strong pharmacological toolbox which can be used to investigate the potential roles of ENaC in modulating central hallmarks in OvCa.

1.5.3 Additional pathways for Na^+ entry in cancer cells

In addition to ENaC, numerous other Na^+ channels and transport mechanisms in the plasma membrane contribute to Na^+ homoeostasis in mammalian cells, many of which are dysregulated in cancers. The predominant driving force for Na^+ is down the electrochemical gradient from the extracellular space into the cytosol (section 1.5). As such, altered expression and function may account for the increased $[\text{Na}^+]_i$ that is a hallmark of numerous tumours (refer to section 1.6.3). This section will provide an overview of other candidates most likely to contribute to altered Na^+ homoeostasis in cancer.

Altered pH homoeostasis is a central hallmark of the tumour microenvironment (see section 1.3) (Liberti and Locasale, 2016). Elevated glucose uptake and metabolism to allow increased aerobic glycolysis is a signature of many cancers and leads to acidosis of the cytosol due to increased lactate secretion: a phenomenon generally referred to as the Warburg effect (Liberti and Locasale, 2016). In order to overcome intracellular acidification (pH_i) cancer cells must increase the availability and activity of acid extrusion machinery (Pedersen, Hoffmann and Novak, 2013). One such acid-extruding family of transporters are NHE antiporters (Birkeland, Koch and Dechant, 2020). The continuously maintained inward electrochemical Na^+ gradient established to a large extent by Na^+/K^+ ATPase also establishes the gradient for NHE exchangers. NHEs facilitate the

extrusion of H^+ from the cytosol via Na^+ . This electroneutral 1:1 antiport mechanism for extracellular Na^+ is a central transport mechanism in pH homeostasis (Yue Loo et al., 2012). The best characterised and most widely studied isoform in cancer, NHE1 demonstrated elevated activity / expression numerous cancers, including breast cancer, gastric cancer, lung cancer, and OvCa (Hosogi et al., 2012; Li et al., 2009; Matthews, Ranson and Kelso, 2011; Wang et al., 2018). Another Na^+ -dependent transporter implicated in pH homeostasis is the electroneutral Na^+/HCO_3^- cotransporter SLC4A7 (also known as NBCn1) (Boron et al., 1997). SLC4A7 imports HCO_3^- into the cell down the Na^+ gradient and neutralises H^+ from increased glycolytic activity, thus generating H_2O and CO_2 . SLC4A7 is upregulated in hypoxic tumours (Gorbatenko et al., 2014).

In considering ENaC, perhaps the most notable of candidates to mention are the acid-sensitive ion channel (ASIC) family (Boscardin et al., 2016). ASICs are H^+ activated channels broadly expressed in neuronal tissue; they are closely related to ENaC, sharing $\approx 25\%$ sequence homology (Boscardin et al., 2016). The family consist of five subunits ASIC1, ASIC2, ASIC3, ASIC4, and ASIC5 and form functional homotrimeric or heterotrimeric channels similar to ENaCs (Gründer and Chen, 2010). They are non-voltage gated ion channels and exhibit a high selectivity for Na^+ ions (Gründer and Chen, 2010). A number of studies have implicated increased expression and activity of ASICs in cancer. In glioblastoma multiforme, ASIC sensitive currents are present in high-grade gliomas and absent in low-grade gliomas and astrocytes; they have been shown to contribute to increased proliferation and migration (Berdiev et al., 2003; Rooj et al., 2012; Liu et al., 2016). Decreased pH_e , a critical property of the tumour microenvironment, may result in increased P_o of ASICs thus potentially contributing to elevated $[Na^+]_i$ in cancers (Gründer and Chen, 2010).

Dysregulated Ca^{2+} homeostasis is a signature of cancer cells and has been linked to multiple tumour hallmarks such as sustained proliferation, migration and invasion. Multiple Ca^{2+} transporters are upregulated in cancer and have been shown to alter Ca^{2+} pathways. However, since it is such a ubiquitous second messenger central to many cellular pathways, the nature of altered Ca^{2+} signalling in cancer is not completely understood. The sodium-calcium exchanger (NCX) however is upregulated in multiple cancers including melanoma, prostate and breast cancer. It demonstrates markedly different behaviour when compared to normal tissue such as cardiac myocytes (Rodrigues, Estevez and Tersariol, 2019; Long et al., 2016; Besson et al., 2015). NCX is an antiporter that is dependent on V_m and the existing Na^+ and Ca^{2+} gradients. When operating in ‘forward mode’, NCX imports 3 Na^+ ions in exchange for extrusion of 1 Ca^{2+} ion (Baartscheer et al., 2011). However, with a reversal potential of ≈ -20 mV, NCX can operate in ‘reverse mode’; extruding 3 Na^+ ions for the import of 1 Ca^{2+} ion (Baartscheer et al., 2011). Evidence for predominant reverse mode operation of NCX in cancers is growing. In PC3 prostate cancer and highly metastatic melanoma cell lines addition of the reverse-mode inhibitor KB-R7943 attenuated $[\text{Ca}^{2+}]_i$ (Long et al., 2016; Sennoune et al., 2015). Thus, it is plausible to speculate that the persistent permeability to Na^+ afforded by a cell also expressing ENaC may markedly alter the activity of NCX in cancer.

Other Na^+ permeant ion channels demonstrate altered expression / function in cancers. The N-methyl-D-aspartate (NMDA) receptor is a non-specific, ligand gated cation channel that are activated by glycine and glutamate and predominantly expressed in neuronal tissue (Cummings and Popescu, 2015). Increased expression has been shown in small-cell lung cancer, breast cancer, ovarian and neuroblastoma and pharmacological

inhibition of these receptors reduced tumour growth (North et al., 2017).

Na^+ -dependent glucose transporters (SGLTs) also avail of the inward Na^+ gradient and are responsible for glucose reuptake in the proximal tubule of the nephron (Ghezzi, Loo and Wright, 2018). Increased glycolytic flux in cancers due increased aerobic glycolysis requires greater function of glucose uptake machinery; indeed SGLTs are shown to be over-expressed in pancreatic and prostate cancers (Scafoglio et al., 2015).

In summary, the established inward Na^+ gradient creates the driving force for multiple Na^+ import / export mechanisms. Altered expression / function may result in the increased Na^+ permeability known to be a signature of numerous cancers. This is discussed in greater detail in subsequent sections (see section 1.6.3).

1.5.4 ENaC in the hallmarks of cancer

While numerous studies have demonstrated a role for Na_V channels in cancer (Roger et al., 2015; Besson et al., 2015), the data for ENaC is limited. Altered expression profiles of ENaC subunits have been linked to proliferation, migration, invasion and metastasis in numerous cancers. Table 1.1 provides evidence of all current studies demonstrating altered ENaC expression and function in cancer. The roles for ENaC are primarily implicated in two critical properties of cancer: proliferation and migration. Central to these individual studies is the observation that ENaC facilitates a persistent inward Na^+ current, modulation of which with amiloride and its derivatives or knock down approaches alters proliferation and invasion (Table 1.1). To date, no studies have assessed the functional involvement of ENaC in OvCa. The subsequent sections will thus take a systematic approach to investigate the role for altered Na^+ permeability in cancer in modulating central tumour hallmarks, and consider how altered function and expression of ENaC may perturb these properties.

Cancer	Subunit	Change	Effects	References
Glioblastoma	α, γ	\uparrow	\uparrow proliferation \uparrow migration	(Kapoor et al., 2011; Rooj et al., 2012; Berdiev et al., 2003)
OvCa	δ	\downarrow	\downarrow upon chemotherapy	(L'Espérance et al., 2008)
HCC	α	\uparrow	\uparrow proliferation \uparrow migration	(Bondarava et al., 2009)
Placenta	\uparrow	α, β, γ	\uparrow proliferation	(Del Mónaco et al., 2009; Marino, Assef and Kotsias, 2013)
Colon	\uparrow	α	\uparrow proliferation	(Ousingsawat et al., 2008)

Table 1.1: Involvement of ENaC in cancer. Evidence of altered expression of ENaC. HCC, hepatocellular carcinoma

1.6 Bioelectric regulation of cell proliferation

Significant progress has been made in understanding the regulation of molecular processes in cell cycle checkpoint machinery. For example a class of tightly regulated proteins, cyclins, have been shown to be differentially expressed at different phases of the cells cycle and allosterically regulate a family of cyclin-dependent-kinases (CDKs); the phosphorylation targets these CDKs enforce correct cell cycle progression (Malumbres and Barbacid, 2005). In contrast bioelectric events, specifically V_m alterations throughout the process, are less well understood but have been shown to regulate checkpoint transitions (Blackiston, McLaughlin and Levin, 2009).

1.6.1 V_m as a primary modulator of cell fate in healthy cells

The best known modulations in V_m are manifested in the generation of the action potential in excitable cells, which involves fluctuations over short time scales (typically in the order of milliseconds). However, non-excitable cells also exhibit marked modulation of V_m over much longer time frames, and substantial evidence exists that it is a key biophysical temporal controller of cell behaviour (Levin, 2014).

The role of V_m in mammalian cells and the contribution from ion channel subtypes have primarily been investigated using pharmacological modulators of specific ion channel targets. While other techniques such as small-interfering RNA (siRNA)

allow a greater degree of specificity, due to the high compensatory capacity of the cell from other constitutive ion channel types, the phenotypic variation of V_m is often masked (Blackiston, McLaughlin and Levin, 2009).

V_m has been demonstrated to be a critical controlling factor in cell proliferation, a process which is regulated by direct alteration of V_m at specific phases within the cell cycle (Wonderlin, Woodfork and Strobl, 1995). Experimental evidence suggests that V_m hyperpolarisation is an essential bioelectric cue in allowing cell progression at G1/S transition (Wonderlin, Woodfork and Strobl, 1995). Experiments across a range of non-excitabile cell types including astrocytes, lymphocytes and kidney fibroblasts demonstrated that pharmacological depolarisation of V_m inhibited G1/S progression (Canady, Ali-Osman and Rubel, 1990; Freedman, Price and Deutsch, 1992; Orr, Yoshikawa-Fukada and Ebert, 1972). At the G2/S transition however, there is an essential V_m hyperpolarisation required immediately preceding DNA synthesis, followed by a sustained depolarisation throughout the process of mitosis (Bregestovski, Medina and Goyda, 1992).

In addition to their role in establishing V_m , ion channels and transporters regulate cell volume (V_{cell}) in non-excitabile cells and cancer cells (Jakobsson, 1980). The vast expression of ion channels and transporters facilitate active transport and passive diffusion mechanisms that allow the rapid modulation of osmotic gradients across the plasma membrane. As a result, there is a strong association between cell volume changes and V_m . It has also been demonstrated that V_{cell} varies throughout the cell cycle (Gazitt et al., 1978).

1.6.2 V_m as an instructive regulator of oncogenesis

While V_m is involved in multiple processes important for cellular homeostasis, there is also growing evidence to suggest it is an important biophysical signal in cellular mitogenesis and oncogenesis. The first relationships between V_m and the proliferative capacity of cells were observed in mature neurons and skeletal muscle cells. These terminally differentiated cells exhibit a hyperpolarised characteristic (typically in the region of -90 to -70mV) in the interphase state and critically they demonstrate an extremely limited potential for mitotic activity (Hodgkin and Horowicz, 1959; Adrian, 1956). Other well differentiated cell types such as renal tubular cells, adipocytes, smooth muscle cells and cells from the adrenal cortex exhibit intermediate levels of V_m (-70 to -50mV) (Girardier, Seydoux and Clausen, 1968; Sullivan, 1968). Cells derived from glandular epithelium, such as liver, thyroid and in addition fibroblasts possess more depolarised levels of V_m in the region of -50 to -40mV (Binggeli and Weinstein, 1986) (see Figure 1-3). In the seminal work of Cone (1971), it was observed that there existed a gradient of V_m in cells from normal tissues that correlated to their proliferative potential. Those that exhibited no mitotic potential such as neurons and skeletal myocytes were hyperpolarised, while cells such as hepatocytes and fibroblasts, which possess the capacity to proliferate under certain conditions such as tissue regeneration and wound healing, were more depolarised in their quiescent (interphase) states (Binggeli and Weinstein, 1986; Girardier, Seydoux and Clausen, 1968). When comparing normal cells in resting states to those in active stages of proliferation, V_m differs significantly. In proliferating renal tubular cells and fibroblasts, V_m levels were in the region of -20 to -10mV; markedly more depolarised than during their quiescent states (Cone and Tongier, 1973; Yang and Brackenbury, 2013).

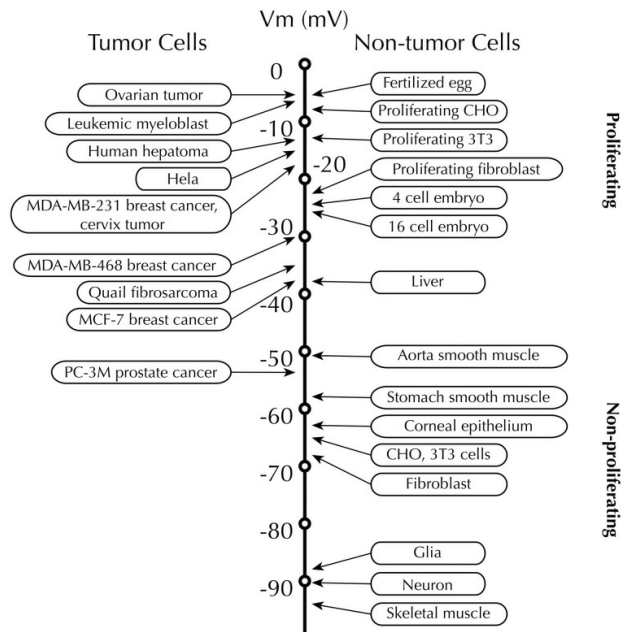


Figure 1-3: V_m as a marker of proliferative capacity. Cancer cells exhibit a depolarised V_m and an increased proliferative capacity. Terminally differentiated cells are hyperpolarised. Non-cancerous proliferating cells are also more depolarised, delineating a role for V_m as an instructive regulator of proliferation. Figure obtained from Brackenbury et al. (2007), originally adapted from (Binggeli and Weinstein, 1986) and with additional data from (Fraser et al., 2005).

The suggestion of a functional relationship existing between V_m and oncogenesis is centred on the association that V_m in cancer cells is persistently more depolarised when compared with normal cells from tissues of the same origin (Cone, 1971; Binggeli and Weinstein, 1986; Yang and Brackenbury, 2013; Binggeli and Cameron, 1980). In considering both *in vivo* and *in vitro* cancer preparations, malignantly transformed cells from ovarian tissue, breast tissue, cervical tissue and gastric tissue all demonstrate markedly depolarised phenotypes when compared to normal equivalents (Binggeli and Weinstein, 1986; Marino et al., 1994). In considering whether a depolarised V_m is simply an epiphenomenon of cancer or whether it is a critical functional regulator in directing cells to a mitogenic and possibly an oncogenic pathway, recent work on *Xenopus laevis* embryonic models have demonstrated a functionally instructive role of V_m in cancer cell proliferation (Lobikin et al., 2012). By functionally expressing a glycine-gated Cl^- channel and then modulating its activity through the addition of the activator ivermectin, V_m could be modulated at localised regions within the organism. Forced cell depolarisation resulted in the induction of a malignant phenotype of proliferation. Furthermore, it was demonstrated that by hyperpolarising the cell through two separate ionic mechanisms (over expression of a K_{IR} channel and artificial control of the Cl^- gradient) that the induction of a malignant phenotype could be suppressed (Lobikin et al., 2012). This seminal study demonstrated two critical points; firstly, that a depolarising insult on a cell was sufficient to direct it towards an oncogenic pathway and secondly, that this process was modulated / suppressed by hyperpolarisation of V_m , not by the activity of specific ion channels and ionic species. Additional evidence also supports the contribution of V_m to other hallmarks of cancer including cell migration and differentiation (Yang and Brackenbury, 2013).

It is well established that a depolarised V_m plays a functionally instructive role in directing a cell towards a mitogenic or oncogenic pathway. However, a conserved mechanism for facilitated depolarisation has not yet been identified across all cancer subtypes. It is postulated that the mechanism may be due to increased/decreased activity of ion channels or an alteration in the activity of Na^+ - K^+ -ATPase. However, differing cancers exhibit a heterogeneous upregulation/downregulation of different K^+ and Na^+ and Cl^- channel subtypes, and no clear functional pattern has been demonstrated (Sundelacruz, Levin and Kaplan, 2009). Investigation into the mechanisms of aberrant bioelectric signalling in cancer has predominantly maintained a ‘channel-centric’ focus, centred on ion channel expression and regulation and assessing the outcome of selective inhibition/activation of specific channel targets on cancer cell viability and proliferation (Yang and Brackenbury, 2013). While these approaches have demonstrated some strong functional relationships between ion channel modulation and tumour behaviour, they offer limited understanding as to how this may impact upon V_m and subsequent tumour fate (Blackiston, McLaughlin and Levin, 2009; Fraser et al., 2005).

One recurrent trait observed during malignant progression is markedly altered Na^+ homeostasis in cancer cells in comparison to normal non-excitable cells (Smith et al., 1978). Increased Na^+ permeability during resting states results in a more depolarised phenotype, and while the evidence suggests that oncogenesis induction by V_m depolarisation is ion-independent, it is likely that altered Na^+ permeability and transmembrane gradient is an important contributor to V_m *in vivo* and thus plays a central role in oncogenesis. The next section will address the evidence for Na^+ as a critical contributor to V_m in cancer.

1.6.3 The importance of Na^+ permeability in cancer

The importance Na^+ contributory depolarisation in cancer is evidenced by markedly altered expression profiles of Na^+ channels observed in numerous metastatic cancers. One of the primary channel families implicated in this phenotype are Na_V channels.

A critical association suggesting that altered Na^+ homeostasis is an important factor in tumourigenesis centres on the observations that $[\text{Na}^+]_i$ has been reported to be markedly elevated in tumour cells across numerous tissue types when compared to their non-malignant counterparts (Cameron et al., 1980). With the advent of energy dispersive x-ray microanalysis (XEDS), an advancement in scanning electron microscopy (SEM) the percentage atomic composition of multiple compartments of mammalian cells was quantifiable (Cameron and Smith, 1980). Across human liver, thyroid, laryngeal and bladder cancers a significant elevation in cytosolic and nuclear concentrations of $[\text{Na}^+]_i$ were detected, often of the order of 2-3 fold magnitude increase in comparison to their non-malignant counterparts (Smith et al., 1978; Zs.-Nagy et al., 1983; Zs. -Nagy et al., 1987; Nagy et al., 1981). Furthermore, in the comparison of tumours of laryngeal origin but of differing stages of malignancy the $[\text{Na}^+]_i$ and nuclear concentration of Na^+ also increased significantly with malignancy while $[\text{K}^+]_i$ remained relatively constant (Zs. -Nagy et al., 1987). It is interesting to note that while a there was a mean increase in $[\text{Na}^+]_i$ between thyroid cancers of increasing malignancy, a degree of each population fell within the distribution of the untransformed thyroid cells. However, due to the sample preparation methods no information exists as to whether cells of increased $[\text{Na}^+]_i$ were located in specific regions of tumours (Smith et al., 1978).

While understanding is increasing of how $[\text{Na}^+]_i$ is altered in cancer, a more complete view of how Na^+ homeostasis is altered across the tumour microenvironment is only

now emerging. Over the past decade, *in vivo* approaches have been developed to assess Na^+ distribution non-invasively using ^{23}Na MRI imaging modalities; these have proved valuable (Poku et al., 2020). While ^{23}Na MRI imaging was first developed approximately 40 years ago, numerous challenges have had to be overcome to increase signal strength and enable quantitative *in vivo* imaging (Poku et al., 2020). The physiological abundance of Na^+ relative to H^+ is considerably lower, which reduces the maximum achievable net magnetisation (Bangerter et al., 2016). Multiple ^{23}Na MRI studies have demonstrated elevated $[\text{Na}^+]$ in tumours (Poku et al., 2020). In malignant gliomas, $[\text{Na}^+]$ is higher in tumour tissue than in normal tissue (Ouwerkerk et al., 2003). In studies of breast cancer, $[\text{Na}^+]$ was $\approx 63\%$ higher in malignant breast lesions when compared to unaffected glandular tissue (Ouwerkerk et al., 2007). These studies were unable to differentiate between the intracellular and extracellular distribution of Na^+ however. A further study able to discriminate between $[\text{Na}^+]_i$ and $[\text{Na}^+]_e$ in glioblastoma, demonstrated that while total $[\text{Na}^+]$ is considerably higher in glioblastoma than normal white matter, the predominant contribution originated from the extracellular volume fraction with the $[\text{Na}^+]_i$ fraction demonstrating a reduction when compared to normal white matter (Nunes Neto et al., 2018). Subsequent observation in prostate and breast cancers however have shown that $[\text{Na}^+]_i$ is elevated and this is in agreement with observations from *in vitro* studies (discussed immediately preceding this paragraph)(Barrett et al., 2018; Jacobs et al., 2004). To date there is one known ^{23}Na MRI study in OvCa. Deen et al used an approach employing an inversion recovery pulse sequence that exploits the difference in the T_1 relaxation times of bound and unbound Na^+ , which enables the derivation of an ‘intracellular weighted sodium’ (IWS) signal (Deen et al., 2019). Total tissue $[\text{Na}^+]$ in peritoneal deposits of OvCa primary origin

was ≈ 57 mM and IWS concentrations were ≈ 31 mM. When compared to total Na^+ and IWS $[\text{Na}^+]$ signals in skeletal muscle, concentrations were ≈ 33 mM and 21 mM respectively (Deen et al., 2019). In summary these studies demonstrate that elevated $[\text{Na}^+]$ signatures in cancer are the net effect of elevated $[\text{Na}^+]_i$ and $[\text{Na}^+]_e$, and the relative distribution between the two compartments may vary with tumour type and histology.

In non-malignant cell types, there exists a difference in $[\text{Na}^+]_i$ between rapidly dividing cells in comparison to slowly dividing cell types. In comparing *in vivo* rat and mice cell populations, there is a positive correlation between increased $[\text{Na}^+]_i$ levels and the mitotic index of the cells (Cameron et al., 1980). The mitotic index (MI) is defined as the ratio of the number of cells in a population undergoing mitosis to those cells not undergoing mitosis (Campbell, 1983). In the study in question, rapidly dividing cells were distinguished from cells with normal or ‘slow’ growth characteristics as those which had a MI of 1.5% or greater and demonstrated a mild but significant elevation in $[\text{Na}^+]_i$. Furthermore, there exist clear distinctions in increasing $[\text{Na}^+]_i$ levels from normal to rapidly dividing cells to malignantly transformed cells, suggesting a role of $[\text{Na}^+]_i$ in cellular mitotic activity (Smith et al., 1978; Cameron et al., 1980). Furthermore, in considering *in vitro* cell culture models of non-cancerous Chinese Hamster Ovary (CHO) and 3T3 mouse embryonic fibroblast cell lines, cells demonstrate an elevated $[\text{Na}^+]_i$ and a depolarised V_m during the lag phase and early stages of active growth (Cone and Tongier, 1973). As cell density increases and growth rate inversely decreases, there is a density-dependent reduction in $[\text{Na}^+]_e$ and a concomitant hyperpolarisation of V_m (Bingeli and Weinstein, 1986; Smith et al., 1978). Upon cell contact, V_m becomes terminally hyperpolarised and $[\text{Na}^+]_i$ returns to lower levels and mitotic

activity is blocked (Cone and Tongier, 1973). In contrast, mitotic activity in cancer cells and in vitro cancer cell line models is not altered by contact inhibition, indicating that there is a possible role of an elevated $[\text{Na}^+]_i$ in directing cells to a more mitogenic or possibly an oncogenic pathway (Binggeli and Weinstein, 1986).

While there exists a correlation between elevated levels of $[\text{Na}^+]_i$ and increased mitogenic potential, there is also evidence to suggest that Na^+ may be a critical mediating factor in mitogenesis and oncogenesis (Cone, 1971). The mammalian liver possesses the remarkable capacity to regenerate after partial hepatectomy (Fausto, 2004). Upon stimulation by a variety of factors, mature hepatocytes have the capability to proliferate both *in vivo* and *in vitro* and initiate DNA synthesis and increase in $[\text{Na}^+]_i$ influx has been shown to be associated with the induction of a proliferative state (Binggeli and Cameron, 1980). Addition of amiloride results in the cessation of hepatocyte proliferation upon stimulation from additional factors (Koch and Leffert, 1979). Furthermore induction of mitogenesis in neurons in vitro, a capacity they do not normally possess, is achievable through pharmacological elevation of $[\text{Na}^+]_i$ using the cardiac glycoside ouabain, an inhibitor of $\text{Na}^+\text{-K}^+\text{-ATPase}$ (Cone and Cone, 1976).

It has also been demonstrated that upon induction of tumourigenesis *in vivo* by known carcinogens, cells experience a rise in $[\text{Na}^+]_i$ in their transformation to a malignant phenotype (Zs.-Nagy et al., 1983; Nagy et al., 1981; Comolli, Rossetti and Cremaschi, 1991). A critical role of elevated $[\text{Na}^+]_i$ in tumourigenesis is further suggested through the pharmacological targeting of Na^+ influx in tumour induced mice. Amiloride treated mice showed a significant reduction of tumour growth and a concomitant reduction in $[\text{Na}^+]_i$ levels.

The first attempt to systematically address the marked change observed in Na^+

homeostasis was posited by Cone et al (Cone, 1971). This unifying theory suggested a direct relationship between the critically altered bioelectric properties associated with cancer; elevated $[\text{Na}^+]_i$, and a depolarised V_m . It is likely that the accumulation of $[\text{Na}^+]_i$ occurs through increased Na^+ permeability due to a higher membrane conductance to Na^+ , either facilitated by increased Na^+ -permeable channel expression or increased activity/open-probability of constitutive Na^+ channels on cancer cells, or a combination of both mechanisms (Fraser et al., 2014; Xu et al., 2016). Furthermore, while limited in number, some studies have demonstrated a direct relationship between increased Na^+ plasma membrane permeability and neoplastic potential (Wonderlin, Woodfork and Strobl, 1995; Rooj et al., 2012).

Since the first proposition of this theory, there have been huge developments in methods of identification for functional transmembrane proteins and ion-channel complexes both in terms of structure and functional role (Behrends, 2012). This has led to the identification of a strong association between Na^+ channel over-expression and malignant transformation (Fraser et al., 2005). However, there is no clear association between specific Na^+ channel subtypes and cancer oncogenic potential (Roger et al., 2015). For example several members of the voltage gated sodium channels (Na_V) have been shown to be functionally expressed in differing cancer subtypes; $\text{Na}_V1.7$ in breast, lung and prostate cancer; $\text{Na}_V1.6$ in cervical cancer (Diaz et al., 2007; Hernandez-Plata et al., 2012; Diss et al., 2001; Roger et al., 2007). In addition, known splice variants of the Na_V channel family have been identified in malignant tissues, of which the best characterised to date is $\text{Na}_V1.5$ in breast cancer (Nelson et al., 2015). In MDA-MB-231 breast cancer cells, a mild persistent contribution of Na^+ to V_m was conferred by Na_V channels and abolished on addition of 30 μM TTX (a selective inhibitor of

Na_V channels) (Yang et al., 2020a). Increased expression of $\text{Na}_V1.5$ *in vivo* has been shown to correlate with increased metastatic potential (Nelson et al., 2015). Interestingly, $\text{Na}_V1.5$ expressed in breast cancer is a neonatal isoform (n $\text{Na}_V1.5$) that is not normally expressed in mature adult cells (Onkal et al., 2008). Critically, it has been shown that n $\text{Na}_V1.5$ permits a greater persistent Na^+ conductance than the comparative adult splice variant (Onkal et al., 2008). In the emergent evidence regarding Na^+ channel expression in cancer there then is a key point to consider; is the higher metastatic potential conveyed by increased conductance of particular Na^+ channel subtypes suggestive that the most important attribute of metastatic potential is increased Na^+ membrane permeability? Furthermore, in considering that a channel with a higher Na^+ conductance is preferentially up-regulated in embryogenesis, another physiological state of increased cell plasticity, proliferative and differential capacity, this is further suggestive of the importance of increased Na^+ permeability in mitotic potential.

1.6.4 Cell volume regulation in proliferation and the role of ENaC

Ion channels have been broadly implicated in the regulation of cell volume (V_{cell}) changes in cancer. Indeed, both secretory and absorptive epithelia, from which the majority of cancers arise, exact net solute and water transport via the careful regulation and spatial localisation of numerous ion channels and transporters. In the renal epithelium for example, ENaC localises to the apical membrane, facilitating Na^+ resorption from the lumen (Bhalla and Hallows, 2008). During the process of cell proliferation it is of course inevitable that there is a facilitative increase in V_{cell} at some time point, often termed the regulatory volume increase (RVI) (Lang et al., 2000). Equally, a re-

duction in V_{cell} is a critical event associated with the induction of apoptosis, termed an apoptotic volume decrease (AVD) (Lang et al., 2000).

There is strong evidence for the regulatory role and altered expression profiles of ion channels in V_{cell} in cancer. In NG108-15 neuroblastoma cells, pharmacological inhibition of K^+ channels, or supplementation with Cs^+ , resulted in cell swelling which acted to fully inhibit proliferation at an increase of V_{cell} by $\approx 25\%$ (Rouzair-Dubois and Dubois, 1998). In addition, inhibition of K^+ or Cl^- conductances in C6 rat glioma cells also resulted in an increase of V_{cell} with a corresponding reduction in proliferation (Rouzair-Dubois et al., 2000). Importantly though, the same authors showed that V_{cell} changes following inhibition with K^+ or Cl^- blockers were not correlated with V_m changes, demonstrating the capacity of ion channel modulation to alter proliferative capacity independently of bioelectric state (Rouzair-Dubois et al., 2000).

Certainly, cell volume changes are a critical component regulating progression through the cell cycle. Indeed, inhibition of proliferation can generally be achieved by forced cell shrinkage, whereas stimulation can often be achieved by cell swelling (Rouzair-Dubois and Dubois, 1998). Accordingly, cell volume is generally the smallest at G0/G1 and demonstrates RVI through S and G2. Conversely, regulatory volume decrease (RVD) has been shown to be an essential process in mitosis. Glioma cells were shown to undergo a cell shrinkage during mitosis, most enhanced at M phase (Rouzair-Dubois et al., 2000). Furthermore, forced cell swelling with hypertonic culture medium increased cell volume at M phase and resulted in a 30 % reduction in the number of cells undergoing divisions (Habela and Sontheimer, 2007).

The underpinning principles governing the regulation of V_{cell} are best described by the long known pump-leak model (PLM) (Kay and Blaustein, 2019). The intracellular

space is enclosed in a flexible plasma membrane that possesses persistent permeability to water and small ionic species. The cytoplasm also contains a relatively large fraction of impermeant ions, predominantly anions (here denoted as X^z , where z is the valency as described above¹). As summarised in section 1.5, the primary monovalent ions, Na^+ , K^+ and Cl^- , the 3 primary contributors to membrane permeability, are asymmetrically distributed across the plasma membrane (K^+ high in cytosol, Na^+ & Cl^- high in extracellular space). Thus, the non-uniform distribution of ions and molecules across the membrane exert osmotic gradients on the cell. However, since the cell maintains a ‘steady-state’ equilibrium and V_{cell} is not continuously expanding or contracting, it is evident that the osmolarity of the cytosol is equal to that of the extracellular space. Through regulation of ion channels and concurrent activation of pump machinery, cells can regulate continuous ion flows in both directions across the membrane and thus maintain a stable volume. This process, consisting of 2 concurrent compensatory mechanisms combining to maintain a stable V_{cell} , is elegantly illustrated by the following process: intracellular impermeant molecules, X^z , establish a relatively large osmolarity gradient. In addition, due to their net negative charge, they establish a Donnan effect and thus attract positively-charged counterions to preserve electroneutrality (Sperelakis, 1995). The inward-flow of Na^+ however, will be accompanied with an osmotically obliged inward-flow of water, which will result in an increase in V_{cell} without limit, which will inevitably result in cell rupture unless ions are actively pumped out. This critical compensatory process is primarily accomplished by the ATP-dependent pump Na^+/K^+ -ATPase; by actively extruding Na^+ , the gradient is

¹While proteins do contribute to total X, it is a relatively small fraction (< 10 mOsm). The major contribution to X consists of small metabolites, many containing negatively charged phosphate groups such as ATP. This metabolite fraction accounts for ≈ 90 mOsm/liter of the total cell osmolarity; ≈ 290 mOsm/liter

restored. This is the underpinning mechanism of the pump-leak model and thus relies on the continued cycling of Na^+ influx through leak channels, balanced by Na^+ efflux through Na^+ - K^+ -ATPase. Thus, in cell systems such as cancer, where it is thought that cells may possess a relatively high permeability or leak conductance to Na^+ , the question of whether this leak conductance contributes to V_{cell} increases arises.

Studies implicating the role of ENaC in V_{cell} changes in cancer are sparse. However, there is some evidence for a role of ENaC in RVI. In HepG2 hepatocellular carcinoma cells, silencing of ENaC- α with siRNA resulted in a near complete impairment of RVI following hypertonic challenge, whereas in control conditions cells exhibited $\approx 25\%$ recovery. This observation was also correlated with a reduced rate of proliferation in HepG2 cells when treated with different ENaC inhibitors (amiloride & flufenamate) (Bondarava et al., 2009). Similar observations were made in the D54-MG glioblastoma multiforme cell line. Treatment with amiloride or psalmotoxin 1 (an inhibitor of ASIC1) abolished RVI recovery following hypertonic challenge. Similar observations were also made following partial replacement of Na^+ with the impermeant replacement NMDG⁺ (Ross et al., 2007). To date there are no known studies assessing the role of ENaC on V_{cell} in OvCa, and thus it is necessary that this be assessed.

1.7 Ion channels in cell migration

1.7.1 Cell migration

Cell motility is a property that is critical in tissue homeostasis under normal tissue remodelling and in disease states. Indeed, there are very few cells that do not possess motile properties at one point in their life cycle. During gastrulation, cells are required to migrate to distant sites within the embryo in order to form the three germ layers

(ectoderm, mesoderm and endoderm) (Keller, 2005). Tissue homeostasis and organ development after birth requires migratory processes. During inflammation, circulating blood leukocytes are required to migrate into locations of inflammation and orchestrate tissue repair (Nourshargh and Alon, 2014). In wound healing (discussed in detail later), upon damage to the skin, keratinocytes and fibroblasts move to the site of insult (Rodrigues et al., 2019).

While the functional roles of cell migration vary in different physiological states, the diverse mechanisms by which a cell responds to an external cue and crucially, migrates towards it in a directed manner, are underpinned by a critical cell property: cell polarity. For a cell to migrate directionally, it must specify an axis of polarity in which it can organise the machinery that governs motility. This polarisation manifests to alter cell morphology to determine a front and back of a cell. The frontal part of a migrating cell is generally characterised by relatively thin organelle-free protrusions in the direction of migration from the cell soma (Charras and Sahai, 2014). The cell body encompassing the nucleus forms the rear part of the cell (Sheetz et al., 1999). Migration is then achieved through a highly coordinated cyclic process involving protrusion of the anterior region through activation of migratory machinery, such as actin filament polymerisation, and a retraction of the cell rear mediated by contractile machinery such as myosin II (Sheetz et al., 1999; Cramer, 2010).

1.7.2 The role of cell deformability in motility

While the mechanisms by which soluble factors such as chemoattractants describe the cellular response to migrate through these heterogeneous environments have been studied intensively, the direct adaptations of the cell in response to dramatic changes in mechanical properties of the tumour micro-environment (TME) have only become

appreciated in the last decades.

The ability of a cancer cell to metastasise is underpinned by its capacity to adapt to the dramatic changes in the TME. The physical properties of the primary tumour are determined by the heterogeneous cell population comprising cancer cells, fibroblasts, stromal cells and leukocytes surrounded by ECM. In aqueous environments such as a cancer cell experiences in malignant ascites and during circulation after undergoing intravasation, the mechanical properties are defined by the fluid viscosity (η), and the shear forces due to fluid and blood flow. Therefore, it is of critical importance for cancer cells to modulate their mechanical properties in order to facilitate adequate motility through the metastatic cascade.

Seminal studies assessing the mechanical properties of cancer cells at differing levels of metastatic potential have demonstrated critical differences. Mechanical measurements of cancer cells of increasing metastatic and invasive potential have demonstrated that they are often ‘softer’ or more deformable than their less metastatic counterparts (Swaminathan et al., 2011). More specifically, the elastic or Young’s modulus (E), which is a marker of how easily a material can deform, demonstrates a decrease with increasing invasiveness when compared to non-malignant counterpart models ². In a study of human melanoma cell lines utilising atomic force microscopy (AFM), SBCL2 and WM115 melanoma cell lines were more deformable when compared to normal human epidermal melanocytes (Weder et al., 2014). Similar relationships have also been observed in cancers of the prostate, bladder and breast, and it has been suggested that mechanical deformability may have prognostic application in assessment of metastatic

²Young’s modulus (E) is described by the relationship $E = \frac{\sigma}{\epsilon} = \frac{F/A}{\Delta l/l}$ where σ is the stress in force (F) per unit area A and ϵ is the strain in compression (Δl) per unit length (l).

capacity of primary tumour biopsies and effusions. (Khan, Santos and Hussain, 2018; Abidine et al., 2015; Rother et al., 2014; Kwon, Gunasekaran and Eom, 2019).

One potential theory to explain the increased deformability or ‘compliance’ of tumour cells may be found in considering the mechanical properties of solid tumours. Tumours are often considerably stiffer or more rigid than the tissue in which they reside due to expansion within a confined space resulting in a subsequent rise in interstitial pressure (Butcher, Alliston and Weaver, 2009). This is thought to be attributed to increased number and activity of cancer associated fibroblasts (CAFs), which in turn leads to increased secretion and deposition of large amounts of ECM components and results in a more fibrotic and ‘stiff’ phenotype (Paszek et al., 2005). By subsequently modulating their mechanical properties, cancer cells residing in tumours can counteract the effects of increased stromal pressure by enhancing their deformability and subsequent invasive potential (Butcher, Alliston and Weaver, 2009). Indeed, in AFM measurements of solid mammary tumours obtained by needle biopsy, the tumour core, which was densely populated with tumour cells, demonstrated a marked reduction in E when compared to peripheral regions, which were predominantly comprised of fibrotic tissue (Plodinec et al., 2012).

In addition to observations in primary tumours, increased cell deformability is also a property observed in metastatic transformation in numerous cancers. During transmigration across the endothelial layer in intravasation, and the mesothelial layer as is thought to occur in OvCa peritoneal dissemination, cancer cells are often required to ‘squeeze’ through spaces considerably smaller than the diameter of the cell. Thus, the ability of a cell to reorganise shape is a central parameter in order to reach the ECM layer beneath. Once in the ECM, cells encounter a variety of ECM-free spaces known as

gaps/pores, and trails that are due to the heterogeneous composition of fibrillar proteins and the degree of cross-linking between them (Charras and Sahai, 2014; Wolf et al., 2009). In situations where these pores are considerably smaller than the cell diameter, cells undergo shape deformations and migrate through them in an amoeboid manner, thus facilitating continued migration (Wolf and Friedl, 2011). While the cytoplasm has a relatively low viscosity and comprises the softest component of the cell, nuclear stiffness magnitudes are often 2 - 10 times higher, and thus nuclear deformation or compliance is a limiting factor in cell translocation through small spaces (Khan, Santos and Hussain, 2018). In aqueous environments encountered during the metastatic cascade, such as malignant ascitic fluid and during haematogenous spread, cell deformability is also a central adaptation to facilitate continued survival. Following intravasation and ascitic transition, cells encounter fluid flows which elicit shear stress to which cells must adapt. Indeed, cancer cells display greater resistance to shear stresses than normal cells (Northcott et al., 2018). Physiological levels of shear stress (5 - 30 dyne/cm²) enhances migratory capacity in MDA-MB-157 and BT-549 breast cancer cell lines (Ma et al., 2017). OvCa cell lines cultured under physiological shear fields *in vitro* resulted in the development of a pro-invasive phenotype when injected intraperitoneally into athymic nude mice (Ip et al., 2016). Hence the ability of a cell to deform is a principal property facilitating cancer dissemination.

1.7.2.1 Role of deformability in OvCa

With recognition of the increased role of deformability in tumour progression, increasing attention has been placed on OvCa, due in part to its highly metastatic phenotype (Ketene et al., 2012).

The mechanisms through which cells regulate cell stiffness are underpinned by the

capacity to undergo cytoskeletal remodelling (Pegoraro, Janmey and Weitz, 2017). While cell soma of migrating cells is typically softer than border regions undergoing active protrusion, total cell stiffness can be described by the degree of actin polymerisation (Hofmann et al., 1997). Actin polymerisation had been shown to be directly regulated by alterations in V_m in endothelial cells (Callies et al., 2011). Alterations in V_m are sensed by the cortical actin network and directly influence the ratio of filamentous actin to globular actin (G-actin) monomers which in turn regulates cytoskeletal stiffness (Kasas et al., 2005; Azadi et al., 2019). A depolarisation of V_m by increasing extracellular K^+ results in a softening of endothelial cells (Oberleithner et al., 2009). Furthermore, ENaC interactions with the cytoskeleton have been shown to directly modulate ENaC activity. Berdiev et al demonstrated that short actin filaments resulted in increased activity in α, β, γ -ENaC channels inserted in planar lipid bilayers (Berdiev et al., 1996). Further work revealed that F-actin binds directly to the ENaC- α subunit, delineating a clear relationship between ENaC activation and cytoskeletal interaction (Mazzochi et al., 2006). To date, there are no known studies assessing the functional modulation of ENaC activity in regulating cell stiffness in metastatic cancers and it remains a valuable question.

1.7.2.2 Consequences of ion channel perturbation in migration

Situated within the plasma membrane, ion channels and transporters serve as ideal candidates to transduce external cues and subsequently modulate the cellular response. As may be expected, the functional roles in which ion channels act to regulate cell migration are associated with the diverse homeostatic mechanisms by which ion channels regulate cell function. These include the regulation of $[Ca^{2+}]_i$, V_m and pH_i , perturbations of which have been associated with modulations of the migratory response.

Since multiple ionic species and channel families are implicated in regulation of V_m , cell volume, etc., the consequences of alterations in these biophysical properties in cell migration will first be considered.

In the MDA-MB-231 metastatic breast cancer cell line, NHE1 has been shown to be important in invasion as a regulator of H^+ efflux. Importantly, H^+ efflux is increased by activity of $Na_V1.5$. They also demonstrate co-localisation with membrane rafts containing caveolin-1. Inhibition with 30μ TTX resulted in reduced invasion (Brisson et al., 2011). This study, demonstrates a role for ion channels in coupling ionic fluxes in modulating migration. Others have shown that $Na_V1.5$ modulates migratory capacity in MDA-MB-231 via a Na^+ facilitated depolarisation (Yang et al., 2020a). Thus demonstrating the diverse roles by which ion channels can modulate motility.

1.7.2.3 The Ca^{2+} hypothesis and V_m alterations

The plasma membrane potential (V_m) modulates similar functions in a migrating cell as those in any other eukaryotic cell. As both temporal and indeed spatial modulations of V_m are critical in other physiological states, such as progression through the cell cycle for example, similar observations have been identified in actively migrating cells.

Of the multitude of V_m modulations that occur during cell migration, one of the most critical is likely to be the instrumental role V_m plays in establishing the driving force of Ca^{2+} influx. As one of the most characterised second messengers in physiology, the cellular responses due to increases in $[Ca^{2+}]_i$ in different physiological states is highly variable. However, cell migration has been shown to be a Ca^{2+} dependent process due to the presence of many Ca^{2+} regulatory proteins in the migratory machinery (Wei et al., 2012). In the majority of mammalian cells, there exists an $\approx 10,000$ -fold inward Ca^{2+} gradient across the plasma membrane, with a similar gradient existing between

the endoplasmic reticulum and the cytoplasm (Wei et al., 2012). Seminal studies by Fay and colleagues first made the observations that gradients of $[Ca^{2+}]_i$ exist across the front to rear of a migrating eosinophil, with a steadily increasing gradient towards the rear of the cell (Snyderman and Goetzl, 1981). Rises in Ca^{2+} at the rear of the cell have direct effects on the cell migration machinery. At relatively high $[Ca^{2+}]_i$ concentrations of the order of $\approx 1 - 10 \mu M$, the actin severing protein gelsolin is active, resulting in the shortening of actin filaments and critically leaving them capped, thus inhibiting actin polymerisation and membrane protrusion at the cell rear (Sun et al., 1999). Conversely, at $[Ca^{2+}]_i$ concentrations of $< 1 \mu M$ that have been observed in the frontal regions of migrating cells, gelsolin dissociates from the actin filament, exposing new sites of polymerisation and thus facilitating the formation of membrane extensions (Yin et al., 1981).

Subsequently, in a cell expressing voltage-independent Ca^{2+} channels, hyperpolarisation of V_m would increase Ca^{2+} influx. In the MDA-MB-435 metastatic breast cancer cell line, a small-conductance Ca^{2+} -activated K^+ channel, SK3 is expressed (Potier et al., 2006). Increased activity would result in V_m hyperpolarisation and has been shown to enhance cell migration, most likely by increasing Ca^{2+} influx (Potier et al., 2006). Similarly IK1, an intermediate-conductance Ca^{2+} -activated K^+ channel in MDCK-F retinal epithelial cells enhances cell migration, and demonstrated a retraction of the rear pole of the cell (Schwab et al., 2006). Conversely, in a cell expressing voltage-dependent Ca^{2+} channels, V_m depolarisation would act to increase Ca^{2+} influx. Inhibition of T-type voltage-gated Ca^{2+} channels in U87 human glioblastoma cells with endostatin resulted in attenuated voltage-dependent Ca^{2+} and a corresponding reduction in cell migration (Zhang et al., 2012).

There are other potential mechanisms by which V_m depolarisation may act to increase Ca^{2+} influx. If functional NCX is expressed, V_m depolarisation may result in predominant reverse mode operation; resulting in Ca^{2+} influx with corresponding Na^+ efflux. In NG2 oligodendrocyte progenitor cells, GABA induced depolarisation resulted in increased $[Ca^{2+}]_i$ that activated an Na_V current and a persistent non-inactivating Na^+ current. This was shown to facilitate reverse mode NCX, and increased NG2 migration .

1.7.3 Roles for ENaC and V_m in cell migration

Numerous studies have demonstrated the importance of the regulatory role of V_m on the migratory capacity of cells. Upon stimulation of wound healing, bovine corneal endothelial cells, rabbit corneal epithelial cells and Madin-Derby canine kidney cells exhibited a significant depolarisation in V_m , when compared to the cell population not actively participating and isolated from the wound edge (Justet et al., 2013). Depolarisation was associated with an increase in $[Na^+]_i$ and a concomitant rise in $[Ca^{2+}]_i$. Subsequent treatment of the aforementioned cell lines with amiloride or phenamil resulted in a marked reduction of wound closure relative to control, whereas treatment with aldosterone or forskolin (drugs which increase insertion of ENaC in the plasma membrane) resulted in an increased rate of wound healing. Indeed, irrespective of the mechanism by which cells migrated, whether by actin cable formation or through lamellipodial cell crawling, ENaC inhibition resulted in a significant reduction in migratory capacity. Of note, however, bovine aortic endothelial cells demonstrated no discernible changes in $[Na^+]_i$ or $[Ca^{2+}]_i$ during wound healing. However, treatment with amiloride and phenamil significantly attenuated the rate of wound healing (Justet et al., 2013). Similar patterns were observed in BeWo cells, a cell line of trophoblastic origin (Del

Mónaco et al., 2009). The potential roles for ENaC in modulating migration are summarised in the cartoon depicted in Figure 1-4.

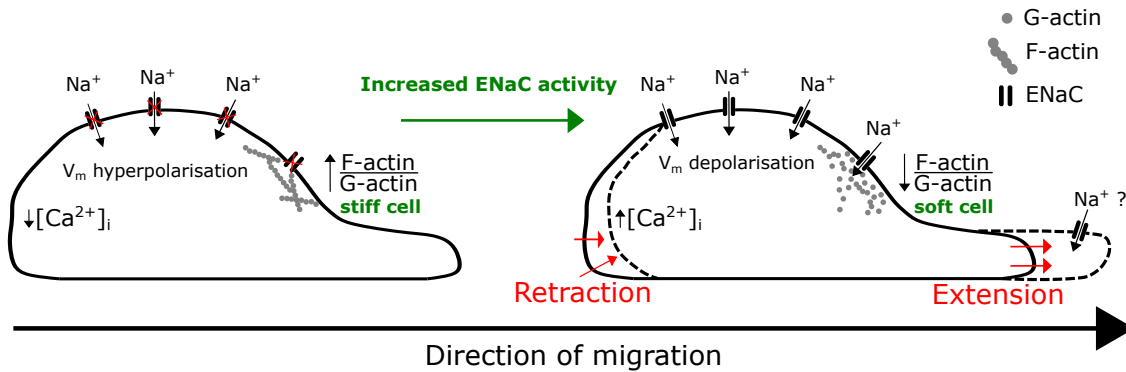


Figure 1-4: Cartoon showing potential mechanisms by which ENaC activity may modulate migration. Persistent conductance of ENaC results in increased Na^+ influx and subsequent V_m depolarisation. In the presence of voltage-dependent Ca^{2+} conductances, subsequent depolarisation may increase $[\text{Ca}^{2+}]_i$ dependent contractile machinery, thus facilitating retraction at the cell rear. V_m manifests as a high electrical field generated across the thin plasma membrane, which can invoke conformational change upon adjacent actin molecules. V_m hyperpolarisation results in F-actin formation and a ‘stiff’ phenotype, whereas depolarisation promotes depolymerisation (F-actin to G-actin), leading to increased cell deformability. Finally, increased ENaC conductance at the leading edge may mediate local volume increases and formation of cell protrusions.

1.8 Galvanotaxis in cancer

As the physiological relevance of the V_m in non-excitabile cells is becoming more apparent, the existence of other steady-state bioelectric phenomena is also receiving greater recognition. One such phenomenon is the presence of long-distance persistent endogenous electric field gradients within tissues. Cells present within such tissues are often sensitive to these persistent direct-current (DC) voltage gradients and respond to them in multiple physiological processes including developmental biology, tissue remodelling, and metastases (McCaig et al., 2005). Indeed, the first observations by Galvani and Volta of steady-state potentials in frogs and mammals pre-date identification of transient / dynamic field potential in tissues (Geddes and Hoff, 1971). These dynamic

changes however, have manifested in physiological tools such as electroencephalography and electrocardiography, and are generally much better understood in physiology than their steady-state counterparts (Binnie and Prior, 1994; Geselowitz, 1989).

1.8.1 Characterisation of external endogenous electric fields

As mentioned above, in contrast to an EF existing across a single cell (V_m), EFs are derived across the extracellular space, and as such establish a non-uniform gradient which decreases with increasing distance from the point of origin. This serves to establish a persistent voltage gradient over a tissue in a particular direction / orientation. The result is a directional voltage ‘cue’ that serves to describe the subsequent physiological response. In static tissue, this response may manifest as the re-orientation of tissue structure and cellular growth (galvanotropism) in alignment with the external field (Zhao, 2009).

1.8.2 The physiological EF

As discussed in section 1.5, in the absence of free electrons in physiological environments, the charge carriers that allow current flow are charged ions, predominantly the monovalents Na^+ and Cl^- , which are present at the highest concentrations in the extracellular fluid. In the presence of a persistent electric field, there will be subsequent current flow in the direction of the field. The magnitude of the current will be dependent on the ionic gradient and, critically, the bulk resistivity of the solution, which will act to oppose current flow. The bulk resistivity of physiological solutions is $\approx 100 \Omega \cdot \text{cm}$ (McCaig et al., 2005). The resultant voltage gradient derived per unit difference is described by a simple variant of Ohm’s law $E = J \cdot \rho$ where, E is the electric field in V/cm (or mV/mm), J is the current density (in A/cm^2) and ρ is the resistivity of the

solution. Crucially, J and subsequently E are vectors, meaning that they have magnitude and importantly, direction, which is the critical property that implicates EFs as spatially orientated signalling candidates in tissues, cells, and on cells existing in tissue / fluid interfaces (McCaig et al., 2005; Cortese et al., 2014).

The magnitude of persistent endogenous EF varies in different physiological systems. Using sharp electrode techniques, the potential across tissue layers has been measured in numerous physiological states. Voltage gradients often exist along the length of the developing embryo. In the axotol, voltage gradients of 75-100 mV/mm were measured in the extracellular space existing under neural plate epithelium at the head end of the embryo, whereas EFs at the tail end were considerably lower at approximately 30 mV/mm (Shi and Borgens, 1995). In other situations, for example limb regeneration of the newt, the current densities measured close to the limb stump using non-invasive vibrating-probe micro electrodes, were 10 - 100 $\mu\text{A}/\text{cm}^2$, resulting in a field potential of ≈ 60 mV/mm (Borgens, Venable and Jaffe, 1977; Altizer et al., 2002). To contextualise the magnitude of these steady-state EFs, to depolarise a neuron, the resultant field gradient would be approximately 1-2 V/mm; 1-2 orders of magnitude higher (McCaig et al., 2005). Nevertheless, these low-magnitude, steady state currents have important roles in directing tissue organisation in physiological systems (McCaig and Zhao, 1997). The next section will describe the establishment of these voltage gradients and the physiological situations in which they arise.

1.8.2.1 The transepithelial potential

All organs are encapsulated in an epithelial layer that is in some cases a single continuous layer, or, in other cases such as the skin, comprised of multiple layers. The primary purpose of which is to control the bi-directional transport of ions, small molecules and

macro molecules (Palmer, 2017). As V_m of a single cell has been shown to have a central role in regulating membrane transport and initiating cell signalling events, the electric properties of the epithelium form a functional syncytium to affect similar events across it (Pu, Cao and McCaig, 2015). A critical property of epithelia that enables this is cell polarity. While the distribution of ion channels and transporters is considered to be uniform when considering V_m , this is not the case in epithelial layers. In the majority of epithelial layers studied, Na^+ channels are predominantly located within the apical membrane (the outward facing side), whereas the majority of K^+ channels and Na^+/K^+ ATPase transporters are located on the basolateral membrane. Na^+ channels situated on the apical side facilitate the flow of Na^+ ions down their concentration gradient, leaving a net negative charge on the outside of the apical membrane. Na^+/K^+ ATPase at the basolateral membrane extrudes Na^+ and imports K^+ , maintaining gradients. Background or 'leak' K^+ channels on the basolateral membrane allow diffusion of K^+ out of the cell, down the concentration gradient, hence establishing a net positive charge on the external basolateral surface. The circuit is completed by the paracellular slow flow of ions between cells connected by tight junctions. This asymmetric persistent field potential across epithelial cells is known as the transepithelial potential (TEP). Considering the Nernstian potentials for Na^+ and K^+ , it is conceivable that the total TEP existing across an epithelial layer can be as high as 130 mV with respect to the apical membrane ($V_{te} = V_a - V_b : -70 - +60$). However, this is rarely the case. The net effect is a persistent potential difference across the epithelium. In most situations this is positive basolaterally (as above), but altered ion channel / transporter activity and ionic gradients can act to reverse this equilibrium, and this varies between tissue types. For example, in the human intestine, the TEP is ≈ -25 mV, lumen (apical) negative

(Archampong and Edmonds, 1972). In human peritoneal mesothelial cells however, the transmesothelial potential (TMP) is ≈ 0.5 mV, apical positive (Li et al., 2001).

In the event of ‘wounding’ and disruption of epithelial layer integrity, a short circuit occurs locally. In considering the basolateral positive TEP described above, the field potential at the wound centre drops to 0 mV (Tai, Tai and Zhao, 2018). Moving laterally away from the wound site, the unwounded, intact epithelium is still maintaining a basolaterally positive voltage across it (Tai, Tai and Zhao, 2018). The result is the establishment of a negative field gradient pointing towards the wound centre. Distally from the wound site, the undamaged cells will work to maintain an inwardly positive voltage, resulting in the persistent establishment of a negative field vector pointing to the site of injury. This phenomenon is known as the wound potential and plays a key role providing a galvanotactic cue to directed re-epithelialisation and closing of the wound (Nuccitelli, 1992; Zhao, 2009). Keratinocytes by their nature respond to a cathodal field response because it directs their migration to the centre of wound insult (Allen, Mogilner and Theriot, 2013; Guo et al., 2015; Yang, Charles, Hummler, Baines and Isseroff, 2013). The wound potential has been shown to persist for many hours / days and is established immediately after disruption, whereas chemotactic gradients can take a number of hours to be established (Zhao et al., 2006).

1.8.3 Galvanotaxis and metastatic disease

Metastatic dissemination is critically determined by the ability of a cancer cell to migrate and invade in response to external stimuli in a directed manner, and is likely to be a multi-cue mediated effect (Lara Rodriguez and Schneider, 2013). Endogenous EFs present in the tumour microenvironment provide yet another cue to influence the migration and invasion of individually or collectively migrating cells in numerous can-

cers.

In prostate cancer, the effects of persistent dcEFs of 3 V/cm on a highly metastatic MAT-LyLu rat cell line resulted in a strong cathodally-directed pattern of migration, whereas a weakly metastatic counterpart cell line, AT-2 derived from the same tumour exhibited no appreciable directed migration in an electric field (Djamgoz et al., 2001). Weakly metastatic MCF-7 human breast cancer cell lines demonstrate a weak cathodal response in an external EF of 3 V/cm (Fraser et al., 2005). In contrast however, the MDA-MB-231 cell line, a model of highly metastatic human breast cancer, demonstrates a strongly anodal response (Fraser et al., 2005). Importantly, the difference in directional response is known to correlate with the polarity of endogenous transepithelial potentials present in the tumour locality. The TEP of the rat prostatic duct is ≈ -10 mV, lumen negative (Wellings and Jensen, 1973). Formed of a cuboidal-like epithelium, and with a cell thickness of ≈ 20 μm , the subsequent EF gradient that would be established across the lumen is - 5 V/cm relative to the basal side. This may provide metastatic cancer cells in the vicinity with the cue to invade through.

Data on the galvanotactic response in metastatic disease remains relatively sparse. Studies in lung cancer derived cell lines also demonstrate effects of external EFs. H1975 cells, a model of large cell carcinoma (LCC), showed cathodal migration and increased migration in the presence of fields of 2 - 6 V/cm, whereas another LCC cell line (H460) demonstrated a very weak response (Li et al., 2017). Lung adenocarcinoma cell lines A549 and CL1-5 showed cathodal and anodal responses respectively, whereas the HCC827 cell line showed increased migration rate but limited directional response (Li et al., 2017; Hou et al., 2014; Yan et al., 2009).

The mechanisms driving galvanotaxis are still not well understood. However, mount-

ing evidence suggests that they are modulated by critical properties of the metastatic niche and local environment. In glioblastoma multiforme (GBM), a disease characterised by the invasion and spread of metastatic cancer cells along white matter tracts, where persistent EFs are present the galvanotactic cue, has also been demonstrated (Huang et al., 2016). U87, C6 and U251 glioma cell lines exhibited cathodal migration *in vitro* in external EFs of 2 V/cm (Li et al., 2013). Furthermore, cell - ECM interactions, which are known to be critical components of the metastatic niche, have also been shown to modulate the galvanotactic response (Huang et al., 2016). Brain tumour initiating cells (BTICs), a sub-population of GBM thought to be capable of continued proliferation and differentiation, migrated towards the anode when cultured on poly-D-ornithine/laminin coated surfaces. However, when cultured in a 3D model comprising hyaluronic acid and collagen 1, the same cells exhibited a cathodal response (Huang et al., 2016). These results demonstrate that biochemical properties of the tumour microenvironment are critical modulators of the subsequent galvanotactic response.

1.8.4 V_m perturbations in regulation of galvanotaxis

The process by which cells ‘sense’ and orientate in response to an external EF is unclear. There are a number of proposed theories for a cellular sensor of an external EF. The first proposed mechanism involves membrane electrophoresis; the non-uniform redistribution of membrane-bound ligands/receptors upon exposure to an external EF (Sarkar et al., 2019; Poo, 1981; Loof, 1986). The second potential mechanism, electro-osmotic flow, involves the ‘solvent-drag’ of water by free cations attracted to the cathode (McLaughlin and Poo, 1981).

One other potential mechanism by which cells ‘sense’ an external EF involves localised changes in V_m (Mycielska and Djamgoz, 2004). Immediately upon application

of an external EF, a cell becomes polarised; the field across the plasma membrane and hence the localised V_m will be inhomogeneous across the cell; the most pronounced differences will occur at the regions perpendicular to the EF field lines (Lee and Grill, 2005). In considering an example of a cell in a uniform external EF of 1 V/cm with a length of 100 μm , the voltage drop across the cell would be 10 mV. The bulk resistivity of the cytosol is many orders of magnitude lower than the resistance of the plasma membrane, as such the current passing through the cell will result in the vast majority of the voltage drop experienced across the membrane (Lee and Grill, 2005; Borys, 2013). As a result, the same cell will experience a 5 mV hyperpolarisation in V_m at the cell surface facing the positive pole (anode) and a 5 mV depolarisation in V_m at the cell surface facing the negative pole (cathode) (Nuccitelli, 2003). This differential V_m across the cell will influence the inward driving force on ions at opposing surfaces of the polarised cell; cations will experience an increase in driving force at the hyperpolarised anodal facing surface (Funk, 2015). Conversely, there will be reduced driving force on cations at the depolarised cathodal surface (Funk, 2015). This differential ion influx across the surfaces of a cell in an external EF has been suggested to establish intracellular ion concentration asymmetry that may subsequently influence cell motility. Since perturbations in localised V_m changes are thought to influence the galvanotactic capacity of cells, the question arises as to whether macroscopic approaches to alter V_m have an effect on galvanotaxis. In the single cell organism *Dictyostelium discoideum*, V_m alteration resulted in altered galvanotactic capacity Gao et al. (2011). Membrane depolarisation via high extracellular K^+ replacement, electroporation or changes in extracellular pH significantly impeded the galvanotactic response. Importantly however depolarisation did not affect cell motility or the chemotactic response in these cells, sug-

gesting the existence of differential sensing mechanisms between these two directional cues Gao et al. (2011).

Other evidence for V_m depolarisation in metastatic dissemination is emerging. In *Xenopus laevis* tadpole models, selective depolarisation of ‘instructor’ cells at the tip of the tail results in marked long-distance signal propagation that altered the function of all melanocytes within the tadpole (Lobikin et al., 2012; Chernet and Levin, 2014). A small but conserved cell population in *Xenopus* express the Glycine-gated chloride channel (GlyCl). Use of the specific GlyCl channel opener ivermectin results in increased Cl^- permeability and efflux and subsequent depolarisation (Lobikin et al., 2012). The melanocyte population exhibits properties of increased proliferation and increased migratory capacity, with the ability to invade and colonise distant tissue and form ‘induced tumour-like strictures’ (ITLS) (Blackiston et al., 2011). Interestingly this effect was blocked by forced hyperpolarisation of differing mechanisms. Artificial alteration of the extracellular Cl^- gradient or transfection with a K_{ir} channel, $K_{ir}4.1$, resulted in a partial blockade in ITLS formation (Lobikin et al., 2012). This is suggestive that V_m depolarisation alone, independently of the ionic mechanism is the critical modulator in inducing a ITLS phenotype. These observations suggest that depolarisation of a small number of instructor cells can result in the development of ITLS at distance in *Xenopus* models. Indeed, depolarisation of instructor cells at the tail could induce ITLS in the head region; at a distance of $\approx 1-2$ mm (Blackiston et al., 2011; Lobikin et al., 2012). It important to note however that this model for long distance development of ITLS may not be down to a galvanotaxis mediated migration of instructor cells, but is more likely due to induced serotonergic signalling on neighbouring cells. Depolarisation of instructor cells results in increased secretion of serotonin; a mechanism

itself that can induce a hyperpigmented phenotype (Lobikin et al., 2012). Treatment of *Xenopus* larva with the serotonin inhibitor fluoxetine, before selective depolarisation of instructor cells blocks down-stream melanocyte hyperpigmentation (Lobikin et al., 2012).

Taken together, it is clear that V_m alterations can impact upon the migratory capacity of cancer cells. However limited data exists for the role of ENaC in modulating the galvanotactic cue. As a constitutively open channel with the potential to modulate V_m , it is an attractive candidate for allowing differential Na^+ at the front and rear of a cell when placed in an external EF. A single study has implicated ENaC as a candidate ‘sensor’ of an external EF. In human keratinocytes exposed to a field of 3 V/cm, addition of 100 μM amiloride or 20 μM phenamil resulted in a mild reduction of directional cell migration in an EF (Yang, Charles, Hummler, Baines and Isseroff, 2013). Furthermore, overexpression of ENaC- α in the H441 lung epithelial cell line that are weakly galvanotactic promotes EF dependent translocation (Yang, Charles, Hummler, Baines and Isseroff, 2013). Interestingly, knock-down of ENaC- α abolishes the galvanotactic response in human keratinocytes but does not alter cell migration speed (Yang, Charles, Hummler, Baines and Isseroff, 2013). This places ENaC as a candidate sensor of an external EF, and suggests that it is not directly involved in the underpinning cell migration machinery in galvanotaxis.

There is as yet no evidence for a role of the galvanotactic cue in OvCa. However, in light of other observations it remains an important questions to address. In considering further that there is evidence for V_m alteration in effecting a cells ability to ‘sense’ an external EF, it may be that there is a role for an Na^+ conductance present within OvCa cells in modulating this cue.

1.9 Rationale, hypothesis and aims

Alterations in bioelectric signalling, namely V_m are gaining greater interest for their potential roles in directing tumourigenesis and cancer progression. Altered Na^+ homeostasis and ENaC activity and their potential contribution to V_m remain poorly understood in cancer however. Further understanding of the mechanisms by which ENaC and altered Na^+ homeostasis contribute to the central hallmarks of OvCa; sustained proliferation and metastatic spread may prove insightful to further understanding the pathogenesis of a cancer subtype that has demonstrated limited improvements in survival outcomes in recent decades.

ENaC and altered Na^+ homeostasis are likely to play a role in controlling central tumour hallmarks in OvCa. ENaC has been shown to modulate proliferative capacity in tumourigenic and non-tumourigenic cell populations and potentially confers cells with increased plasticity or ‘stemness’ and as such could participate in the maintenance of the cancer stem cell population. Increased activity of ENaC is thus has been shown to facilitate V_m depolarisation and cytoskeletal remodelling and subsequently promote cell migration . Furthermore, persistent external EFs may provide a directional cue for metastatic spread in numerous cancers and ENaC as a constitutively open channel is centrally placed as a potential ‘sensor’ of the galvanotactic cue. There is increasing evidence that altered Na^+ conductances are a central property of cancer cell progression in numerous subtypes and as such it is critical to address whether ENaC plays a role in the progression of OvCa.

1.9.1 Hypothesis

The central hypothesis presented in this study is that ENaC regulates V_m , and subsequently regulates proliferation and migratory capacity in OvCa. It is further hypothesised that OvCa cells migrate preferentially in the presence of external EFs and ENaC and as a modulator of V_m may act as a regulator of galvanotaxis in OvCa.

1.9.2 Aims

To test this hypothesis, the following aims are addressed in each chapter:

1. To assess whether Na^+ and ENaC contribute to V_m in OvCa, the patch clamp method in $I=0$ current clamp mode was employed to determine V_m values when recorded in the absence and presence of Na^+ and upon addition of amiloride in SKOV-3 and OvCa_{asc} cells.
2. To assess the role of ENaC and Na^+ on proliferation in OvCa. Proliferation of SKOV-3 and OVCAR-3 cells in the presence of amiloride were assessed. Effect of elevation of $[\text{Na}^+]_e$ was then assessed. The effect of ENaC inhibition on V_{cell} changes in proliferating SKOV-3 was also assessed.
3. To assess the role by which ENaC contributed to OvCa progression. mRNA levels of the ENaC- α & ENaC- δ were compared between normal ovarian tissue (NO), FIGO₃₋₄ solid tumour and OvCa_{asc} samples. It was then assessed by flow cytometry whether ENaC- α is preferentially expressed in cancer stem cell populations in OvCa_{asc}. The contribution of ENaC to migration in OvCa cell lines was then assessed. A role for ENaC in controlling cell stiffness was then assessed using AFM force-probe measurements.

4. To assess whether OvCa cells are galvanotactic. Galvanotaxis assays in OvCa_{asc} are conducted in the presence and absence of external EF Secondly, it was assessed whether ENaC plays a role in EF directed cell migration. Finally, it was assessed whether Na⁺ influx and V_m modulation impact the galvanotactic cue.

Chapter 2

Materials and Methods

2.1 Drugs

Amiloride hydrochloride hydrate (CatA7410, Sigma, UK) was dissolved in dimethyl sulfoxide (DMSO) (Sigma, UK) at 100 mM, and dispensed into 50 μ l aliquots. Phenamil mesylate (3379, Tocris Bioscience, UK) was dissolved in DMSO at 50 μ M and dispensed into 30 μ l aliquots. Phenytoin (PHR1492, Sigma) was dissolved in 75 mM NaOH at 180 mM. Riluzole hydrochloride (Cat0768, Tocris Bioscience, UK) was dissolved in DMSO at 100 μ M and dispensed into 20 μ l aliquots. All aliquots were stored at -20°C until use. A fresh stock solution was used once and remaining stock was discarded after use.

2.2 Cell culture and processing of primary cells from tissue and ascites

The following sections detail all cell lines used in this study, including sub-culture and storage. The isolation and purification of cells from primary OvCa ascites is detailed next, followed by the processing of normal ovarian and primary OvCa tumour tissue

samples. All cell culture procedures were performed in a sterile Class II safety cabinet using aseptic technique. Prior to cell culture, the cabinet was wiped down with 70% industrial methylated spirit (IMS).

2.2.1 Cell lines

2.2.1.1 Cell lines used in this study

The OvCa cell lines used in this study are outlined in table 2.1, detailing their histological features, source and site of isolation.

Name	Histology	Site of origin	Prior treatment	Source
SKOV-3	Serous G1/2	Ascites	Thiotepa ^a	ECACC 91091004
OVCAR-3	High grade serous G3	Ascites	Multi-chemo ^{a,b,c}	ATCC HTB-161
OVCAR-8	High grade serous G3	Unknown	Multi-chemo ^a	
A2780	adenocarcinoma	Primary tumour	none	ECACC 93112519
MCF-7	adenocarcinoma	Pleural effusion	none	ECACC 86012803

Table 2.1: Properties of OvCa cell lines used in this study. Prior treatment: *a* alkylating agent, *b* platinum therapy, *c* other.

All cell lines were cultured in RPMI-1640 media containing L-glutamine and phenol red (Gibco, Thermo Fisher Scientific, UK) supplemented with heat-inactivated foetal bovine serum (FBS, Sigma, UK) (10 % for SKOV-3, OVCAR-8 & A2780 and 20 % for OVCAR-3). Media were supplemented with 1,000 units/ml penicillin and 1,000 µg/ml streptomycin (P/S) (Sigma, UK). This recipe is hence referred to as complete growth medium (CGM). Cell lines were routinely maintained in T25 or T75 tissue culture treated flasks (Thermo Fisher Scientific, UK) in a humidified incubator (5 % CO₂ / 95% air).

Experiments in all cell lines were carried out in a window of maximally 6 passages. Cells were tested every three months for mycoplasma contamination and confirmed to be negative.

2.2.1.2 Rationale for choice of cell lines, ascites and primary tumours

No one cell line defines the characteristics of OvCa. It was therefore decided to use the SKOV-3 and OVCAR-3 cell line as they are of ascites origin and are well characterised OvCa cell lines (Hallas-Potts, Dawson and Herrington, 2019). The A2780 adenocarcinoma cell line was chosen since it originates from the primary OvCa tumour. The OVCAR-8 serous adenocarcinoma cell line was used in migration studies as a comparison since it is known to exhibit markedly different migration and invasive capacities than SKOV-3 and OVCAR-3 cells (Hallas-Potts, Dawson and Herrington, 2019). MCF-7 cells were used as a comparison in electrophysiology experiments since they have previously been shown to exhibit persistent permeability to Na^+ and numerous studies have characterised V_m values (Wonderlin, Woodfork and Strobl, 1995; Fraser et al., 2005; Marino et al., 1994). Due to the limitations with using cell lines that may no longer resemble nor recapitulate the original phenotype, cells isolated from malignant ascites from women with OvCa were used as a more likely representative population of OvCa. SKOV-3 cells were used in all studies except chapter 6.

2.2.1.3 Sub-culture

Upon reaching 60 - 80% confluence, cell lines were sub-cultured under aseptic conditions in a Class II laminar flow hood (Panasonic, UK). All reagents were pre-warmed (37°C) before use. Spent media was aspirated and cells were washed twice in Ca^{2+} & Mg^{2+} -free Hank's Balanced Salt Solution (HBSS) (Gibco, Thermo Fisher Scientific, UK) (3 ml and 7 ml for T25 and T75 respectively). Following washing, cells were immersed in 2 (T25) or 4 (T75) ml of 0.05% trypsin-EDTA and incubated at 37°C for 2-4 minutes until cells detached as assessed under a light microscope. Detachment of OVCAR-3, OVCAR-8 and A2780 cells was aided by gentle tapping. Immediately upon

cell detachment trypsin was inactivated by addition of FBS (1 and 3 ml for T25 & T75 respectively), followed by mixing and further dilution with HBSS (7 ml) and transfer to 15 ml Falcon tubes. Tubes were then centrifuged (120 x g) for 5 minutes, supernatant aspirated, the pellet resuspended in HBSS; this process was repeated twice. Upon completion of washing, the cell pellet was resuspended in 10 ml of the respective CGM, and 20 % (SKOV-3, OVCAR-8 and A2780) or 25 % (OVCAR-3) of the cell suspension was transferred to a new flask containing 5 (T25) or 12 (T75) ml of pre-warmed CGM. Cells were returned to the incubator and allowed to adhere for 24 hours, after which media was aspirated and replaced with fresh CGM. Media was aspirated and replenished every 2-3 days, depending on the extent of monolayer confluency.

Where necessary, cell counts were determined using a Countess II cell counter (Invitrogen, Thermo Fisher Scientific, UK). After washing (see above), cells were resuspended in 5 ml (T25) or 10 ml (T75) of their respective CGM and mixed gently using a Pasteur pipette. Then, 10 μ l of the cell suspension was mixed (1:1) with 0.4 % trypan blue solution (Bio-Rad, UK), and 10 μ l of mixture then loaded into a Countess slide for cell counting.

2.2.1.4 Cryopreservation and resuscitation of cells

Mycoplasma-free cell lines were periodically cryopreserved in LN₂ (\approx -196°C). Cells were detached, washed and centrifuged as described in the previous section 2.2.1.3. Upon the formation of a pellet, cells were resuspended in freezing medium consisting of 90 % CGM and 10 % DMSO (Sigma, UK). The cell suspension was then dispensed into 1 ml aliquots in cryovials (Corning, UK) containing 2×10^6 cells. Cryovials were then placed on ice for 20 minutes to cool gradually, then transferred into a foam freezing container (Sigma, UK), stored at -80°C for 24 hours and transferred into LN₂ for long

term storage.

At the point of cell resuscitation, a cryovial was removed from LN₂ storage, transferred to the cell culture hood and cap loosened by holding a kimwipe around the lid in order to release residual LN₂. The cap was then tightened and part-submerged in a water bath (37) using a pair of disinfected (70% IMS) forceps. When the solution was 90% defrosted, the vial was removed from the water bath, wiped down thoroughly with a kimwipe soaked with 70% IMS and transferred into the cell culture cabinet.¹ Defrosted cryovials were then transferred to the cell culture hood and transferred to a Falcon tube containing warmed CGM in order to reduce the concentration of DMSO. Cells were then counted as detailed in section 2.2.1.3 and added to a T25 or T75 flask containing pre-warmed CGM at the volume detailed above (section 2.2.1.3). Cells were then placed in the incubator and left to adhere undisturbed overnight, following which media was aspirated and replenished with CGM.

2.2.1.5 Cell culture coating

Collagen type 1 solution from rats tail (Sigma, UK, C3867) was diluted to a working concentration of 40 µg/ml with ddH₂O in a sterile 50 ml Falcon tube. Contents were swirled gently to ensure complete mixing, and appropriate amount (500 µl/cm²) added to tissue culture dishes, coverslips or electrotaxis (ET) chambers. Lids/covers were replaced and plates incubated at RT for 2 hours, after which solution was carefully aspirated. Surfaces were then washed (x 3) with sterile PBS, remaining PBS carefully aspirated and allowed to dry in a cell culture hood with the lids/roof cracked slightly open for 2 hours. Upon drying, dishes were carefully placed in clean polyseal bags and stored at 4 for up to two weeks.

¹The user removed outer glove layer and discarded them at this point to ensure there was no carry-over contamination from the water bath introduced into the class II cabinet.

2.2.2 Primary cells from OvCa ascites

2.2.2.1 Collection and maintenance

Ascitic fluid (300 ml - 4 L) from participants undergoing paracentesis, diagnostic biopsy or cytoreductive surgery were collected from participants in the study: 'Biological Properties and Alterations of the Tumour Microenvironment Governing Ovarian Cancer Progression (OM)', (REC ref: 17/EM/0453) study at the Royal Derby Hospital under full ethical approval between September 2018 and December 2018. Participants were identified by members of the gynaecological oncology team upon clinical admission based on their clinical presentation, imaging studies and the results of serum CA-125 (cancer antigen-125) levels. Diagnosis of OvCa was confirmed after histological analysis by the Pathology department at the Royal Derby Hospital. In instances where participants were later diagnosed with cancer of non-ovarian origin the samples were removed from the study and destroyed. Characteristics of samples collected are detailed in table 2.2.

Following isolation, cells from OvCa ascites isolates (herein referred to as OvCa_{asc}) were cultured in Medium 199 (Gibco) and MCDB 105 medium (Sigma, UK) mixed at a 1:1 ratio supplemented with 20% heat-inactivated FBS and P/S (1,000 units/ml and 1,000 µg/ml respectively, herein termed OSE CGM). Cells were maintained in a humidified incubator (5 % CO₂ / 95% air). All experiments on cells from OvCa_{asc} samples were undertaken within the 1st passage and cells were not sub-cultured in an effort to reduce the effects of the culture environment on cell properties; the maximum incubation time was 72 hours. To this effect cells were seeded directly into wells, coverslips and ET chambers (detailed in relevant sections). Media was aspirated and

Table 2.2: Clinical characteristics of participants from which OvCa_{asc} were collected

Participant identifier	Age	Origin	Histopathology	Grade	Stage	Neoplastic cells present in ascites	Collection method
OM1	60	PPO	SA	G3	IIIC	Yes	UGP
OM2	64	OvCa	SA	G3	IVA	Yes	UGP
OM3	73	PPO	SA	G3	IIIC	Yes	UGP
OM4	63	OvCa	SA	G3	IIIC	Yes	UGP
OM5	66	OvCa	SA	G3	IIIC	Yes	UGP
OM7	60	OvCa	SA	G3	IVA	Yes	PCS
OM8	79	OvCa	SA	G3	IIIC	Yes	UGP
OM9	62	PPO	SA	G3	IVB	Yes	UGP
OM11	53	OvCa	SA	G3	IIIC	Yes	UGP
OM12	78	PPO	SA	G3	IIIC	Yes	UGP

PPO, primary peritoneal origin; SA, serous adenocarcinoma; UGP, Ultrasound-guided paracentesis; PCS, primary cytoreductive surgery.

replaced 24 hours post seeding and periodically after depending on cell density. All experiments with OvCa_{asc} unless otherwise stated were performed on collagen-1 coated surfaces (procedure detailed below) as cell adherence was observed to be markedly better than TC plastic or fibronectin.

2.2.2.2 Cell purification using percoll step density gradients

Ovarian cancer cells present within ascitic effusions were isolated / enriched using density gradient centrifugation. Working concentrations of Percoll™ gradients were prepared by diluting 100% Percoll™ (Sigma, UK) with the appropriate volumes of filter-sterilised 10x HBSS (Ca²⁺ and Mg²⁺-free) and ddH₂O as per table 2.3. Once prepared, gradients were stored at 4°C and used within a month.

For initial characterisation of the ascitic cell population, a complete density gradient was prepared by adding 5 ml of 50% stock into the bottom of a 30 ml corex glass centrifuge tube and then carefully layering 2 ml of the respective concentrations in de-

Final percoll conc. (%)	Percoll (ml)	ddH ₂ O (ml)	10x HBSS (ml)	Final volume (ml)
60	30	15	5	50
55	27.5	17.5	5	50
50	25	20	5	50
45	22.5	22.5	5	50
40	20	25	5	50
20	10	35	5	50

Table 2.3: Composition of percoll stock solutions for OvCa_{asc} cell purification

scending order. Ascitic fluid was transferred into 50 ml falcon tubes and centrifuged at 200 x g (RT) for 5 minutes, the supernatant removed and kept for purification and the pellet re-suspended in 1 ml of HBSS. The volume of ascites collected varied widely between participants (\approx 300 ml and 4 L) and as a result relative cell densities were also markedly different. Optimal loading of cells in PercollTM gradient was achieved by combining the cell suspensions from four 50ml falcon tubes and carefully layering on top of 20% layer. Corex tubes were then placed in a SL 16R swing bucket centrifuge (Thermo, UK) and spun at 1200 x g (4°C) for 30 minutes. Upon completion of the spin cycle, the centrifuge was allowed to decelerate slowly to prevent mixing of the upper layers. After this initial centrifugation, multiple samples demonstrated a similar profile of sedimentation, with single cells and small cell aggregates (spheroids) numbering \approx 5 - 15 cells located at the 45 - 50% interface and larger spheroids numbering \approx 10 - 100 cells located at the 35 - 40% interface. Subsequent density gradients were prepared as follows; 5 ml 50%, 5 ml 40%, 5 ml 20% to allow adequate resolution of the cell fractions. Cell fractions were then collected using a pasteur pipette, transferred into a 15 ml falcon tube, washed twice in 10 ml HBSS by centrifugation (100 x g, for 5 minutes) and assessed for viability using 0.4% trypan blue (Bio-Rad, UK). Upon washing, pellets were then resuspended in OSE CGM for downstream processing (detailed in the rele-

vant sections) or resuspended in FBS supplemented with 10% DMSO and frozen down for cryopreservation in the same manner and cell density as described above (section 2.2.1.4). All experiments on OvCa_{asc} cells (excluding patch clamp) were undertaken on culture plastic coated with collagen 1 (50 $\mu\text{g}/\text{ml}$) (Sigma, UK) .

2.2.3 Normal Ovary (NOv) and OvCa primary tumour processing

Tissue samples from normal ovarian tissue (NOv) and primary OvCa tumours (FIGO₃₋₄T) used in this thesis were previously collected as part of the study: ‘A prospective study to examine the expression of EAG1 and HERG1 potassium channels in ovarian cancer’ under full ethical approval (REC ref: 08/H0405/71). At the point of surgical resection, sections of NOv or primary OvCa tumours were resected and placed into 7 ml sterilin polystyrene bijoux containers (Thermo, UK) and immediately snap-frozen in LN₂, transported to the laboratory and stored at -80°C until processed further. Tumour grade was confirmed by histological analysis by the Pathology department. Clinical and histological characteristics are presented in table 2.4.

2.3 Membrane potential recordings using the current clamp I=0 patch clamp method

Cells were harvested as per the protocol described in section 2.2.1.3, re-suspended in their relevant CGM on 1.5 10mm diameter poly-D-lysine (Sigma, UK) coated (1mg/ml) coverslips and incubated in standard culture conditions. V_m measurements were undertaken after 1 day in culture. The cover slips with adherent cells were placed in a 5ml perspex plastic recording chamber and fixed to the bottom with a small amount of

Table 2.4: Clinical characteristics of participants from which NOv or FIGO₃₋₄T samples were collected

	Participant identifier	Age	Classification	Histopathology	Grade	Stage	Collection method
NOv	S4	46	NOv	-	-	-	TLH+BSO
	S6	44	NOv	-	-	-	TLH+BSO
	S7	37	NOv	-	-	-	TAH+BSO
	S21	68	NOv	-	-	-	TLH+BSO
	S38	67	NOv	-	-	-	TLH+BSO
	S39	50	NOv	-	-	-	TLH+BSO
	S51	52	NOv	-	-	-	TLH+BSO
	S73	69	NOv	-	-	-	TAH+BSO
	S113	56	NOv	-	-	-	TLH+BSO
	S115	44	NOv	-	-	-	TLH+BSO
FIGO₃₋₄T	S42	54	OvCa	SA	G3	IIIB	PCS
	S65	57	OvCa	EA	G3	IIIC	PCS
	S90	50	OvCa	SA	G3	IIIB	PCS
	S96	50	OvCa	SA	G3	IIIC	PCS
	S103	70	OvCa	SA	G3	IIIC	PCS
	S112	89	OvCa	SA	G3	IIIB	PCS

NOv, normal ovary; FIGO₃₋₄T, FIGO stage 3-4 primary tumour

TLH, total laparoscopic hysterectomy; TAH, total abdominal hysterectomy; BSO, bilateral salpingo oophorectomy

SA, serous adenocarcinoma; EA, Endometrioid adenocarcinoma

petroleum jelly (Sigma, Poole, UK).

The whole-cell I=0 current clamp method was chosen to measure V_m since dialysis of the cytosol is achieved. This allows for complete control of the Na^+ gradient, thereby allowing for the resting permeability to Na^+ to be assessed independently of any contribution from unknown $[Na^+]_i$. Other methods for V_m measurement are well described, namely the sharp microelectrode approach. While this approach is considered to be the classical method for measuring V_m , it has been shown result in a sustained V_m depolarisation in small cells (of the order of size of cancer/epithelial cells) (Ince et al., 1986). Hence this is the rationale for selection of the whole-cell I=0 patch clamp method. The

advantages/disadvantages of both methods are discussed at length in Appendix A.

Patch pipettes were pulled from thick-walled borosilicate glass of 1.5mm outer diameter and 0.86mm internal diameter (Linton Instrumentation, Norfolk, UK) using a Sutter P-1000 patch clamp puller (Sutter Instruments, California, USA). Pipettes were filled with an internal solution (ISS, detailed in table 2.5). Values for CaCl_2 and EGTA were computed to achieve 50nM free Ca^{2+} at 25°C using the algorithm determined by Schoenmakers et al (Schoenmakers et al., 1992). Tip diameters were approximately 2 μM wide and fire-polished using a Narishige MF-830 microforge (Narishige International Ltd, London, UK) and were between 3 – 5 $\text{M}\Omega$ when filled with ISS solution. Membrane potential recordings were undertaken using an Axopatch 200B amplifier (Molecular Devices, Wokingham, UK) and pCLAMP 10 data acquisition software (Molecular Devices, Wokingham, UK). A Burleigh PCS-5200 micromanipulator (Burleigh Instruments, New York, USA) was used in the formation of seals between the pipette and cell surface.

Solution	NaCl	KCl	MgCl ₂	CaCl ₂	NMDG-Cl	ChCl	HEPES	EGTA	Ca ²⁺	pH
PSS	135	5	1	1	-	-	10 (Na ⁺)	-	-	7.2
Na ⁺ -free NMDG-Cl	5	5	1	1	130	-	10	-	-	7.2
ISS	5	140	1	1	-	-	10 (K ⁺)	1	50 nM	7.2

Table 2.5: Patch clamp solutions. All values were in mM unless otherwise stated. Acidic solutions were titrated to the required pH using the OH-ion shown in brackets, alkali solutions were titrated down using HCl. PSS: extracellular physiological salt solution, ISS: intracellular patch pipette solution.

All recordings were made at room temperature (RT) (22-25°C) with either PSS or Na⁺-free NMDG. Upon the establishment of a seal in the cell-attached configuration, cells were held at -10mV in voltage-clamp mode, the seal was assessed for tightness using a 10mV, 100ms unipolar square-wave test pulse; cells under 2G Ω were rejected. The seal

was then allowed to stabilise for up to 2 minutes and then the whole-cell configuration was achieved using the mouth-suction technique. Cells then compensated for whole-cell capacitance ($C_{whole-cell}$) and access resistance (R_{access}) and only those with $R_{access} < 30M\Omega$ were used. Within 30 seconds of achieving whole-cell configuration the amplifier was then switched over to $I=0$ current-clamp mode; V_m was continuously recorded at a sampling rate of 10KHz and filtered at 1KHz using a Bessel filter. The criterion for selecting cells to begin experiments on was to assess whether V_m was stable for at least 60 seconds when recorded in PSS. Cells were superfused with test solution for up to 10 minutes or until the V_m response had plateaued. V_m values were then recorded in control conditions by computing the mean value over 60 seconds immediately prior to changeover to test solution (drug or Na^+ -free PSS). V_m values in test conditions following wash-in were computed as the mean over a 60 second period immediately after reaching steady-state response or after 200 seconds, whichever happened first, using Clampfit software (Molecular Devices, Wokingham, UK). Cells were then reperfused with PSS to ensure that any change observed in V_m was not due to flow-induced perfusion effects or cell damage.

The junction potential between ISS - Na^+ -free-PSS solutions was measured as described by Neher and corrected for post hoc (Neher, 1992*a*). In order to derive a direct relationship between Na^+ and K^+ the chloride concentration $[Cl^-]$ was set equal ($[Cl^+]_i = [Cl^+]_e = 140mM$) (E_{Cl} was set to 0mV and had no contribution to V_m) in all electrophysiological solutions throughout experiments. As a result, irrespective of whether there exists a persistent permeability to Cl^- in the cell lines assessed it will have no contribution to V_m in this experimental setup.

A minimum of 4 cells were recorded from in all experiments and pooled as the

combined n of at least 2 independent repeats. Data were imported into Graphpad Prism and statistical analysis performed as detailed in section 2.15.

2.4 Scratch wound assays

Cell migration in OvCa cell lines was assessed using scratch wound healing assays. Cells were cultured as described in section 2.2.1.1 and upon reaching $\approx 60-80\%$ confluence were detached as described in section 2.2.1.3. Upon washing, the cell pellet was resuspended in the respective CGM and cells were seeded at a density of 4×10^5 cells / well into 6-well Costar culture coated plates. Plates were then incubated for ≈ 48 hours until they had reached $\approx 85 - 90 \%$ confluence, at which point media was aspirated and replaced with serum starve medium (SSM; 98 % RPMI, 1 % P/S, 1 % FBS) and incubated for a further 24 hours in order to inhibit cell proliferation (Liang, Park and Guan, 2007)². Upon serum starvation, plates were removed from the incubator and a centrally placed scratch was made along the diameter of the well with a sterile 200 μ l pipette tip thus creating a cell-free line. A custom template was then affixed to the bottom of the plate delineating ‘windows’ or reference regions lined along the wound, allowing imaging of the same region over the experiential timecourse. Cells were then washed (x3) in HBSS to remove detached cells and debris, resuspended in SSM and returned to the incubator for 1 hour to allow cells at the wound edge to re-adhere following mechanical disturbance. Wells were then replenished with vehicle (0.1 % DMSO) or amiloride (0.1, 1, 10, 50 & 100 mM) dissolved in SSM. The vehicle and entire dose range were assessed on a single 6-well plate. Immediately upon treatment 5-6 regions per wound were photographed (defined as t=0) with a Zeiss Axiovert 25

²The effects of reduced serum (1 %) over a duration of 72 hours (24 h serum starve + experimental time) were assessed by addition of trypan blue and shown to have a limited effect of cell viability.

inverted microscope (20x). The plate was replaced in the incubator and the process repeated at 24 & 48 hours post-wound. Images were loaded into Image-J and migration was quantified by drawing an ROI (region of interest) around the cell-free area. Cell migration was expressed as the fraction of the area filled with cells at 24 and 48 hours relative to the wound area at $t=0$; $t=24$ or $48_{area} / t=0_{area}$. further statistical testing was performed with Graphpad Prism detailed in section 2.15. Experiments using all cell lines (SKOV-3, OvCAR-3 and A2780) were repeated 3 times independently.

2.5 Wound stimulation experiment

Cells were seeded in 90 mm cell culture plates in CGM at 2×10^6 cells/plate and allowed to grow to approximately 80% confluence at which point media was replaced with low-serum media for 24 hours. Upon completion of serum starvation, a single plate was harvested as follows: The wound stimulated population was created by introducing multiple parallel wounds along the length of the plate, spaced 6 mm apart with a 200 μ l pipette tip using a custom-made template. Cells were then washed 3 times with HBSS to remove dislodged cells at the wound border and SSM added (1% FBS) for a further 24 hours. Cells were lysed, and the lysate stored for ENaC- α expression by western blotting in the same manner as described in section 2.6. Wound stimulated expression of ENaC- α was assessed by normalising to a population undergoing the same conditions without scratch wounding. Wound reduction was confirmed by the assessment of wound area in defined regions under a light microscope at the time of wound stimulation and at the end of the experiment using the same method as in section 2.4. The entire experimental procedure was repeated in 3 independent experiments for each cell line tested.

2.6 Western blotting

2.6.1 Cell lysis and protein extraction

For protein extraction from both cell lines and primary tissue the same homogenisation buffer (HB) was used, which had the following composition in mM: 320 sucrose, 10 tris-base, 50 KCl, 1 EDTA & 0.5% (v/v) igepal. All constituents excluding igepal were added and the solution was then adjusted to pH 7.4 using dropwise addition of 5 M HCl. Following this, igepal was added and the solution was titrated to the required volume with dH₂O. Solution was stored at 4°C and used within one month. Shortly before cell lysis, 10 ml of HB was aliquoted to which 1 Pierce protease and phosphatase inhibitor cocktail tablet (A32959, Thermo) was dissolved.

Igepal was selected as the detergent of choice since the non-ionic properties have been shown to achieve sufficient lysis of the plasma membrane while resulting in minimal lysis of nuclear membranes (Shehadul Islam, Aryasomayajula and Selvaganapathy, 2017).

The following sections detail the procedures for protein harvest from OvCa cell lines and primary tissue.

2.6.1.1 Cell lines

Cell lines were cultured in 100 mm petri dishes as per section 2.5, removed from the incubator and washed (x3) with HBSS. After washing, dishes were placed on ice and cells were immediately lysed by addition of 600 μ l HB and dislodged with a rubber policeman. Homogenates were then transferred to 1.5 ml eppendorf tubes and sheared on ice twenty times with a 19 g needle and syringe and sonicated on wet ice for 15 minutes. Eppendorfs were then removed, cells sheared as before and centrifuged at 2,000 x g at 4°C in a EBA 12R fixed rotor centrifuge (Hettich, UK) for 5 minutes.

The supernatant was then transferred to a fresh eppendorf and centrifuged at 23,000 x g (4°C) for a further 60 minutes. Membrane enriched supernatant was then carefully removed, transferred to a fresh tube and stored at - 80 °C until further analysis.

2.6.1.2 Primary NOv and OvCa tissue

For extraction of protein from NOv and solid OvCa samples, previously snap-frozen samples (refer to section 2.2.3) were partially defrosted on ice and 100 mg of tissue was weighed out, then transferred to a homogenisation tube containing 1 ml of ice-cold HB. Samples were then homogenised with an Ultra-Turrax T25 (IKA, Oxford, UK) using short bursts, and placed on ice between cycles to reduce sample heating. Samples were then transferred to 1.5 ml eppendorf tubes and centrifuged in the same manner as described in the section 2.6.1.1.

2.6.2 Protein determination

Protein concentration determination was accomplished using the bichinchoninic (BCA) method (Walker, 1994). In 1.5 ml eppendorf tubes, 10 μ l of sample lysates were diluted in 40 μ l homogenisation buffer of the composition stated in section 2.6.1 (1:5 dilution). A protein standard curve was created by dissolving bovine serum albumin (Sigma, UK) in homogenisation buffer to obtain a top standard of 3 mg/ml followed by serial dilution with homogenisation buffer to achieve the following standards (mg/ml): .15, .3, .6, 0.9, 1.2, 1.5, 1.8, 2.1, 2.4 & 3. Samples and standards were maintained on ice until use. Upon preparation of sample dilutions and protein standards, 10 μ l duplicates of each tube were loaded into clear, non-sterile 96-well polystyrene plates (Greiner, UK) placed on a cool block throughout. A duplicate sample of homogenisation buffer was also added to determine the background contribution of buffer. Immediately after, 90 μ l of BCA/4% copper II sulphate pentahydrate (50:1 ratio) was added to the respective

wells and incubated at 37°C for 30 minutes. Following incubation, absorbance was read at 562 nm in an (Thermo, UK) plate reader. Unknown concentrations were determined by interpolation after construction of a standard curve.

2.6.3 SDS-PAGE and Immunoblotting

After protein concentration determination, samples were diluted with the appropriate volume of HB and then mixed at a 1:1 ratio with 2x Laemmli sample buffer (Bio-Rad, UK) and vortexed. Samples were then heated to 70°C for 15 minutes and immediately placed on ice. Upon cooling and vortexing, 40 μ g of sample were loaded in duplicate onto 10-well 10% hand-cast tris-glycine polyacrylamide denaturing gels (SDS-PAGE). Gels were run in duplicate at 40 mA constant current for 50 minutes. Upon completion, gel casts were disassembled and gels were placed on nitrocellulose membranes sandwiched between 2 pieces of blotting paper and sponge. Sandwiches were then placed in a transfer tank containing chilled running buffer (4°C) and transferred a 100 V for 90 minutes. After this, membranes were placed in trays containing 0.1 % (w/v) Ponceau-S solution in 5% acetic acid (Sigma, UK) for 10 minutes with gentle rocking. Membranes were then washed (x 3) in dH₂O and imaged with Quantity One software (BioRad, UK). Following acquisition of images, membranes were washed (x 3) in TBS-T for 5 minutes to remove Ponceau-S. Membranes were then blocked in 5 % non-fat dried milk dissolved in TBS-T for 2 hours at RT and rinsed twice in TBS-T. Membranes were then transferred to trays containing ENaC- α antibody (PA1-920A, Thermo, UK) (1:500 in 3% non-fat dried milk in TBS-T) and incubated with gentle rocking overnight (4°C). Membranes were removed and washed (x 6) at RT for 5 minutes in TBS-T and incubated in goat-anti-rabbit alkaline phosphatase antibody (1:3000 diluted in 3% marvel in TBS-T) (A3687, Sigma) for 90 minutes at RT with

gentle rocking. Blots were washed as above, drip-dried using a kimwipe and 2.5 ml of substrate with enhancer (50 μ l) (BioRad, UK) added with a pasteur pipette; then blots were incubated in the dark for 10 minutes. Chemiluminescence was performed using Quantity One software (BioRad, UK). Lanes were normalised to the respective Ponceau-S total protein stain (Sander et al., 2019).

Blotting buffer was of the composition in mM: 192 glycine, 25 Tris, pH 8.4. Running buffer was of the composition in mM: 192 glycine, 25 Tris, pH 8.4. TBS-T was of the composition in mM: 20 Tris, 500 NaCl, 0.01 % Tween 20, pH7.4.

2.7 Cell proliferation assays

Cell viability (used as a marker of the number of living cells) in SKOV-3 and OVCAR-3 cell lines was assessed by the resazurin reduction method. Upon reaching \approx 80 % confluence, cells were detached and washed as described above. Cell were then counted and seeded into tissue-culture treated 96-well clear flasks (CostarTM, Corning, UK) at 5×10^3 cells / well³ at a working volume of 100 μ l. Plates were then incubated under standard conditions for 3 hours to allow cells time to adhere sufficiently. A stock solution of resazurin was prepared by dissolving 27.6 mg of resazurin sodium salt (199303, Sigma) in 100 ml of RPMI-1640 to create a 1.1 mM solution. All subsequent steps were undertaken in low-light conditions to reduce photobleaching. The solution was then sterilised with a 0.22 μ m cellulose acetate syringe filter (Star Labs, Uk), aliquoted into 7 ml foil-wrapped bijou SterilinTM containers (3 ml), stored at -20°C and used within 2 months. A working concentration of resazurin was prepared by diluting resazurin stock in the respective complete growth medium to obtain a final

³Seeding density for cell lines in this study was determined by the construction of a seeding density dependent curve. Refer to appendix B.1

concentration of 100 μM . Upon adherence (t_0) or following the required incubation time (t_{24} , t_{48} , t_{72}), media was gently aspirated and designated wells were resuspended in 10 μl resazurin solution. Plates were loosely wrapped in foil and placed in the incubator for 2 hours. Upon incubation, cell viability was assessed with a Fluroskan Ascent *FL* (Thermo, UK) filter-based fluorescence plate reader (560 nm excitation, 590 nm emission) by taking a single reading in the centre of each well. Three sequential readings per well were taken over a period of 45 seconds and data were then averaged. Values expressed in relative fluorescent units (RFU) were then imported into Microsoft Excel (2013) and the average RFU values from wells containing resazurin+CGM were subtracted from the remaining wells to yield background-corrected values. IC_{50} and IC_{25} values for amiloride and phenytoin were derived by fitting data normalised to vehicle controls at t_{24} , t_{48} , t_{72} time points with a hill-slope curve.

Upon measurement of the t_0 reading, plates were transferred to the class II cabinet, the remaining wells aspirated and resuspended in CGM + drug in replicates of 4 for each time point. Amiloride concentrations were prepared from a 100 mM stock solution dissolved in DMSO and diluted to 0.1, 1, 10, 50 & 100 μM . The vehicle control was CGM + 0.1 % DMSO. Phenytoin treatments were prepared from a 180 mM stock solution of 75 mM NaOH diluted in CGM to 5, 50, 100, 200 μM . Vehicle control was CGM + 208 μM NaOH. Cells were then returned to the incubator and fluorescence was measured at the required timepoints as described above. Upon completion of t_{24} and t_{48} readings, media was aspirated and remaining wells were resuspended in fresh treatments.

In order to ensure that cells were growing as expected over the experimental duration, a 'no drug' control was included on each experimental plate. Upon adherence,

media was aspirated from 3 wells, resazurin solution was added in triplicate and cells were incubated in the same manner as described above (designated the t_0 time point). This process was repeated at all subsequent time points (t_{24} , t_{48} , t_{72}). Data were then imported to Graphpad Prism, normalised to t_0 and fitted with the exponential growth equation to determine cell doubling time. The details of the fitting and mathematical determination of doubling time are detailed in Appendix B.1.

Experiments using amiloride and phenytoin were repeated a minimum of 5 times independently for each cell line. Cell proliferation assays were conducted with assistance from BSc student Lyndsay Wilkinson.

2.8 Effect of Na^+ gradient on cell proliferation

In order to assess further whether Na^+ influx is important in driving the proliferation capacity of the cell, either directly or by modulation of V_m , an experiment altering the inward Na^+ gradient was designed. The experimental approach was based on addition of monovalent salts to the standard RPMI 1640 medium (the medium in which cells were cultured under normal conditions). This approach means that addition of monovalents to the medium will result in the increase of solution osmolality, which limits the concentration range over which the monovalent ions can be varied.⁴ The osmolality of RPMI-1640 after addition of sodium bicarbonate is 279 mOsm/kg $\text{H}_2\text{O} \pm 5\%$ (Sigma-Aldrich, 1998). Plasma has an osmolality of ≈ 290 mOsm/kg and subsequently, cell culture media compositions varying between 260 - 320 mOsm/kg are considered acceptable. The osmolality was varied to a maximum of 339 mOsm/kg, equating to a maximum addition of 30 mM NaCl (equating to a 60 mM increase in

⁴A more robust experimental approach aimed at maintaining solution osmolality by substituting Na^+ with impermeant ions was attempted. However, there were significant issues with media preparation and salt solubility. Therefore, this approach was abandoned.

osmolarity) or 30 mM choline chloride (ChCl) accordingly.

Upon reaching 70 - 80 % confluence, SKOV-3 or OVCAR-3 cells were trypsinised and seeded in 96-well plates for resasurin-resofufin reduction assays in the same manner as in section 2.7. Since osmolarity is altered by the addition of NaCl (as described above) an equimolar concentration of choline chloride was added to corresponding control wells. In order to account for osmotic pressure changes induced by addition of NaCl or ChCl, the osmotic diuretic mannitol was added to corresponding control wells at twice the concentration in mM as NaCl or ChCl (a 1 M NaCl/ChCl solution has an osmolarity of 2 Osmol/L, twice that of mannitol which does not dissociate in solution). All conditions were repeated in triplicate. A minimum of 5 independent experiments were carried out for each cell line. Treatments were normalised to control (CGM) at their respective time points.

2.9 Cell cytotoxicity assays

Cytotoxicity in SKOV-3 and OVCAR-3 cells was assessed after 72 hours using SYTOX green nucleic acid stain (ThermoFisher Scientific, Paisley, UK). Cells were detached, washed and seeded in Costar 96-well plates then treated with amiloride or phenytoin at the same concentrations and manner as described in section 2.7. Following incubation, 5 μ l of 110 μ M SYTOX green stock prepared in HBSS was added to each well to a final concentration of 5.2 μ M. Plates were wrapped in foil and then transferred to the incubator for 10 minutes. Fluorescence was then measured at 485 nm excitation, 520 nm emission. Plates were then removed, and a 10 μ l of 2.2% (vol/vol) Triton X-100 stock prepared in PBS was added to each well to achieve a final concentration of .21%. This step was performed to achieve maximum cell lysis. Cells were then incubated

(37°C) for a further 5 minutes and measured as above. The percentage cytotoxicity was then computed by dividing the first fluorescent RFU values by those measured after lysis in Microsoft Excel (2013). Data were then imported into GraphPad Prism and further statistical analysis performed as described in section 2.15. Experiments were repeated 5 times independently.

2.10 RT-qPCR experiments

2.10.1 RNA extraction

RNA extraction was accomplished using the Qiagen RNeasy mini kit (Qiagen, Manchester, UK), a procedure utilising the well-established solid-phase extraction method comprising a silica-based membrane (Tan and Yiap, 2009). In all cases the cells were initially lysed / disrupted using RLT buffer that contains a high concentration of the strong chaotropic salt guanidine thiocyanate supplemented with β -mercaptethanol (143 mM) to further inhibit endogenous RNase activity and prevent degradation. All further references to RLT contain β -ME at this concentration. All buffers (RLT, RW1 & RPE) used in this section are proprietary components of the RNeasy mini kit and as such their composition is confidential. All subsequent steps were undertaken using sterile filter pipette tips.

2.10.1.1 Cell line monolayers

For cell line monolayers, cells were seeded in single wells of a 6-well plate and grown until 70 - 80 % confluency. Cells were then washed once with PBS and re-suspended in 350 μ l RLT buffer and moved into suspension using a rubber policeman. The suspension was transferred into a 1.5 ml eppendorf tube and mixed by sequential pipetting to ensure that no cell clumps persisted. The mixture was often frozen at this point and stored (-

80 °C) for later extraction.

Upon homogenisation, an equal volume of 70 % ethanol was added to the lysate and mixed by pipetting. Sample lysate up to a volume of 700 μ l was then transferred onto an RNeasy spin column placed within a 2 ml collection tube and centrifuged for 15 seconds at $8 \times 10^3 \times g$ and the flow-through was then discarded. Any additional sample lysate was then transferred to the same spin column and successive repeats were undertaken as above until the entire sample was processed. A volume of 350 μ l RW1 buffer was then added to the spin column and centrifuged for 15 seconds ($8 \times 10^3 \times g$) to wash the membrane. Upon discarding flow-through in the collection tube, 500 μ l of RPE buffer was added to the spin column, centrifuged and discarded as per the previous step. The column was then subjected to a final wash by adding a further 500 μ l as above and centrifuging at $8 \times 10^3 \times g$ for 2 minutes in a new collection tube to allow the column to dry fully, thereby ensuring that no residual ethanol was carried over into the RNA elution. The spin column was then transferred into a 1.5 ml eppendorf. 50 μ l of RNase-free water was then added into the spin column and centrifuged at $8 \times 10^3 \times g$ for 1 minute to elute RNA.

Upon elution, samples were immediately placed on ice and subsequently stored at -80 °C until further quantification of RNA integrity and downstream synthesis of cDNA.

2.10.1.2 Primary ovarian tissue and OvCa tissue

RNA was extracted from primary normal ovarian and OvCa tissue using FastPrepTM Lysing Matrix D ceramic beads (1.2 - 1.4 mm) in 2ml polypropylene screw-cap tubes (MP Biomedicals, UK). Tissue samples stored at -80 °C (refer to section 2.2.3 for sample collection and storage method) were allowed to partially defrost on ice and 60 - 80 mg of tissue was transferred into a lysing matrix D tube containing 600 μ l RLT

buffer. Tissue was then homogenised using an MP Fast Prep 24 (MP Biomedicals, UK) for 3 x 40 seconds at rate of 6 m/s. Homogenisation tubes were placed on ice for 5 minutes between each cycle to reduce friction mediated sample heating. Homogenisation tubes were then centrifuged at $12 \times 10^3 \times g$ for 3 minutes to pellet any cellular debris. Supernatant was then added to a sterile 1.5 ml eppendorf, and RNA extraction was performed using the same procedure described in section 2.10.1.1 starting paragraph 2.

2.10.1.3 Primary OvCa_{asc} cells

Cells from the ascitic fluid of participants with ovarian cancer were isolated and cryopreserved in aliquots of 2×10^6 cells/vial, as described in section 2.2.2.2. For RNA extraction, the cell vials were defrosted via gentle warming in a water bath as described in section 2.2.1.4. Immediately upon complete thawing, the suspensions were transferred to 13 ml of pre-warmed (37 °C) PBS and centrifuged at 100 x g for 5 minutes. The supernatant was then aspirated and the pellet was resuspended in 350 μ l of RLT buffer and mixed by pipetting to ensure no cell clumps were present, transferred to a sterile 1.5 ml eppendorf and then processed for RNA as per the procedure described in 2.10.1.1. Since the cell number varied between samples and RNA concentration was typically lower than yields from cell lines, the elution volume of RNase-free water was chosen to be 30 μ l.

2.10.1.4 Spectrophotometry and RNA integrity

A nanodrop ND-1000 spectrophotometer was used to quantify sample RNA concentration and contamination. To ensure consistency, measurement sessions were always preceded by running a blanking cycle; a sample volume (1.6 μ l) of elution buffer (RNase-free water) was loaded and 'blanked' and subsequently verified in read mode to assess the uniformity of baseline response. Sample concentrations of RNA extractions

were then quantified. Absorption ratios of 260/280 and 260/230 nm were quantified to assess the extent of protein and organic contaminants (chaotropic salts) respectively. Absorbance ratios between 1.8 - 2.2 and 2.0 - 2.2 for 260/280 and 260/230 nm ratios respectively were considered acceptable for subsequent cDNA synthesis. Samples were maintained on ice throughout this process.

Qualitative assessment of RNA integrity, extent of degradation and genomic DNA contamination were routinely assessed by agarose gel electrophoresis.

2.10.1.5 Synthesis of cDNA

cDNA was synthesised from RNA in volumes of 20 μ l reactions according to the manufacturers instructions using a High-Capacity cDNA reverse transcription kit and a DNA Engine Dyad Thermocycler (MJ research, Waltham, USA). Reverse transcription mixtures contained 2 μ l 10xRT buffer, 0.8 μ l dNTP mix, 2 μ l random primers, 1 μ l RNAase inhibitor, 3.2 μ l nuclease free water, 1 μ l reverse transcriptase and 10 μ l RNA solution. All samples were transcribed at 120 ng RNA. The temperature cycle was 25°C for 10 min, 37°C for 2 hours and 85°C for 5 mins. All cDNA samples were stored at -80°C until qPCR analysis.

2.10.2 qPCR

Gene amplifications were performed with a CFX Connect Real-Time PCR system (Watford, Hertfordshire, UK). All qPCR experiments were conducted using Taqman hydrolysis probes (Thermo Fisher Scientific, UK). qPCR of each sample was performed in triplicate, containing 2 μ L cDNA solution, 10 μ L 2x Taqman Universal Master Mix, 0.7 μ L Taqman Gene Expression Assay and 7.3 μ L H₂O. Reactions were performed by initial denaturation at 95 °C for 10min followed by 50 cycles of denaturation at 95 °C for 15 s and annealing/extension at 60 °C for 1 min. All experimental plates contained

no template (NT) and -reverse transcriptase (-RT) controls to assess the presence of extraneous nucleic acid and genomic DNA contamination. The details of all primers used in this study, including assay ID, amplicon length and reaction efficiencies are presented in table 2.6. Reference genes were determined using Genex (Multid software, Sweden) using the Genorm and Normfinder algorithms according to the manual and are also indicated in table 2.6. All Taqman probes selected for use in this study were selected to anneal to exons on both sides of an intron (exon-spanning), in order to discriminate between amplification of cDNA and potentially contaminating genomic DNA.

Taqman hydrolysis probes are oligonucleotides that contain a donor fluorescent moiety located at the 5'-end and an acceptor (quencher) on the 3'-end and as such do not emit fluorescence when intact (Mackay, 2004). The probe is designed to bind to a specific region of the target DNA that is located between the two primers. During the extension phase, the bound hydrolysis probe is degraded by the 5'→3'-exonuclease activity of DNA polymerase, resulting in the dissociation of the fluorescent moiety from the quencher and a subsequent increase in fluorescent intensity (Livak et al., 1995). Thus, Taqman hydrolysis probes add an increasing degree of specificity over intercalating dyes such as SYBR green, since increases in fluorescence are only observed by probe cleavage within the amplicon product. This mechanism however is not compatible with melting dissociation curves at the end of the amplification run due to free fluorophores in the assay solution (Shen, 2019). qPCR reaction efficiencies were determined by performing a 5-step dilution series from initial cDNA solutions (120 ng/μl). For cell lines, a series of 1:10 dilutions was performed. For experiments undertaken in primary tissue (NOv, FIGO₃₋₄T and OvCa_{asc} samples), dilutions were 1:5 for HPRT, GUSB,

Gene name	Assay ID	Amplicon length (bp)	SKOV-3		OVCAR-3		Primary tissue	
			E (%)	R ²	E (%)	R ²	E (%)	R ²
HPRT1 *†	Hs02800695_m1	82	106	0.98	98	0.99	92	0.92
YWHAS *	Hs03044281_g1	106	90	0.99	94	0.99	-	-
GUSB †	Hs00939627_m1	96	-	-	-	-	97	0.93
RPLP0 †	Hs00420895_gH	76	-	-	-	-	98	0.96
SCNN1a	Hs00168906_m1	63	85	0.99	99	0.99	93	0.98
SCNN1d	Hs00936289_m1	68	-	-	-	-	84	0.97
SCN5A	Hs00165693_m1	85	-	-	-	-	82	0.99

Primary tissue refers to NOv, FIGO₃₋₄T and OvCa_{asc} samples.

Table 2.6: Primer information of reference and target genes used in this study. * and † denote reference genes used in cell lines and primary tissue respectively. All assays were completed using Taqman hydrolysis probes (Thermo Fisher Scientific, UK), assay ID is the unique assay identifier.

RPLP0 and SCN5A (Na_v1.5) and 1:2 for SCNN1a (ENaC- α) and SCNN1d (ENaC- δ).
The PCR efficiency (E (%)) was calculated from the equation: $E = (10^{\frac{1}{m}} - 1) \times 100$,
where m is the slope of the linear regression line fitted as the log-transform of the cDNA
concentration vs the C_T values (Kubista et al., 2006) (reaction efficiencies detailed in
Table 2.6).

PCR work was conducted with assistance from BSc student Kasheir Rowe.

The size of the nucleic acid transcripts was determined by resolving the qPCR
product of two selected samples from NOv and FIGO₃₋₄T and cell lines on a 1%
agarose gel containing ethidium bromide, 5 μ L RNA solution, 2 μ L of 10x blue juice gel
loading buffer were mixed and gently pipetted into wells. Gels were run at 90 V for 30
minutes and quantified under UV exposure on a Chemidoc (BioRad, UK). qPCR data
was then imported into Genex (BioRad, UK) and analysed using the double-delta CT
method (Livak and Schmittgen, 2001).

2.11 Immunofluorescence

2.11.1 Microscopy

Prior to immunofluorescence (IF) experiments, cell lines were subcultured until reaching 70 - 80 % confluency, trypsinised and resuspended in CGM as per section 2.2.1.3. Cells were then seeded in 24-well plates at 50 and 100 x 10³ cells/well for cell lines and primary cell isolates respectively, and allowed to adhere for 12 - 18 hours. Cell lines were allowed to proliferate until reaching \approx 40 - 50 % confluence, thus enabling the assessment of single & isolated cells.

Upon achieving required cell densities, cells were removed from the incubator and allowed to equilibrate to RT for 10 minutes before proceeding; all subsequent steps unless otherwise specified were undertaken at RT. Media was then carefully aspirated with a 3 ml pasteur pipette and cells were washed twice for 5 minutes with 1 ml PBS while gently shaken using a gyro-rocker. After washing, PBS was aspirated and cells were re-immersed in 300 μ l 4 % chilled paraformaldehyde (PFA) for 5 minutes. Fixative was then carefully aspirated and cells underwent sequential washes with PBS (x 3) to remove residual PFA. Permeabilisation was achieved by incubation for 5 minutes in 0.5 % igepal (NP-40) in PBS⁵. Subsequently, cells were washed with PBS, solution aspirated as above and incubated in PBS/glycine/BSA solution for 20 minutes to inactivate any residual PFA. Thereafter, PBS/glycine/BSA solution was aspirated; cells were washed in PBS (x 3) as above. Immuno-blocking was achieved through addition of 250 μ l of 20 % goat serum in PBS for 30 minutes⁶. When the blocking step was complete,

⁵The non-ionic detergent igepal was chosen since optimal staining of membrane-bound proteins is achieved.

⁶In all cases the 2^o antibodies were raised in goat and thus serum from the same species was chosen as blocking agent to reduce off-target binding

solution was aspirated and cells were resuspended in 200 μ l of primary antibody at the appropriate dilution in 20 % goat serum/PBS, and placed at 4 °C with gentle shaking for 12 - 18 hours. Table 2.7 details the target, species, dilution factor and supplier of all 1° antibodies used for IF microscopy.

1° antibody	Host	Clone (#clone)	Isotype	Dilution	Company (#Cat)
ENaC- α	R	poly	IgG	1:50	Thermo (PA1-920A)
pan-Cytokeratin	M	poly	IgG	1:50	SIGMA (C2931)
EpCAM	R	poly	IgG	1:50	AB (AB71916)
MUC16	R	mono (EPSISR23)	IgG	1:25	AB (AB71916)
FGFR4	M	mono (5B5)	IgG1	1:50	AB (AB44971)
CD45	M	mono (2B11 + PD7/26)	IgG1	1:25	Dako (M0701)

R, rabbit; M, mouse; mono, monoclonal; poly, polyclonal
 Thermo, Thermofisher Scientific, UK; SIGMA, Sigma, UK
 AB, Abcam, Cambridge, UK; Dako, Agilent Dako, Agilent Technologies, CA, US

Table 2.7: Primary antibodies used in IF experiments.

Following incubation with the 1° antibody, plates were allowed to equilibrate on the bench for 10 minutes. The 1° antibody solution was then aspirated and washed (x 3) with PBS in the same manner as described above. After the last wash, PBS was aspirated and the solution replaced with 250 μ l of PBS / goat serum containing goat whole-molecule IgG FITC-conjugated 2° antibody (1:50) raised against rabbit or mouse (goat anti-rabbit IgG-FITC; F0382, Sigma, UK; goat anti-mouse IgG-FITC; F0257, Sigma, UK), depending on the host species of relevant 1° antibody. After addition, plates were wrapped in foil and incubated with gentle rocking at RT for 30 minutes. After incubation, cells were washed in PBS (x 3) in dimmed light, taking care to recover between cycles, and finally resuspended in PBS. Cells were often protected from light and stored at 4° for up to 24 hours before imaging. Controls consisted of omitting the 1° antibody and replacing with an equal volume of PBS.

Images were acquired using a Zeiss Axiovert 25 inverted microscope equipped with a halogen light source and a DP70 CCD camera (Olympus Ltd, UK). Fluorescent

excitation of the fluorophore fluorescein isothiocyanate (FITC) was achieved with a filter cube fitted with a BP-450-490 excitation and LP-520 emission filter and a FT510 dichroic mirror. Images were captured with Cell^F software, and an associated bright field and fluorescent image was captured for each field of view assessed. The auto-expose feature in Cell^F was used to obtain proper white / black balance. Cell line experiments were repeated 3 times independently.

2.11.2 IF characterisation of OvCa_{asc} primary isolates

Malignant effusions from OvCa are known to contain a heterogeneous cell population consisting collectively of cancer cells and stromal cells. The stromal cell population of malignant ascites is comprised of fibroblasts, mesothelial cells, adipocytes, bone marrow-derived stem cells and immune cells. In order to identify the tumour cell population, an IF approach using multiple cell markers was designed. EpCAM was selected to identify cancerous cells present within OvCa_{asc} isolates. EpCAM is a 40 kDa transmembrane-spanning glycoprotein that is shown to be highly expressed in numerous epithelial carcinomas, including those of gastrointestinal, pancreatic and ovarian origin; it is often highly expressed in metastatic lesions (Nguyen et al., 2017; Spizzo et al., 2011; Wintzell et al., 2012; Porcel et al., 2019). Another benefit of EpCAM in the detection of cancerous cells present in OvCa_{asc}, is its capacity to differentiate metastatic carcinoma cells from mesothelioma and reactive mesothelial cells, both of which are negative for EpCAM (Oda et al., 2016). In order to identify cancer cells of OvCa origin present within OvCa_{asc} samples, MUC16 (also known as CA125) was chosen since it is expressed on the surface of OvCa cells and is routinely used for diagnosis. CAF were identified by the intensity of staining for FGFR4; a marker expressed on normal fibroblasts and in CAF. Though no one marker has been shown to definitively identify fibroblasts, FGFR4

positive staining combined with morphological assessment of adherent fibroblasts, based on their spindle shape and low staining for epithelial markers such as EpCAM, provides a method to identify fibroblasts or CAFs. Immune cell contamination was assessed using the commonly used marker CD45.

To assess the heterogeneity of cell types present in OvCa_{asc} samples, four samples were analysed; OM5, OM8, OM11 and OM12. The same protocol was used as that described in section 2.11. The target, species, dilution factor and supplier of all 1° antibodies used for characterisation are provided in Table 2.7. The relative cell populations were assessed by qualitative assessment of positive staining counts for the respective markers divided by the total number of cells in the field of view. Positive staining of individual populations were then expressed as % positive of total cell number. Three fields of view were assessed for each OvCa_{asc} sample. It should be noted that this approach is not quantitative since the exposure time of the light source can not be controlled accurately. Furthermore, cell populations are only stained with a single antibody and an approach using a co-staining approach utilising confocal or wide-field microscopy would provide a more definitive method to differentiate cell subtypes.

Representative images of IF staining for EpCAM, MUC16, FGFR4 and CD45 consisting of brightfield and associated IF image of the same field of view in sample OM5 is shown in Figure C-1 in Appendix C. In 4 OvCa_{asc} samples assessed (OM5, OM8, OM11 and OM12), $\approx 85\%$ of cells were positive for EpCAM; EpCAM⁺, $84.9\% \pm 11.2$ (mean \pm SD, $n = 4$ of 4 independent experiments, Figure C-1A and B, Figure C-2). Similarly the MUC16⁺ population was $84.3\% \pm 7.8$ (Figure C-1C and D, Figure C-2). The fibroblast marker, FGFR4 demonstrated low staining across all samples ($3.8\% \pm 1.8$, Figure C-2). The FGFR4⁺ cell population was shown to consist of cells with

distinct processes or spindle like morphologies (Figure C-1E and F). CD45⁺ staining was very low across all 4 samples assessed ($1.6 \% \pm 1.2$, Figure C-1G and H, Figure C-2).

This work was conducted with assistance from BMedSci student Vanessa Huang.

2.12 Flow cytometry

2.12.1 OvCa_{asc} panel

A 6-colour flow cytometry panel was designed to assess the differential staining of ENaC- α in OvCa_{asc} sub-populations. OvCa_{asc} cells were defrosted as described in section 2.2.1.4, washed and resuspended in 1ml PBS. Cell populations were confirmed to contain very few erythrocytes following Percol isolation (detailed in section 2.2.2.2), and as such RBC lysis treatment was not necessary. Spheroids were removed from the cell preparations with a 40 μ m cell strainer. Then 1 μ l Zombie-NIR viability dye (423105, Biolegend, UK) was added to eppendorfs, and cells were incubated under low light conditions for 15 min. Staining was then stopped by addition of 500 μ l blocking buffer (PBS+0.1% BSA) and cells were incubated for a further 15 minutes. Characteristics and dilution of fluorophore-conjugated 1^o antibodies used for identification of cell populations are detailed in Table 2.8. ENaC- α antibody (PA1-920A, Thermo, characteristics in Table 2.7) was conjugated to the CY5 fluorophore using the CY5 Fast conjugation kit (ab188288, Abcam) as per the protocol described by the manufacturer, dilution factor was 1:100. Cells were then centrifuged (100 x g for 3 minutes), resuspended in 100 μ l of antibody cocktail as specified, and incubated in the dark for 20 minutes. Following incubation, cells were centrifuged and resuspended in 100 μ l of PBS containing 0.5 % paraformaldehyde (PFA) (Sigma, UK), and incubated for 30

minutes in the dark at 4°C. After fixation, cells were centrifuged and resuspended in permeabilisation buffer (PBS + 0.5 % igeal(Sigma, UK)) and incubated at RT for a further 20 minutes. Following incubation cells were centrifuged and resuspended in PBS containing 0.5 % PFA.

A MoFlo Astrios equipped with 7 lasers (Beckman Coulter, UK) was used for this study. Since the experiment was a 6 colour panel (requiring a 6 x 5 compensation matrix, or 30 individual adjustments), spectral overlap was corrected for using in-built computer-aided compensation algorithms within the Astrios software. OvCa_{asc} cells were fixed, blocked and permeabilised as per the procedure described above and stained with a single fluorochrome per sample (single colour controls) at the same dilution as detailed in (Table 2.8). Unstained OvCa_{asc} cells, prepared as above but without incubation of a fluorochrome, were chosen as the negative control to ensure that there was no contribution of autofluorescence to the compensation matrix. The cell yield varied widely between samples and as such 10,000 events were acquired based on the FSC (forward scatter) and SSC (side scatter) parameters. Flow cytometry data was analysed by importing FCS (flow cytometry standard) into Kaluza 2.1 software (Beckman Coulter, UK). Doublet discrimination was performed by generating FSC-A vs FSC-H plots (FSC-Area vs FSC-Height) on the x and y axes respectively. Viable cells were gated on Zombie NIR (detailed in paragraph above). Zombie-NIR is an amine reactive fluorescent dye that is impermeant to live cells, but permeant to cells with compromised membranes and thus allows the discrimination of live vs dead cells in the population that is to be fixed (Perfetto et al., 2010). In order to remove leukocytes from the datasets, the population of cells were gated on CD45 and termed the CD45⁻ cell population. Cancer cells were identified by gating on EpCAM; a cell surface marker

expressed on carcinomas of multiple origins (further information and rationale provided in section 2.11.2). The cancer stem cell (CSC) markers CD44 and CD117 were chosen since they have been previously shown to identify CSC populations in OvCa cells lines and primary OvCa malignant ascites cells (Zhang et al., 2008). Percentage of cell sub-populations were calculated by dividing the absolute number of the respective gate by the total number of CD45⁻ viable gated population. Data were then imported into Graphpad Prism and analysed as described in section 2.15.

Antibody	Host	Clone	Isotype	Fluorochrome	Dilution	Company (#Cat)
EpCAM	M	VU1D9	IgG1	PE	1:50	CS (8995)
CD45	M	2D1	IgG1, κ	Alexa Fluor 488	1:20	BL (368535)
CD44	Rat	IM7	IgG2b, κ	Brilliant Violet 711	1:100	BL (103057)
CD117(c-kit)	M	104D2	IgG1, κ	Brilliant Violet 421	1:20	BL (313215)

R, rabbit; M, mouse; PE, phycoerythrin

CS, Cell Signalling Technology, UK; BL, Biolegend, London, UK

Table 2.8: Primary conjugated antibodies used in flow cytometric characterisation of OvCa_{asc} populations.

2.12.2 Assessment of apoptosis

The extent of apoptosis in SKOV-3 cells following treatment with amiloride was assessed using a FITC Annexin V/Dead cell apoptosis kit (V13242, Invitrogen, Molecular Probes, Thermo, UK). Annexin V binds in a calcium-dependent manner to phosphatidylserine (PS), which is located on the cytoplasmic surface on the plasma membrane of healthy cells. However, in cells undergoing apoptosis membrane flippases translocate PS to the outer surface of the membrane, thereby marking the cell for phagocytosis by macrophages (Schutte et al., 1998). Propidium iodide (PI) is a nucleic acid binding dye that only stains cells with compromised plasma membranes (Schutte et al., 1998).

SKOV-3 cells were split as described in section 2.2.1.3 and seeded in T25 flasks

at 400×10^3 cells/flask in triplicate, then allowed to adhere for 6 hours. Adherence was assessed by light microscopy. Upon adherence, media was aspirated and cells were resuspended in CGM + vehicle (0.1% DMSO) or CGM in the presence of 10, 50 or 100 μM amiloride respectively. Cells were then incubated for 48 hours and trypsinised as above, washed in cold (4°C) PBS, and resuspended in Annexin-binding buffer in aliquots containing 100×10^3 cells in 100 μl volumes. A 2.5 μl volume of FITC Annexin-V and 1 μl of PI working solutions were added to the cell suspensions as per the manufacturers instructions, and incubated for 15 minutes at RT. Following incubation, a further 400 μl of Annexin-binding buffer was added. The suspension was then mixed gently using a 1000 μl pipette and transferred to standard FACS tubes (Thermo, UK). Cells were then transferred to a carousel and samples were analysed using a FC5000 (Beckman Coulter, UK); fluorescence emission was measured at 530 and 575 nm respectively. The compensation matrix was generated manually through use of unstained and single-stain controls. Flow cytometry data was analysed by importing FCS (flow cytometry standard) into Kaluza 2.1 software (Beckman Coulter, UK). Doublet discrimination was performed using the method described in section 2.12.1. Since it was known that amiloride at a high dose ($100\mu\text{M}$) induced cytotoxicity in SKOV-3 cells (assessed by SYTOX green assay), it was not necessary to include a known apoptosis inducing control (such as etoposide (Mizumoto, Rothman and Farber, 1994)) and gating was performed on single stained populations of 100 μM amiloride treated cells.

A minimum of 10^3 events were recorded for each experiment and repeated on three separate occasions.

2.12.3 Determination of V_{cell}

Cell volume changes of SKOV-3 cells following treatment with amiloride were determined by assessment of cells in suspension. SKOV-3 cells were split as described in section 2.2.1.3 and seeded in T25 flasks at 400×10^3 cells/flask in triplicate, then allowed to adhere for 6 hours. Adherence was assessed by light microscopy. The treatment protocol was performed in exactly the same manner as for assessment of apoptosis (section 2.12.2).

Since it was observed that there was significant cytotoxicity by live / dead staining with flow cytometry at 48 hours (see section 4.2.1), an approach to systematically discriminate cells undergoing apoptosis or those in late apoptosis / necrosis from the viable cell population was designed. Since Ca^{2+} present at low mM concentrations is essential for annexin V binding to phospholipids, it was decided to undertake experiments in the proprietary formulation used in the associated kit. The osmolarity of 1 x annexin-binding buffer is 297.5 mOsm/kg H_2O , a value similar to RPMI medium when supplemented with 10 % FBS (see section 2.8), thus any acute changes in cell volume due to osmolarity differences in media and the removal of drug / vehicle would not have been determined in the current experiment and this is a limitation. As a result, the time that cells were maintained in annexin buffer was kept to a minimum (< 30 minutes).

Cell volume measurements were undertaken using an Amnis ImagestreamTM imaging flow cytometer (Luminex, Austin, TX, US) with the capability to record high resolution 2D brightfield and corresponding fluorescent images of cells in suspension, and subsequently perform morphometric measurements in a cell by cell fashion. Events were gated for single cells and compensated for spectral overlap in the same manner

as described in section 2.12.2. The viable, apoptotic and necrotic / late apoptotic cell populations were determined respectively using IDEAS (Luminex, Austin, TX, US) detection and analysis software. Single viable cells were then fit with a tight 'mask' on the brightfield channel to spatially distinguish the entire cell area from that of the background (Dominical, Samsel and McCoy, 2017). The number of pixels within the mask were then converted to μm^2 (1 pixel = $0.25 \mu\text{m}^2$) to obtain a 2D area of the cell. Assuming that the cells tended towards spherical objects in suspension ⁷, the cross sectional area in a 2D projection is described by the area A :

$$A = \pi r^2$$

where A and r are the area and radius of a circle respectively. The volume for a sphere, V with equivalent area A in a 2D projection can subsequently be described as:

$$V = \frac{4}{3}\pi \left(\frac{A}{\pi}\right)^{\frac{3}{2}}$$

where volume is in μm^3 . To then convert to litres (l), values were multiplied by 10^{-15} and expressed in femtolitres (fl). Individual area values in pixels for cell populations were imported into Graphpad Prism and the volume computed in fl as per the equation above. A minimum of 1500 events were recorded for each experiment and repeated on three separate occasions.

⁷The circularity of the mask, which is a measure of the degree of deviation from a circle, was quantified across all treatments and assessed to be close to that of an ideal circle

2.13 Cell stiffness measurements as assessed by atomic force microscopy force spectroscopy

To determine the effect of amiloride on modulating cell stiffness in A2780 cells, atomic force microscopy (AFM) mechanical measurements were conducted on single adherent cells. Cells were subcultured and trypsinised as described in section 2.2.1.3 then seeded in cell culture treated 60 mm dishes at 600×10^3 cells/dish and allowed to adhere overnight. The AFM used in experiments was a Dimension ICON multimode 8 (Bruker, UK) equipped with an objective lens to align cells with the probe head. The probes used in this study were DNP (Bruker, UK) with a nominal spring constant of 0.06 N/M. Measurements were conducted in PSS of the composition detailed in Table 2.5 at RT. In order to exclude the effects of cytoskeletal interactions between cells only isolated cells were measured. Calibration, prior to commencement of cell measurements, was achieved in air using the thermal vibration method and fitted with a Lorentzian function to determine the spring constant (Lévy and Maaloum, 2002). The indentation region selected was directly over the nucleus of the cells and indentation depth was set to 1 μM . Young's modulus (E) was determined by fitting with a Hertz contact model (Kontomaris, 2018) using the Force Curve Analysis macro implemented in Microsoft Excel 2010 written by Professor Xinyong Chen, School of Pharmacy, University of Nottingham. A 6 x 10 array (row x column) spaced 0.5 μm apart of force curves was obtained for each cell. The average Young's modulus for each cell was determined by computing the mean of the array matrix. Data was then imported into Graphpad Prism and statistical analysis performed as described in section 2.15.

Since the absolute magnitude of Young's modulus varied between cells, a paired

sample approach was undertaken. Culture dishes were removed from the incubator, CGM aspirated and cells then resuspended in PSS, and allowed to equilibrate for 30 minutes before commencement of experiments. Measurements for each cell were then undertaken and upon completion, amiloride was carefully added to the dish with a 200 μl pipette and allowed to equilibrate for 60 minutes. After equilibration, measurements were then repeated on cells in the same sequence as acquired in control conditions. This approach thus meant that cells experienced a different ‘exposure window’ to the presence of amiloride, i.e. the measurement time of a single cell took ≈ 10 minutes, the the last cell to be measured would be exposed to amiloride for ≈ 50 minutes longer before data acquisition (the maximum number of cells measured in a single experiment did not exceed 6). As such any temporal effect of amiloride on cell stiffness may influence measurements differently, depending on the sequence position.

2.14 Galvanotaxis

The following sections detail all aspects of the galvanotaxis experiments undertaken in this thesis, including fabrication of electrotaxis (ET) chambers, seeding of cells and application of electric fields (EF). Image acquisition and data processing are then described. Finally, quantitative parameters used to assess directed cell migration are described and derived where necessary.

2.14.1 Preparation of silver chloride electrodes

AgCl/Cl electrodes for application of EFs were prepared in the same manner as for patch clamp experiments. Annealed silver wire, 1 mm \varnothing was cut into lengths of 3 - 4 cm and immersed in household bleach (NaClO); wire was then placed in a glass petri dish for at least 12 hours. Bleach was then discarded and electrodes were washed many

times in ddH₂O, allowed to dry on a kimwipe and stored at RT until required.

2.14.2 Preparation of agar salt bridges

Plastic aspiration pipettes of 4 mm internal diameter (Starlabs, UK) were cut down to approximate 15 cm lengths with a hot scalpel and then bent to approximately 90° over a bunsen burner at both ends to produce a U shape. 2% w/v agar (Sigma, UK) was added to Steinberg's solution (composition detailed in 2.14.3), then heated gently in the microwave to allow the agar to dissolve and then allowed to cool to approximately 60°C. Bridges were filled with agar using a 3 ml pasteur pipette in a continuous motion to prevent the formation of air bubbles and allowed to set at RT. Bridges were immersed in Steinberg's solution and stored for up to 2 weeks at 4°C.

2.14.3 Media and solution composition

Since all galvanotaxis experiments were undertaken outside a humidified CO₂ incubator, cell culture media was required to maintain pH in a CO₂-independent manner. For OvCa_{asc} experiments, both Medium 199 and MCDB 105 contained 25 mM HEPES and OSE CGM preparations required no modification for ET experiments. OSE CGM preparations were observed to maintain stable pH levels over the experimental durations tested.

Steinberg's solution was of the following composition (mM): 60 NaCl, 0.7 KCl, 0.8 MgSO₄·7H₂O, 0.3 mM CaNO₃·4H₂O, 1.4 tris-base, pH 7.4. Addition of NaCl & KCl were prepared from 1 M stock solutions, the remaining components were added directly. Upon preparation, the solution was autoclaved and stored at 4°C for up to 1 month.

For experiments assessing the effects of Na⁺ replacement on galvanotaxis, it was necessary to design proprietary solutions. Since it was known that OvCa_{asc} samples

displayed little change in cell morphology and adherence when maintained for durations of 2 - 3 hours in PSS and NMDG-PSS of the composition detailed in Table 2.5, formulations based on these solutions were designed. The concentrations of Ca^{2+} and Mg^{2+} in ET buffers were calculated to match those present in OSE CGM, since it is known that $[\text{Ca}^{2+}]_e$ often influences galvanotactic capacity in many cell types (Fang et al., 1998; Borys, 2013). The compositions of 'Basal' and Na^+ -free ET buffers are detailed below. In both cases they were supplemented with 20% FBS to match concentrations used in OSE CGM.

Basal ET buffer composition (mM): 135 NaCl, 5 KCl, 1.3 CaCl_2 , 0.7 MgCl_2 , 25 HEPES, pH 7.4

Na^+ -free ET buffer (mM): 135 NMDG-Cl, 5 KCl, 1.3 CaCl_2 , 0.7 MgCl_2 , 25 HEPES, pH 7.4

2.14.4 Construction of electrotactic chambers

Electrotactic chambers were constructed similarly to the method described by Song et al (Song et al., 2007). A custom stencil was used to mark a centrally placed rectangle of 22 mm length by 10 mm width in 90 mm Corning cell culture treated polystyrene dishes (Fisher Scientific, UK). Number 1 glass coverslips, 22 mm x 22 mm (SLS, UK) were cut in half using a tungsten carbide scribe, sterilised in 70% ethanol and dried in a 60°C oven. In a class II cabinet, cover glass strips were fixed in place using DC 3140 silicone adhesive (Dow Corning, UK), taking care to ensure that they lined up correctly with the edges of the stencilled rectangle, and allowed to set overnight.

Glass wells were constructed from coverslips to fit exactly within the sides of the electrotactic chamber, in order to allow cell seeding only in the chamber region. Number 2 glass coverslips, 22 mm x 22 mm were cut in half as described above and assembled to

form a rectangular well with internal dimensions 21.56 mm x 9.56 mm. Coverslips were affixed using DC 732 silicone sealant (Dow Corning, UK), and allowed to set overnight. Wells were sterilised in 70% ethanol for at least 1 hour, dried in a 60°C oven and used immediately. After cell seeding, wells were washed, sterilised and reused as described above. ET chambers were coated with collagen 1 (40 µg/ml).

2.14.5 Chamber seeding

In preparation for ET experiments, wells were removed from the oven and transferred to a class II cabinet in a sterile container and set in place between the chamber sides using forceps. A 500 µl cell suspension of OvCa_{asc} was added to the chamber to yield a cell density of 100 x 10³ cells / cm². Cells were then placed in a humidified incubator and allowed to adhere for 18-24 hours.

2.14.6 Application of electric fields

For ET experiments, chambers were removed from the incubator, then the majority of the media was aspirated and the glass well was removed. Cells were then washed gently with the respective warmed ET media (37 °C) to remove non-adherent cells. After washing, a thin strip of DC 4 silicon grease (Dow Corning, UK) was applied along the length of the chamber sides with a sterile cotton swab (Fisher Scientific, UK) and a 22 mm x 22 mm number 2 coverslip forming the chamber roof was glued on, taking care to ensure that it was pressed down as tightly as possible to reduce the Joule effect (cell heating) (McCaig et al., 2005). This resulted in the formation of a chamber with dimensions 22 mm x 10 mm x 0.15 mm (see Figure 2-1A).

Silicone grease dams were then built up from each end of the ET openings ensuring good contact with the edges, creating 2 media reservoirs. The working volume of each

reservoir was approximately 7 ml. Care was taken to ensure that the volumes were equal to prevent the establishment of a flow gradient through the chamber (see Figure 2-1A).

Upon preparation of the ET chamber the dish was transferred to the ET holder (pre-heated to 37 °C). ET media was topped up using gentle drip wise addition to both chambers simultaneously, and the chamber was allowed to equilibrate for 15 minutes before the start of experiment. The current was applied through 2 reservoirs ($\approx 10\text{ml}$) containing Steinberg's solution, coupled to the ET chamber via salt bridges (see Figure 2-1B). AgCl/Cl electrodes partially submerged in the reservoir were connected to a EPS 600 DC power supply (PSU) (Pharmacia Biotech, UK) via a custom made $20\text{K}\Omega$ 20-turn resistance box (R_{var} in Figure 2-1C), which allowed fine tuning of applied voltage throughout the duration of the experiment.

The PSU was ramped up to steady-state over 3 seconds and the potential across the chamber was monitored by thin AgCl/Cl electrodes positioned at the ends of the chamber connected to a high impedance voltmeter (Rapid electronics, UK) (see Figure 2-1B). The field was expressed as a function of Volts per centimetre (V/cm), for example if the field required was 5 V/cm, the potential necessary to be developed across the length of the chamber would be 11 V (2.2 cm x 5 V/cm) (refer to figure 2-1B).

Throughout the experiment, media was aspirated and replenished using custom made pasteur pipette droppers with a narrow aperture from both reservoirs of the chamber, taking care not to apply a flow gradient over the cells. This process was repeated at 30 minute intervals until cessation of the experiment.

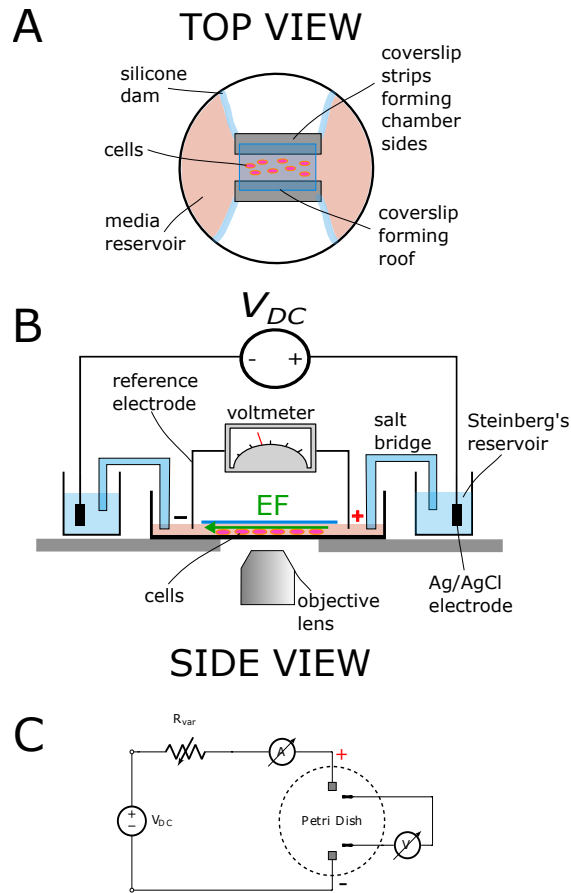


Figure 2-1: Experimental setup for application of external electric fields to OvCa cells. (A) Top view of electro-tactile chamber. Chambers were assembled in a standard 100 mm cell culture treated dishes. Strips of coverslips are affixed parallel to each other 10 mm apart. Cells are seeded in a retaining well seated between coverslip strips and upon adherence, an additional cover slip is fixed on top thus forming the chamber roof. Dams built up from high vacuum silicon grease form the media reservoirs, allowing periodic replacement of media throughout the experiment. (B) Side view. Salt bridges comprising agar (2%) dissolved in Steinberg's provided electrical coupling to the system. One end is placed in media reservoir, the other is submerged in a beaker containing Steinberg's. The circuit is connected through the DC power supply (V_{DC}) by Ag/AgCl electrodes coupled to salt bridges through the Steinberg's reservoir. Reference electrodes connected to a voltmeter are positioned at the ends of the central EF chamber allowing continuous tuning of applied EF over the course of the experiment via a series variable resistance box (R_{var}). (C) Equivalent circuit of ET setup. Current flow over the experiment duration is assessed with a series ammeter to ensure it remains relatively constant. R_{var} consists of two 10-turn wire-wound resistors connected in series allowing fine tuning of EF. + and - denote the anodal and cathodal electrode respectively.

2.14.7 Image acquisition

Time lapse microscopy was performed on an IX51 inverted phase-contrast microscope (Olympus, UK). All images were captured with a 20x 0.45 NA air objective. Images were captured with a Cannon EOS 7D CMOS camera mounted to the microscope via a photo tube and time-lapse imaging was controlled using Cannon EOS utility suite.

The temperature of the electrotaxis chamber was regulated using a custom-made setup comprising of an Inkbird ITC-308 relay switched temperature controller driving a silicone heater mat (RS components, UK), mounted onto the underside of the ET chamber holder. All experiments were carried out at 37° C. The temperature regulation system was switched on at least 1 hour prior to the beginning of experiments to allow the chamber holder to reach a steady state.

Immediately prior to the application of electric field a reference image was taken and subsequent images were taken at 2 minute intervals.

2.14.8 Image analysis

Time lapse images were converted to stacks and processed using FIJI , an open-source distribution of Image J (version 1.52g) and analysed using the Manual Tracking plugin, in order to determine the two dimensional position of a cell with respect to time (Schindelin et al., 2012). Cells which were observed to be undergoing division during the experiment were excluded from further analysis. Cells which migrated out of the field of view during the experiment were tracked until they left the field of view, and the positional information was recorded with the remaining tracks.

2.14.9 Quantitative parameters of cell migration

Different properties of cell locomotion were further quantified using several parameters which have been reported previously in cell migration experiments. All metrics were quantified using the Chemotaxis tool apart from directedness, for which a custom script was written using MATLAB (appendix D).

1. **Directional cosine.** The angle θ was defined as the angle between the cell migration vector and the external EF vector (see figure 2-2). The directional cosine D is then defined as:

$$D = \cos \theta \quad (2.1)$$

In a cell migrating straight towards the anode or cathode, θ is 0° or 180° and the cell would have a cosine value of 1 or -1 respectively. Conversely, cells migrating orthogonally to the EF vector would have a cosine value of 0. Thus this provides a marker of net directional bias in an external EF (refer to Figure 2-2).

2. **Accumulated distance (Dis_{ACC}).** This describes the total path length (μm) that the cell has travelled over the course of the experiment (refer to Figure 2-2).
3. **Euclidean distance (Dis_{EUC}).** This describes the length of cell displacement from the cell start point to the x,y position (refer to Figure 2-2).
4. **||Forward migration index (||FMI).** The forward migration index is a measure of the efficiency with which a cell moves preferentially in response to an external cue such as an EF. Here, the parallel (||) FMI describes the migration of cells in a

direction parallel to the EF vector (always defined as the x-axis / horizontal axis in this study). For a single migrating cell, the ||FMI is then described as:

$$||FMI = \frac{x_{end\ point}}{Dis_{ACC}} \quad (2.2)$$

where $x_{endpoint}$ and Dis_{ACC} are both in μm . For a cell population the ||FMI is then described by:

$$||FMI = \frac{1}{n} \sum_{i=1}^N \frac{x_{end\ point,i}}{Dis_{ACC,i}} \quad (2.3)$$

where n is the total number of cells from i to N .

5. **Percentage of cells crossing criterion boundary (P_C).** To quantitatively assess meaningful cell translocation towards an extracellular cue, the percentage of cells migrating directedly across a threshold boundary was defined. The threshold corresponded to the median Dis_{EUC} value that the cells achieved in control conditions, centered 66° around the anodal axis which described a cell with a cosine value of ≥ 0.84 (refer to the schematic depicted in figure 2-3).

Upon quantification of parameters, values were exported as tab-delimited text files and further statistical analysis was undertaken using Graphpad Prism.

2.14.10 Assessment of ENaC inhibition and Na^+ replacement on galvanotaxis in OvCa_{asc} samples

To assess whether OvCa_{asc} samples were galvanotactic, experiments were carried out in the absence and presence of an external EF of 5 V/cm. Each OvCa_{asc} sample was seeded in duplicate in ET chambers as described in section 2.14.5. The control

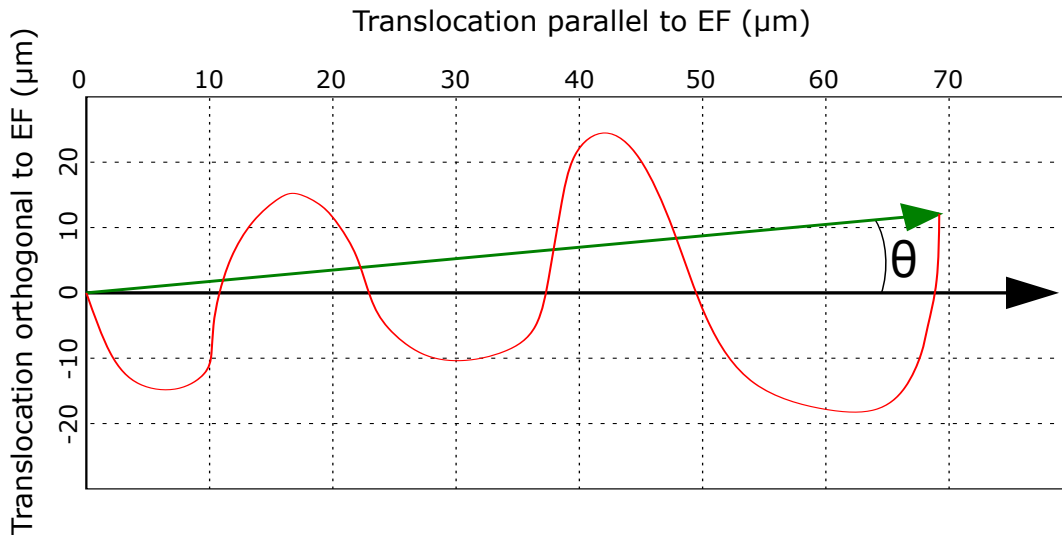


Figure 2-2: Schematic of the trajectory of a cell migrating within an electric field (EF). Black arrow denotes the direction of the EF vector from cathode to anode. The red line indicates the total path length that the cell has taken (Dis_{ACC}). The green line demonstrates the net displacement of the cell from the origin (Dis_{EUC}). θ denotes the angle between the EF vector and the the cell displacement vector. $\cos \theta$ then describes the extent of directionality which which a cell migrates to the anode or cathode (1 and -1 respectively).

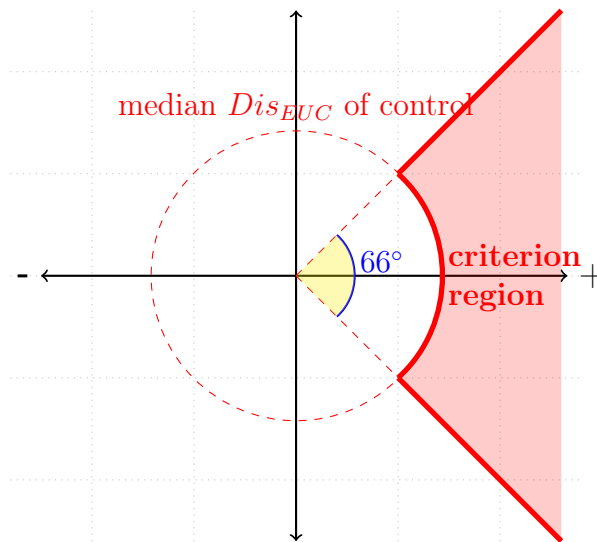


Figure 2-3: Schematic depicting the threshold boundary (criterion boundary) for distance and directionality for cells migrating in an external EF (shaded red region). The threshold for Dis_{EUC} (dashed red line) was defined as the median distance that cells migrated in control conditions in the same external EF strength. The directional threshold was centered 66° about the anode which corresponded to a cosine value of ≥ 0.84 . - and + denote the position of the cathodal and anodal pole respectively.

condition was thus 0 V/cm. The effects of an external EF were quantified by comparing the migration parameters (section 2.14.9) to those quantified in the presence of a field of 5 V/cm. Migration was assessed over 60 minutes in both conditions.

Assessment of the effect of ENaC inhibition on galvanotaxis of primary OvCa_{asc} cells was assessed by treatment with pharmacological inhibitors of ENaC. Prior to application of electric fields, ET chambers fitted with ET wells were removed from the incubator, media aspirated, and resuspended in media containing vehicle (0.2 % DMSO), amiloride (100 μ M) or phenamil (20 μ M). Chambers were then placed in a humidified incubator (100% air) for 1 hour. Then, chambers were removed and a roof and reservoirs added as described in section 2.14.6. Galvanotaxis was assessed for 2 hours in each condition in the manner described above (section 2.14.8), maintaining the presence of drug or vehicle throughout the course of the experiment. All three conditions were undertaken as individual experiments on each OvCa_{asc} samples and the effect assessed as the difference relative to vehicle (0.2 % DMSO).

For Na⁺ replacement experiments, ET chambers were removed from the incubator, aspirated and replaced with a basal ET buffer or Na⁺-free ET buffer (compositions described in section 2.14.3) supplemented with 20 % FBS. Chambers were placed in a humidified incubator (100 % air) for one hour prior to commencement of ET experiments. Dependence of Na⁺ on galvanotactic migration was assessed by pairwise comparison of OvCa_{asc} samples in Na⁺-free ET buffer to conditions containing [Na⁺]_e in the normal physiological range (basal ET buffer). Cells were first validated to migrate with similar properties in basal ET buffer as those observed in OSE CGM.

Statistical analysis of ET experiments is detailed in section 2.15.1.

2.15 Statistical analysis

All statistical analysis was undertaken using GraphPad Prism 8.2.1. Unless otherwise specified population data are presented as mean \pm SD (standard deviation) of n observations of x independent experiments, where n refers to the number of individual cells/experiments. Significant differences between sample/treatment groups were assessed using the students t-test (paired or unpaired specified in the relevant results sections) or one-/two-way ANOVA for two or more groups respectively. When comparing 3 or more groups to a control condition with ANOVA, Dunnett's post-hoc test was used. When expressing differences between samples, data was expressed as the mean value with 95 % confidence intervals; mean [95% LCI , 95% UCI] (LCI, lower confidence interval; UCI, upper confidence interval) (Drummond and Tom, 2012). Values of $p < 0.05$ were assumed to describe significance in all tests. Normality tests were performed on data when using parametric tests.

For determination of differences in cell volume, relative frequency distributions across all treatment conditions exhibited marked positive kurtosis ($+ 2.23 \pm 0.14$, mean \pm SD, lowest n = 1918) with large outliers. Populations were defined as non-normally distributed as assessed by the D'Agostino & Pearson omnibus test and Anderson-Darling test ($p < 0.0001$). As such, the non-parametric Kruskal-Wallis test was used with Dunn's multiple comparisons post-hoc test to compare treatment groups to control (Dunn, 1964).

2.15.1 Galvanotaxis experiments

Quantitative metrics of directed cell migration used in galvanotaxis experiments are described in section 2.14.9.

Data of individual populations of each OvCa_{asc} sample are presented as mean \pm SEM (standard error of the mean) and statistical difference relative to the respective control conditions assessed using the Mann-Whitney U (MWU) test (two-tailed). N denotes the number of cells tracked and is described in the tables of associated sections. When two individual treatments were used for each individual OvCa_{asc} sample tested, pair-wise MWU comparisons were assessed relative to control conditions.

When assessing the net effect of ENaC inhibition or Na⁺ replacement on combined OvCa_{asc} samples ET parameters, data was presented as mean \pm SD and significance assessed using the paired students t-test (two-tailed) or one-way ANOVA for 2 or 3 groups respectively and termed the grouped mean.

Chapter 3

Assessment of Na^+ and ENaC contribution to V_m in OvCa

3.1 Introduction

There are numerous reports that cancer cells exhibit a depolarised V_m . When compared to their non-malignant counterparts, hepatomas, thyroid cancers and fibrosarcoma exhibited more depolarised phenotypes (Jamakosmanovic and Loewenstein, 1968; Binggeli and Cameron, 1980; Binggeli and Weinstein, 1986). This depolarised phenotype has been suggested to confer cancer cells with increased replicative potential (Blackiston, McLaughlin and Levin, 2009). Hyperpolarisation of tumour initiating cells (TIC) from hepatomas; a cell population thought to be central in contributing to pathogenesis, proliferation and invasion, resulted in a reduction in proliferation (Bautista et al., 2014). Exposure of hepatoma TIC cells to the GABA_A receptor agonist muscimol, resulted in V_m hyperpolarisation with concomitant reduction in proliferative capacity (Bautista et al., 2014).

While the observation of depolarised V_m values has been reported in numerous cancers, little evidence exists for the basal values of V_m in OvCa. A single study published by Redmann et al in 1972 reported that tumour cells isolated from human enzymatically dissociated OvCa tumours were highly depolarised (V_m values of -2 to -6 mV) using microelectrodes (Redmann et al., 1972). It should be noted however that in this study there was no characterisation of the tumour grade or even any putative staging information provided which makes it challenging to infer a causative relationship with V_m (Redmann et al., 1972).

A number of studies have identified an increased contribution to V_m of Na^+ in other tumour types (Binggeli and Weinstein, 1986). In MCF-7 breast adenocarcinoma and mammary tumours of mice it was shown that Na^+ contributed to membrane depolarisation (Wonderlin, Woodfork and Strobl, 1995; Shen et al., 1978). Increased Na^+ mediated depolarisation has also been suggested to partially account for low V_m values in Shay chloroleukemic tumour cells (Schaefer et al., 1972). In addition, other studies have demonstrated markedly elevated $[\text{Na}^+]_i$ values across a broad range of cancers and these provide further evidence for increases in P_{Na^+} in tumourigenesis (Nagy et al., 1981).

While increased Na^+ permeability has been shown to contribute to the depolarised phenotype in cancer, there is still a question as to which channels are implicated in facilitating this increased Na^+ influx. It has been hypothesised that Na_V channels may modulate V_m (Roger et al., 2015). If V_m values are depolarised to a point where Na_V channels possess a window current then persistent Na^+ influx is facilitated and may act to depolarise V_m further. However further depolarisation would likely result in channel inhibition and cessation of Na_V mediated Na^+ influx. In MDA-MB-231 breast cancer

cells, knock-down of $\text{Na}_V1.5$ or addition of $30 \mu\text{M}$ tetrodotoxin (an inhibitor of Na_V channels) resulted in $\approx 10 \text{ mV}$ hyperpolarisation (Yang et al., 2020a) suggesting a role for Na_V modulation of V_m .

There is a paucity of investigations of ENaC in cancer and hence a lack of evidence of a role for ENaC modulations of V_m . As a constitutively open channel, ENaC is a good candidate for maintaining V_m depolarisation observed in cancer cells (Bhalla and Hallows, 2008). In glioblastoma multiforme, multiple cell lines possess an amiloride sensitive current that acts to depolarise V_m , inhibition of which (at $100 \mu\text{M}$) markedly attenuates cell migration (Rooj et al., 2012). Interestingly this Na^+ current is not detectable in normal human astrocytes or low grade gliomas (Berdiev et al., 2003). Human hepatocellular carcinoma HepG2 cells have also been shown to exhibit ENaC- α mediated currents which could be abolished with amiloride ($50 - 300 \mu\text{M}$) or flufenamate (Bondarava et al., 2009). This ENaC mediated conductance appeared to play a central role in proliferative potential; inhibition with $30 - 100 \mu\text{M}$ amiloride resulted in a $\approx 50\%$ reduction in proliferation (Bondarava et al., 2009). Further evidence for tumourigenesis mediated by increased Na^+ and ENaC conductance is suggested in studies of adenomatous polyposis coli (APC) negative mice ($\text{APC}^{\text{Min}/+}$) with a much higher risk of developing colon cancers (Ousingsawat et al., 2008). APC is a tumour suppressor gene implicated in the suppression of canonical Wnt signalling pathway; this pathway is important in tumourigenesis and is mutated in $> 90\%$ human colonic cancers (Aoki and Taketo, 2007). Rectal potential measurements and Ussing chamber studies on isolated colonic epithelium in $\text{APC}^{\text{Min}/+}$ mice demonstrated increased Na^+ absorption via ENaC and increased expression of α, β, γ -ENaC in the proximal and distal colon (Ousingsawat et al., 2008). Taken together there is evidence to suggest an increased

Na⁺ permeability mediated by ENaC that may facilitate a sustained depolarisation in cancer, but no clear evidence exists in OvCa.

Thus, the aims of this study were to measure V_m values in OvCa cell lines and OvCa_{asc} primary cells using the I=0 current clamp patch clamp method. Then to assess the contribution of persistent P_{Na^+} to V_m . The MCF-7 cell line, a breast cancer model that has been relatively well characterised for V_m values was also assessed for comparative analysis. Pharmacological modulators of K⁺ channels were next used to assess the differing contribution of K⁺ between cancer types. Finally ENaC contribution to V_m in SKOV-3 cells was also assessed using the ENaC inhibitor, amiloride.

3.2 Results

3.2.1 The contribution of persistent Na⁺ permeability to V_m in OvCa and MCF-7 cells

V_m values of SKOV-3 cells were determined with the I=0 patch clamp method by recording potentials in normal [Na⁺]_e physiological salt solution (PSS) for 60s and measuring the extent of hyperpolarisation upon perfusion of Na⁺-free (NMDG⁺-PSS) solution to the bath as described in section 2.3. In PSS SKOV-3 cells exhibited a markedly depolarised V_m of -3.6 ± 3.6 mV (figure 3-1A & B). Upon perfusion with NMDG⁺-PSS cells hyperpolarised to -19.4 ± 13 mV exhibiting a significant hyperpolarisation of -15.8 mV $[-22.1, -9.5]$ (pooled data n=14 of 4 independent experiments, $p < 0.05$, one-way ANOVA Dunnett's post hoc test) (see figure 3-1B). However, while this was significant, a subpopulation of cells (n = 5) exhibited a limited hyperpolarisation. A subset of cells were assessed for recovery of V_m by re-perfusion of PSS and exhibited almost complete return to baseline values (-3.2 ± 2.9 mV, $p > 0.05$ relative to PSS, n

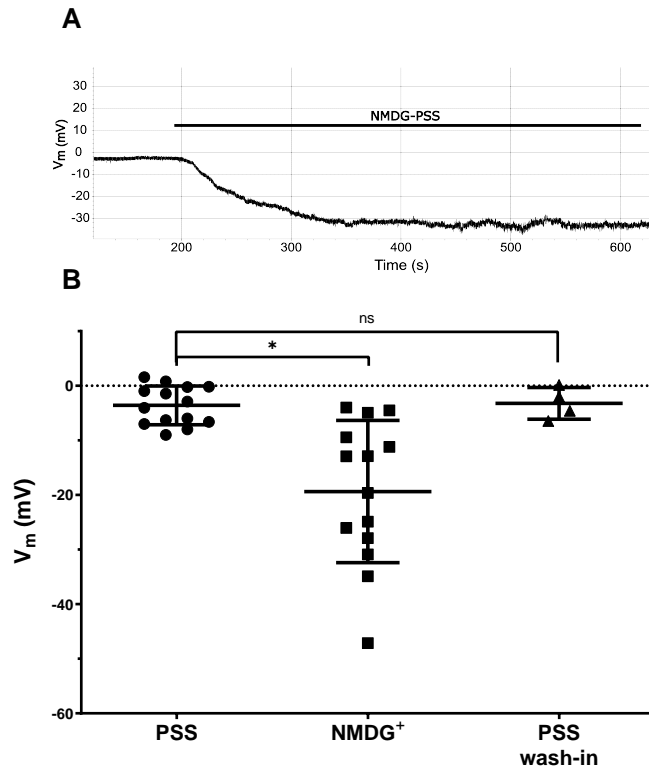


Figure 3-1: The contribution of Na^+ to V_m in SKOV-3 cells. $I=0$ current clamp recording of V_m in PSS for 60s and upon wash-in of NMDG-PSS at plateau of response after switching solutions. (A) Representative recording of V_m (B) Graph shows change in V_m with NMDG-PSS and on washout. Combined data ($n=14$) of paired measurements of 4 independent experiments (PSS wash-in; $n=4$, 3 independent measurements). Error bars denote mean \pm SD, * denotes significance ($p < 0.05$) as assessed by one-way ANOVA with Dunnett's post-hoc test.

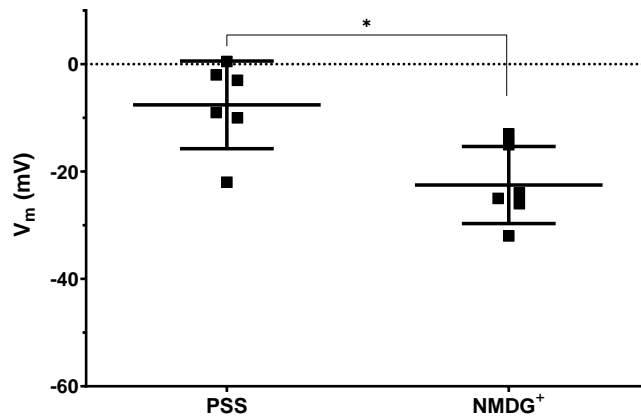


Figure 3-2: The contribution of Na^+ to V_m in MCF-7 cells. $I=0$ current clamp recording of V_m in PSS for 60s and upon plateau of response following perfusion of NMDG-PSS. Combined data ($n=6$) of paired measurements from 2 independent repeats. Error bars denote mean \pm SD, * denotes significance ($p < 0.05$) as assessed by paired t-test.

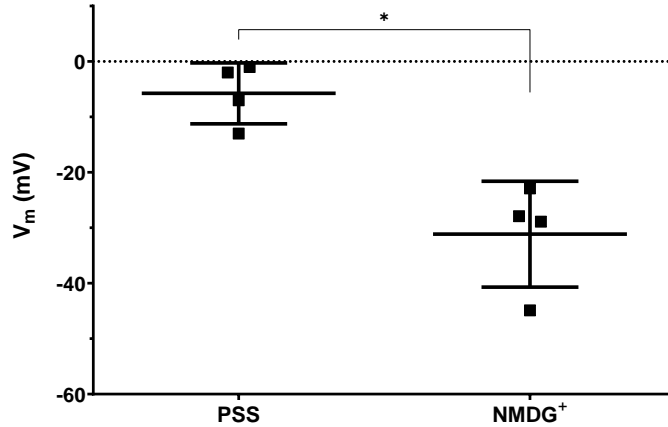


Figure 3-3: The contribution of Na^+ to V_m in OvCa_{asc} cells. $I=0$ current clamp recording of V_m in PSS for 60s and upon plateau of response following perfusion of NMDG-PSS. Combined data ($n=4$) of paired measurements in OM5, OM8 and OM12 from 3 independent experiments. Error bars denote mean \pm SD, * denotes significance ($p < 0.05$) as assessed by paired t-test.

= 4 of 3 independent experiments).

Recordings of V_m in MCF-7 cells in PSS were -7.6 ± 8.2 mV which, upon replacing PSS with NMDG-PSS hyperpolarised cells to -22.5 ± 7.2 mV ($n = 6$ of two independent experiments, $p < 0.05$, figure 3-2). It was next assessed what the basal values of V_m were in OvCa_{asc} cells. These cells also exhibited a markedly depolarised phenotype; -5.8 ± 5.5 mV ($n=4$) in PSS. Upon wash-in of NMDG-PSS OvCa_{asc} cells hyperpolarised to -31.2 ± 9.5 mV (combined data $n=4$ from samples OM5, OM8 and OM12, $p < 0.05$, paired t-test refer to figure 3-3).

3.2.2 Effect of riluzole on V_m in SKOV-3 and MCF-7 cells

In observing that Na^+ contributed to V_m depolarisation in SKOV-3 and MCF-7 cells it was next sought to assess whether K^+ conductances modulated V_m in SKOV-3 and MCF-7 cells using riluzole as a broad spectrum modulator of K^+ channels. It activates K_{Ca} channels including both intermediate-conductance ($\text{K}_{Ca3.1}$) and small-

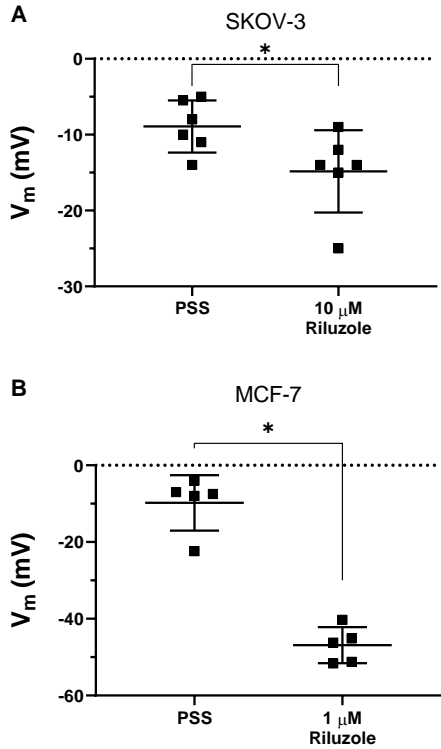


Figure 3-4: The effect of riluzole on V_m in (A) SKOV-3 and (B) MCF-7 cells. $I=0$ current clamp recording of V_m in PSS for 60s and upon wash-in of NMDG-PSS at plateau of response. Combined data ($n=6$ and 5 for SKOV-3 and MCF-7 cells respectively) repeated twice independently. Error bars denote mean \pm SD, * denotes significance ($p < 0.05$) as assessed by paired t-test.

conductance ($K_{Ca2.1}$, $K_{Ca2.2}$ & $K_{Ca2.3}$) (Coleman et al., 2014) channels, and inhibits $K_V11.1$ (Pillozzi et al., 2018)

Upon perfusion of cells with riluzole at 10μ M, SKOV-3 cells underwent mild hyperpolarisation; PSS V_m -8.9 ± 3.4 mV; PSS + 10μ M riluzole -14.8 ± 5.4 mV ($p < 0.05$, combined $n=6$ of two individual experiments, see figure 3-4A). Perfusion of 1μ M riluzole in MCF-7 cells however evoked significant hyperpolarisation by ≈ 40 mV (-9.8 ± 7.2 to -46.9 ± 4.7 mV, $p < 0.05$, combined $n=6$ of 2 individual experiments) (figure 3-4B).

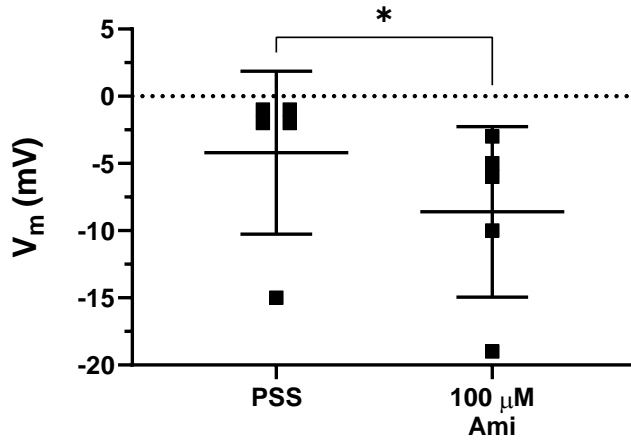


Figure 3-5: The effect of amiloride on V_m in SKOV-3 cells. $I=0$ current clamp recording of V_m in PSS for 60s and upon plateau of response following perfusion with NMDG-PSS. Combined data (n=5) of paired measurements repeated twice independently. Error bars denote mean \pm SD, * denotes significance ($p < 0.05$) as assessed by paired t-test.

3.2.3 The contribution of ENaC to V_m in SKOV-3 cells

Finally, since it was observed that Na^+ contributed to V_m in OvCa cells it was next assessed to what extent ENaC-mediated conductance modulated V_m . Upon perfusion with 100 μ M amiloride, cells underwent a mild but sustained hyperpolarisation; PSS, $-4.2 \text{ mV} \pm$; PSS + 100 μ M amiloride, $-8.6 \pm 6.3 \text{ mV}$ (n=5, of 2 independent experiments $p < 0.05$, see figure 3-5); the amiloride concentration used is similar to that required to elicit a response in other cancer cell types (Rooj et al., 2012; Ross et al., 2007; Kapoor et al., 2011).

3.3 Discussion

This study sought to assess the contribution of Na^+ to V_m in OvCa. It is shown here that the V_m of both SKOV-3 cells and cells from primary OvCa_{asc} isolates are profoundly depolarised. Moreover, there is a persistent membrane permeability to Na^+

which may contribute to a significant extent to the depolarised phenotype observed. Riluzole resulted in V_m hyperpolarisation in both SKOV-3 and MCF-7 cells but to markedly different magnitudes. Finally it was shown that amiloride, at similar doses to those in other cancer studies ($\approx 100 \mu\text{M}$) results in a mild V_m hyperpolarisation in SKOV-3 cells Rooj et al. (2012).

3.3.1 Effects of Na^+ replacement on V_m in OvCa and MCF-7 cells

Firstly, V_m recorded in SKOV-3 cells exhibited a markedly depolarised phenotype with a strong convergence between individual V_m values when measured in PSS. No difference was noted between basal V_m values in SKOV-3 cells or OvCa_{asc}.

Measurements of V_m in MCF-7 cells also demonstrated a markedly depolarised phenotype and exhibited a persistent permeability to V_m . These V_m values are markedly more depolarised ($\approx 30 \text{ mV}$ more depolarised) than those recorded by other investigations using sharp microelectrode and whole cell current clamp methods (Marino et al., 1994; Fraser et al., 2005). Wonderlin et al measured V_m in MCF-7 cells using the sharp microelectrode method and reported median V_m values of -23 mV in unsynchronised cells in a much larger sample population ($n=188$) which is closer to values observed here yet still markedly more hyperpolarised (Wonderlin, Woodfork and Strobl, 1995). It is important to significantly increase the number of recordings moving forward.

Across all cell types assessed in this study with NMDG only partial hyperpolarisation was observed upon impermeant replacement of Na^+ . Indeed K^+/Na^+ permeabilities in all OvCa and MCF-7 measurements were closer to unity and not significantly different from one another. Thus while Na^+ mediated depolarisation is a contributory factor to

the V_m , the data is suggestive of a reduced contribution of K^+ channel conductance that would act to hyperpolarise V_m . Indeed a number of K_V channels have been shown to be down regulated in cancers of renal, gastric, breast, skin and cervical origin (Serrano-Novillo et al., 2019).

The utilisation of the conventional whole-cell patch clamp method in this study enables complete control of the monovalent and divalent ionic transmembrane gradients across the plasma membrane and thus allows for the resting membrane permeability to Na^+ to be independently investigated. However, V_m is established as a product of K^+ and Cl^- transmembrane gradients in addition to Na^+ and limited data exists for cytosolic concentrations of these ions for the cell lines in this study. In order to derive a direct relationship between Na^+ and K^+ , the Cl^- concentration was set equal ($[Cl^-]_i = [Cl^-]_e = 140mM$) (E_{Cl} was set to 0mV and had no contribution to V_m) in all electrophysiological solutions throughout experiments. Normally $[Cl^-]_i$ is lower than $[Cl^-]_e$ resulting in a negative reversal potential (E_{Cl}) (Wright, 2004). Studies in brain gliomas have demonstrated upregulation of numerous members of the ClC chloride channel family and it has been suggested that they may enhance ability to transport Cl^- (Olsen et al., 2003). In a study of MCF-7 cells, artificial manipulation of the Cl^- gradient did not affect V_m , suggesting that there is a limited persistent membrane permeability to Cl^- (Wonderlin, Woodfork and Strobl, 1995). It remains to be seen to what extent Cl^- contributes to V_m in OvCa.

While the contribution of Na^+ to V_m in OvCa cells is significant, it is relatively small (≈ 20 mV) and so it is important to consider whether limitations of the whole-cell patch clamp for V_m measurements are due in part to these observations. Upon achievement of a tight seal following cell access, the intracellular contents are dial-

ysed with the contents of the pipette solution (many orders of magnitude greater than V_{cell}), resulting in abolition of the cytosolic gradient over the duration of the experiment (Neher, 1992*b*). The concentration of certain molecules and ions are important for channel function. For example, the weak K_{ir} channel K_{ATP} is gated by ATP and any changes in intracellular concentration of said molecule depending on the physiological state of the cell (eg progression through the G0/G1 phase of the cell cycle) would not be observable due to the concentration being clamped to the pipette contents with whole-cell patch clamping (Enkvetchakul and Nichols, 2003). Indeed significant differences in K_{ATP} inhibition have been observed between the whole-cell and perforated (a method that achieves limited dialysis of cytosolic contents) patch methods (Liu et al., 1997; Ishibashi, Moorhouse and Nabekura, 2012). In INS-1 rat β islet cells transfected with $K_{ir}6.2$ (a K_{ATP} subunit), V_m measurements were ≈ 20 mV more depolarised in perforated patches when compared to whole-cell recordings, further indicating the regulatory capacity of the cytosolic contents (Lin et al., 2005). In whole-cell recordings the phenomenon of ‘rundown’ has been reported mostly for Ca^{2+} currents as essential cytosolic factors required to maintain current activation are dialysed out of the cell causing downstream changes in current amplitudes (Fenwick, Marty and Neher, 1982). In bovine chromaffin cells Ca^{2+} currents exhibited this rundown phenomenon over ≈ 10 -15 minutes. Furthermore, there were no observed changes in channel kinetics observed, indicating that it is the number of channels available for activation rather than their unitary conductance or P_o which decays during rundown (Fenwick, Marty and Neher, 1982). As such cytosolic dialysis through the patch clamp method could alter V_m measurements in SKOV-3 cells. In considering Na^+ specifically, $[Na^+]_i$ was clamped at 5 mM in all experiments. $[Na^+]_i$ in cancer cells may be higher however (10 - 15 mM)

(Roger et al., 2007). There are other considerations for $[\text{Na}^+]_i$ mediated alteration of V_m in cancer cells. If functional NCX exchangers are present in the plasma membrane then $[\text{Na}^+]_i$ may be essential for modulating the driving force of the exchanger. Evidence is growing for the function of NCX in ‘reverse mode’ in cancer, which would result in an NCX mediated hyperpolarisation via increased Na^+ efflux (Sennoune et al., 2015; Rodrigues, Estevez and Tersariol, 2019; Long et al., 2016). In patch clamp measurements of rat endothelial cells from intact aorta preparations addition of the reverse mode NCX inhibitor KB-R7943 resulted in a sustained depolarisation (Bondarenko, 2004). As such it is necessary to address the contribution of $[\text{Na}^+]_i$ to V_m in SKOV-3 and OvCa_{asc} cells by conducting V_m current clamp measurements at different $[\text{Na}^+]_i$. Another approach that would prove insightful in further understanding the contribution Na^+ to V_m is the perforated patch approach. This approach results in reduced dialysis of the cytosol and could be considered in future experiments (Ishibashi, Moorhouse and Nabekura, 2012). The classical method of recording V_m directly is by using sharp microelectrodes. This approach for small cells has been superseded by the whole cell patch clamp technique which causes less damage to cells than impalement and introduces less noise. The sharp microelectrode method also suffers from the introduction of a shunt resistance (R_s , of the order of 50 - 200 M Ω) component which can effectively be thought of as a ‘short circuit’ or leak current to the bath electrode and has been shown to significantly underestimate V_m in small cells following impalement (Ince et al., 1986). Future experiments using the sharp microelectrode method to compare V_m values with patch clamp recordings would prove useful. In addition to invasive measurements of V_m , use of voltage-sensitive fluorescent dyes would prove insightful since they preserve the contents of the cytosolic compartment. Negatively charged oxonol based dyes such

as DiBAC₄(3) have been used extensively to study slow V_m kinetics in intact cells and a comparison with V_m patch clamp measurements in OvCa cells will help to further address concentration dependent effects of $[Na^+]_i$ on V_m (Baxter et al., 2002; Wolff, Fuks and Chatelain, 2003).

Whole-cell voltage clamp studies on SKOV-3 cells in the absence and presence of amiloride were undertaken, however whole-cell conductances in SKOV-3 cells were very small and voltage steps from a -10 mV holding potential to -100 mV, while demonstrating some inhibition on inward current, were not large enough to prove significant. In considering that amiloride inhibits other Na^+ mediated conductances such as NHE1, ascribing the effects of amiloride induced hyperpolarisation to ENaC inhibition must be treated with caution (Masereel, 2003). Other approaches such as current injection in current clamp mode while monitoring cell input resistance would help to further address this (Odgen, 1994).

Another limitation of this study is the relatively low number of V_m measurements that were undertaken in OvCa_{asc} cell isolates. To date only 4 independent measurements were determined across 3 different OvCa_{asc} derived cells. While cells collectively exhibited a relatively depolarised phenotype, limited conclusions on Na^+ contribution to V_m can be drawn from this investigation. It is likely that there may be differences in growth profiles and invasive capacity between the individual OvCa_{asc} samples. It is thus plausible that OvCa_{asc} samples could exhibit markedly different V_m distributions (Cone, 1971; Binggeli and Weinstein, 1986; Fraser et al., 2005). To date, however, differences in the clonogenic capacity and invasive capacity of OvCa_{asc} samples have not been assessed. It is of note that significant differences between OvCa_{asc} samples in another bioelectric property, galvanotaxis (described in Chapter 6.2.3) have been observed in

this thesis. This highlights the bioelectric heterogeneity between respective samples and the importance of considerably larger population sizes in future investigations involving patient samples.

In addition to the limited sample sizes of V_m measurements in OvCa_{asc}, this study did not investigate V_m values and Na⁺ permeability of OvCa cells derived from the primary tumour site. Fraser et al demonstrated that V_m values in breast cancer were inversely correlated with metastatic potential; highly metastatic MDA-MB-231 cells were \approx twice as depolarised (\approx -20 mV) as weakly metastatic MCF-7 cells (\approx -40 mV) (Fraser et al., 2005). It would thus prove insightful to assess whether V_m values of cell populations enzymatically dissociated from different regions of the primary ovarian tumour exhibit different V_m distributions and indeed, whether any difference exists between paired isolates from the primary site and malignant ascites.

3.3.2 Effects of riluzole on V_m in SKOV-3 and MCF-7 cells

Upon perfusion with riluzole SKOV-3 and MCF-7 cells exhibited a marked hyperpolarisation, though to differing extents. MCF-7 cells strongly hyperpolarised by approximately 40 mV to a value relatively close to E_K , while SKOV-3 cells at a 10-fold higher dose demonstrated only mild hyperpolarisation (5-10 mV).

Riluzole was chosen as a broad modulator of K⁺ channels; it is an activator of K_{Ca} channels, including both K_{Ca}3.1, K_{Ca}2.1, K_{Ca}2.2 and K_{Ca}2.3) (Coleman et al., 2014) channels. It has also been shown to inhibit of K_V11.1 (Pillozzi et al., 2018). Riluzole blocks inactivated Na_V channels at doses \approx 10 fold higher than the highest concentration (10 μ M) used in this study and as such is unlikely to contribute to the V_m hyperpolarisation observed in SKOV-3 and MCF-7 cells (Benoit and Escande, 1991).

There are other reports of riluzole induced hyperpolarisation in tumour cells. Rilu-

zole (10 μM) induced strong hyperpolarisation in the colorectal cancer cell lines HCT-116 and HCT-8 with magnitudes remarkably similar to those observed in MCF-7 cells in this study (Pillozzi et al., 2018). $\text{K}_{\text{Ca}3.1}$ currents have been identified in MCF-7 cells and shown to regulate V_{m} (Ouadid-Ahidouch et al., 2004). Notably, $\text{K}_{\text{Ca}3.1}$ inhibition or knock-down significantly reduced proliferation and induced cell-cycle arrest in the G1 phase; a transition where V_{m} hyperpolarisation is required (Faouzi et al., 2016; Blackiston, McLaughlin and Levin, 2009).

The reason why riluzole yielded a much more moderate hyperpolarisation in SKOV-3 cells relative to MCF-7 cells is not clear. $\text{K}_{\text{Ca}3.1}$ currents have been detected in SKOV-3 cells and identified by molecular methods (Robles-Martínez et al., 2017). Molecular expression of HERG1 has been identified in SKOV-3 cells as part of previous studies in our lab, yet there remains no electrophysiological evidence for functional HERG currents (Asher et al., 2011). It is possible that riluzole is both inhibiting HERG and activating $\text{K}_{\text{Ca}3.1}$, which would result in two opposing effects on V_{m} . Future studies should focus on further characterising the effects on V_{m} using more specific blockers (E-4031) (Asher et al., 2011; Ishii et al., 2003).

In summary, hyperpolarisation of V_{m} via methods independent of blocking Na^+ mediated depolarisation present differing approaches to counteract the sustained depolarisation phenotype in cancer and are promising future avenues of research. Indeed riluzole mediated hyperpolarisation in prostate cancer cell lines has demonstrated promising results in mediating proliferative potential and increased response to platinum therapy when co-administered (Pillozzi et al., 2018; Benavides-Serrato et al., 2020). Due to the heterogeneity of ion channel expression between cancer subtypes and the observations that riluzole is less effective in causing V_{m} hyperpolarisation in OvCa, it is clear that a

cancer specific approach is required (Prevarskaya, Skryma and Shuba, 2010).

3.3.3 Amiloride results in V_m hyperpolarisation in SKOV-3 cells

It was demonstrated that perfusion with amiloride caused a mild hyperpolarisation on V_m of SKOV-3 cells. Other studies consistent with our observations that ENaC contributes to persistent V_m depolarisation in cancer have been reported. For example, inhibition of NG108 hybridoma cells with amiloride resulted in a persistent hyperpolarisation of V_m (O'Donnell and Villereal, 1982). Moreover this effect was abolished in high extracellular K^+ conditions suggesting that the effects of amiloride-induced hyperpolarisation are carried by an inward Na^+ current (O'Donnell and Villereal, 1982).

ENaC channels are present in the apical membranes of numerous epithelia such as in the collecting duct of the nephron, sweat glands, the mesothelium and the respiratory tract (Garty and Palmer, 1997). Typical half-maximal inhibition (IC_{50}) concentrations of amiloride in these tissues however are $\approx 100nM$, values much lower than any observed V_m hyperpolarisation in SKOV-3 cells. Similar concentrations of amiloride to those required here were also required in D54-MG cell lines and primary glioblastoma multiforme cells (Rooj et al., 2012; Ross et al., 2007; Kapoor et al., 2011). Another plausible explanation is that native ENaC channels in SKOV-3 cells are formed of only α and β subunits (McNicholas and Canessa, 1997). McNicholas and Canessa demonstrated that ENaC channels formed of only α and β subunits in *Xenopus* oocyte expression models demonstrated IC_{50} concentration ≈ 20 -fold higher relative to channels formed from α and γ subunits alone (McNicholas and Canessa, 1997). More potent analogues of amiloride, namely benzamil and phenamil have been characterised and thus it is necessary to assess whether they effect a similar response. Furthermore future studies employing ENaC- α knock-down approaches will prove insightful in assessing the extent

to which ENaC conductances contribute to the V_m in OvCa.

3.4 Conclusions

This study has demonstrated that OvCa cells possess a relatively high permeability to Na^+ that significantly contributes to the depolarised phenotype exhibited in the disease. What is clear however is that ENaC currents alone only partially account for P_{Na^+} . While this may be in part due to the poor inhibition by amiloride at high doses as observed here and in other tumour types (discussed above), it is also plausible that other as yet unidentified conductances contribute significantly to increased P_{Na^+} .

A relatively small depolarisation of V_m can lead to significant functional consequences. Depolarisation of V_m has significant consequences on cell behaviour and tumour hallmarks such as differentiation, proliferation directed cell migration and evasion of apoptosis (Yang and Brackenbury, 2013; Sundelacruz, Levin and Kaplan, 2009; McCaig and Zhao, 1997). ENaC depolarises OvCa cells and inhibition of this conductance modulates tumour properties. In mice with hepatoma or mammary adenocarcinoma implanted subcutaneously, injection with amiloride reduced tumour area by 50% and interestingly also resulted in concurrent reductions in cytosolic $[\text{Na}^+]_i$ concentrations (Sparks et al., 1983). It is suggestive therefore that ENaC targeting may prove beneficial in studies of other cancers.

Taken together it is demonstrated for the first time that a persistent Na^+ permeability, in part mediated by ENaC, contributes to a relatively high degree to sustain the depolarised phenotype observed in an OvCa cell line and indeed in primary OvCa_{asc} cells. The implications of V_m alterations in tumour cell behaviour span multiple hallmarks, and subsequent chapters focus on the evidence for Na^+ and ENaC mediated

depolarisation in modulating the OvCa phenotype.

Chapter 4

The effects of Na^+ flux on proliferation in OvCa cells

4.1 Introduction

It has long been known that V_m is strongly associated with proliferative capacity in numerous mammalian cell types and influences important pathways in cell division: DNA synthesis and mitosis and critically, progression through the cell cycle (Binggeli and Weinstein, 1986; Blackiston, McLaughlin and Levin, 2009; Sundelacruz, Levin and Kaplan, 2009). Terminally differentiated cells with little or no mitotic potential generally exhibit a pronounced hyperpolarised phenotype (≈ -90 to -70 mV). Conversely, cells with a high replicative capacity such as embryonic cells and indeed cancer cells generally exhibit a markedly depolarised phenotype. Cone first posited in the 1970's that these observations may be more than phenotypic and that in fact there exists a functional relationship between V_m and mitotic potential. Indeed, V_m hyperpolarisation has been shown to block mitotic capacity in a reversible manner (Cone, 1971).

Conversely, hyperpolarisation of mature neurons *in vitro* has been shown to stimulate mitosis (Cone and Cone, 1976).

Cancer cells, undifferentiated cells and rapidly proliferating cells possess a depolarised V_m when compared to their non-malignant counterparts and this has been proposed as a ‘sustaining proliferative signal’ (refer to section 1.6). V_m changes are also associated with progression through the cell cycle. Generally, cells are required to undergo hyperpolarisation at the G1/S checkpoint to progress into S phase (Orr, Yoshikawa-Fukada and Ebert, 1972).

In addition to their pivotal role in modulating V_m and intra and extracellular ion concentrations, ion channels have been shown to play a critical role in the modulation of cell volume (V_{cell}). Through modulation of intracellular monovalent ion concentrations, subsequent changes in cytosolic tonicity result in osmotically obliged water fluxes facilitated by aquaporins and ion channels act to alter V_{cell} . Numerous investigations have implicated the role of ion channels in the dysregulated control of cell cycle progression in cancer with those for ENaC already described in Chapter 1 section 1.6.4. There are no known studies assessing whether alterations in ENaC activity may perturb V_{cell} changes in OvCa and it is important that this be addressed.

Subsequently, this study aimed to assess the role of ENaC and Na^+ in modulating cell proliferation in OvCa. To address this, it was first assessed whether treatment of SKOV-3 and OVCAR-3 cells with amiloride modulates cell proliferation. Next, it was evaluated whether inhibition of Na_V channels with phenytoin modulates proliferation. It was then assessed whether increased $[Na^+]_e$ serves to modulate proliferative capacity in OvCa cell lines. Finally it was assessed whether ENaC regulates V_{cell} changes in proliferating cells.

4.2 Results

4.2.1 Effects of amiloride on proliferation of OvCa cell lines

The effects of amiloride on cell proliferation was assessed using the resazurin reduction assay as an index of the number of viable cells. Cells were seeded at 5×10^3 cells/well and incubated over 72 hours in the presence of amiloride (0.1 - 100 μM) or vehicle (0.1% DMSO) and quantified as percentage proliferation relative to control (refer to section 2.7). All experiments were repeated a minimum of five times independently with each concentration carried out in replicates of four. In vehicle control conditions cells exhibited a similar growth profile to cells cultured in the presence of CGM alone ('no drug', refer to Figure 4-1 A, 3.4 % [-10.6,17.7] reduction relative to control, $p > 0.05$). Amiloride at low doses (0.1 & 1 μM) had no effect on cell proliferation over the observed time course in SKOV-3 or OVCAR-3 cells. In SKOV-3 cells, higher doses of amiloride resulted in a significant reduction in the number of viable cells detectable 24 hours post treatment and persisting over the duration of the experiment, resulting in a reduction relative to control at 72 hours post treatment of 17.7 % [5.9,29.6], 36.6 % [23.9,49.2] and 90.3 % [79.0,101.6] at 10, 50 & 100 μM (mean 95% [lower CI, upper CI], $n = 6$) respectively (Figure 4-1A) corresponding to an IC_{50} of approximately 58 μM (Table 4.1). Amiloride treatment in OVCAR-3 cells also resulted in a significant reduction in the number of viable cells at higher doses (Figure 4-1 B). However, this was only detectable 48 hours post-treatment and considerably less potent than as observed in SKOV-3 cells: reduction relative to control 72 hours post-treatment of 28.7 % [9.5,47.9] and 47.7 % [28.5,66.9] at 50 and 100 μM ($n=5$) respectively and a subsequent IC_{25} of approximately 38 μM (see Table 4.1).

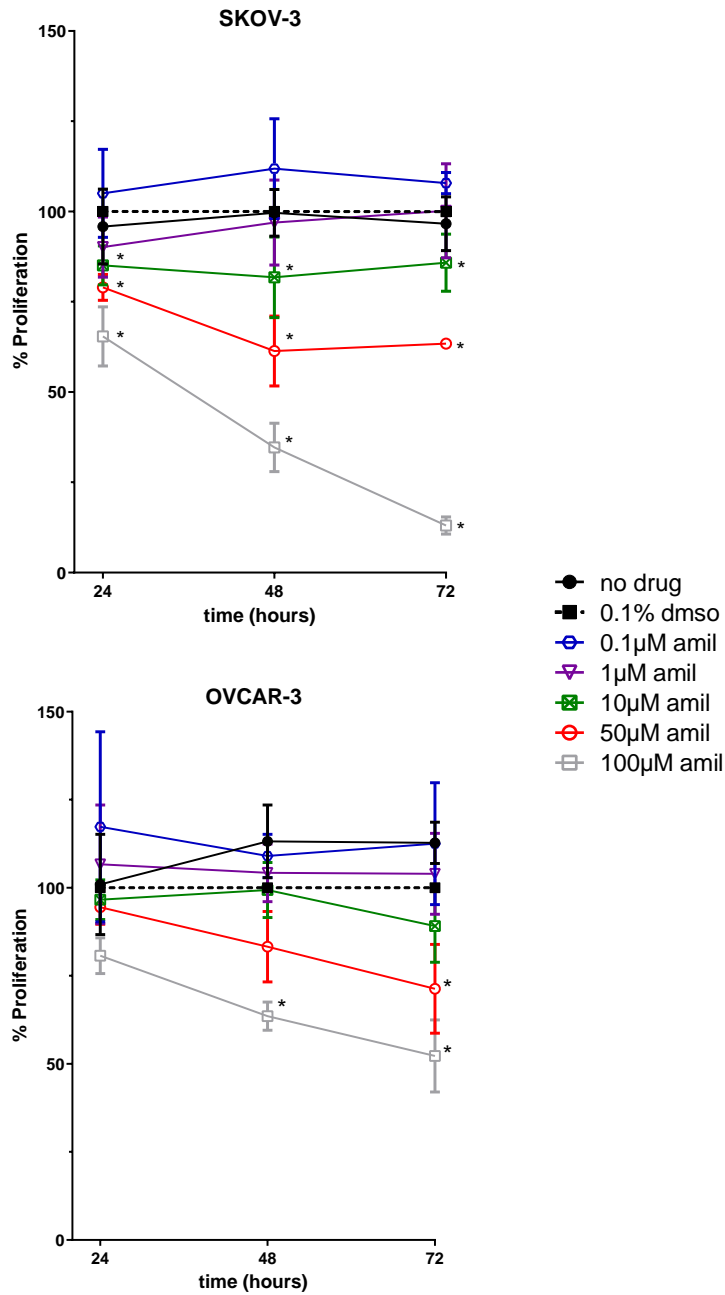


Figure 4-1: Cell proliferation of SKOV-3 and OVCAR-3 cell lines over 72 hours following treatment with amiloride in SKOV-3 (A) and OVCAR-3 (B) cells. Error bars represent the mean \pm SD of 6 and 5 independent experiments with each condition carried out in replicates of 4 in SKOV-3 and OVCAR-3 cells respectively. Where error bars are not visible they are smaller than size of the data point. * denotes significant difference relative to control (0.1 % DMSO) as assessed by one-way ANOVA with Dunnett's post-hoc test.

Cell line	Time (h)	IC ₂₅ (μ M)	IC ₅₀ (μ M)	r^2
SKOV-3	48	20 [12, 33]	63 [47, 84]	0.83
	72	42 [36, 50]	58 [52, 66]	0.93
OVCAR-3	48	70 [57, 86]	142 [100, 202]	0.80
	72	38 [23, 65]	113 [69, 186]	0.72

Data are presented as mean and 95% CI [lower limit, upper limit]
red values indicate those extrapolated out of range

Table 4.1: Summary of cell proliferation parameters in SKOV-3 and OVCAR-3 cell lines following treatment with amiloride

In SKOV-3 cells, incubation with amiloride demonstrated a dose dependent increase in cytotoxicity observed at 72 hours as assessed by SYTOX green (see section 2.9). When cultured in the presence of vehicle (0.1 % DMSO), relative cell cytotoxicity when compared to complete cell lysis was 15.0 ± 3.0 % (mean \pm SD, $n = 4$) and there was no observable difference when cultured in the presence of 0.1 and 1 μ M amiloride respectively ($p > 0.05$, one-way ANOVA, Dunnet's post-hoc test). When treated at doses of 10 and 100 μ M amiloride, cells exhibited a significant increase in cytotoxicity to 35.8 ± 14.8 % and 48.6 ± 17.6 % ($n = 4$, $p < 0.05$) respectively (Figure 4-2). This trend of increased cytotoxicity was also observed at 50 μ M amiloride, however, it was not significantly different to control. In contrast, OVCAR-3 cells treated with amiloride showed no significant difference in cytotoxicity relative to control, with a considerably lower basal cytotoxicity in control conditions (3.0 ± 0.3 %, $p > 0.05$, Figure 4-2).

Since SKOV-3 cells treated with amiloride demonstrated a dose-dependent cytotoxicity profile at 72 hours and conversely, OVCAR-3 cells exhibited no increase relative to control, it was next assessed whether differential activation of apoptotic pathways between the two models could in part explain this observation. SKOV-3 cells were seeded in T25 flasks in triplicate and cultured in the presence of control (0.1 % DMSO) or amiloride, trypsinised at 48 hours post treatment, washed and then stained with an-

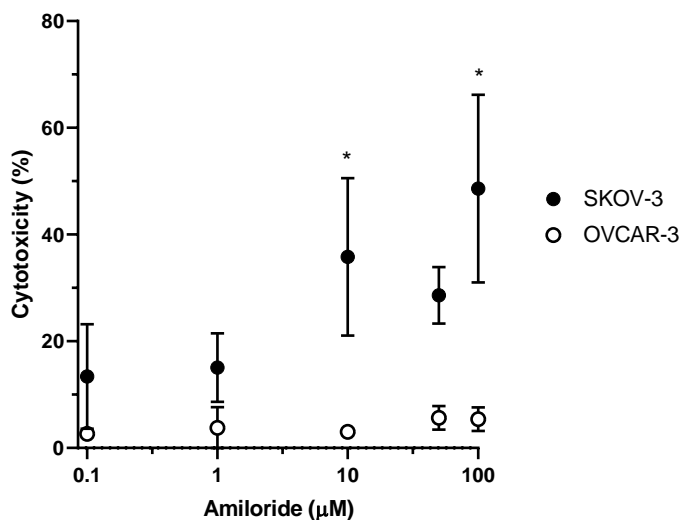


Figure 4-2: Cell cytotoxicity of SKOV-3 and OVCAR-3 cell lines 72 hours after treatment with amiloride. Percentage cytotoxicity is defined as the RFU in the presence of treatment divided by the RFU when cells were treatment with Triton X-100 to achieve complete cell lysis. Error bars represent the mean \pm SD of 4 independent experiments. * denotes significant difference ($p < 0.05$) relative to control condition (.1 % DMSO) as assessed by one-way ANOVA with Dunnet's post-hoc test.

nexin V and propidium iodide (PI) to differentiate between cells undergoing apoptosis and dead cells (refer to section 2.12.2). Since lower doses of amiloride (0.1 and 10 μ M) demonstrated no significant reduction in cell proliferation in SKOV-3 cells, treatments chosen for assessment were 10, 50 and 100 μ M.

Following treatment with 0.1 % DMSO for 48 hours, 88.10 ± 0.89 % (mean \pm SD % of total gated cells) of cells were viable. A further 9.41 ± 0.85 % stained for annexin V alone, indicating the induction of apoptotic pathways (Figure 4-3). There was minimal dual staining for PI and annexin V (1.16 ± 0.57 % respectively), indicating that vehicle treatment for 48 hours demonstrated a minimal necrotic effect or likelihood of detection of cells in late apoptotic stages. Amiloride at the lowest tested dose of 10 μ M demonstrated no significant decrease in the viable cell fraction (88.41 ± 2.25) or apoptotic fractions (9.50 ± 0.93). When treated with 50 μ M amiloride however, the

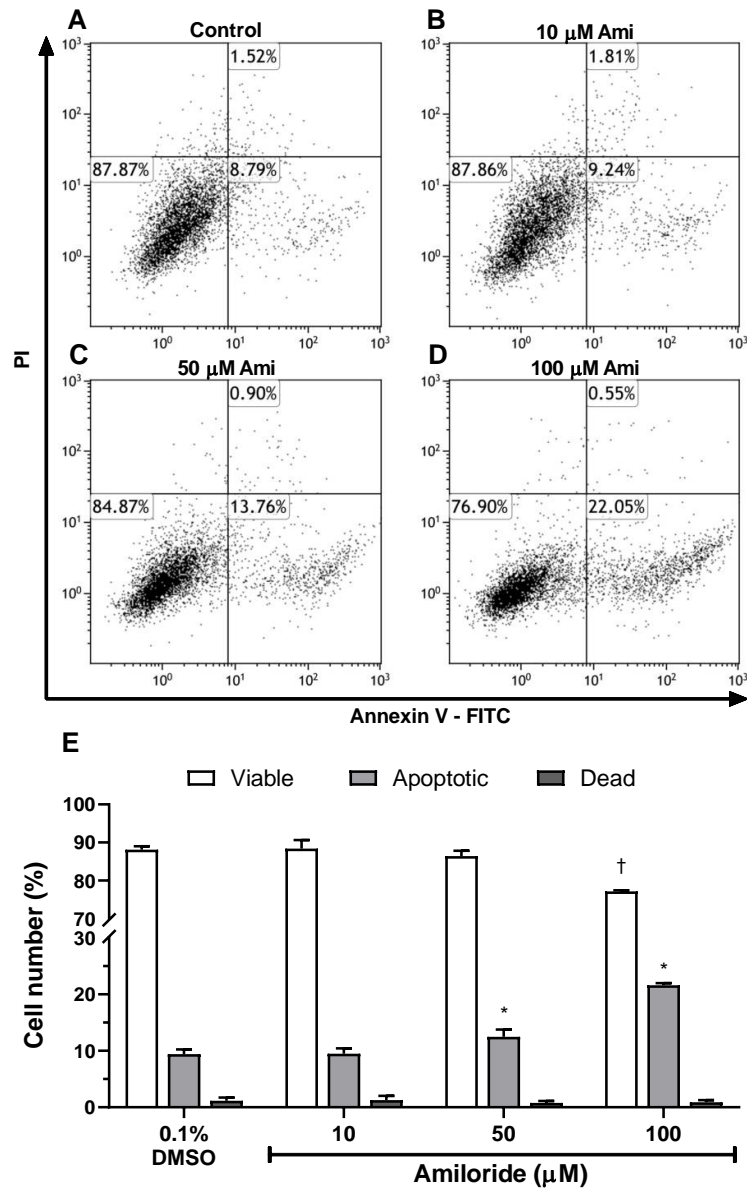


Figure 4-3: Assessment of apoptosis by flow cytometry in SKOV-3 cells following treatment with amiloride (10 - 100 μM) for 48 hours. Cells were stained with FITC-conjugated annexin-V (x-axis) to identify cells undergoing apoptosis and co-stained with propidium iodide (PI) (y-axis) which describes cells with compromised membranes that are necrotic or in the late stages of apoptosis. The lower left quadrant indicates viable cells, the lower right represents annexin-V positive/PI negative cells and indicates cells undergoing early apoptosis. The upper right quadrant denotes annexin-V positive/PI positive cells and thus indicates late apoptosis or necrotic (dead) cells. Percentages in each quadrant represent the % fraction of total gated cells (A - D) Representative scatter plots when cultured in the presence of 0.1 % DMSO, 10, 50 and 100 μM amiloride respectively. (E) The percentage of viable, apoptotic and dead cells relative to the total number of gated cells following treatment with vehicle or amiloride. Error bars denote mean \pm SD of 3 individual experiments. † denotes significant difference relative to control conditions in viable cell population. * denotes significant difference relative to control conditions in apoptotic cell population. Significance was set at $p < 0.05$ and assessed by two-way ANOVA with Dunnett's post-hoc test.

early apoptotic fraction exhibited a mild but significant increase to 12.50 ± 1.27 % ($p < 0.05$, two-way ANOVA, Dunnett's post-hoc test) with no detectable difference in the viable fraction relative to control. This effect was further enhanced following treatment with $100 \mu\text{M}$ amiloride, where the apoptotic fraction was observed to increase to 21.62 ± 0.37 , with a corresponding decrease in viable fraction to 77.18 ± 0.26 , thus demonstrating a dose dependent effect of amiloride on induction of apoptosis.

4.2.2 Effects of phenytoin on proliferation of OvCa cell lines

In observing that ENaC inhibition resulted in a reduction in cell proliferation in SKOV-3 and OVCAR-3 cells it was next tested whether voltage gated Na^+ (Na_V) channel inhibition also demonstrated a role for growth modulation in OvCa cell lines. Using the same approach as above, a resazurin reduction assay was performed over 72 hours in the presence of phenytoin (5 - $200 \mu\text{M}$), an inhibitor of Na_V channels (Nelson et al., 2015). In SKOV-3 cells, treatment with phenytoin at doses of 5 and $50 \mu\text{M}$ respectively showed no difference in cell proliferation relative to control over the observed time. When treated with 100 and $200 \mu\text{M}$ phenytoin, significant reductions in cell proliferation were observable 72 and 48 hours post treatment respectively, resulting in a reduction relative to control at 72 hours of 25.4 [6.3, 44.4] % (mean [95 % lower CI, upper CI]) and 49.9 [30.1, 68.9] % for 100 and $200 \mu\text{M}$ respectively ($n = 6$, $p < 0.05$, one-way ANOVA with Dunnett's post-hoc test), corresponding to an IC_{50} of approximately $148 \mu\text{M}$ (Table 4-5). In contrast, in OVCAR-3 cells, phenytoin treatment resulted in a reduced effect on cell proliferation with a significant reduction only observable at 72 hours post treatment at higher doses of drug: 14.5 [0.9, 28.1] % and 23.6 [10,37.2] % reduction relative to control at 100 and $200 \mu\text{M}$ respectively ($p < 0.05$).

In observing that treatment with phenytoin reduced the number of viable cells in

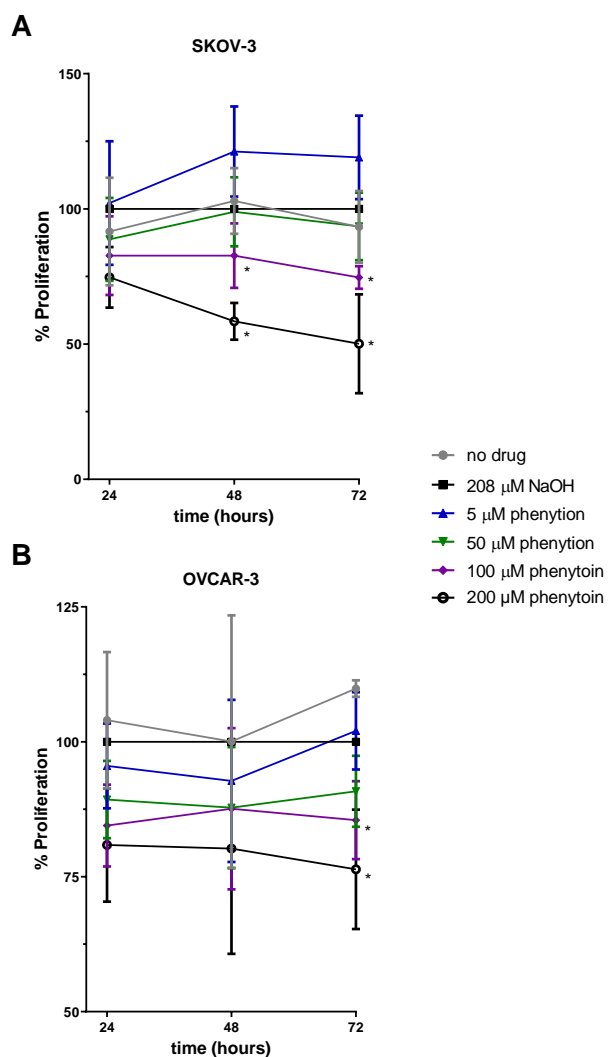


Figure 4-4: Cell proliferation of SKOV-3 and OVCAR-3 cell lines over 72 hours following treatment with phenytoin in SKOV-3 (A) and OVCAR-3 (B) cells. Error bars represent the mean \pm SD of 6 and 5 independent experiments in SKOV-3 and OVCAR-3 cells respectively. Where error bars are not visible they are smaller than size of the data point. * denotes significant difference relative to control as assessed by one-way ANOVA with Dunnett's post-hoc test.

SKOV-3 and OVCAR-3 cells, it was again sought to determine to what extent this was due to cytostatic or cytotoxic effects of the drug using SYTOX green as described above. In SKOV-3 cells, when cultured in the presence of vehicle (208 μ M NaOH), relative cell cytotoxicity when compared to complete cell lysis (0.2 % (vol/vol) Triton X-100) was 19.5 ± 6.6 % (mean \pm SD, n = 4) 72 hours post-treatment (Figure 4-6). When treated

Cell line	Time (h)	IC ₂₅ (μM)	IC ₅₀ (μM)	r ²
SKOV-3	48	68 [39, 121]	184 [136, 250]	0.80
	72	56 [30, 105]	148 [108, 203]	0.80
OVCAR-3	72	285 [136, 596]	-	0.72

Data are presented as mean and 95% CI [lower limit, upper limit]
values indicate those extrapolated out of range

Figure 4-5: Summary of cell proliferation parameters in SKOV-3 and OVCAR-3 cell lines following treatment with phenytoin

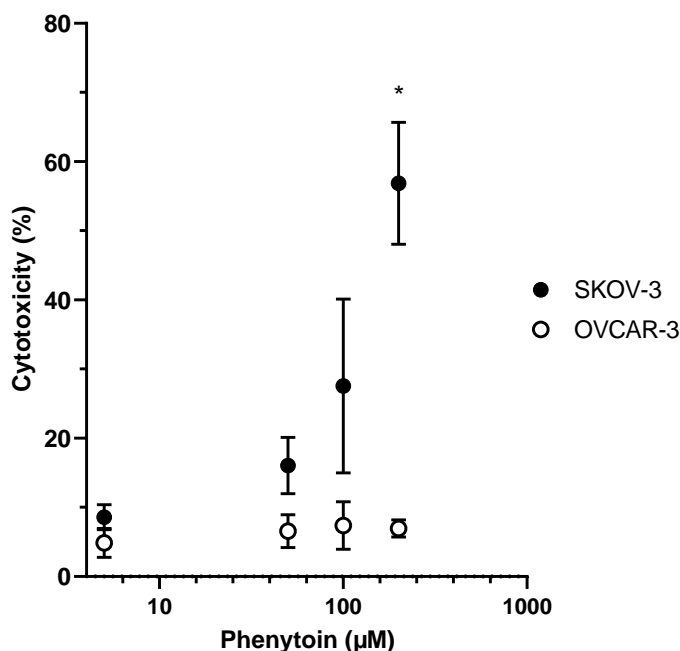


Figure 4-6: Cell cytotoxicity of SKOV-3 and OVCAR-3 cell lines 72 hours after treatment with phenytoin. Percentage cytotoxicity is defined as the RFU in the presence of treatment divided by the RFU when cells were treated with Triton X-100 to achieve complete cell lysis. Error bars represent the mean \pm SD of 4 individual experiments. * denotes significant difference ($p < 0.05$) relative to control condition as assessed by one-way ANOVA with Dunnett's post-hoc test.

with phenytoin (5 - 200 μM), SKOV-3 cells exhibited a trend of dose-dependent increase in cytotoxicity at 72 hours. However, this was only significantly increased at the highest dose of 200 μM, with a 37.4 [22.5, 52.3] % (mean [lower 95% CI, upper 95% CI] increase relative to control (n = 4, $p < 0.5$, one-way ANOVA, Dunnett's post-hoc test). However, OVCAR-3 cells demonstrated no significant difference relative to vehicle over 72 hours;

3.9 ± 2.1 ($n = 4$) in $208 \mu\text{M NaOH}$, a value similar to that observed when supplemented with amiloride.

4.2.3 Effects of Na^+ gradient on proliferation

Given the observation that amiloride and phenamil inhibited proliferation, potentially via Na^+ channels of OvCa cell lines, it was then assessed whether the alteration of Na^+ influx directly was sufficient to modulate proliferative capacity. This was assessed by the direct addition of NaCl, ChCl or mannitol to the culture medium and assessed over 72 hours using the resazurin reduction assay as described above (refer to section 2.8) (5 independent experiments of each condition in triplicate). In SKOV-3 cells, CGM supplemented with 15 or 30 mM NaCl resulted in a significant reduction in cell proliferation by -45.3% [$-24.2, -66.3$] and -54.9% [$-19.0, -90.8$] respectively relative to control at 72 hours post-treatment ($p < 0.05$ two-way ANOVA, Dunnett's post-hoc test, $n=5$). There was no detectable dose-dependent response in NaCl addition at 72 hours, however, a small reduction in proliferation in the presence of 30 mM NaCl was detectable as early as 24 hours post treatment (-14.5% [$-0.5, -29.6$] change relative to control, $p < 0.05$) (see Figure 4-7). Conversely, treatment of OVCAR-3 cells with NaCl resulted in a mild but significant increase in proliferation over the observed time. A trend of increased proliferation was evident but not statistically significant until 72 hours post treatment, with a similar increase observed upon addition of either 15 or 30 mM NaCl; 15 mM: $+26.1\%$ [$+7.4, +44.8$], 30 mM: $+26.8\%$ [$+8.2, +45.5$] change relative to control.

Treatment of cell lines with equimolar concentrations (relative to NaCl treatments) of choline chloride, a condition whereby Na^+ is replaced with an impermeant ion and Cl^- is preserved, also resulted in a difference in proliferation of the two tested cell lines.

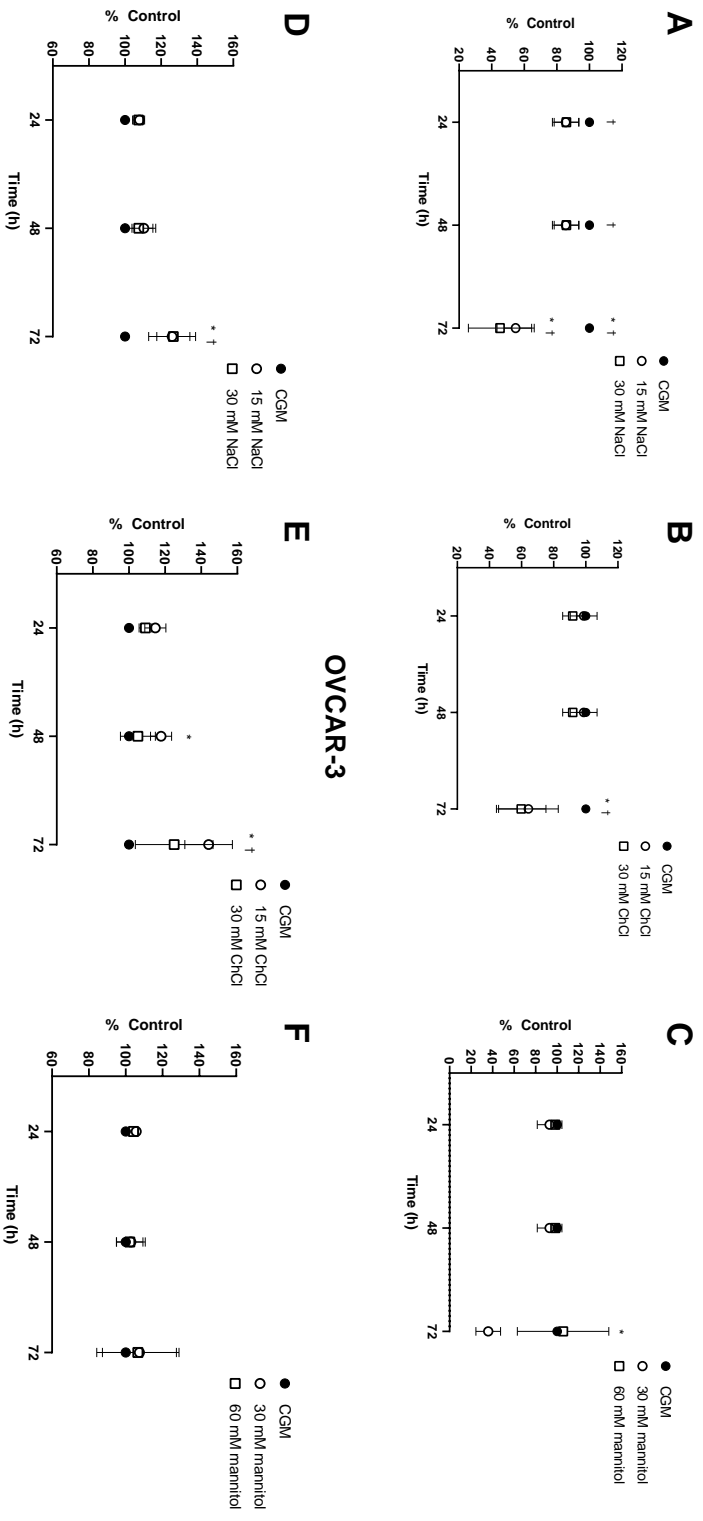


Figure 4-7: Assessment of the role of $[Na^+]_e$ on the proliferation rate of SKOV-3 and OVCAR-3 cells. SKOV-3 and OVCAR-3 cells were treated with 15 and 30 mM NaCl (A and D respectively), 15 and 30 mM ChCl (B and E respectively) or 30 mM and 60 mM mannitol (C and F respectively). Error bars represent the mean \pm SD of 5 independent experiments with each condition carried out in triplicate. * denotes significant difference ($p < 0.05$) relative to control condition (CGM) at the same time point following treatment with 15 mM NaCl, 15 mM ChCl or 30 mM mannitol respectively. † denotes significant difference ($p < 0.05$) relative to control condition (CGM) at the same time point following treatment with 30 mM NaCl, 30 mM ChCl or 60 mM mannitol respectively. Assessed by two-way ANOVA with Dunnett's post-hoc test.

In SKOV-3 cells, treatment with ChCl resulted in a similar attenuation in proliferation as observed when the CGM was supplemented with NaCl, though the extent of growth inhibition was marginally lower; 15 mM ChCl: - 35.7 % [- 1.4, - 70.0], 30 mM ChCl: - 40.2 % [- 11.8, -68.6] relative to control, with no significant dose-dependent difference observable. In contrast, treatment of OVCAR-3 cells with 15 or 30 mM ChCl resulted in an increase in cell proliferation relative to control conditions of + 44.1 % [+ 25.4, + 62.8] and + 25.0 % [+ 6.6, + 43.7] respectively; a response markedly similar to that exhibited by NaCl addition.

In order to assess to what extent changes in proliferation were due to osmolyte induced hypertonicity, mannitol was added to CGM at twice the concentration in mM of the respective concentrations of NaCl and ChCl respectively (refer to 2.8). In SKOV-3 cells, no difference in resazurin intensity was detected relative to control condition upon addition of 30 or 60 mM mannitol over 48 hours. However, at 72 hours post treatment, 30 mM mannitol resulted in a marked reduction in cell proliferation; - 64.0 % [- 42.7, - 85.3] change relative to respective control. In contrast, addition of 60 mM mannitol demonstrated no detectable difference relative to control conditions.

4.2.4 Effects of amiloride treatment on V_{cell}

Since amiloride treatment of OvCa cell lines resulted in reduced proliferation, it was next assessed whether these effects were mediated by modulating V_{cell} . Effects of amiloride on V_{cell} were assessed in log-phase proliferating SKOV-3 cells after 48 hours. An incubation time of 48 hours was chosen since a relatively large fraction of cells were still viable following treatment with amiloride. Mean V_{cell} in control conditions (0.1 % DMSO) was 233 ± 58 fl. Treatment with amiloride at 10 and 50 μ M resulted in volumes of 229 ± 51 and 230 ± 55 fl respectively, with no significant difference relative

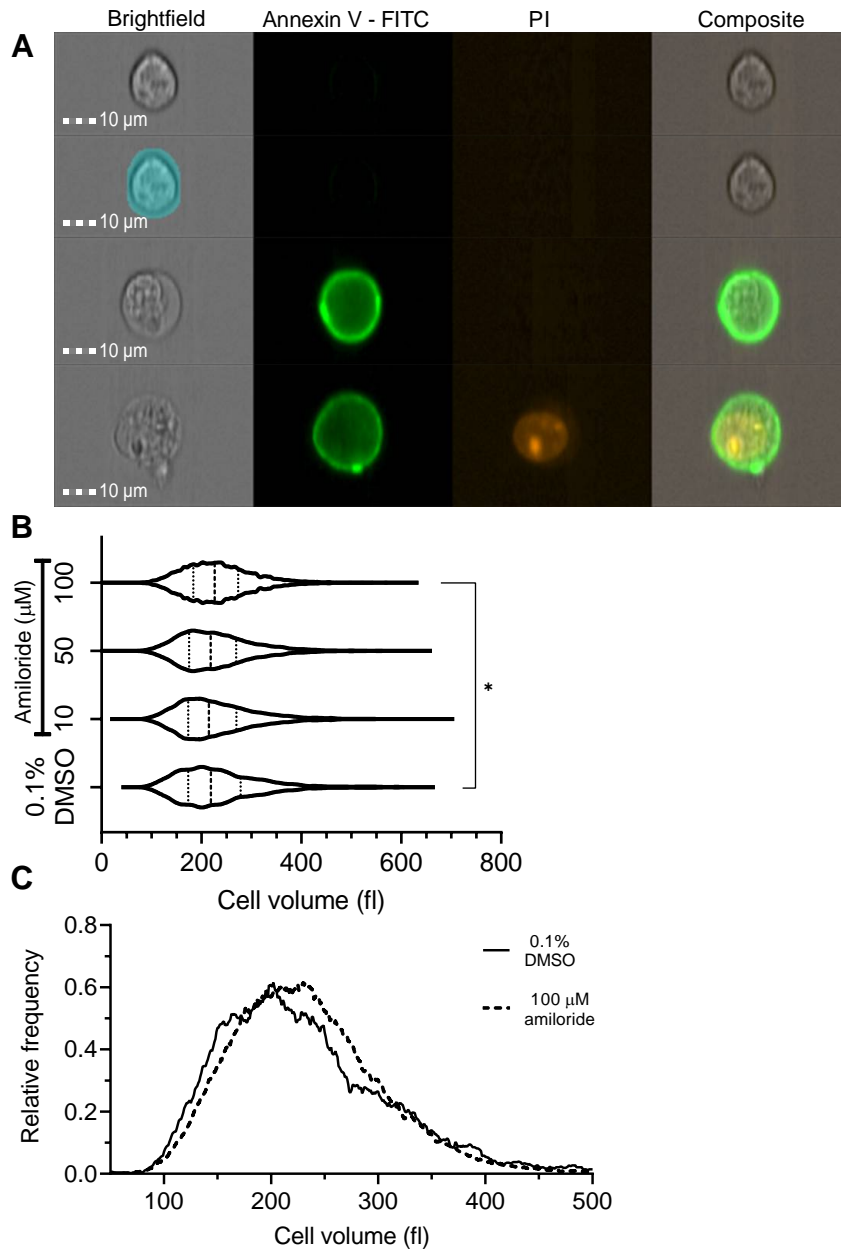


Figure 4-8: Cell volume determination of SKOV-3 cell lines 48 hours post-treatment with amiloride (10 - 100 μM) (A) Measurement of cell diameter and discrimination of apoptotic and dead cell fractions. Top to bottom: Example of a gated viable cell demonstrating no staining for Annexin V, or propidium iodide (PI), below, representation of same cell with mask (blue) representing the 2D cell area in pixels. Lower 2: a cell undergoing apoptosis and a necrotic / late apoptotic cell. (B) Violin plot of cell volume populations in fl. Thin and thick dashed lines denote IQR and mean respectively. * denotes significant change relative to control of 3 independent experiments with a minimum of 1000 events recorded per experiment ($p < 0.05$, tested by Kruskal-Wallis with Dunn's post-hoc test). (C) Relative frequency distributions of cell volume in the presence of control (0.1 % DMSO) and 100 μM amiloride treatment. Scale bar, 10 μm

to control as assessed by Kruskal-Wallis with Dunn's multiple comparison test ($p > 0.05$, $n=3$). Treatment with 100 μM amiloride however, resulted in a small increase relative to control conditions to 235 ± 45 fl ($p < 0.05$), however this equates to a mean V_{cell} change of $\approx 1\%$ relative to control conditions and significance was likely due to the high sensitivity of non-parametric rank tests and the high sample size (Vargha, Delaney and Vargha, 1998).

4.3 Discussion

Here, evidence for a functional role of the epithelial Na^+ channel in modulating growth in OvCa is presented for the first time. Treatment of OvCa ascites derived cell lines with amiloride modulates proliferation. In addition, Na_V channel inhibition also reduces OvCa proliferation. Furthermore, mild increases in $[\text{Na}^+]_e$ yielded a reduction in the rate of proliferation of SKOV-3 cells and conversely a mild increase in OVCAR-3 cells. It was also demonstrated that ENaC does not serve to modulate V_{cell} in proliferating SKOV-3 cells.

4.3.1 ENaC inhibition reduces proliferation in OvCa cell lines

ENaC function has been intensively investigated in polarised epithelia, notably in the principal cells of the distal nephron, bladder and lung airway, and in ducts of sweat glands, as a critical element in Na^+ transport across the epithelial layers and subsequent modulator of osmoregulation (Garty and Palmer, 1997; Bhalla and Hallows, 2008). There have been a very limited number of studies of ENaC in cancer and none in ovarian cancer (Rooj et al., 2012; Bondarava et al., 2009).

The results of our *in vitro* experiments suggest that ENaC functionally modulates the proliferation of ascites-derived OvCa cells, since blocking ENaC channels with the

channel selective blocker amiloride reduced the number of cells progressing through cell division. Previous work, pioneered by seminal studies undertaken by Clarence D. Cone established a direct link between mitotic potential and the degree of V_m hyperpolarisation (Cone, 1971). Subsequent studies revealed that alterations in V_m with proliferative activity served as a functional regulator of proliferative capacity and not merely as an observational correlate in multiple cell types (Cone, 1971; Cone and Cone, 1976). While changes in V_m occur through the cell cycle, tumourigenic cells in multiple cancer types also demonstrate changes in V_m throughout cell cycle checkpoints but, on the whole, maintain a more depolarised phenotype than their non-malignant counterparts (Wonderlin, Woodfork and Strobl, 1995; Marino et al., 1994). Importantly, under normal electrochemical gradients, as is thought to occur in the fluid of malignant ascites, ENaC transports Na^+ into the cell with the capacity to affect membrane depolarisation. Amiloride treatment of SKOV-3 cells resulted in a strong inhibition in cell proliferation at higher concentrations (Rooj et al., 2012; Bondarava et al., 2009). SKOV-3 cells have a depolarised V_m much closer to the reversal potential for Na^+ than many known mammalian cell types (≈ -2 to -10 mV, refer to chapter 3). Patch clamp experiments (see section 3.3.3) showed that amiloride induced a mild hyperpolarisation of V_m in SKOV-3 cells. The data presented here therefore suggest that the constant influx of Na^+ may contribute to a depolarisation in membrane potential required to maintain sustained proliferation. It is important to note however that a significant fraction of cells underwent apoptosis when treated with amiloride at higher doses, and as such the findings should be interpreted with caution. Similar observations were also made in OVCAR-3 cells. However, the total reduction in proliferation was somewhat lower. This may be in part due to increased doubling time of OVCAR-3 cells. In order

to attribute this effect to a reduction in depolarisation induced sustained proliferation, it is necessary to determine V_m values in OVCAR-3 cells and thus future studies must address this.

The findings presented here are consistent with those observed in other tumour types. In U87MG, D54-MG and primary glioblastoma multiforme cells, treatment with benzamil (an amiloride derivative) reduced cell proliferation and demonstrated a reduction in inward Na^+ currents. Notably, their results were very similar when cells were cultured in low- Na^+ medium, further supporting the contributory role of Na^+ induced depolarisation (Rooj et al., 2012). Other studies in multiple myeloma cell lines demonstrated similar results: H929, and JJn3 cells treated with amiloride (100uM to 1mM) resulted in a significant reduction in cell proliferation detectable at 48 hours. Amiloride treatment also induced apoptosis in a dose dependent manner (Rojas et al., 2017).

While amiloride has been widely characterised as a selective inhibitor of ENaC it is also known to inhibit NHE antiporters (Teiwes and Toto, 2007). Reported NHE1 IC_{50} values for amiloride vary widely, in studies conducted in low $[\text{Na}^+]_e$ values vary between 5 - 50 μM , although in the presence of physiological $[\text{Na}^+]_e$ values of 1 mM have been reported (Teiwes and Toto, 2007). At the higher treatment concentrations used in this study it is possible that amiloride is exerting an inhibitory effect on NHE1. NHE antiporters have been widely reported to be overexpressed in cancer and inhibition with pharmacological blockers results in attenuated proliferation in the gastric adenocarcinoma cell line, MKN28 and small cell lung cancer SCLC H446/CDDP cells (Hosogi et al., 2012; Li et al., 2009). Moreover inhibition of NHE in SKOV-3 and CAOV-3 OvCa cell lines resulted in a significant reduction in proliferation (Corradi

and Wallert, 2020). The IC_{50} value for NHE1 of the amiloride derivative benzamil is $150 \mu\text{M}$, conversely however the IC_{50} for ENaC is $\approx 400 \text{ nM}$ (xin Zhuang et al., 1984; McNicholas and Canessa, 1997). As such future approaches assessing the effect of ENaC on OvCa proliferation using benzamil as a more selective inhibitor of ENaC would prove insightful.

There were differential effects of amiloride on the extent of necrotic cells as indicated by SYTOX green. No significant dose-dependent effect of amiloride was observed in OVCAR-3 cells despite a reduction in proliferation. Conversely, SKOV-3 cells exhibited a dose dependent increase in necrotic signal, which could be in part attributed to a corresponding dose dependent increased extent of apoptosis. ENaC inhibition by amiloride in glioma cell lines and primary isolates has been shown to increase accumulation of cells in G0/G1 phase, and resulted in a reduction of cells in S and G2/M (Rooj et al., 2012). Conversely in HepG2 cells, amiloride treatment resulted in an increase in the number of cells at the G2 transition (Bondarava et al., 2009). One possible explanation of the observed differential effects of amiloride on the cell cycle lies in the consideration that, prior to entering G1 or following transition through G2 into M, V_m is depolarised (Boonstra et al., 1981; Sachs, Stambrook and Ebert, 1974). Thus, in SKOV-3 cells that exhibit a significantly higher rate of proliferation and thus are much more likely to enter into the cell cycle, it is plausible that amiloride blockade of depolarisation may also result in an accumulation of cells at G2/M, and account for the increased apoptotic effect observed. It is noteworthy that increased Na^+ has been observed immediately prior to G2 and this lends further weight to the hypothesis that Na^+ plays a role in G2 transition (Boonstra et al., 1981). In OVCAR-3 cells it may be that the persistent contribution of Na^+ -mediated depolarisation is less, and that ENaC acts in

a permissive manner to allow entry into the cell cycle. Thus it is plausible that the cell may be held at G0/G1, which would account for the reduced and practically absent increase in cell death as assessed by SYTOX green. A similar explanation for ENaC mediated entry into the cell cycle has been posited in adult neural stem cells. ENaC was shown to be a key regulator of adult neurogenesis and exhibited greater expression with increased stemness (Petrik et al., 2018). Indeed, neuronal stem cells (NSCs) of the mouse neuronal subependymal zone (SEZ) demonstrated $\approx 80\%$ positivity for ENaC- α , whereas in neuroblasts it was only $\approx 20\%$. Moreover, inhibition with benamil, or following ENaC- α knock down, resulted in a 2-fold reduction in the number of cell divisions (Petrik et al., 2018). It is hard to conclude further whether this a viable explanation unless it is assessed whether differential ENaC mediated conductances manifest throughout the cell cycle. Further work would take an electrophysiological approach and measure ENaC mediated conductances after cell cycle synchronisation at different checkpoints in the absence and presence of amiloride, in a manner similar to that performed by Wonderlin et al (Wonderlin, Woodfork and Strobl, 1995).

Since it was hypothesised that ENaC activity facilitated a persistent Na-mediated depolarisation that served to sustain proliferative capacity in OvCa cells, it was next determined whether increasing $[\text{Na}^+]_e$ would serve to increase proliferative capacity. Interestingly, differential results were observed between cell lines. OVCAR-3 cells demonstrated a mild increase in proliferation when cultured in elevated $[\text{Na}^+]_e$. Increasing $[\text{Na}^+]_e$ by 30 mM would only serve to mildly increase E_{Na} , but may constitute the necessary V_m depolarisation required to enter the cell cycle. Indeed the proliferation rate was observed to be stable when NaCl was further increased from 15 to 30 mM. Increased proliferation in supraphysiological $[\text{Na}^+]_e$ in vascular smooth muscle cells has

also been observed (Wu et al., 2016). Conversely, SKOV-3 proliferation rates dropped substantially in elevated $[\text{Na}^+]_e$. One possible explanation of this may lie in the observation that V_m values reported here in SKOV-3 cells are one of the most depolarised phenotypes recorded (Binggeli and Weinstein, 1986). Successful cell cycle transition relies on significant hyperpolarisation between G1/S, and a persistent albeit small Na^+ facilitated depolarisation may impede this transition. Cell cycle analysis in high $[\text{Na}^+]_e$ environments would provide further insight and must subsequently be addressed. Alteration in V_m also serves to regulate Ca^{2+} influx; V_m hyperpolarisation generally increases the inward driving force for Ca^{2+} (see Chap 1, section 1.7.2.3). As such, a further depolarisation may result in compromised Ca^{2+} homeostasis, a critical second messenger and regulator of proliferation (Varghese et al., 2019; Munaron, Antoniotti and Lovisolo, 2004). Conversely however an increased driving force for Na^+ may also facilitate an increase $[\text{Ca}^{2+}]_i$, an event that has been shown to drive apoptotic pathways. NCX operating in ‘forward mode’ imports 3 Na^+ ions in exchange for extrusion of 1 Ca^{2+} ion. With a reversal potential reported to be ≈ -20 mV, NCX can operate in ‘reverse mode’; extruding 3 Na^+ ions for the import of 1 Ca^{2+} ion. Evidence is growing for ‘reverse mode’ operation being the predominant mode in cancer. In PC3 prostate cancer cell lines the NCX reverse mode inhibitor KB-R7943 significantly attenuated cell migration as assessed by wound healing and transwell assays (Long et al., 2016). In highly metastatic C8161 human melanoma cells NCX has been shown to operate in ‘reverse-mode’, however in the lowly metastatic C8161 melanoma cell line NCX operates in forward mode (Sennoune et al., 2015). Importantly, an increased Na^+ influx has been shown to drive ‘reverse-mode’ NCX mediated Ca^{2+} influx in neurons and astrocytes of mouse neocortex, inhibition of which with KB-R7943 resulted in reduced Na^+ efflux

and subsequent Ca^{2+} efflux, conferring tissue with a neuroprotective effect following chemical induced ischemia (Gerkau et al., 2018). There is as yet no functional evidence for NCX activity in SKOV-3 or indeed OVCAR-3 cells however NCX activity in cisplatin resistant A2780 (A2780cis) cells has been identified (Pelzl et al., 2015). Thus, it is plausible that an increased driving force from elevated $[\text{Na}^+]_e$ serves to increase NCX mediated $[\text{Ca}^{2+}]_i$ elevation, subsequently inducing apoptosis in SKOV-3 cells and accounting for the observed reduction in cell viability. Ultimately, an approach assessing the degree of apoptosis following elevated $[\text{Na}^+]_e$ treatment such as the PI/Annexin V flow cytometry approach used in this study will prove insightful. Furthermore the assessment of NCX activity with patch clamp studies in SKOV-3 and OVCAR-3 cells will further elucidate whether this is a viable explanation. There exists further evidence for the role of increased Na^+ influx in the induction of apoptotic pathways in cancer. In primary HUVEC vascular endothelial cells, elevation of $[\text{Na}^+]_e$ to 173 and 188 mM resulted in a dose-dependent induction of apoptosis (Jakic et al., 2017). In the human lymphoma Jurkat cell line, subpopulations identified displaying early markers of apoptotic pathways demonstrated significant increases in $[\text{Na}^+]_i$ (Bortner and Cidlowski, 2003). Furthermore, upon part replacement of Na^+ with choline, RVD, an early process in the induction of apoptosis was abolished (Bortner and Cidlowski, 2003). Further weight is lent to the hypothesis that a large influx of Na^+ initiates apoptosis. Viral vector delivery of ASIC channels in a constitutively open state into glioma cells resulted in significant Na^+ entry and cell death (Tannous et al., 2009). Overall, the results from this study indicate that persistent Na^+ influx has a biphasic role in regulating cell proliferation and induction of apoptosis in ovarian cancer. A more robust experimental approach centred on maintaining solution osmolarity through substitution of Na^+ with

impermeant ions (refer to section 2.8) would facilitate titration of Na^+ over a greater physiological range, and may prove insightful in further understanding the regulatory roles of Na^+ permeability in cancer.

There are other suggested roles by which ENaC may be involved in cell division. Studies of ENaC in human erythroblastic and myeloblastic cell lines have shown a strong translocation to the plasma membrane region demarcating the mother and daughter cells during cell division (Mirshahi et al., 2000). α -ENaC has been shown to interact with components of the cytoskeleton via interactions with actin, spectrin and cortactin (Berdiev et al., 1996; Zuckerman et al., 1999; Ilatovskaya et al., 2011). These interactions have been shown to modify channel open conductance and may provide a possible role for amiloride induced reduction of cell proliferation by modulating Na^+ influx locally, without systemically altering V_m .

4.4 Na_V channel inhibition reduces proliferation in OvCa cell lines

In considering the observations that SKOV-3 cells exhibited a reduction in proliferation when treated with either amiloride or phenytoin, it must be considered whether the effects were due to a convergent mechanism of attenuated Na^+ influx through the inhibition of differential Na^+ conductances. Further credence is lent to this hypothesis in the observation that in patterns of Na_V expression in numerous cancers, the α -subunit is always expressed and Na_V currents are shown to be more prominent in increasingly aggressive cancer models (Besson et al., 2015). Furthermore, weakly metastatic A549 pulmonary adenocarcinoma cells lack functional expression of Na_V channels and do not possess a Na_V currents and are weakly metastatic (Campbell, Main and Fitzger-

ald, 2013). When transfected with $\text{Na}_V1.7$, A549 cells exhibit a marked increase in invasive capacity, pointing to the fact that I_{Na} is the critical requirement for Na_V induced alterations in proliferative and invasive properties in cancer (Campbell, Main and Fitzgerald, 2013). The degree of channel interdependence on observed cancer cell proliferation lends further credence to the consideration that OvCa cells require Na influx to maintain proliferative signalling and that in part, this acts as a depolarising cue.

While phenytoin is well characterised as an inhibitor of Na_V channels, it is also known to modulate other ion channels. In HEK 293 cells stably transfected with HERG, patch clamp studies demonstrated a significant reduction in HERG-specific tail currents upon perfusion of phenytoin (IC_{50} or $240 \mu\text{M}$). Previous data from this lab has demonstrated that HERG is functionally expressed (as assessed by western blot and IF) in SKOV-3 cells (Asher et al., 2011). Furthermore inhibition of HERG with E-4031 and ergtoxin resulted in a significant reduction of proliferation in SKOV-3 cells (Asher et al., 2011). In addition to K^+ channels, phenytoin is also known to inhibit Ca_V channels. In patch clamp studies of human hippocampal granule cells, phenytoin demonstrated a concentration-dependent inhibition of high-voltage activated Ca^{2+} currents (Schumacher et al., 1998). Phenytoin has also been show to inhibit T-type $\text{Ca}_V3.1$ and $\text{Ca}_V3.2$ Ca^{2+} currents in HEK 293 transfected cells and T-type currents in neuroblastoma N1E-115 cells (Todorovic, Perez-Reyes and Lingle, 2000; Yaari, Selzer and Pincus, 1986). There is also evidence of a role for T-type Ca^{2+} channels in modulating proliferative capacity in ovarian cancer. Treatment of A2780 and HO8910 OvCa cell lines with NNC 55-0396 or mibefradil, pharmacological inhibitors of T-type Ca^{2+} channels, resulted in a significant reduction in cell proliferation (Li et al., 2011). Fur-

thermore, knock down of $\text{Ca}_V3.1$ and $\text{Ca}_V3.2$ with siRNA also attenuated proliferation (Li et al., 2011). It is not known however whether T-type Ca^{2+} channels are functionally expressed in SKOV-3 and OVCAR-3 cells. As a result the potential inhibitory effects of phenytoin on proliferation of SKOV-3 and OVCAR-3 cells must be interpreted with caution. Future work must assess the effect of more potent inhibitors of Na_V channels such as TTX on cell proliferation in OvCa cell models (Lee and Ruben, 2008). In addition, patch clamp studies to assess the presence of Na_V currents in SKOV-3 and OVCAR-3 cell lines would prove insightful.

4.4.1 ENaC does not regulate V_{cell} in proliferation of OvCa cells

Here it is demonstrated that inhibition of ENaC results in no detectable regulatory volume changes in proliferating SKOV-3 cells. Conversely, studies in HepG2 hepatocellular carcinoma and high grade glioma demonstrated a role for ENaC in RVI (Ross et al., 2007; Bondarava et al., 2009). Considering the observations here that ENaC inhibition results in reduced rates of proliferation, it is thus likely that ENaC modulates other physiological parameters essential for cell division such as V_m .

4.4.2 Conclusion

In summary, inhibition of ENaC likely by inducing a mild hyperpolarisation served to reduce the number of proliferating cells in both SKOV-3 and OVCAR-3 cell lines. Sustained V_m depolarisation by elevated $[\text{Na}^+]_e$ results in an increase in the number of cells entering into the cell cycle. Finally inhibition of ENaC by amiloride is unlikely to modulate V_{cell} changes in proliferating SKOV-3 cells.

Chapter 5

Differential regulation of ENaC in OvCa and the role in modulation of migratory properties

5.1 Introduction

In the past two decades evidence has grown supporting a causative link between increased Na_V activity and enhanced metastatic potential of cancer cells. Increased expression of $\text{Na}_V1.5$ and $\text{Na}_V1.7$ in breast and prostate cancer respectively has been correlated with metastatic potential (Fraser et al., 2005; Diss et al., 2001). Furthermore metastatic breast cancer cells have been shown to overexpress the foetal splice-variant of $\text{Na}_V1.5$; a channel with a greater unitary conductance than the adult form, inhibition of which results in a marked reduction in migratory capacity (Brackenbury et al., 2007). These observations of increased Na_V channel activity in metastatic cancers mediated by differential channel subunits suggest that the property of primary importance is

the facilitation of a sustained Na^+ conductance alone. High grade serous OvCa is a highly aggressive disease and is characterised by extensive invasion and seeding of the peritoneum (Tan, Agarwal and Kaye, 2006). In observing that ENaC partly conveys SKOV-3 cells with a persistent depolarised phenotype (Chapter 3), and as a constitutively open channel, it may prove insightful to assess the differential expression of ENaC with OvCa progression.

There are some critical similarities in the physiological properties of cancer and normal stem cells; the capacity for self-renewal, ability to differentiate, the ability to migrate and metastasise, evasion of apoptosis and increased membrane transporter activity (Wicha, Liu and Dontu, 2006). Indeed, with the advent of molecular probes and the development of animal models, greater support is lent to the hypothesis that tumours are also driven by cell sub-populations with increased stem cell-like properties, termed cancer stem cells (CSC) or tumour initiating cells (TIC). In the last two decades, tumour sub-populations with enhanced self-renewal capacity have been identified in breast, prostate and colon tumours (Al-Hajj et al., 2003; Collins et al., 2005; O'Brien et al., 2007; Ricci-Vitiani et al., 2007). Evidence for altered bioelectric properties of normal stem cells is provided in the observation that V_m seems to exist at a more depolarised state, and V_m hyperpolarisation has been shown to correlate with increasing stem cell maturation (Sundelacruz, Levin and Kaplan, 2009). In view of this relationship, it is plausible that a depolarised V_m may facilitate the maintenance of an undifferentiated population of CSCs. Thus, the question arises as to whether a persistent inward Na^+ current, which would act to depolarise V_m , may provide a sustaining signal in the maintenance of the CSC phenotype, and hence this potentially implicates a role for ENaC. Numerous sub-populations of cells with increased self-renewing and

differential capacity have been identified (Lupia and Cavallaro, 2017). Cell surface markers have long been considered to denote cell sub-populations with increased ‘stemness’ in numerous cancers (Collins et al., 2005; Nguyen et al., 2017). Indeed in OvCa, EpCam⁺/CD44⁺ levels correlated with poor outcome and demonstrated higher levels at the time of disease recurrence (Gao et al., 2015; Križanac et al., 2018). A recent study however, has demonstrated that CD44⁺/CD117⁺ cell subpopulations may serve to identify the OvCa CSC population. Injection of 100 CD44⁺ / CD117⁺ cells derived from high grade serous disease into athymic nude mice resulted in the propagation of original tumours (Zhang et al., 2008). Conversely, injections of 10⁵ CD44⁻/CD117⁻ cells were nontumorigenic (Zhang et al., 2008). This is the rationale for assessing differential ENaC expression in OvCa_{asc} cells of differing tumourigenic capacity.

Numerous studies have demonstrated the importance of the regulatory role of V_m on the migratory capacity of cells. Upon stimulation of wound healing, bovine corneal endothelial cells, rabbit corneal epithelial cells and Madin-Derby canine kidney cells exhibited a significant depolarisation in V_m , when compared to the cell population not actively participating and isolated from the wound edge (Justet et al., 2013). Depolarisation was associated with an increase in $[Na^+]_i$ and a concomitant rise in $[Ca^{2+}]_i$. Subsequent treatment of the aforementioned cell lines with amiloride or phenamil resulted in a marked reduction of wound closure relative to control, whereas treatment with aldosterone or forskolin (drugs which increase insertion of ENaC in the plasma membrane) resulted in an increased rate of wound healing (Justet et al., 2013). Indeed, irrespective of the mechanism by which cells migrated, whether by actin cable formation (directed actin-filament formation from the cell cortex to the cell edge) or through lamellipodial cell crawling, ENaC inhibition resulted in a significant reduction in migra-

tory capacity (Justet et al., 2013). Considering that studies in chapter 3 demonstrated a role for ENaC in modulating V_m in SKOV-3 cells, it is plausible that ENaC mediated depolarisation may confer the cell with increased migratory capacity.

During migration through heterogeneous environments and subjection to markedly different physical and physiochemical forces, cancer cells must acquire the ability to modulate their biophysical properties (Emon et al., 2018). One biophysical property that has gained increasing recognition for modulation of metastatic potential is cell deformability (Azadi et al., 2019). It is generally well accepted that cancer cells are ‘softer’ or more deformable than their non malignant counterparts (Lekka, 2016). Furthermore, increased cell deformability has been shown to correlate strongly with increased invasive capacity, furnishing cancer cells with the ability to adjust to ECM components of increasing densities and thus facilitating them with a greater capacity to escape their primary site (Wullkopf et al., 2018). One critical component shown to regulate cell stiffness is the degree of actin polymerisation the cell is subjected to. In a seminal study in endothelial cells, it was demonstrated that V_m alterations directly impact the degree of actin polymerisation and subsequently cell stiffness (Callies et al., 2011). Depolarising cells resulted in a decreased ratio of F-actin to G-actin that led to cell softening, whereas conversely hyperpolarisation reversed the relationship and resulted in cell stiffening (Callies et al., 2011). Several other studies have also demonstrated cell softening by application of cytochalasins (drugs that promote depolymerisation of F-actin) in chicken cardiocytes, COS-7 monkey fibroblasts and in human and rat fibroblasts (Hofmann et al., 1997; Kasas et al., 2005; Rotsch and Radmacher, 2000). In observing that ENaC confers SKOV-3 cells with a sustained depolarisation, an interesting question arises: does inhibition of ENaC in an OvCa model increase cell stiffness, which is in

turn a critical regulator of invasive capacity?

Therefore the aims of this chapter were to address whether ENaC- α exhibits an altered expression profile in OvCa, and whether ENaC plays a functional role in modulating the migratory response in OvCa. To address this, RTqPCR analysis for ENaC- α & ENaC- δ was determined between NOv, FIGO₃₋₄T and OvCa_{asc} samples and in OvCa cell lines; functional translation was confirmed by WB and IF. Next, it was determined whether positive staining for ENaC- α is associated with OvCa_{asc} populations of differing tumourigenic potential using flow cytometry. Migration was assessed in SKOV-3, OVCAR-8 & A2780 OvCa cell lines using scratch assays, in the absence and presence of amiloride. Finally, atomic-force microscopy (AFM) force-probe measurements were utilised to assess whether ENaC regulates cell stiffness in A2780 cells.

5.2 Results

5.2.1 Expression of ENaC subunits in OvCa

In SKOV-3 and OVCAR-3 cell lines, mRNA levels of the ENaC- α subunit were next assessed using RTq-PCR. ENaC- α subunits were expressed in both cell lines with C_q values detectable below 30. Comparison of relative mRNA levels ($2^{-\Delta\Delta C_q}$) of ENaC- α between the two cell types revealed an approximate 3-fold increase in ENaC- α expression in OVCAR-3 cells when compared to SKOV-3 cells (Figure 5-1 A). Expression of ENaC- α , as assessed by immunofluorescence, yielded positive staining across both cell populations. Indeed almost no cells were observed to be immunonegative in either cell line (see Figure 5-1 B-E). Negative controls were clear (Figure 5-1 F-G).

It was next assessed whether changes in ENaC expression were associated with OvCa using RT-qPCR (refer to section 2.10). Comparison of mRNA levels for ENaC-

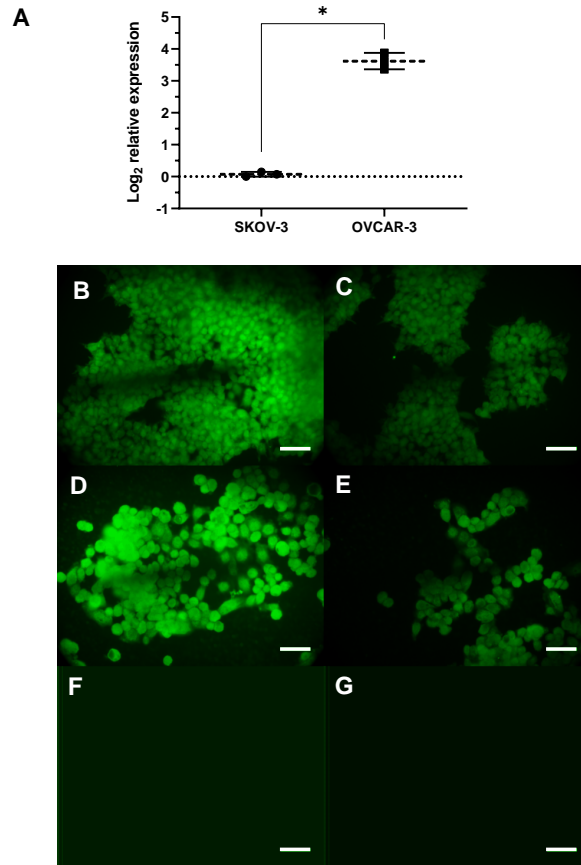


Figure 5-1: Expression of ENaC- α in SKOV-3 and OVCAR-3 cell lines. (A) RT-qPCR expression of ENaC- α , data is presented as mRNA expression relative to the lowest Δ ct values between cell lines ($n = 3$ of 3 independent repeats) Immunofluorescence staining for Pan-cytokeratin (B,D) and ENaC- α (C,E) in SKOV-3 and OVCAR-3 cells respectively. Negative controls for Pan-cytokeratin (F) and ENaC- α (G) Scale bar = 50 μ m (IF experiments repeated 3 times independently). Error bars represent mean \pm SD, * represents significant difference ($p < 0.05$) as assessed by unpaired t-test.

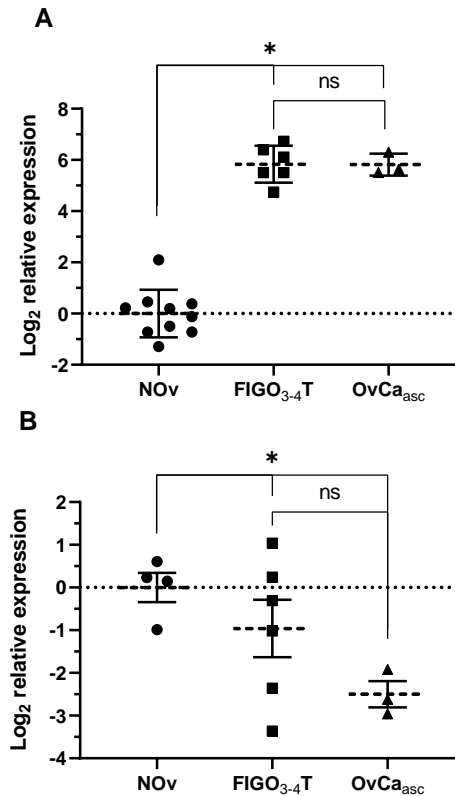


Figure 5-2: Alterations in mRNA expression of ENaC subunits in NOv, FIGO₃₋₄T primary tumours and OvCa_{asc} malignant ascites samples subjects. Relative expression of ENaC- α (A) and ENaC- δ (B) subunits. Data is presented as log₂-fold change relative to NOv. Error bars, mean \pm SD, * represents significant difference ($p < 0.05$) as assessed by one-way ANOVA with Dunnett's multiple comparison test. ENaC- α samples: NOv n=10, FIGO₃₋₄T n=6, OvCa_{asc} n=3. Data was repeated twice independently. ENaC- δ samples: NOv, n=4; FIGO₃₋₄T, n=6; OvCa_{asc}, n=3. Individual samples detailed in text.

α revealed approximately 60 ($\approx 2^6$) times greater expression in the FIGO₃₋₄T group when compared to NOv tissue samples (Figure 5-2A (n = 6 & 10 respectively, +5.83 [+4.55,+7.12] relative to NOv, $p < 0.05$ one-way ANOVA, Dunnett's multiple comparison test)(Samples used: S4, S6, S7, S21, S38, S39, S51, S73, S113, S115, S42, S65, S90, S96, S103, S112). OvCa_{asc} also exhibited a very similar increase in expression relative to NOv (+5.82 [+4.50,+7.13], $p > 0.05$), with no discernable up/down regulation detectable between primary FIGO₃₋₄ tumours and malignant ascites (Figure 5-2A, n = 3 for OvCa_{asc}, +0.02 [-1.35,+1.39], relative to FIGO₃₋₄T samples: OM4, OM7, OM9).

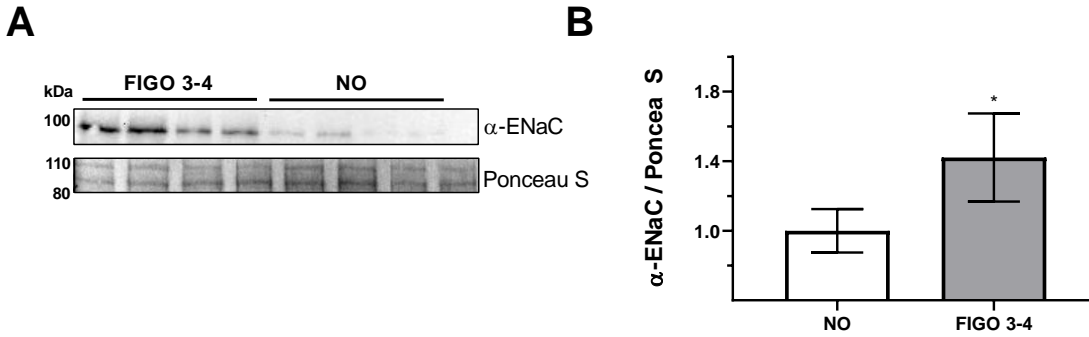


Figure 5-3: Expression of ENaC- α in normal ovary and high grade OvCa. (A) Representative western blot of total ovarian and tumour lysates, upper panel displays primary ENaC- α band at approximately 100 kDa normalised to total protein Ponceau S loading control (lower panel). (B) Relative expression of ENaC- α in FIGO₃₋₄T normalised to Ponceau S. Error bars represent mean \pm SD of two independent repeats. * denotes significance relative to NOv. Samples: S4, S7, S113, S115, S65, S90, S96 and S112

Conversely, comparison of ENaC- δ revealed no significant change in expression levels between NOv and FIGO₃₋₄T tumours; results were markedly varied between samples, demonstrating both up and down regulation relative to NOv (-0.96 [-3.66,+1.74], relative to NOv, n = 4 & 6 for NOv and FIGO₃₋₄T respectively.) However malignant ascites (OvCa_{asc}) samples demonstrated a clear down regulation of ENaC- δ ; approximately three times lower than in NOv (see figure 5-2B, -2.50 [-4.38,-0.62], n = 4 and 3 for NOv and OvCa_{asc} respectively) (Samples used: S4, S21, S38, S73, S42, S65, S90, S96, S103, S112, OM4, OM7, OM9).

It was next investigated whether the observed differences in mRNA levels of ENaC- α subunits in NOv and FIGO₃₋₄T corresponded with differences in protein expression using western blotting (refer to section 2.6). FIGO₃₋₄T samples demonstrated a mild but significant up-regulation to +1.42 [+1.20,+1.64] relative to NOv samples 1.0 [0.90,1.10] (figure 5-3, n = 4 in each group of two independent repeats, p < 0.05) (Samples used, NOv: S4, S7, S113 and S115, FIGO₃₋₄T: S65, S90, S96 and S112).

5.2.2 Expression of Na_V channels in OvCa

It was next sought to characterise whether alteration in Na_V channel expression was associated with OvCa. The Na_V1.5 isoform was chosen since it has shown to be functionally upregulated in primary ovarian tissue (Gao et al., 2010). Relative mRNA levels ($2^{-\Delta\Delta Cq}$) of NaV_{1.5} were compared between NOv and FIGO₃₋₄T samples (see figure 5-4). mRNA levels in FIGO₃₋₄T were downregulated approximately 3-fold when compared to NOv samples (-1.6 [-2.72,-0.48] $p < 0.05$, combined $n = 6$ & 10 for FIGO₃₋₄T and NOv respectively of 2 independent repeats. All samples in table 2.4 were used in this experiment).

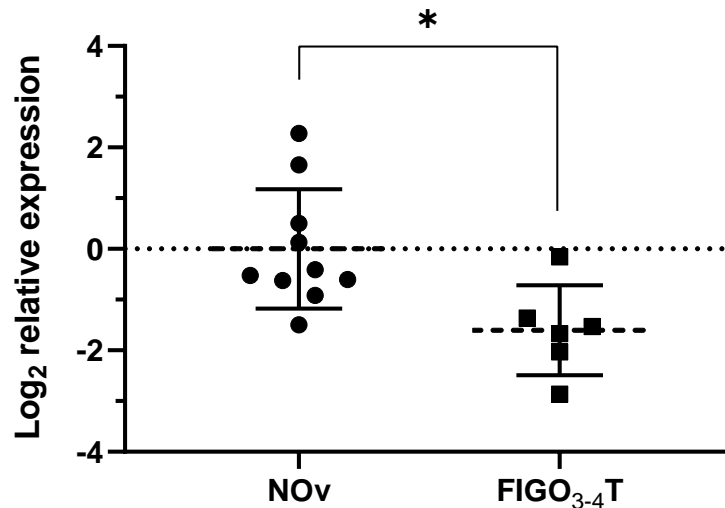


Figure 5-4: Alterations in mRNA expression of NaV1.5- α subunits in normal ovarian tissue (NOv) and FIGO₃₋₄T primary tumours. Data is presented as log₂-fold change relative to NOv. Error bars, mean \pm SD, of 6 & 10 FIGO₃₋₄T and NOv samples repeated twice independently. All samples in table 2.4 were used in this study. * represents significant difference ($p < 0.05$) as assessed by unpaired t-test.

5.2.3 Flow cytometry of OvCa_{asc}

Given that ENaC was functionally expressed in effusions from malignant ascites, it was next sought to assess differential ENaC- α staining in sub-populations of differing

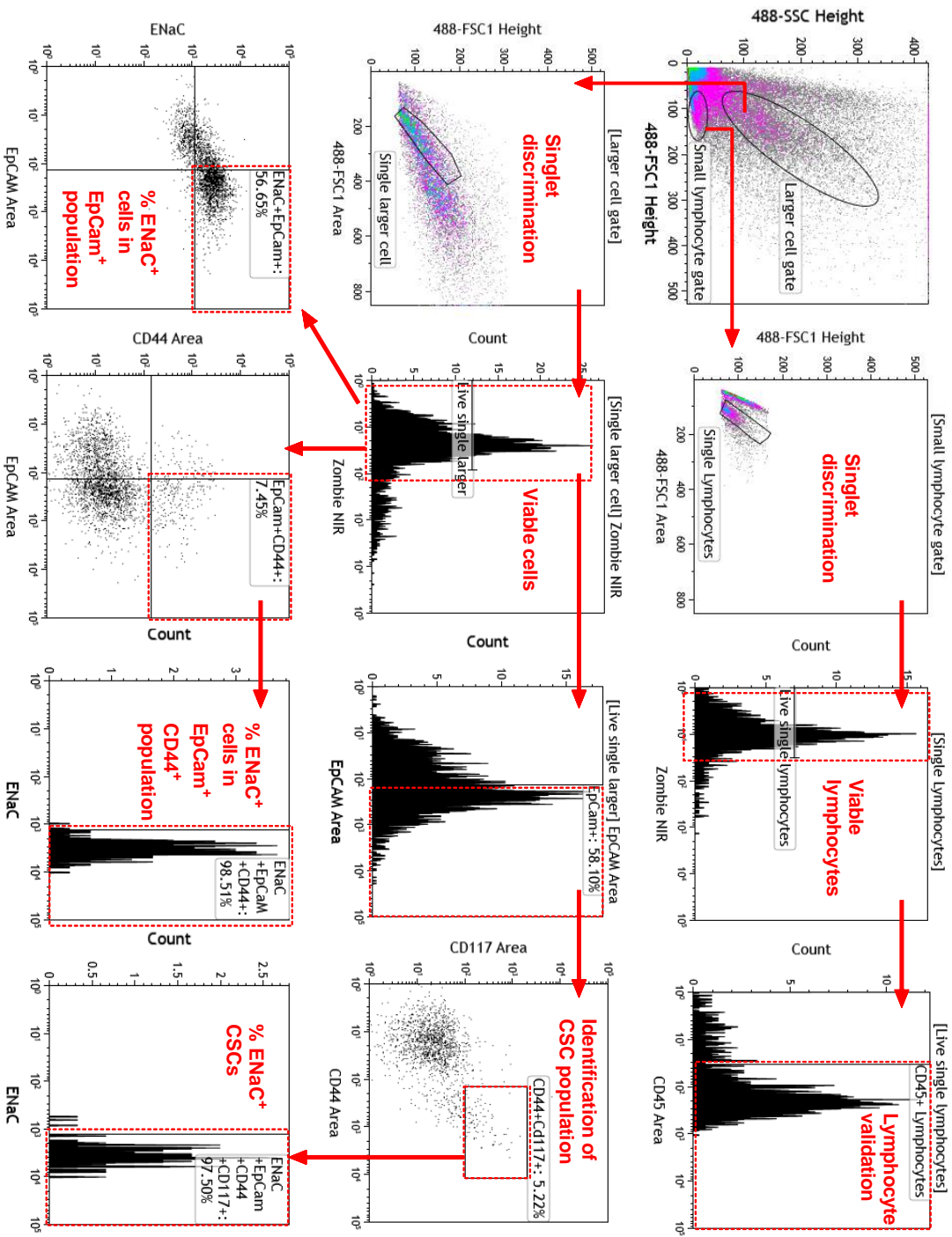


Figure 5-5: Gating strategy to identify OvCa cell populations of differing tumorigenic potential and assessment of differential ENaC⁺ populations. Lymphocytes were discriminated from a larger cell population through FSC & SSC characteristics and positive staining for CD45. Viable cells were then gated using Zombie-NIR amide-sensitive dye. A distinct population of EPCAM⁺ CD44⁺ CD117⁺ could be identified (middle row, last graph). Percentages denote the fraction relative to the parent gate. Data from OM7

tumourigenic capacity / plasticity using flow cytometry. Six OvCa_{asc} primary samples were assessed in this study (OM4, OM7, OM8, OM9, OM11, OM12, refer to section 2.2.2.1 for clinical characteristics of samples and section 2.12.1 for details of flow panel). Experiments were repeated twice independently.

It was first assessed to what extent ENaC- α^+ staining was associated with cells positive for EpCam, a cancer cell marker (Spizzo et al., 2011). EpCam⁺ expression in the CD45⁻ cell population varied significantly in the 6 samples assessed (39.3 ± 30.1 % EpCam⁺ cells / total parent gate, refer to figure 5-5). ENaC expression within EpCam⁺ cells demonstrated a similar degree of variability with minimum and maximum ENaC- α^+ fractions of 30.5 and 94.1 % of total EpCam⁺ cells respectively. Mean percentages of total EpCam⁺ cells between ENaC- α^- and ENaC- α^+ sub-populations were not significantly different; 41.6 ± 26.7 % and 58.4 ± 26.7 % respectively ($p > 0.05$, paired t-test, figure 5-6A).

CD44⁺ populations among the CD45⁻ cells also exhibited high variability between samples (35.1 ± 34.2 % CD44⁺ in CD45⁻ cell population). While there was a trend of increase in the ENaC- α^+ fraction of cells, this was not significant; CD44⁺ENaC- α^- 35.7 ± 24.3 , CD44⁺ENaC- α^+ 64.3 ± 24.3 % ($p > 0.05$, figure 5-6B).

Since tumour initiating cells of different carcinomas have been identified by a CD44⁺EpCam⁺ signature (Zheng et al., 2017), it was next assessed whether ENaC was associated with this cell population. Four samples exhibited greater than 90 % positivity for ENaC- α in the CD44⁺EpCam⁺ population, however the sample difference proved insignificant; CD44⁺EpCam⁺ENaC- α^- 22.1 ± 27.8 %, CD44⁺EpCam⁺ENaC- α^+ 77.9 ± 27.8 % ($p > 0.05$, figure 5-6C).

Finally, it was assessed whether differential staining of ENaC- α was observed in cell

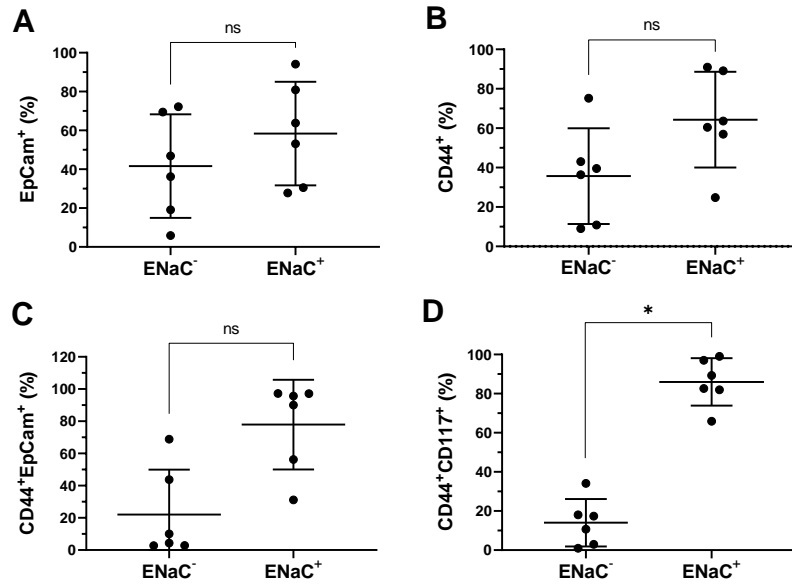


Figure 5-6: Fraction of ENaC- α^+ cell populations in OvCa ascites cells of differing tumourigenic potential as assessed by flow cytometry. Percentages indicates the fraction relative to the total number of parent target cell populations of (A) EpCAM $^+$, (B) CD44 $^+$, (C) CD44 $^+$ EpCAM $^+$ and (D) CD44 $^+$ EpCAM $^+$ CD117 $^+$. Populations were identified through the gating strategy described in figure 5-5. Error bars denote mean \pm SD, ns: not significant, * denotes significant difference relative to control ($p < 0.05$) as assessed by paired t-test, $n = 6$ OvCa_{asc} samples (OM4, OM7, OM8, OM9, OM11, OM12) repeated twice independently.

populations staining for EpCam $^+$, CD44 $^+$ and CD117 $^+$, a population recognised as having increased clonogenic and tumour initiating capacity in OvCa. The EpCam $^+$ CD44 $^+$ CD117 α^+ population constituted $5.1 \pm 3.7\%$ of total viable CD45 $^+$. Triple positive cells exhibited strong positive staining for ENaC- α ; EpCam $^+$ CD44 $^+$ CD117 $^+$ ENaC- α^- accounted for $14.0 \pm 12.1\%$ vs EpCam $^+$ CD44 $^+$ CD117 $^+$ ENaC- α^+ cells that contributed $86.0 \pm 12.1\%$ of the parent population (figure 5-6D, $p < 0.05$). In conclusion, ENaC- α demonstrates increasing positivity with OvCa stem cell markers.

5.2.4 Effect of ENaC inhibition on OvCa migration

In order to assess the effect of ENaC on collective cell migration, scratch assays were employed using SKOV-3, OVCAR-8 and A2780 (3 independent repeats) cell lines.

Wounding was assessed in the presence and absence of amiloride (0.1 - 100 μM) added 1 hour after wounding. Migration was assessed over 48 hours and quantified as the reduction in wound area relative to $t=0$ in the respective conditions (see section 2.4).

In control conditions cell lines exhibited markedly differing rates of wound closure over the observed time. In the SKOV-3 cell line, the wound area relative to $t=0$ after 24 and 48 hours decreased significantly to 0.56 ± 0.15 and 0.24 ± 0.13 units respectively (mean \pm SD, $n = 3$, $p < 0.05$, 2-way ANOVA with Dunnett's post-hoc test). The rate of wound closure in control conditions in OVCAR-8 and A2780 cell lines was markedly reduced relative to SKOV-3 cells. However, OVCAR-8 and A2780 cell lines still demonstrated a significant reduction in wound area at 48 hours post-wound; OVCAR-8, $T_{24}/T_0 = 0.65 \pm 0.20$ and $T_{48}/T_0 = 0.57 \pm 0.19$; A2780, $T_{24}/T_0 = 0.80 \pm 0.09$ and $T_{48}/T_0 = 0.57 \pm 0.13$ ($n = 3$, $p < 0.05$).

Low doses of amiloride (0.1 - 10 μM) resulted in no significant reduction in wound closure when compared to vehicle control at 24 or 48 hours post wound in all three cell lines tested ($n = 3$, $p > 0.05$ 2-way ANOVA with Dunnett's post-hoc test). In the SKOV-3 cell line, 50 μM amiloride resulted in a significantly attenuated rate of wound closure detectable at 24 hours; $T_{24} = -0.34$ [-0.66 , -0.08] and $T_{48} = -0.40$ [-0.66 , -0.13] (mean [95 % LCI , UCI] reduction relative to control, $p < 0.05$ 2-way ANOVA as above). At 100 μM amiloride, there was no further significant decrease in wound closure when compared to 50 μM treatments; $T_{24} = -0.29$ [-0.51 , -0.06] and $T_{48} = -0.36$ [-0.59 , -0.14]. In OVCAR-8 cells a mild reduction in wound closure was only observed at 100 μM at 24 hours; $T_{24} = -0.15$ [-0.30 , 0.0] with no further reduction observed at 48 hours; $T_{48} = -0.16$ [-0.31 , -0.01]. In A2780 cells, a mild reduction in wound closure was only detectable at 100 μM after 48 hours; $T_{48} = -0.10$ [-0.19 , -0.01] 100

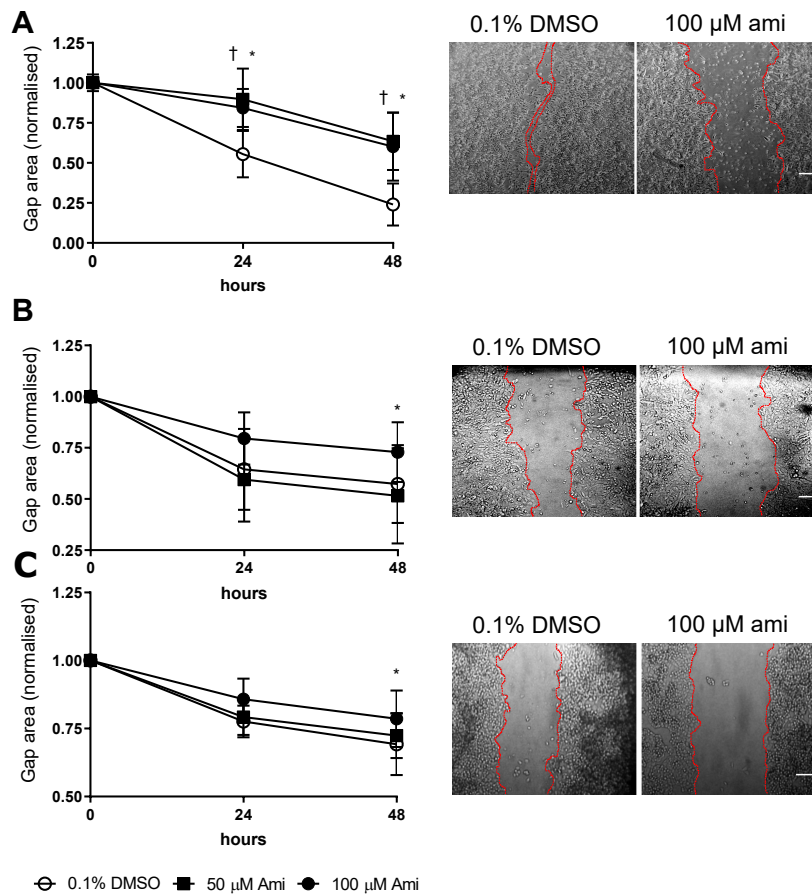


Figure 5-7: Effect of amiloride on cell migration as assessed by scratch assays. (A - C) Relative reduction in wound closure over 48 hours in the presence of 50 & 100 μM amiloride in SKOV-3, OVCAR-8 and A2780 cell lines respectively (left) and representative images (right). Error bars denote mean \pm SD. † and * denote a significant reduction relative to control conditions of 50 & 100 μM amiloride respectively as assessed by two-way ANOVA, $n=3$ of 3 independent experiments.

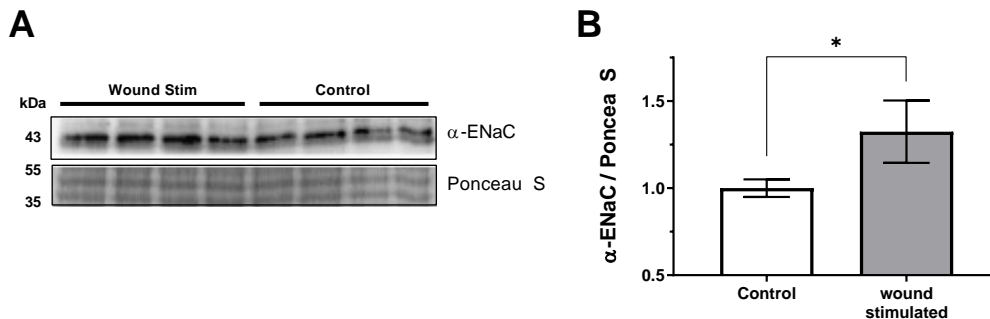


Figure 5-8: Alterations in expression of ENaC- α in SKOV-3 cells during migration stimulated conditions. (A) Representative western blot of SKOV-3 cells in control and wound stimulated 24 hours post treatment, upper panel displays primary ENaC- α band at approximately 43 kDa normalised to total protein Ponceau S loading control (lower panel). (B) Relative expression of ENaC- α normalised to Ponceau S. * denotes significance relative to control by paired t-test. Error bars represent mean \pm SD, of 3 independent experiments.

μM respectively.

A degree of cytotoxicity was observed in cell lines treated with higher concentrations of amiloride (50 and 100 μM); this was particularly evident in SKOV-3 cells at 48 hours post wounding (Figure 5-7). Results from chapter 4 (Figure 4-2) demonstrated a significant cytotoxic effect of amiloride on SKOV-3 cells; this may confound conclusions of amiloride in mediating OvCa migration observed here.

It was next assessed whether alterations in functional ENaC expression were observed during wound healing in SKOV-3 cells, using western blotting. Densitometric analysis of wound stimulated population at 24 hours post-scratch revealed a significant up-regulation of ENaC- α of 1.33 [1.15,1.50] relative to control conditions (mean [95% LCI,UCI], of 3 independent repeats, unpaired student's t-test, refer to figure 5-8).

5.2.5 Effect of ENaC inhibition of cell stiffness

Since cell stiffness has been shown to be inversely correlated with increased metastatic potential (Swaminathan et al., 2011), it was assessed whether ENaC played a functional role in modulating cell compliance using AFM force spectroscopy in A2780 cells (refer to section 2.13). A2780 cells were selected since they originate from a primary OvCa tumour. Due to the slow diffusion of drug after manual addition, and since this was a pilot study, a high dose of amiloride was chosen to elicit maximum effect. In control conditions (PSS), cells exhibited a relatively soft phenotype with a mean Young's modulus (E_m) of 1.78 [1.59,1.98] ($n = 11$). Upon addition of amiloride, cells exhibited an ≈ 3 -fold increase in cell stiffness; $E_m = 5.13$ [5.02,5.23], $p < 0.05$, paired t-test.

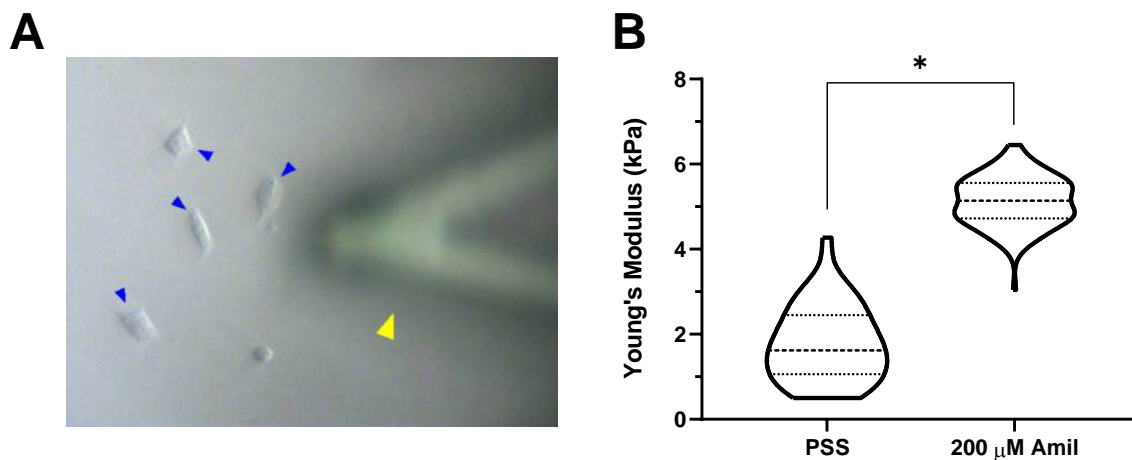


Figure 5-9: Effect of amiloride treatment on cell stiffness of A2780 cells. (A) Isolated cells were chosen to discount cell-cell adhesive interactions (blue arrows), yellow arrow indicates cantilever located at start position. A 6×10 array spaced $0.5 \mu\text{m}$ apart of force curves was obtained located over the nucleus to reduce effect of underlying substrate. (B) Violin plot of Young's modulus values obtained for 11 cells in control conditions and re-probed following incubation with $200 \mu\text{M}$ amiloride (amil) for 1 hour. (Top and bottom lines represent the max and min values. Dashed and dotted lines indicate median and quartiles. * denotes significance ($p < 0.05$), paired t-test of two independent experiments.)

5.3 Discussion

The results presented in this chapter demonstrate an altered expression profile of ENaC in OvCa. α -ENaC demonstrates increased expression in high-grade FIGO₃₋₄ solid tumours, in the OvCa_{asc} samples and in cell line models of OvCa ascites, while conversely ENaC- δ exhibits a downregulation in FIGO₃₋₄T and OvCa_{asc}. However, Na_v1.5 also displays down-regulation in OvCa_{asc} compared to NOv. It was also observed that cells of increased tumourigenic potential or 'stemness' exhibited greater ENaC- α^+ staining. The second part of this chapter demonstrated that ENaC plays critical roles in cell migration in OvCa cell lines and modulates biophysical properties important for cell migration.

ENaC channels have been shown to exist in different stoichiometry in *in vitro* exper-

iments, however only channels containing α or δ -ENaC alone, or in combination with other subunits, can form functional Na-conducting channels (McNicholas and Canessa, 1997; Kosari et al., 1998). The physiological relevance of channels comprising different subunits is suggested by the observation that Na⁺-absorbing epithelia of differing origins contain all four known subunits of the channel. In lung epithelia some cells only contain α and γ subunits, whereas as in colonic epithelia only the α subunit is expressed (Canessa et al., 1994; Hummler et al., 1996). As such, the lack of β or γ subunits does not obviate ENaC currents and hence this was the rationale for assessing differential expression of the α and δ subunits. While a down regulation of mRNA for ENaC- δ was observed, functional protein expression was not assessed in this study. It is important to address this to further understand the contribution of ENaC- δ to the progression of OvCa and differential expression in cell lines. The results presented here demonstrate a marked upregulation of mRNA for ENaC- α in FIGO₃₋₄T and OvCa_{a_{sc}}, confirmed by WB and IF. In the current study design no correlation could be drawn between the metastatic potential of excised tumour biopsies and ENaC- α mRNA levels. It is thus hard to conclude whether such changes in expression have an impact on the metastatic progression of disease. It should also be noted that relative levels of mRNA for ENaC- α have to date not been assessed in low-grade OvCa biopsies; a disease with limited metastatic potential. Further studies would help to differentiate between the potential roles for ENaC- α in OvCa progression. Furthermore, the observation that there was no significant change in mRNA levels of ENaC- α between FIGO₃₋₄T and OvCa_{a_{sc}} samples is evidence to suggest that ENaC plays a limited role in metastatic dissemination from the primary site; it may be that ENaC upregulation is a relatively early event in the progression to a metastatic phenotype.

Considering that ENaC inhibition has been shown to attenuate proliferative and migratory capacity in OvCa cell lines in this study, and that it has been shown to contribute to the depolarised phenotype exhibited in OvCa, it is plausible that up-regulation of ENaC- α , a subunit responsible for functional Na⁺ conductance, contributes to the malignant phenotype in OvCa. Furthermore, BeWo cells, a trophoblastic cell type derived from malignant gestational choriocarcinoma, demonstrated an increase in migration rate and inward Na⁺ currents when treated with aldosterone, a compound known to increase insertion of ENaC into the plasma membrane (Marino, Assef and Kotsias, 2013). Future studies would over-express ENaC- α in OvCa models to investigate whether increased expression confers cells with greater proliferative and migratory potential. High-grade gliomas have been shown to express members of the ENaC and ASIC family. Importantly these channels are absent in low-grade gliomas and normal astrocytes, a finding similar to that observed here (Berdiev et al., 2003; Rooj et al., 2012).

Given that increased levels of ENaC- α mRNA were observed in OvCa samples, it is important to consider how this may translate to altered functional activity of ENaC in OvCa. In the mpkCCDc14 renal cortical collecting duct cell line, the majority of ENaC channels reside in intracellular vesicles and are not present in the plasma membrane (Edinger et al., 2012). It was further shown that insertion of ENaC in the apical membrane was markedly down-regulated when aldosterone was removed from cell culture media (Edinger et al., 2012). Furthermore, in COS-7 kidney fibroblast and human embryonic kidney HEK293 cell lines transfected with α , β and γ subunits, \approx 98 % of total cellular assembled ENaC channels were located in the endoplasmic reticulum (Prince and Welsh, 1998). Multiple processes regulate the intracellular trafficking and

membrane insertion of ENaC, such as the ubiquitin ligase Nedd4-2 and glycosylation, and this has been shown to be a dynamic process (Staub et al., 2000; Ergonul, Frindt and Palmer, 2006). As such, limited inference can be drawn from the marked increase of ENaC- α mRNA observed in OvCa. Other studies in human glioma cells have utilized techniques such as total internal reflection fluorescence (TIRF) microscopy to assess surface expression / membrane insertion of ENaC and such approaches would prove useful here (Kapoor et al., 2011).

Interestingly, FIGO₃₋₄T samples demonstrated a down regulation in mRNA levels of Na_V1.5. This observation is in opposition with that observed by others (Gao et al., 2010). It should be noted that limited data on stage and grade is provided by the authors, however considering that 11 samples in the OvCa group presented with lymph node metastasis, it is likely that a subset were relatively high grade tumours. Furthermore, the authors used non-quantitative (RT-PCR) methods for determination of relative gene expression and thus the magnitude of effect between normal ovarian and OvCa samples must be interpreted with some caution (Gao et al., 2010). While the Na_V1.5 subunit was chosen since it has previously been shown to be upregulated in OvCa tissue, it is possible that Na_V channels formed from other subunits exhibit altered regulation in OvCa. In primary derived human neoplastic mesothelioma cells, functional Na_V currents are thought to be predominantly carried via Na_V1.2, Na_V1.6 and Na_V1.7 α subunits (Fulgenzi et al., 2006). In metastatic MDA-MB-231 breast adenocarcinoma cell lines, the predominant α -subunit is thought to be Na_V1.5 (Brackenbury et al., 2007). It is important to assess differential expression of other Na_V subunits in future studies of OvCa.

In scratch assay migration models, OvCa cell lines exhibited a reduction in migratory

capacity when treated with amiloride. Other researchers have also reported a role for ENaC in cancer cell migration. Addition of amiloride resulted in a significant decrease in wound closure in the BeWo cell line (Del Mónico et al., 2009). Further investigations by the same group revealed that treatment with aldosterone, a known upregulator of ENaC surface expression, resulted in enhanced migratory response and increased inward current (with physiological Na^+ in bath solution) detected by patch-clamp studies; these responses were subsequently abolished by treatment with amiloride (Marino, Assef and Kotsias, 2013). Other studies assessing wound healing in cells of endothelial and epithelial origin demonstrated that cells at the leading edge of scratch assays were depolarised and demonstrated increased Na^+ influx and elevated $[\text{Ca}^{2+}]_i$. Amiloride attenuated this effect, and resulted in significant reductions in cell migration (Justet et al., 2013). These authors propose that increased ENaC activity at the membrane facilitates V_m depolarisation sufficient to allow cytoskeletal reorganisation and $[\text{Ca}^{2+}]_i$ influx, potentially through increased activity of NCX (Justet et al., 2013). The effect of ENaC inhibition on V_m during cell migration was not assessed directly in this study, however considering that amiloride results in a mild V_m hyperpolarisation in SKOV-3 cells from patch clamp studies (see chapter 3), it is plausible that ENaC facilitates migration in OvCa cell lines in a similar manner. Future studies assessing the effect of V_m perturbations directly on OvCa migration, will provide insight as to whether ENaC provides a depolarising cue or is also involved in orchestration of cell machinery via other mechanisms, such as Na^+ dependent calcium influx. Approaches such as increasing $[\text{K}^+]_e$ and titration of extracellular Na^+ with impermeant replacements will increase our understanding of the distinct roles of Na^+ in OvCa migration. While the results in all three cell lines are significant, the confounding effects of amiloride-induced

cytotoxicity observed require the conclusions to be interpreted with caution.

Increased evidence for the role of ENaC in OvCa cell migration is provided by the observations that protein expression of ENaC- α was increased in a wound stimulated population of SKOV-3 cells. This cell line was selected since inhibition of ENaC with amiloride resulted in the greatest reduction in wound closure. Furthermore, since only assembled channels containing ENaC- α or ENaC- δ are constitutively active, this was the rationale for assessing alterations in ENaC- α . Increased localisation of the α , β , & γ ENaC subunits at the wound edge was observed in BeWo cells, supporting the hypothesis that ENaC plays a participatory role in stimulating the migratory phenotype (Del Mónico et al., 2009). However other studies have demonstrated that increased expression of ENaC is not a requirement, but that increases in activity alone are sufficient to promote migration (Marino, Assef and Kotsias, 2013). Alterations of ENaC- α levels in wound stimulated populations of OVCAR-8 and A2780 cells have not been assessed to date; it remains to be seen whether functional ENaC activity is a requirement for cell migration.

It was identified that $\approx 80\%$ of EpCAM⁺/CD117⁺/CD44⁺ cells were positive for ENaC- α , with decreasing ENaC- α ⁺ fractions in cells of decreased tumourigenic potential. Other investigations have made associations between the presence of ENaC and proliferation / self-renewal. A recent study in mouse adult neuronal stem cells (NSCs) of the subependymal zone (SEZ) found that $\approx 80\%$ of cells were positive for ENaC- α while progenitor cells exhibited some 60% positivity. Interestingly, only $\approx 20\%$ of terminally differentiated neuroblasts were positive for ENaC- α , further suggesting a role for ENaC in clonogenic potential (Petrik et al., 2018). Furthermore it was demonstrated that ENaC- α inhibition in isolated NCSs, via knock down or following treatment with

amiloride or benzamil, markedly reduced the number of cell divisions the cells underwent, demonstrating a clear role for ENaC in adult neurogenesis (Petrik et al., 2018). In adult stem and progenitor cells of the pulmonary epithelium, ENaC- α is increasingly expressed in ATII and club progenitor cells and bronchioalveolar stem cells; these are cells with increased migratory and proliferative capacity that participate in endothelial development and repair (Matalon, Bartoszewski and Collawn, 2015; SMITH et al., 2000). In considering the observations in Chapter 3 suggesting a role of ENaC mediated proliferation in OvCa cell lines, it is plausible that ENaC may play a role in the maintenance of plasticity in OvCa CSCs. To date, clonogenic and migratory assays have not been undertaken in EpCAM⁺/CD117⁺/CD44⁺ cells of OvCa_{asc} and it remains to be seen whether ENaC does modulate OvCa CSC properties. As to whether ENaC contributes significantly to V_m in this cell population, patch clamp experiments must be undertaken. Isotype controls were not included in the design of this cell line panel, but would be important to determine whether there is non-specific binding of the target antibody through Fc-receptors (Hulspas et al., 2009). In light of this, the data must be interpreted with some caution and efforts must be made to select adequate isotype controls (selecting antibodies of the same heavy chain and light chain class) for all antibodies included in the experiment (Hulspas et al., 2009). Another type of control that would prove useful in determining the antibody specificity would be positive cell line controls (Maecker and Trotter, 2006). For example, the mpkCCDc14 mouse cortical collecting duct cell line is a well characterised positive control for ENaC- α (Zhang et al., 2019). This cell line should be negative for the leucocyte marker. Thus, this approach using positive controls known to stain negative another marker in the antibody panel is also important to undertake in future experiments (Maecker and Trotter, 2006).

Force spectroscopy measurements utilising AFM demonstrated a marked increase in the stiffness of A2780 cells when treated with amiloride. To date there are no other studies assessing the effect of ENaC inhibition on cell deformability in cancer. Studies assessing the deformability of primary OvCa ascites cells and OvCa cell lines using a magnetic tweezer method demonstrated a clear relationship between cell compliance and migratory and invasive capacity. Cancer cells with the highest invasive and migratory capacity were \approx five times less stiff than those that were poorly invasive (Swaminathan et al., 2011). Similarly, HEY and HEY A8 cells were much softer than non-malignant mouse ovarian surface epithelial cells (IOSE) and demonstrated a marked increase in transwell migration and invasion when compared to IOSE cells (Xu et al., 2012). Thus there is a clear relationship between increased cell deformability and enhanced migratory capacity. Patch clamp studies from this thesis demonstrate that persistent permeability to Na^+ in OvCa cell lines and primary OvCa isolates exerts a depolarising effect on cells, and that this is partly facilitated by ENaC conductance. The importance of V_m in regulating cell stiffness has been demonstrated in endothelial cells (Callies et al., 2011). Indeed, inhibition of ENaC with amiloride reduces the migratory capacity of OvCa cells. In light of our observations, it is likely that ENaC acts to provide a persistently depolarising cue, thus reducing the electric field across the plasma membrane and promoting depolymerisation of F-actin tending towards G-actin. Since OvCa cells possess an ENaC-independent (or amiloride insensitive) Na^+ conductance, further elucidation of the contribution of Na^+ mediated depolarisation is essential. Future experiments employing wash-in of impermeant replacements such as NMDG^+ and Ch^+ will prove insightful.

The experimental approach used in AFM studies necessitated addition of amiloride

to the experimental dish manually; this was performed immediately after the acquisition of the last cell in control conditions (PSS). Since it was important to allow sufficient time for diffusion of drug stock solution, an incubation time of 1 hour was chosen, after which point cells were measured in the same order as in control conditions. This approach meant that cells were subject to different ‘exposure windows’ to amiloride depending on the order they were assessed. In addition, since this was a pilot study, a dose of 200 μM amiloride was chosen in order to elicit maximum effect. However, it is possible that amiloride at this concentration may be exerting off-target effects on NHE exchangers, since IC_{50} values have been quoted as between 50 μM - 1 mM dependent on $[\text{Na}^+]_e$ (Cassel et al., 1988). Studies in hepG2 hepatocellular carcinoma cells demonstrated amiloride-sensitive Na^+ currents at high concentrations (300 μM) in patch clamp experiments and it is plausible that the effects of amiloride on A2780 cell stiffness are due to ENaC inhibition, however the results must be interpreted with some caution. Future approaches allowing rapid perfusion over a time course of minutes would provide further insight on the temporal dependence of amiloride on OvCa cell deformability. In addition, it is also necessary to assess the effect of amiloride on cell stiffness at lower concentrations (1 - 100 μM).

While A2780 cells were chosen for this study as a solid tumour model of OvCa, the results observed raise interesting questions as to whether ENaC is important in regulating cell stiffness in cells originating from malignant ascites. The ability of a cell to undergo deformation is a key factor in metastatic dissemination and has been shown to correlate with invasive capacity in OvCa cell derived from malignant ascites (Swaminathan et al., 2011). It is thus important to assess the contribution of ENaC to cell stiffness in SKOV-3, OVCAR-3 and OVCAR-8 cell lines and in primary derived

OvCa_{asc} cells in future studies.

In summary, ENaC- α is upregulated in OvCa samples and exhibits increased expression in putative CSC populations. ENaC demonstrates upregulation in migration stimulated populations, and treatment of OvCa cell lines with amiloride attenuates migratory capacity. ENaC also appears to play a role in maintaining a deformable phenotype in an OvCa cell line model; a property associated with increased invasive capacity.

Chapter 6

The migration of OvCa cells in an external electric field and the role of ENaC, Na^+ and V_m

6.1 Introduction

The mechanisms by which OvCa metastasises from the primary tumour site are still poorly understood. OvCa cells have been shown to exhibit a tropism for the adipose rich omentum (Motohara et al., 2019). In considering however that OvCa_{asc} derived cells are highly metastatic, it important to assess other potential gradients that may modulate motility and directional migration and invasion (Weidle et al., 2016).

Numerous mammalian cells demonstrate the ability to ‘sense’ naturally occurring endogenous EFs and show directional migration. Indeed a role for galvanotaxis has been proposed in wound healing; keratinocytes exhibit cathodal migration which directs them to migrate towards the wound centre upon disruption of the epithelium (Zhao, 2009;

Guo et al., 2015).

In recent years, evidence has grown of a functional role for galvanotaxis in the metastatic progression of cancer. This is based on the seminal observations by Djamgoz et al in rat prostate cancer cells. There it was shown that the weakly metastatic AT-2 cell line exhibited a poor migratory response in the presence of external EFs (3 V/cm) (Djamgoz et al., 2001). Conversely, the strongly metastatic MAT-LyLu cell line, derived from the same tumour, exhibited a strong cathodal migration pattern when exposed to an EF (Djamgoz et al., 2001). The relevance of this observation becomes apparent when it is considered that one of the first sites of local invasion in prostate cancer are prostatic epithelial ducts (Szatkowski et al., 2001). The transepithelial potential (TEP) of a prostatic duct has been measured to be ≈ -10 mV, lumenally negative, which with a thickness of 20 μm would manifest as a field gradient of 5 V/cm (Szatkowski et al., 2001). Hence, there is a potential galvanotactic cue driving metastatic spread. Additionally, other cancer cell types have been tested in external EFs of physiological strengths *in vitro* and have been shown to demonstrate diverse galvanotactic capacity. Two sub-clones derived from the CL1 lung adenocarcinoma cell line have demonstrated diverse results. CL1-0 cells demonstrate low invasiveness *in vitro* and corresponding weak galvanotactic capacity. However, the CL1-5 sub-clone exhibits greater invasive capacity and marked anodal galvanotaxis (Tsai et al., 2013). In addition, other effects of EFs have been shown to modulate growth of cancer spheroids, indicating clear instructive roles of endogenous EFs in modulating tumour behaviour (Wartenberg, Hescheler and Sauer, 1997; Sauer et al., 1997).

The mechanisms by which galvanotactic cells respond to or ‘sense’ external electric fields are still poorly understood. Numerous theories have been proposed, such

as electrophoretic redistribution of membrane-bound ligands and proteins, and ‘sensing’ of bulk-water movement (Poo, 1981; Lammert, Prost and Bruinsma, 1996; Sarkar et al., 2019; McLaughlin and Poo, 1981). Another proposed mechanism by which cells ‘sense’ an external EF involves localised changes in V_m at the poles of the external EF (McCaig, Song and Rajnicek, 2009). Indeed, changes in V_m modulate galvanotactic capacity in Dictyostelium cells (Gao et al., 2011). Depolarisation of cells via electroporation or acidic conditions resulted in a marked reduction in galvanotactic migration. Conversely however, there was no reduction in the chemotactic capacities on cells under the same treatments (Gao et al., 2011). There is also a correlation between V_m values and galvanotactic capacity in breast cancer cells. Weakly metastatic MCF-7 cells have a V_m of ≈ -30 to -40 mV, whereas strongly metastatic MDA-MB-231 cells have a V_m of -20 mV (Wonderlin, Woodfork and Strobl, 1995; Fraser et al., 2005). Thus, understanding the effects of V_m perturbations on cell migration in an EF remain important in characterising the galvanotactic cues directing migration of cancer cells.

Recent evidence has emerged for the role of ENaC in mediating the directionality of EF induced migration in keratinocytes, cells essential for skin epidermal repair upon wounding. Inhibition of ENaC by phenamil, a derivative of amiloride, resulted in a marked reduction in directed cell migration in the presence of an external EF (Yang, Charles, Hummler, Baines and Isseroff, 2013). Furthermore, depletion of ENaC- α , the primary conductance mediating subunit, resulted in complete abolishment of a galvanotactic response, presenting ENaC as an interesting candidate sensor of an external EF (Yang, Charles, Hummler, Baines and Isseroff, 2013). There is evidence for ENaC in regulating wound healing in human choriocarcinoma, bovine aortal endothelial cells, bovine corneal endothelial cells, rabbit corneal epithelial cells and Madin-Darby canine

kidney cells via a facilitated V_m depolarisation at the wound edge (Del Mónaco et al., 2009; Justet et al., 2013). In considering that work in this study implicated ENaC in modulating the migration of OvCa cells lines (refer to Chapter 5, section 5.2.4) and the identification of a sustained depolarising current via patch-clamp studies (refer to chapter 3), it is thus plausible that ENaC may play a role in modulating the migration of OvCa_{asc} in an external EF.

Subsequently, this study aimed to investigate the galvanotactic cue in cancer and the role of Na⁺ and ENaC mediated Na⁺ fluxes. To address this it was first investigated whether OvCa_{asc} were galvanotactic. Secondly, it was assessed whether ENaC plays a role in EF directed cell migration. Finally it was assessed whether Na⁺ influx and V_m modulation modulate the galvanotactic cue.

6.2 Results

6.2.1 Investigation of galvanotactic response in OvCa_{asc} isolates

It was first sought to assess whether OvCa_{asc} populations exhibited directional migration in the presence of an electric field. Migration of OvCa_{asc} cells in the absence and presence of an electric field (5 V/cm) was carried out as described in section 2.14 and quantitative analysis of cell migration was performed using the parameters detailed in section 2.14.9.

A representative time-lapse image of an OvCa_{asc} derived cell line (OM5) in the absence and presence of an external EF is shown in Figure 6-1. A subset of cells (numbered 1-5) were tracked and exhibited random migration in the absence of an external EF (Figure 6-1 A-C). Upon application of an external EF however, some cells (numbered 3, 4 & 5) exhibited marked anodal translocation (Figure 6-1 D-F).

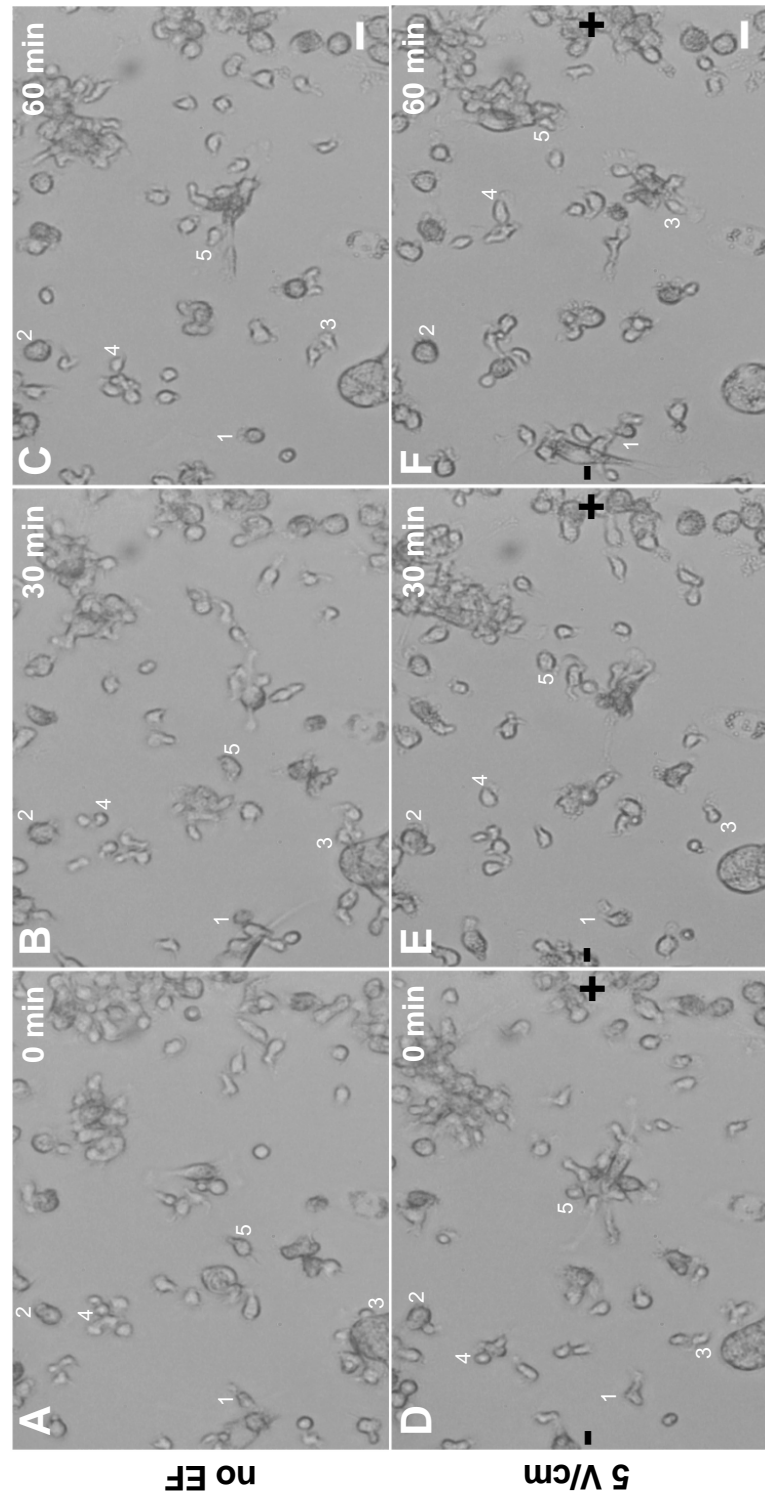


Figure 6-1: Representative bright field time-lapse photographs of 5 separate cells from OM5 taken from the same field of view over 60 minutes in the absence of an EF (A-C). An EF of 5 V/cm (D-F) was then applied and cells tracked for a further 60 minutes (cells labelled 1-5). Cells in no EF demonstrated random migration (A-C). In the presence of an EF cells demonstrated significant movement towards the anode. Polarity indicated with '+' (anode) and '-' (cathode). Scale bar, 20 μ m.

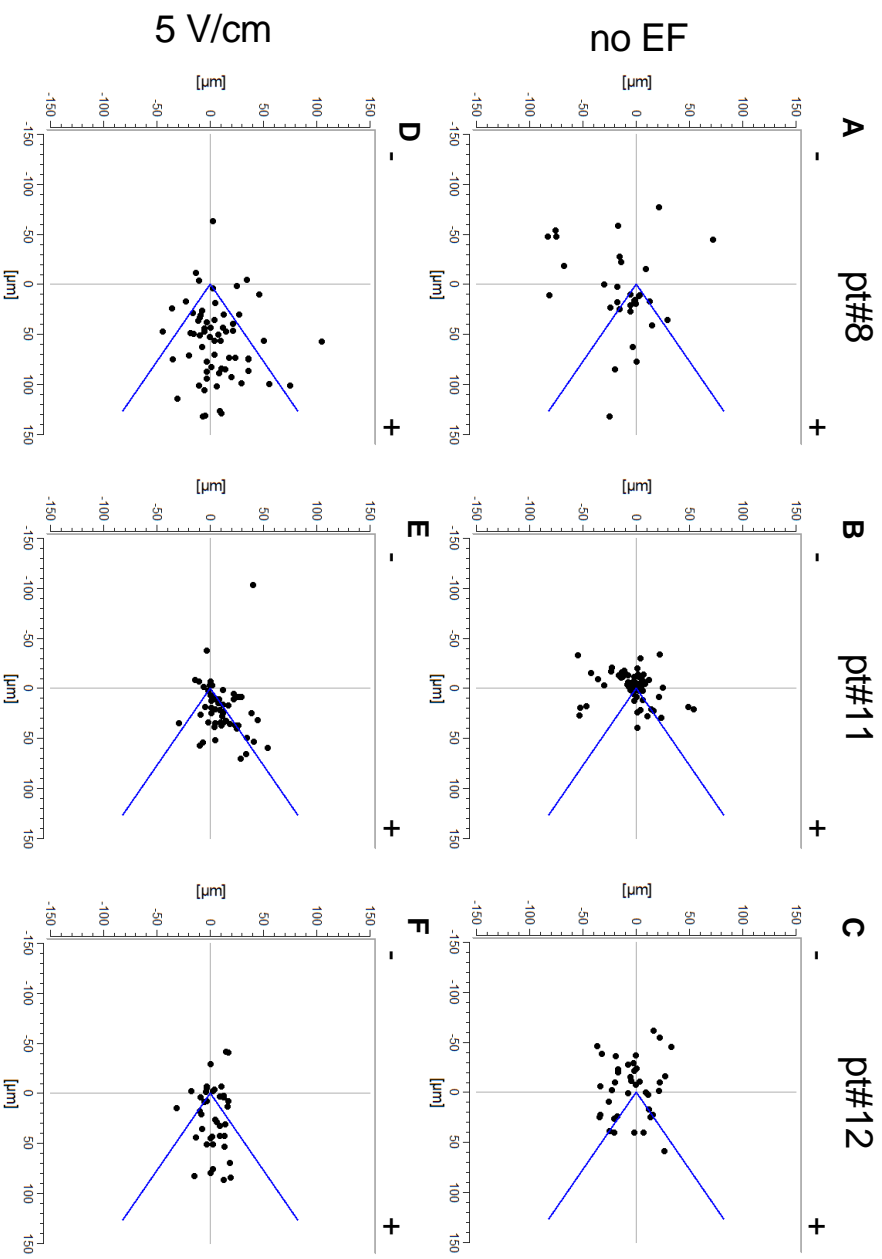


Figure 6-2: Composite trajectories of cells (dots) from *OvCaasc* samples OMs8, OMI1 and OMI2 respectively migrating in the absence (A-C) and in the presence of an EF (D-F). After computer-aided tracking the position of a cell before and after 60 minutes in the absence or presence of an EF, the initial point was placed at the origin (0,0) and the final location of each cell was plotted as a single 'dot' on the circular graph. '+' and '-' denote anode and cathode respectively; the anode was always placed at the right side of the diagram. Blue lines demarcate a region centred 66° about the anode corresponding to a cosine value of $\geq +0.84$.

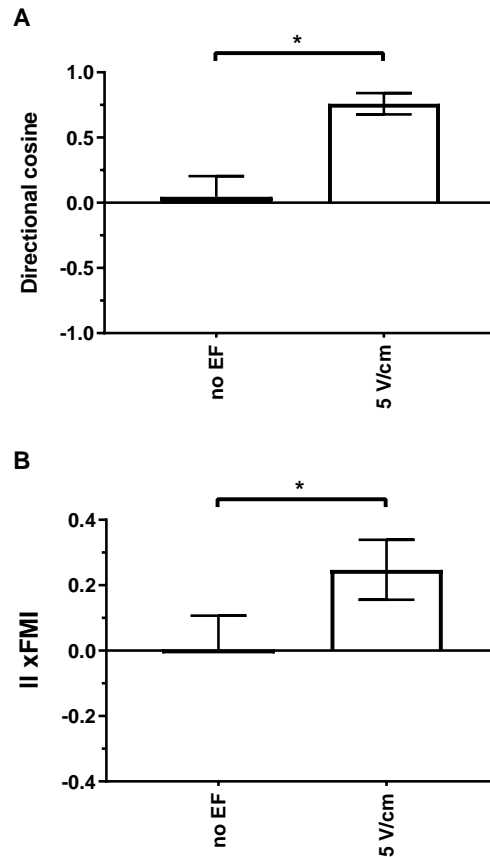


Figure 6-3: The grouped effects of an applied external EF on the galvanotactic properties of primary OvCa_{asc} cell lines in an external EF of 5V/cm. (A) Directional cosine, (B) ||FMI. Error bars represent grouped mean \pm SD of 3 samples: OM8, OM11, OM12. * denotes significance relative to control conditions (no EF) ($p < 0.05$), paired students t-test.

Quantitative metrics for OvCa_{asc} cell lines are presented next.

The quantitative migration data for OM8, OM11 and OM12 are presented in table 6.1. In the absence of an external EF, all 3 samples were observed to migrate randomly (figure 6-2 A-C) with a grouped mean directional cosine value of 0.05 ± 0.16 (mean \pm SD, $n=3$), and no preferential migration parallel to the intended EF axis (grouped mean ||FMI, $+0.003 \pm 0.103$, $n=3$) (figure 6-3). There were however some differences in the accumulated and euclidean distances between samples in the observed time (60 minutes) with OM8 exhibiting \approx twice the distance relative to OM11 (see table 6.1).

Upon application of an external EF however, a significant change occurred in all 3 samples, whereby cells migrated strongly to the anode (figure 6-2) (grouped mean directional cosine = 0.76 ± 0.08 , $n=3$, $p < 0.05$, paired students t-test) with meaningful translocation along the axis of the EF vector (grouped mean $\|FMI = +0.25 \pm 0.09$, $n=3$, $p < 0.05$) (figure 6-3). Thus, while there were limited differences in the distances covered, the directional translocation increased ≈ 4 -fold (table 6.1). This response was observed to be rapid with an observed orientation visible after 2 minutes (the time-lapse interval between successive image acquisition).

Identifier	EF (V/cm)	Directional cosine	$\ FMI$	Accumulated distance (μm)	Euclidean distance (μm)	Speed ($\mu\text{m}/\text{min}$)	N
OM8	no EF	0.21 ± 0.17	0.12 ± 0.06	154 ± 14	47 ± 6	2.66 ± 0.24	31
	5	0.85 ± 0.04	0.35 ± 0.03	174 ± 7	68 ± 4	3.11 ± 0.13	65
OM11	no EF	0.03 ± 0.14	-0.05 ± 0.03	70 ± 4	19 ± 2	1.00 ± 0.07	67
	5	0.71 ± 0.08	0.19 ± 0.03	100 ± 6	32 ± 3	1.43 ± 0.08	56
OM12	no EF	-0.11 ± 0.14	-0.06 ± 0.05	96 ± 7	32 ± 2	1.70 ± 0.12	39
	5	0.71 ± 0.12	0.20 ± 0.04	109 ± 6	34 ± 4	1.88 ± 0.11	40

EF Applied electric field strength
N Total number of cells tracked

Data are presented as means \pm S.E.M.

Metrics in blue denote statistically significant ($p < 0.05$) results relative to the respective no EF control.

Details of statistics and metrics provided in text.

Table 6.1: Quantitative metrics of cell migration in OvCa_{asc} isolates in the presence and absence of an external EF.

6.2.2 Effect of ENaC inhibition on galvanotaxis

In order to investigate whether ENaC activity played a role in galvanotaxis in primary OvCa isolates, an approach using pharmacological inhibition with 100 μM amiloride or 20 μM phenamil in the presence of an EF was employed (refer to section 2.14). The quantitative migration data for OM8, OM11 and OM12 in the absence and

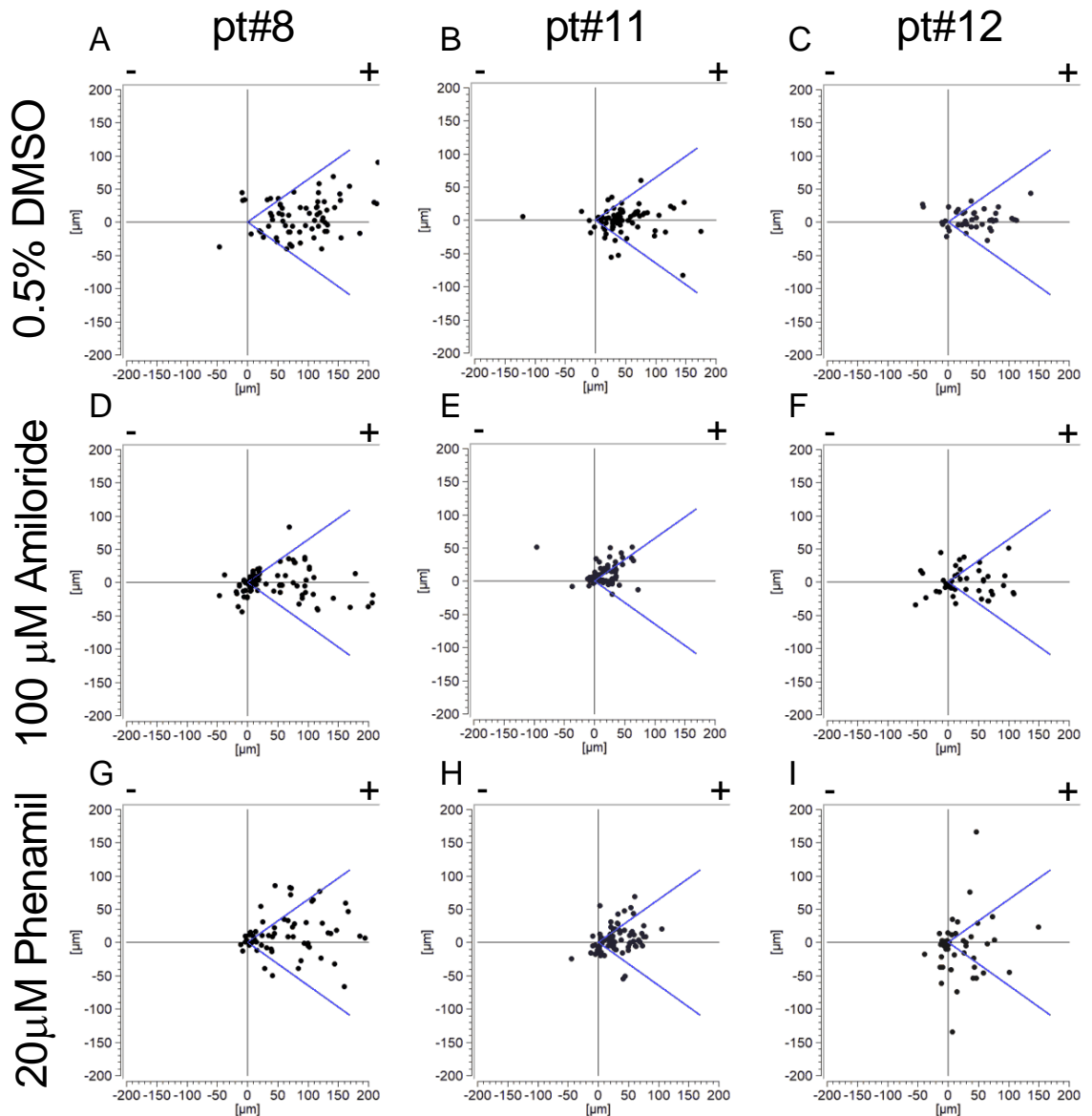


Figure 6-4: The effects of pharmacological inhibition of ENaC on the galvanotactic properties of primary OvCa cell isolates. Treatments were as follows, (A-C) OM8, OM11 & OM12 + 0.2% DMSO respectively, EF of 5 V/cm . (D-F) OM8, OM11 & OM12 + 100 μ M amiloride respectively, EF of 5 V/cm. (G-I) OM8, OM11 & OM12 + 20 μ M phenamil respectively, EF of 5 V/cm. The initial point of each cell trajectory was plotted at the origin (0,0). '+' and '-' denote anode and cathode respectively, the anode was always placed at the right side of the diagram. Blue lines demarcate a region centred 66° about the anode corresponding to a cosine value of $\geq +0.84$.

presence of amiloride or phenamil are presented in table 6.2. In agreement with previous observations, all three isolates tested were observed to migrate towards the anode

Identifier	EF (V/cm)	Perturbation	Directional cosine	FMI	Accumulated distance (μm)	Euclidean distance (μm)	Speed ($\mu\text{m}/\text{min}$)	N
OM8	5	0.1%DMSO	0.858\pm 0.040	0.342 \pm 0.022	266.7 \pm 11.5	96.3 \pm 6.0	2.32 \pm 0.1	67
	5	100 μM Amiloride	0.569 \pm 0.066	0.186 \pm 0.024	172.5 \pm 8.6	50.4 \pm 5.5	1.52 \pm 0.09	87
	5	20 μM Phenamil	0.741 \pm 0.055	0.311 \pm 0.030	239.1 \pm 12.9	91.1 \pm 9.3	2.01 \pm 0.11	68
OM11	5	0.1%DMSO	0.805 \pm 0.050	0.290 \pm 0.025	163.4 \pm 9.1	52.3 \pm 4.3	1.19 \pm 0.06	75
	5	100 μM Amiloride	0.489 \pm 0.086	0.112 \pm 0.022	149.4 \pm 7.8	31.1 \pm 2.9	1.19 \pm 0.06	56
	5	20 μM Phenamil	0.664\pm 0.058	0.245 \pm 0.026	124.9 \pm 8.1	38.2 \pm 2.8	1.06 \pm 0.07	75
OM12	5	0.1%DMSO	0.609\pm0.1	0.203\pm 0.032	190 \pm 10.2	49.5 \pm 5.1	1.7 \pm 0.09	40
	5	100 μM Amiloride	0.42\pm 0.11	0.109\pm 0.030	210 \pm 11.8	44.5 \pm 4.7	1.92 \pm 0.11	42
	5	20 μM Phenamil	0.128\pm 0.091	0.049\pm 0.030	136.9 \pm 17.7	38.5 \pm 5.6	1.14 \pm 0.15	51

EF Applied electric field strength
N Total number of cells tracked

Data are presented as means \pm S.E.M.

Metrics in **blue** denote statistically significant ($p < 0.05$) results relative to the respective no EF control.

Details of statistics and metrics provided in text.

Table 6.2: Quantitative metrics of amiloride and phenamil treatment on OvCa_{asc}

in an external EF of 5 V/cm (Figure 6-4 A-C), (grouped mean directional cosine = 0.76 ± 0.13 , $n=3$). In the presence of amiloride, cell populations also demonstrated an anodal trajectory to differing extents across samples (Figure 6-4 D-F). A clear reduction in directional migration was observed (grouped mean directional cosine = 0.49 ± 0.07 , $n=3$, $p < 0.05$ relative to control) with \approx 2-fold reduction in meaningful translocation towards the anode (grouped mean ||FMI = 0.14 ± 0.04 , $n=3$, $p < 0.05$ relative to control). No change in migration speed was observed across all 3 samples (refer to Table 6.2). A single sample (OM8), demonstrated significant reductions in accumulated and euclidean distances, whereas OM12 showed a small increase in accumulated distance (Table 6.2). In the presence of phenamil, cells also migrated towards the anode (Figure 6-4 G-I), with a mild reduction in directionality observed across all samples (table 6.2). In considering the grouped mean effect however, this was not significant (grouped mean directional cosine = 0.51 ± 0.33 , $n=3$, $p > 0.05$ relative to control). In considering meaningful translocation towards the anode in the presence of phenamil, a

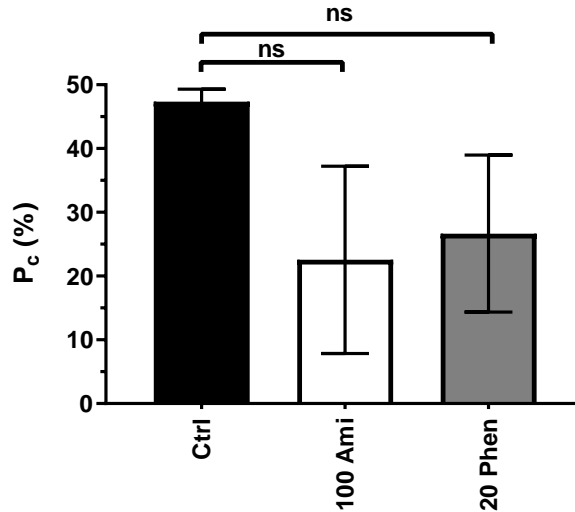


Figure 6-5: Percentage of primary OvCa cell isolates crossing a criterion boundary (P_c) relative to the initial position immediately prior to EF (5 V/cm) application. The threshold was defined as the median euclidean distance migrated of each sample in control conditions translocating in a 66° region centred around 0° (towards the anode). Ctrl; OSE CGM + 0.2 % DMSO, 100 Ami; OSE CGM + 100 μ M amiloride, 20 PHEN; OSE CGM + 20 μ M phenamil. Error bars represent mean \pm SD of 3 samples: OM8, OM11, OM12. ns, not significant ($p > 0.05$), one-way ANOVA with Dunnett's post-hoc test.

single cell line (OM12) demonstrated a significantly attenuated response while others did not (Table 6.2). While sub-populations in each cell line were observed to exhibit a reduced capacity to translocate directedly, this was not significant (grouped mean $\|FMI = 0.20 \pm 0.14$, $n=3$, $p > 0.05$ relative to control)(refer to table 6.2, see Figure 6-4 G-I).

To compare the effects of amiloride and phenamil on the extent of directional migration, an additional parameter P_c (percentage of cells crossing a criterion boundary) was used. P_c is determined by the number of cells crossing a threshold distance, defined as the median euclidean distance in the respective sample control conditions (vehicle + CGM + 5 V/cm) migrating to a region 66° (corresponding cosine value of 0.84) around the anode (see section 2.14.9). In control conditions, approximately half the

cell population in each group crossed the boundary ($P_c = 47.4 \pm 2.0 \%$, $n=3$)(Figure 6-5). Treatment with amiloride resulted in a reduction of the number of cells crossing the threshold (grouped mean $22.6 \pm 14.7n$ $n=3 \%$), however this was not significant (grouped mean difference - 24.8 [- 18.7, - 68.2] $p < 0.05$ one-way ANOVA, Dunnett’s post-hoc test) relative to control (Figure 6-5). Treatment with phenamil resulted in a similar reduction in the number of cells traversing the boundary ($P_c = 26.7 \pm 12.3 \%$, $n=3$) however this was also not significant (grouped mean difference - 24.8 [- 16.1, - 57.5] $p < 0.05$ one-way ANOVA, Dunnett’s post-hoc test) (Figure 6-5). In summary, ENaC inhibition reduced the capacity to migrate directedly in an external EF, however different OvCa_{asc} samples exhibited differing responses in meaningful translocation.

6.2.3 Effect of Na⁺ replacement on primary OvCa_{asc} cells

Identifier	EF (V/cm)	Perturbation	Directional cosine	FMI	Accumulated distance (μm)	Euclidean distance (μm)	Speed ($\mu\text{m}/\text{min}$)	N
OM8	5	ET Buffer + 20% FBS	0.91 ± 0.03	0.49 ± 0.03	172 ± 12	94 ± 9	1.58 ± 0.12	59
	5	Na ⁺ -free ET buffer	0.44 ± 0.07	0.17 ± 0.03	45 ± 4	15 ± 3	0.38 ± 0.03	79
OM11	5	ET Buffer + 20% FBS	0.84 ± 0.05	0.35 ± 0.03	84 ± 6	34 ± 3	0.72 ± 0.05	60
	5	Na ⁺ -free ET buffer	-0.60 ± 0.07	-0.23 ± 0.03	193 ± 10	60 ± 6	2 ± 0.13	58
OM12	5	ET Buffer + 20% FBS	0.64 ± 0.08	0.32 ± 0.04	135 ± 14	59 ± 8	1.44 ± 0.18	44
	5	Na ⁺ -free ET buffer	-0.20 ± 0.12	0.04 ± 0.04	95 ± 22	32 ± 13	0.79 ± 0.19	44

EF Applied electric field strength
N Total number of cells tracked

Data are presented as means ± S.E.M.

Metrics in blue denote statistically significant ($p < 0.05$) results relative to the respective no EF control.

Details of statistics and metrics provided in text.

Table 6.3: Quantitative metrics of external Na⁺ replacement on OvCa_{asc}

In order to assess the role of Na⁺ influx and V_m on the galvanotactic response of primary OvCa_{asc}, an approach using an impermeant replacement of Na⁺ was taken. In basal ET buffer supplemented with 20% FBS at a field strength of 5 V/cm, cells exhibited a net anodal response with similar directional cosine magnitudes observed in

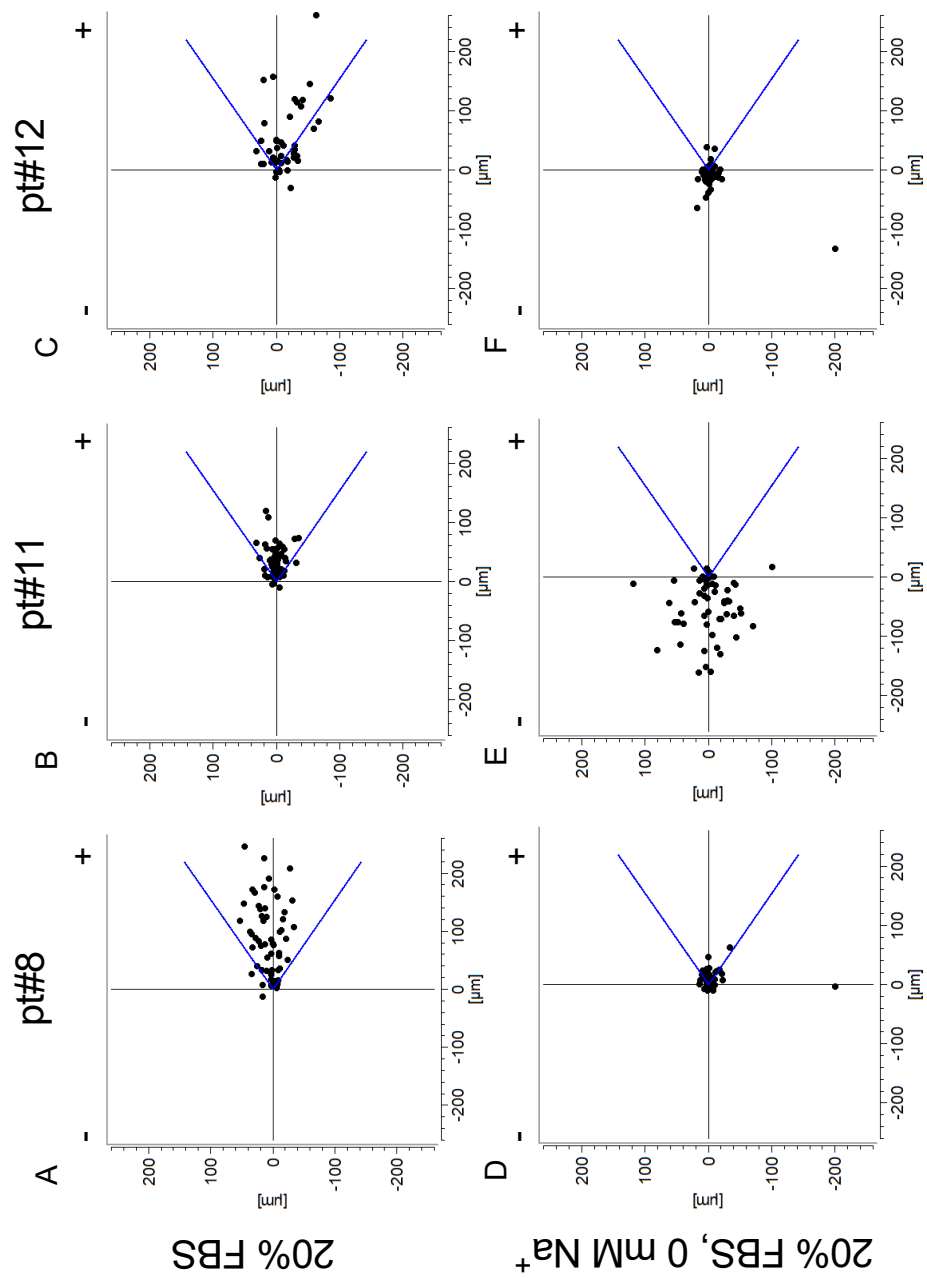


Figure 6-6: The effects of Na⁺ replacement on the galvanotaxis of primary OvCa_{asc} cell isolates. Treatments were as follows, (A-C) OM8, OM11 & OM12 in basal ET buffer + 20% FBS, EF of 5 V/cm . (D-F) OM8, OM11 & OM12 in Na-free ET buffer + 20% FBS, EF of 5 V/cm. The initial point of each cell trajectory was plotted at the origin (0,0). '+' and '-' denote anode and cathode respectively, the anode was always placed at the right side of the diagram. Blue lines demarcate a region centred 66° about the anode corresponding to a cosine value of $\geq +0.84$.

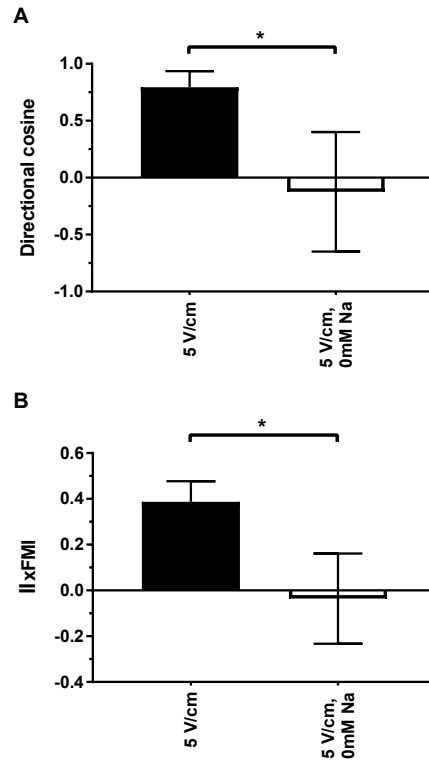


Figure 6-7: The effects of Na^+ replacement on the galvanotactic properties of primary OvCa cell isolates in an external EF of 5V/cm. (A) Directional cosine, (B) $\|\hat{x}\text{FMI}$. Error bars represent mean \pm SD of 3 samples: OM8, OM11, OM12. * denotes significance ($p < 0.05$), paired students t-test.

OSE CGM (directional cosine = 0.79 ± 0.14)(figure 6-6 A-C) and similar extents of directional translocation ($\|\hat{x}\text{FMI} = 0.39 \pm 0.09$)(table 6.3), grouped mean data displayed in figure 6-7. However, on partial Na^+ replacement the anodal response was completely abolished (directional cosine = -0.12 ± 0.53 , $n=3$, $p < 0.05$ relative to control). In 2 of 3 samples tested, cells were unable to translocate meaningfully (figure 6-6, however one sample exhibited a strong cathodal migration (table 6.3) (grouped mean $\|\hat{x}\text{FMI} = -0.04 \pm 0.20$, $n=3$, $p < 0.05$ relative to control).

6.3 Discussion

Here, evidence for OvCa_{asc} migrating directionally in an electric field is presented for the first time. Pharmacological inhibition of ENaC with amiloride and phenamil

results in a reduced galvanotactic capacity of OvCa_{asc}. It is also demonstrated that Na⁺ mediated depolarisation alters galvanotactic behaviour of OvCa cells.

6.3.1 OvCa_{asc} migrate preferentially in an external EF

Cell migration is well recognised as a critical property in the metastatic dissemination of cancer. Gaining greater understanding of the long-range directional cues that persist in ovarian cancer may provide further insight into the mechanisms governing ovarian cancer progression.

Here it is shown for the first time that OvCa_{asc} cells are galvanotactic. In external electric fields of endogenously produced field strengths they exhibit a strongly anodal response.

When OvCa_{asc} cells were plated on collagen 1 coated plastic, all three samples tested demonstrated a strong anodal response. Studies of galvanotaxis in glioblastoma have observed a directional dependence of migration depending on the ECM components present. On poly-L-ornithine/laminin-coated plastic, cells migrated to the anode, however when embedded in 3D collagen/hyaluronan hydrogel, cells exhibited a cathodal response. There is thus a clear physical interaction with the ECM that may serve to modulate the galvanotactic cue (Huang et al., 2016). OvCa cells are known to interact with collagen, indeed in the omentum, a primary metastatic site of dissemination, collagen remodelling by mesothelial cells has been shown to promote invasion (Natarajan et al., 2019). It is important that future studies assess the ECM dependence of OvCa_{asc} galvanotaxis.

There is some evidence that the polarity of endogenous TEP, and hence endogenous EFs, correlate with the directional response in metastatic cell lines. Rat prostate cancer metastatic Mat-LyLu cells are cathodal and the TEP of the rat prostate duct is

luminally negative. The initial direction of invasion early in disease is into the lumen and thus correlates with the directional response of both cell types. In order to further understand the relevance of galvanotaxis in OvCa, it is necessary to identify the electrical dimensions or cues which may direct this response. OvCa metastatic spread is characterised by the formation of peritoneal implants of OvCa cells and spheroids. During formation, OvCa cells migrate towards, attach to, and invade the mesothelium, the cell layer covering the surface of organs in the abdominal cavity (Iwanicki et al., 2011). There is limited information regarding the transmesothelial potential (TMP) in human tissues. The TMP of mesothelial cells grown on polyester inserts was measured to be ≈ 0.5 mV, apically positive when measured using the Ussing chamber setup (Li et al., 2001). The mesothelium consists of a flattened layer of cells that is approximately 2-3 μM thick, which would thus result in an EF of between 1.7-2.5 V/cm across it that is apically positive. Since OvCa_{asc} cells are anodal, this field gradient is inverse and hence is unlikely to act as a directional cue. However, it should be noted that isolated mesothelial cells may not be reflective of *in vivo* TMP measurements, and gold-standard techniques such as vibrating probe measurement on resected healthy and cancerous omental tissue would provide further insight (Reid, Nuccitelli and Zhao, 2007).

It has been suggested that the galvanotactic cue in cancer may begin in the primary tumour and facilitate migration to distant metastatic sites. Surface potential measurements at the tissue surface are lower in breast tumours when compared to normal tissue; a property that has been correlated with metastatic potential (Cuzick et al., 1998). This most likely arises from the fact that transformed cells are substantially more depolarised than normal breast epithelial cells (Fraser et al., 2005; Marino et al.,

1994). As such, a situation could arise in the malignant ovary where EF field gradients exist and provide an anodal cue for metastatic cells to migrate into. Furthermore, in considering that the lining of the ovary is also mesothelial, it is plausible that the TMP (outside positive) may provide a cue for OvCa cells to migrate into the peritoneal fluid. It may then be that the anodal migratory capacity of OvCa_{asc} cells is a retained characteristic from those cells that invade the primary site. However, only OvCa_{asc} cells have been assessed to date and thus it is necessary to test the galvanotactic response of malignant cells derived from solid tumour samples.

In summary, it has been shown that primary OvCa_{asc} cells migrate directedly in external electric fields at cosine values similar to those observed in other highly metastatic cancers. This may prove insightful in further understanding the role of galvanotaxis in metastatic dissemination of OvCa.

6.3.2 ENaC and V_m modulate the galvanotactic cue in OvCa_{asc}

Here, we show that ENaC plays a role in responding to external EFs and modulating the galvanotactic response in OvCa_{asc} cell populations.

Inhibition of ENaC with either amiloride or phenamil resulted in a reduction of EF mediated directional cell migration in primary OvCa cells. However, in the presence of both drugs, cells still demonstrated the ability to ‘sense’ the EF and migrate anodally with a relatively mild reduction in directional response. A dose-dependent effect of amiloride and phenamil was not assessed in this study however, and further investigations utilising ENaC- α knock down or utilising the more potent channel blocker benzamil would prove insightful. Studies of galvanotaxis in human keratinocytes also demonstrated a mild reduction in directional response with the addition of 20 μ M phenamil, an effect similar to our observations (Yang, Charles, Hummler, Baines and

Isseroff, 2013). It is also of note that human keratinocytes migrate towards the cathode whereas OvCa_{asc} cells are anodal (Guo et al., 2015; Yang, Charles, Hummler, Baines and Isseroff, 2013). While ENaC blockade served to reduce the directional response, cells still demonstrated in a strong cathodal response. In the same study depletion of ENaC- α , resulted in the complete abolishment of directional response with no reduction in migration speeds, suggesting that ENaC participated in direction sensing and EF but did not influence the underpinning cell migration machinery. From the observations of Yang et al in keratinocytes and the observations made here in OvCa_{asc}, it is clear that there is a cell-specific subtlety of EFs in controlling EF directed cell migration, suggesting that there exist differing mechanisms through which primary OvCa cells ‘sense’ and respond to an EF (Yang, Charles, Hummler, Baines and Isseroff, 2013). In summary, ENaC may play a regulatory role in ‘sensing’ an EF.

One of the key mechanisms proposed to describe how cells ‘sense’ an external electric field and migrate directionally is based on localised changes in V_m (Borys, 2013). Upon exposure of a cell to an external electric field, the cytosolic fluid becomes polarised leading to negative charge accumulation at the anodal side and positive charge accumulation on the cathodal side. Since the resistivity of the cytoplasm is very low this will result in the bulk of charge being developed across the plasma membrane; this will subsequently result in a V_m hyperpolarisation of the anodal facing surface and a depolarisation of the cathodal facing surface (Lee and Grill, 2005). This mechanism has been proposed to differentially regulate Ca^{2+} influx across the cell; increased $[Ca^{2+}]_i$ at the anodal face and a decreased $[Ca^{2+}]_i$ at the cathodal face (Nuccitelli, 2003). A similar consideration can be applied to Na^+ . Considering a cell that is 15 μm in diameter placed in an EF of 5V/cm, the voltage developed between the two faces of the cell would be 15 mV,

that is, the anode would be 7.5 mV more hyperpolarised and the cathode would be 7.5 mV more depolarised. Assuming an $[\text{Na}^+]_i$ of 5 mM and $[\text{Na}^+]_e$ of 135 mM then E_{Na} at 37°C is 88.1 mV. Then considering that V_m values of OvCa_{asc} are typically -5 mV, Na^+ is 93.1 mV away from equilibrium. However, a 7.5 mV local change in V_m would increase the total driving force for Na^+ by approximately 7.6% at the anode and reduce it by 7.6% at the cathode. Essentially, the established ion asymmetry could set up an intracellular concentration gradient which may influence motility. Other studies in cancer have established a role for Na^+ conductances in galvanotaxis. Na_V channels are over-expressed in metastatic cancers and have been shown to correlate with metastatic potential (Mycielska and Djamgoz, 2004). Metastatic prostate and breast cancer cells exhibit a strong galvanotactic response and interestingly this response is abolished in the presence of TTX, a blocker of Na_V channels (Djamgoz et al., 2001; Fraser et al., 2005). Increased galvanotactic response in MAT-LyLu can be potentiated further by treatment with veratridine, a Na_V channel opener; this results in an enhanced effect of the EF on directed cell migration (Djamgoz et al., 2001). The mechanisms of Na_V mediated cell migration are not well understood, however several theories have been postulated (Mycielska and Djamgoz, 2004). One such theory suggests that increased Na^+ influx would inhibit Ca^{2+} exchange across the membrane hence increasing $[\text{Ca}^{2+}]_i$, a critical regulator of migratory machinery (Borys, 2013). Hence, it is possible that Na^+ influx, independently of a specific ion channel, may serve to direct migration and hence this is a possible explanation for role for ENaC in modulating the galvanotactic response in OvCa_{asc} .

When V_m was hyperpolarised through the part replacement of Na^+ with NMDG⁺ a complete inhibition of anodal migration was observed in OvCa_{asc} cells. The direc-

tional migration of cells differed between samples however. Indeed, 1 sample (OM11) migrated strongly towards the cathode while the other two oriented cathodally but did not migrate meaningfully. The observation that OM11 exhibited strong cathodal migration upon part replacement with NMDG⁺ poses interesting questions. $[Ca^{2+}]_i$ gradients across a migrating cell have profound effects in modulating migratory machinery across numerous cell types (this is discussed at length in section 1.7.2.3). Increases in $[Ca^{2+}]_i$ at the rear of the cell results in the shortening and gelsolin-dependent capping of actin filaments, which ultimately results in inhibition of actin polymerisation and membrane protrusion. A reduction in $[Ca^{2+}]_i$ in the frontal regions of the cell has been shown to result in dissociation of gelsolin from actin filaments, facilitating actin polymerisation and formation of membrane extensions. Evidence is growing for a role of Na⁺-dependent calcium influx in cancer. In rat ventricular myocytes, a persistent Na⁺ influx facilitated by Na_v1.5 results in Ca²⁺ influx via reverse mode function of NCX (Yao et al., 2011). It may be that NCX transporters are expressed differentially across the 3 OvCa_{asc} samples tested in this chapter. It is plausible that the driving force for NCX is reduced upon part removal of $[Na^+]_e$; NCX may thus predominantly be operating in forward mode. Since it has been shown that Na⁺ contributes to a more depolarised phenotype in OvCa_{asc} samples in this thesis, it is also possible that the resultant V_m hyperpolarisation upon replacement of $[Na^+]_e$ with NMDG will increase the driving force for Ca²⁺ uptake via different pathways. Store-operated Ca²⁺ entry (SOCE) has been shown to be an important mechanism mediating Ca²⁺ uptake in numerous cancers (Chen et al., 2019). Dysregulated SOCE pathways and overexpression of the associated plasma membrane pore-forming subunits Orai 1-3, correlate with increased migratory and invasive capacity in breast cancer, cervical cancer, hepatocellular

carcinoma and glioblastoma (Feng et al., 2010; Chen et al., 2011; Yang, Tang, Wang, Zhang, Xu, Shen, Sun and Yang, 2013; Motiani et al., 2013). V_m hyperpolarisation results in persistent Ca^{2+} influx in cerebellar granule neurons . In human myoblasts, V_m hyperpolarisation results in increased Ca^{2+} uptake. The dependence of the galvanotactic response in OvCa_{asc} on Ca^{2+} influx was not the purpose of this study. However it remains an important question whether differential activity/expression of Ca^{2+} influx pathways may explain the markedly different response in OvCa_{asc} samples upon part removal of $[Na^+]_e$. Future studies employing Ca^{2+} -sensitive fluorescent indicators such as Fluo-4 or the widely used ratiometric dye fura-2 in combination with galvanotaxis experiments would prove insightful in assessing the dependence of Ca^{2+} uptake on $[Na^+]_e$ (Lock, Parker and Smith, 2015). Taken together however, it is suggestive that a depolarised phenotype is necessary for strong anodal migration in OvCa_{asc} cells.

It is of note that metastatic cancer cells that are strongly galvanotactic have been shown to be more depolarised than their weakly metastatic and galvanotactic counterparts (Fraser et al., 2005). These observations and the results presented here raise the question as to whether a depolarised V_m facilitates cells to ‘sense’ an electric field.

One other interesting question that arises from this work is whether hyperpolarisation via mechanisms other than the impermeant replacement of Na^+ also modulate the directional response of OvCa_{asc} cells in an EF. Indeed, in a study assessing $K_{ir}4.2$, a member of the inward-rectifying K^+ channel family, in a human corneal epithelial cell line, knock-down resulted in the complete abolishment of cathodal migration and also served to depolarise cells by ≈ 20 mV relative to control siRNA (Nakajima et al., 2015). Interestingly, in the same study transfection of siRNA for $K_{ir}4.2$ into anodal migrating MDA-MB-231 cells also resulted in abolishment of galvanotactic capacity but did not

impair cell migration rates. It is thus likely that V_m modulations predispose cells to ‘sense’ differential galvanotactic cues. Indeed, here it was observed that a single sample exhibited a strongly cathodal response when hyperpolarised, providing further evidence of the EF-sensing modulatory capacity of V_m . Further studies in OvCa_{asc} galvanotaxis must assess the effect of V_m dependence by investigating the effect of intermediate concentrations of impermeant replacements for Na⁺.

Since it has been shown that ENaC induces a sustained depolarisation in an OvCa ascites-derived cell line (refer to chapter 3), one plausible hypothesis is that V_m hyperpolarisation by ENaC inhibition may render the cells less susceptible to V_m perturbations induced across the cell in an external EF; this would explain the attenuated galvanotactic capacity on OvCa_{asc} cells in the presence of amiloride. However, the work in this thesis has to date not assessed whether the effect of ENaC inhibition on galvanotaxis is due to direct perturbations on V_m or indeed due to the potential modulations of other Na⁺-mediated local ionic fluxes across the front and rear of the cells in an external EF, such as potential Na⁺-mediated Ca²⁺ entry mechanisms that may be in part due to the activity of NCX activity in reverse mode, suggested in other cancers. To further elucidate whether V_m perturbations are important in modulating OvCa_{asc} galvanotactic capacity an Na⁺-independent approach could be assessed by manipulation of other ionic gradients present in extracellular medium. The effect of Na⁺-independent hyperpolarisation could be assessed by titration of extracellular K⁺ from 5 mM to 1-2 mM. It is also not outside the realms of possibility to directly assess whether ENaC inhibition results in a reduction in the voltage developed across the two faces of the cell in an external EF. The V_m -sensitive fluorescent dye Di-8-ANEPPS has been used to assess the effect of cell polarisation in an external EF on *Xenopus* oocytes (Lee and

Grill, 2005).

All experiments in this study were undertaken in either cell culture medium or ET buffers (compositions described in section 2.14.3) supplemented with 20% FBS. It is of note that the galvanotactic capacity of numerous primary cell types is dependent on the presence of serum in external medium. In bovine corneal epithelial cells, removal of FBS resulted in abolishment of cathodal migration which was only detectable again when the external EF was increased 2-fold (from 1 V/cm to 2 V/cm relative to control conditions(10%)), however meaningful translocation was still significantly attenuated relative to control conditions (4-fold lower) (Zhao et al., 1996). Furthermore, in studies on human keratinocytes, removal of all growth supplements resulted in a 50% reduction in translocation rate, though cells still exhibited a similar cosine value when compared to cells in the presence of growth factors (Fang et al., 1998). In view of the evidence for growth factors in modulating the galvanotactic capacity of cells, the effect of FBS removal on a single OvCa_{asc} cell line (OM8) was assessed (experiment was undertaken in the presence of ET buffer alone). Interestingly, while cells displayed an orientation parallel to the EF, they exhibited no significant translocation, suggesting the importance of media supplementation with FBS in this cell population. Future investigations would take a titration-based approach to assess the relative minimal concentration of FBS that facilitated galvanotactic migration. While there are numerous growth factors present in serum known to modulate cell behaviours such as proliferation, differentiation and migration (Witsch, Sela and Yarden, 2010), there is evidence for a role of epidermal growth factor (EGF) in the regulation of Na⁺ transport and ENaC activity. Treatment of A6 *Xenopus laevis* kidney cells with EGF resulted in a transient increase in ENaC activity by increasing P_O (Markadieu et al., 2005). However, chronic treat-

ment of A6 cells with EGF resulted in an inhibition of detectable ENaC activity by decreasing the number of channels in the plasma membrane through the modulation of MAPK1/2 pathways (Liu et al., 2009). Other studies of EGF-mediated ENaC regulation in mpkCCD_{c14} renal collecting duct principal cells have shown differential effects on temporal ENaC inactivation however (Levchenko et al., 2010). Consequently, the effects of EGF on ENaC-mediated Na⁺ transport are diverse and exposure-duration specific. Future experimental approaches involving acute exposure windows to cells supplemented with FBS or EGF would further elucidate the extent to which serum supplementation contributes to galvanotactic capacity of OvCa_{asc} cells.

While it was shown that the OvCa_{asc} population was approximately 80% pure for cancer cells (Chapter 2, section 2.11.2), it is important to consider the contributory effect that other populations may have on the total galvanotactic response in OvCa_{asc} samples. Since cells with a spindle like morphology and subsequent staining for FGFR4 were observed, it is likely that a low number of fibroblasts are present in OvCa_{asc} samples. Some evidence exists for fibroblasts in external EFs. Human dermal fibroblasts exhibited relatively slow migration towards the anode in an external EF of 0.5-1 V/cm (Guo et al., 2010). It is thus plausible that a fibroblast population may contribute to a small extent to the anodal phenotype observed in physiological [Na⁺]_e. Other potential confounding cell populations may contribute to the galvanotactic effect observed should be considered. There are to date no known studies of galvanotaxis in mesothelial cell populations, and it remains an interesting whether they also respond to the galvanotactic cue.

In conclusion, this study has demonstrated for the first time that OvCa cells of ascitic origin are galvanotactic. The potential galvanotactic cue for OvCa has to date

not been elucidated, however, in considering that galvanotactic response correlates with metastatic potential, this provides a promising and novel avenue of research in further understanding OvCa dissemination. It is further demonstrated that directed cell migration in an external EF is partly dependent on ENaC-mediated Na^+ influx. Furthermore, V_m depolarisation or Na^+ influx is required to facilitate the anodal phenotype observed.

Chapter 7

Final overall discussion

This work aimed to contribute to the understanding of bioelectric control of ovarian cancer with a focus on the role of Na^+ and specifically ENaC, and their potential role in modulating critical properties of cancer. Since alterations in V_m have been implicated in modulating several different behaviours of a cancer cell, a broad approach was taken. The main findings in this study were:

- OvCa cell line models and OvCa_{asc} are markedly depolarised.
- The depolarised phenotype in ovarian cancer is conferred by an increased P_{Na^+} .
- ENaC contributes to sustained V_m depolarisation in SKOV-3 cells, an OvCa ascites derived cells line.
- ENaC inhibition with amiloride reduces proliferation in SKOV-3 and OVCAR-3 cell lines. Moreover, mild increases in $[\text{Na}^+]_e$ resulted in an increase in proliferation of a slower growing cell line, OVCAR-3.
- mRNA expression for ENaC- α was significantly up-regulated in FIGO₃₋₄T solid

tumours relative to NOv. Levels did not change on progression from primary tumour to malignant OvCa ascites. Protein expression was confirmed by western blotting and IF respectively.

- ENaC- α^+ staining increases with stemness.
- ENaC function facilitates cell migration of OvCa cell lines and is functionally upregulated in a migration stimulated environment.
- ENaC inhibition decreases cell deformability in A2780 OvCa cells, a critical modulator of cell migration.
- OvCa_{asc} cells are strongly galvanotactic: a property which has been shown to correlate with metastatic potential. ENaC modulates the directional migration of OvCa_{asc} cells in an external EF. Furthermore, impermeant replacement of Na⁺ with NMDG abolishes the anodal migratory phenotype, potentially via V_m hyperpolarisation.

It has been relatively well established that malignantly transformed cells exhibit a depolarised V_m in numerous cancers. However, prior to this body of work, there was only one report of V_m values in OvCa (Binggeli and Weinstein, 1986; Yang and Brackenbury, 2013; Redmann et al., 1972). The work presented in chapter 3 using patch-clamp electrophysiology demonstrated that V_m values of SKOV-3 cells and OvCa_{asc} cells are indeed highly depolarised and correlate well with measurements in solid tumours using the sharp-electrode technique. Moreover, it was demonstrated that increased P_{Na⁺} of the plasma membrane contributes to this phenotype to a large extent, as has been suggested by others in breast cancer cell lines (Wonderlin, Woodfork and Strobl,

1995). While a body of work exists on altered ion channel expression profiles in cancer, there is substantially less work focussing on the conductances responsible for sustained depolarisation. Studies in high grade gliomas have also shown that ENaC and ASIC contribute to increased V_m depolarisation, an observation that interestingly is absent in low-grade gliomas and normal astrocytes (Rooj et al., 2012; Berdiev et al., 2003). Others have suggested that persistent V_m depolarisation is partly accounted for by the loss of some hyperpolarising K^+ channels; indeed it may be that this, in part, accounts for our observation that a subset of SKOV-3 cells demonstrated little change in V_m values upon impermeant replacement of Na^+ (Fraser et al., 2005). One other potential explanation for the the markedly different extents of hyperpolarisation exhibited by SKOV-3 cells upon replacement of $[Na^+]_e$ or by addition of high doses of amiloride is that there may be undiscovered persistent Na^+ conductances contributing to a depolarised V_m . One family of ion channels that are promising candidates for increased Na^+ conductance are the transient receptor potential (TRP) channels. The TRP channel family consists of at least 20 individual ion channel proteins, which participate in a wide variety of physiological functions including pain and itch-sensing (Akopian, 2016). Numerous members of the TRP channel family exhibit a relatively high permeability to Na^+ and have been shown to participate in regulating V_m in numerous cell types (Gees, Colsoul and Nilius, 2010). Numerous studies have reported increased expression of TRP channels, particularly those performed in prostate cancer (Prevarskaya, Zhang and Barritt, 2007). Increased expression of TRPC3 has been identified in primary OvCa biopsies; downregulation resulted in reduced proliferation in SKOV-3 cells (Yang et al., 2009). Future studies must thus address the contribution of Na^+ conductances from other, as yet unidentified, channels. Fewer investigations have assessed the possible

contributory role for V_m depolarisation from Na^+ channels. NaV channels have gained the most interest; they show marked over expression profiles in metastatic breast and prostate cancer and partly contribute to sustained V_m depolarisation in metastatic models of breast cancer (Yang et al., 2020*b*). While it was not within the scope of this study, future investigations must address the contribution of NaV channels to V_m in OvCa, including undertaking electrophysiological approaches using the classical Na channel blocker tetrodotoxin.

While the work presented in this study was focussed on investigating the role of ENaC and Na^+ in modulating the bioelectric behaviour of OvCa, ENaC may have a functional role in modulating the bioelectric behaviour of other cancers; namely depolarisation induced sustained proliferation, maintenance of stem cell populations and pro-migratory stimuli. To date, there have only been a small number of studies investigating ENaC function in cancer: for glioblastoma and hepatocellular carcinoma (Rooj et al., 2011; Bondarava et al., 2009). While Ross et al demonstrated a potential role for ENaC in facilitating RVI changes and thus theoretically potentiating glioma cell proliferation, there is a limited amount that can be inferred as to how ENaC current impacts upon disease progression (Ross et al., 2007). Future studies must address functional outcomes of altered ENaC activity.

In considering the modulation of Na^+ fluxes in OvCa, there is one critical component of Na^+ homeostasis that must be addressed. To date this study has not assessed directly whether perturbations in $[\text{Na}^+]_i$ are observed in OvCa. This is a central question, firstly since the method through which V_m measurements were accomplished (the patch clamp technique) is one which results in complete dialysis of the cytosolic compartment over time. Thus, while a depolarising cue was indeed detected in the SKOV-3 cell line and

in OvCa_{asc} cells at 5 mM $[\text{Na}^+]_i$, the contribution of this cue may be substantially reduced if $[\text{Na}^+]_i$ in OvCa cells is elevated. Seminal studies conducted mainly in the 1980s identified elevated $[\text{Na}^+]_i$ levels in the cytosol of rapidly proliferating cells; it was also observed that intranuclear Na^+ concentrations ($[\text{Na}^+]_{i\text{Nucleus}}$) were increased. When $[\text{Na}^+]_i$ and $[\text{Na}^+]_{i\text{Nucleus}}$ levels were assessed in urogenital cancers, they were found to be approximately 4-fold higher than non-transformed cells of the normal human urothelium and those of rat tubular kidney cells (Nagy et al., 1981; Smith et al., 1981). Compelling evidence of a role for ENaC in modulating intracellular Na^+ is further presented by a study involving H6 hepatocellular carcinoma cells implanted in A/J mice: amiloride treatment resulted in a 6-fold reduction in tumour volume with concomitant 2-fold reduction in $[\text{Na}^+]_{i\text{Nucleus}}$ when compared to untreated control (Sparks et al., 1983).

Different strategies were employed to quantify $[\text{Na}^+]_i$. In the first year of study, a method was developed to determine $[\text{Na}^+]_i$ using the ratiometric pH-sensitive dye carboxy-SNARF-1-AM in the presence of the carboxylic ionophore $\text{Na}^+\text{-H}^+$ monensin, adapted from a method to determine $[\text{K}^+]_i$ using the $\text{K}^+\text{-H}^+$ ionophore, nigericin (Balkay et al., 1997). While there was moderate success optimising this method, it does not allow for the concomitant treatment of cells with other pharmacological modulators and as a result, the method was not pursued further. A new ratiometric Na^+ dye, NAGY was identified and subsequently obtained as part of a collaboration; while fluorescent yield was very high, there were problems with stability and as such it was abandoned (Taki et al., 2015). This avenue of research remains central to further understanding the altered Na^+ homeostasis in OvCa. Indeed, earlier this year a study using 3D-cone analysis to study $[\text{Na}^+]_i$ in *ex vivo* peritoneal lesions in HGS OvCa demonstrated a marked increase in intracellular weighted sodium, a marker of $[\text{Na}^+]_i$. This a

promising result, certainly considering the evidence presented here for increased ENaC- α expression, and the demonstration of a persistent amiloride-sensitive contribution to V_m , it lends more weight to the hypothesis that altered Na^+ homeostasis is important in OvCa progression (Deen et al., 2019).

7.0.1 Future work

While the investigations in this study demonstrated interesting findings regarding the potential increased expression of ENaC- α in putative OvCa CSC populations, limited conclusions can be drawn from this preliminary data. CSCs are characterised by their increased capacity for self-renewal (Wicha, Liu and Dontu, 2006). Whether ENaC confers OvCa cells with a persistent depolarising cue and thus facilitates sustained proliferation remains to be determined. Important investigations are required to further attribute increased ENaC- α expression to functional effects on OvCa cell hallmarks. Firstly it is important to address whether the $\text{CD117}^+/\text{CD44}^+$ population in OvCa_{asc} samples exhibit increased replicative potential. To this end, an approach using Fluorescence-activated cell sorting (FACS) to isolate the $\text{CD117}^+/\text{CD44}^+$ cell populations in combination with colony forming assays on double-layered soft agar would prove insightful (Vembadi, Menachery and Qasaimeh, 2019; Rajendran and Jain, 2018). Pharmacological approaches using amiloride would further elucidate whether the OvCa CSCs require an ENaC mediated Na^+ current to sustain proliferation, as has been suggested in neural stem cells (Petrik et al., 2018).

Studies in this thesis investigating altered expression of ENaC focused on the α and δ ENaC subunits. The rationale for this decision centred on the observations of other, that only assembled channels containing an ENaC- α or ENaC- δ result in a functional Na^+ -conducting channel (Canessa et al., 1994). While it was shown that ENaC- α

exhibited marked upregulation in OvCa samples, there are a number of unanswered questions. It has previously been shown that assembled channels containing ENaC- α alone exhibit a markedly reduced unitary conductance when compared to those formed from an α - β - and γ subunit (McNicholas and Canessa, 1997). These observations clearly demonstrate an important role for the β - and γ subunits in modulating channel function, and the question arises as to whether they exhibit altered regulation in OvCa. Indeed, in the IMCD mouse collecting duct cell line, ENaC- γ has been shown to be important in resistance to apoptosis upon exposure to hypotonic stress (Wang et al., 2014). Interestingly, ENaC- β has been suggested to have a tumour suppressive role in gastric cancer (Qian et al., 2017). In a tissue microarray study of chemo-naïve gastric cancer samples, increased expression of ENaC- β was shown to correlate with increased patient survival (Qian et al., 2017). In the same study, overexpressing ENaC- β in four gastric cancer cell lines (AGS, BGC823, MGC803, and MKN45) resulted in a greater fraction of cells undergoing apoptosis and also served to reduce migratory capacity (Qian et al., 2017). In light of these observations, it is important to determine whether the β - and γ - subunits display altered expression profiles in OvCa, and whether they are linked to similar experimental and functional outcomes described such as resistance to apoptosis and patient survival. A key strength of this study was access to human OvCa tissue biopsies, as well as ascites, and these preparations lend themselves well to these investigations given the characterisation we have. Other classical techniques that could be employed include clustered regularly interspaced short palindromic repeat (CRISPR)–Cas-associated nuclease approaches to overexpress particular ENaC subunits in order to determine the impact and relationship of particular subunits on aspects of migration, proliferation and indeed bioelectric characteristics (Li et al., 2020).

One of the key limitations of this study was the pharmacological approach employed to target ENaC function. While pharmacological inhibitors may have non-specific effects compared to molecular approaches, they allow more precise control of the timing of current / channel inhibition. While amiloride is classically characterised as a selective blocker of ENaC, its potential off-target effects, particularly on NHE, have proved a confounding factor in drawing clear conclusions on the regulatory role of ENaC on V_m in OvCa (Cassel et al., 1988). While its derivatives are more potent and somewhat more specific, a systematic approach using benzamil, phenamil and amiloride was not employed; this is important to address by comparing experimental outcomes in a clear and methodical fashion in order to have confidence in the data produced, and to help plan future studies. A number of other approaches can be explored. While inhibition of ENaC may result in off target effects, a channel opener / activator would prove an insightful tool in many of the investigations undertaken in this study. The small molecule specific ENaC activator S3969 has recently become available and demonstrates pronounced activation of ENaC conductance by increasing P_o (Lu et al., 2008). If used in conjunction with amiloride and its derivatives, it may prove useful in determining by whole-cell voltage-clamp and single-channel analysis, whether ENaC contributes to a sustained inward Na^+ current in OvCa.

The observations presented here for the roles of ENaC in promoting sustained proliferation and facilitating migration in OvCa, open up the potential for future clinical trials of ENaC inhibitors in OvCa, as has been suggested by others (Matthews, Ranson and Kelso, 2011). Amiloride is a long-established, licensed potassium-sparing diuretic in clinical use. However in view of this, and given the consideration that ENaC is present in most secretory epithelia, it must be approached with caution. Animal mod-

els thus present an appealing goal for investigating the potential of amiloride in slowing disease progression. While it is recognised that early detection of OvCa remains central to disease-free progression, it is my view that there are as yet unexplored treatment strategies that may improve outcomes in cases where the disease presents at advanced stages of peritoneal dissemination.

In summary, the work presented in this thesis provides further evidence for ENaC in modulating the critical hallmarks of OvCa. This work identifies new avenues of research into the novel approaches to targeting OvCa, and may eventually contribute to improving outcomes for women diagnosed with this insidious disease.

Appendix A

Limitations of patch clamp and sharp microelectrode methods to measure

V_m

While dialysis of the intracellular compartment is greatly reduced using the sharp microelectrode approach (due to a much smaller tip aperture), there are inherent issues in the accurate measurement of V_m in smaller mammalian cells (cells of the order of size including cancer / epithelial cells). The primary cause of underestimation of V_m is due to the introduction of a membrane shunt resistance (R_s) which is created by a hydration layer surrounding the microelectrode interface with the cell membrane upon penetration. Estimations of R_s are between 50 - 200 $M\Omega$. An equivalent circuit and subsequent effect on V_m measurements following introduction of an R_s component by a microelectrode are described in detail in Figure A-1 (figure from (Ince et al., 1986)). The patch clamp method does not suffer from the introduction of an R_s component

due to the formation of a ‘giga- Ω ’ seal ($> 1 \text{ G}\Omega$) between the patch electrode and the cell membrane. As such, this was the rationale for choosing the patch clamp approach for V_m measurement of OvCa cells in this study.

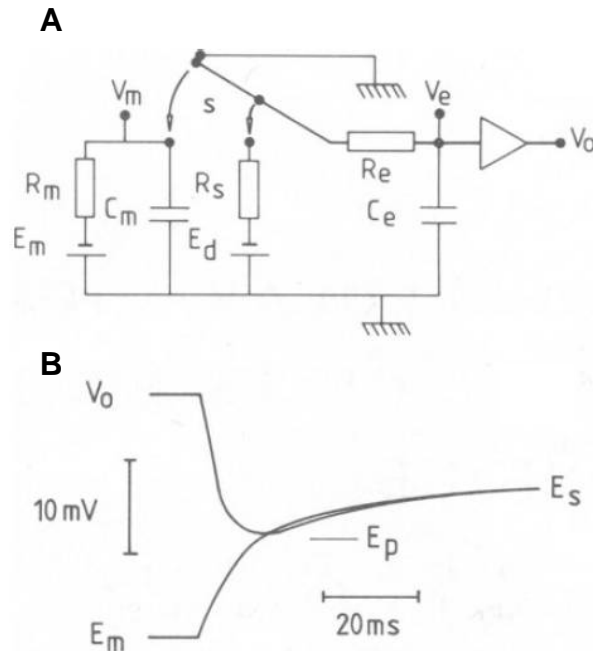


Figure A-1: Effect of the introduction of a transmembrane shunt resistance R_s on V_m measurements using the sharp microelectrode method. (A) Equivalent electrical circuit schematic of V_m measurements using the microelectrode method when an R_s component is introduced. Cell parameters: E_m , cell resting potential; C_m , cell capacitance; R_m , cell resistance. Electrode parameters: R_e , electrode resistance; C_e , electrode capacitance. The microelectrode introduces an R_s component thus creating a diffusion potential, E_d . Closure of switch (S) simulates impalement of the microelectrode. Before impalement, $E_m = V_m$. Following impalement, increased current flow through the newly introduced R_s results in a rapid decrease in V_m so that the actual membrane potential output V_o is considerably lower. (B) A simulated time course of R_s introduced errors in V_o following impalement. R_s results in a sharp positive going deflection of E_m . Before impalement, $V_o = 0 \text{ mV}$. Figure from (Ince et al., 1986)

There are however some drawbacks to the patch clamp approach for V_m measurement. Since the tip aperture of a patch clamp microelectrode is much larger ($\approx 2 \mu\text{m}$), upon formation of a seal the intracellular compartment is subject to dialysis by the pipette solution over the experimental duration. Since the exact fluid composition

of the intracellular compartment is not known, the use of an arbitrary / proprietary intracellular pipette solution (ISS) can also alter V_m due to depleting of intracellular molecules important in regulating ion channel function (Pusch and Neher, 1988).

Appendix B

Optimisation and validation of cell viability assays

B.1 Seeding density optimisation

Determination of optimal cell number and an estimation of the maximal detectable cell number in resazurin reduction cell viability assays was performed by generating a cell density vs resazurin RFU. Upon completion of cell detachment as per section 2.2.1.3, cells were counted as described above and serially diluted to create a range of cell densities (SKOV-3: 2.5×10^3 , 5×10^3 , 10×10^3 , 40×10^3 , 80×10^3 , 100×10^3 ; OVCAR-3: 2.5×10^3 , 5×10^3 , 10×10^3 , 40×10^3 , 80×10^3 cell per $100 \mu\text{l}$). Cells were then seeded in replicates of 6 for each seeding density in a clear 96-well Costar™ cell culture treated plate and incubated under standard conditions for 5-6 hours to allow sufficient time to cells to adhere. Cell viability was then assessed in the same manner as described in section 2.7. Curves were then obtained by fitting cell seeding density vs RFU (relative fluorescent units) with a variable hill slope equation using Graphpad Prism 8 (refer to figure B-1). Subsequent cell viability assays were seeded at 5×10^3 cells / well.

B.2 Validation of cell doubling time

To assess whether cell properties and growth characteristics were in agreement with those documented, growth curves were generated over 72 hours. Cells were seeded in triplicate at 5×10^3 cells/well in their respective CGM. An estimation of cell number

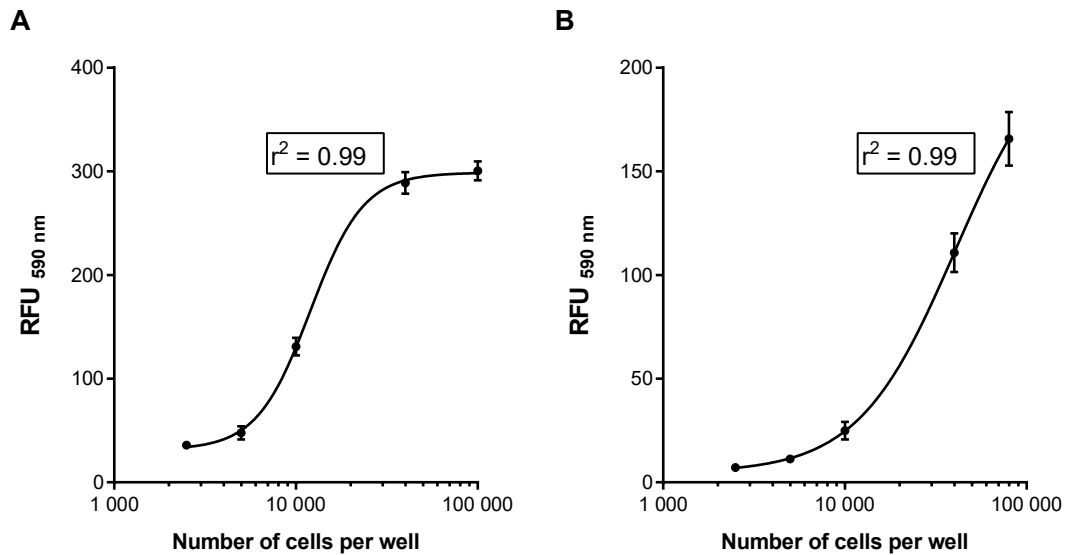


Figure B-1: Cell seeding density vs resazurin fluorescence intensity in (A) SKOV-3 cells and (B) OVCAR-3 cells. Cells were seeded in 96-well plates, allowed to adhere for 5-6 hours in a humidified incubator (37°, air 5% CO₂) and incubated in CGM + 100 μM resazurin for a further 2 hours. Data was fitted with a variable slope hill equation. Data points represent mean ± SD of 6 replicate wells. RFU; relative fluorescent units.

was undertaken using the resazurin reduction method as described in section 2.7. RFU values recorded over the timecourse were normalised to $t=0$ (N_t and N_0 respectively) to approximate the starting number of cells and data points were fitted with the standard exponential growth equation: $N_t = N_0 e^{kt}$, where k is a rate constant: $\ln 2/DT$, where DT is the cell doubling time. DT is thus derived by: $DT = \ln 2/k$ Sherley, Stadler and Stadler (1995). Since fitted data was normalised, the y intersect (N_0) was held at 1.

Calculated values for DT were with the resazurin reduction assay were markedly similar to those quoted elsewhere: SKOV-3; 27.1 [25, 28.3] hours (mean doubling time ± 95% [LCI, UCI]), $r^2 = 0.82$, OVCAR-3; 39.5 [36.7, 42.8], $r^2 = 0.78$ (Hallas-Potts, Dawson and Herrington, 2019).

Appendix C

Primary OvCa ascites (OvCa_{asc}) sample characterisation

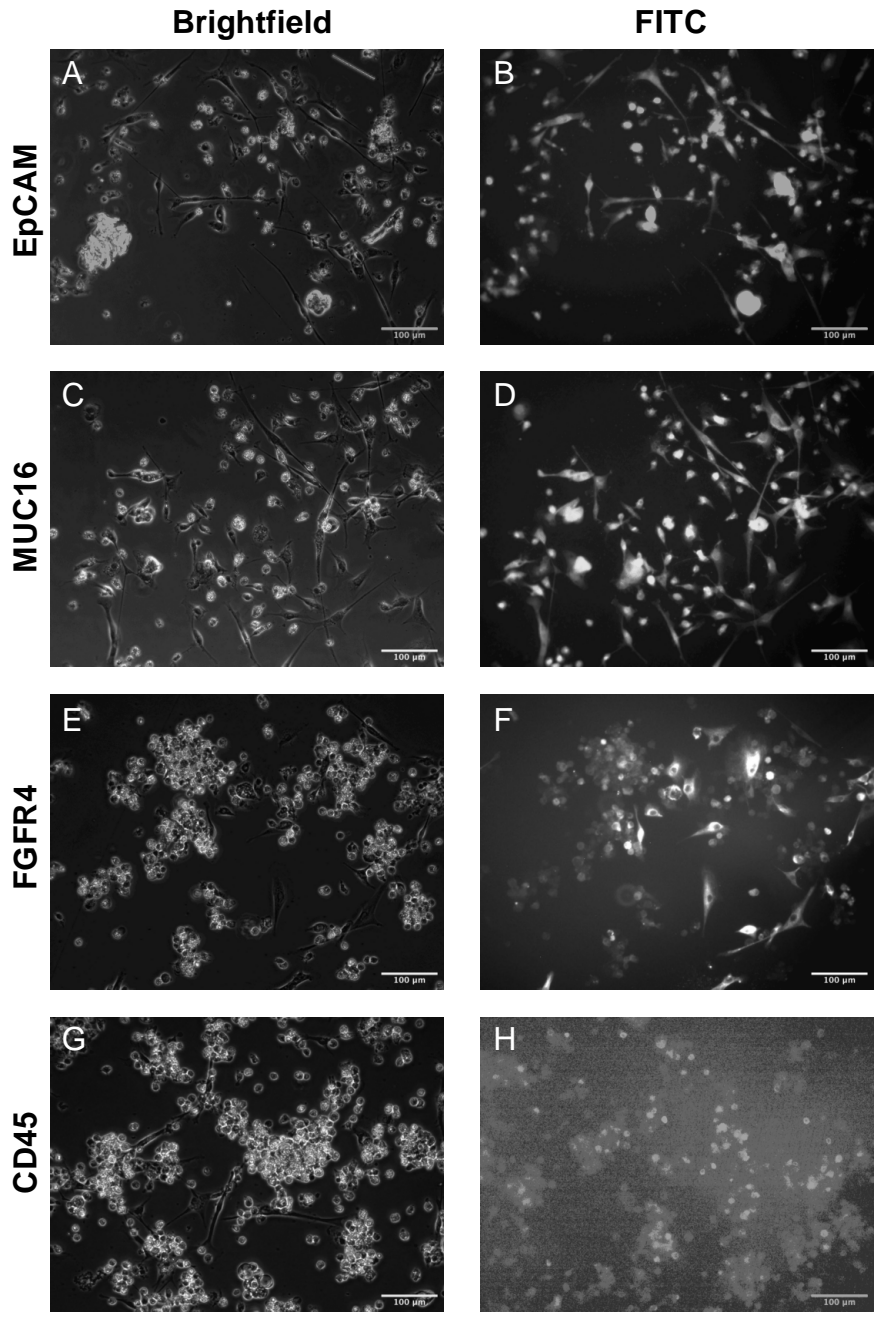


Figure C-1: Reflective images of characterisation of OvCa_{asc} sample OM5 cell surface marker expressed by IF. Scale bars inset.

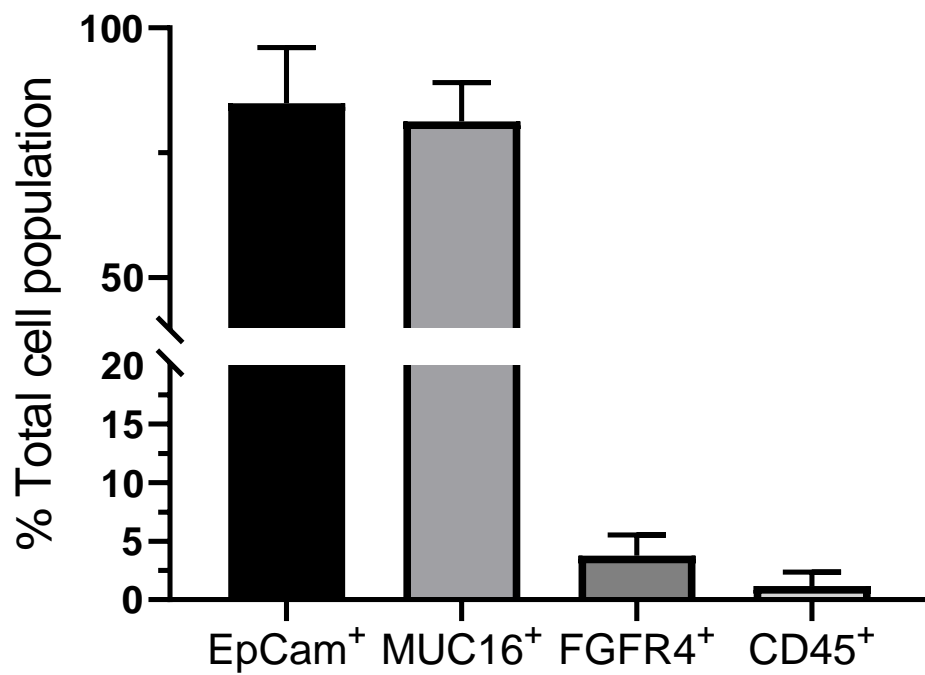


Figure C-2: Assessment of percentage contribution of differing cell populations present within primary isolates of malignant OvCa ascites samples. Cells were qualitatively assessed for positive staining and expressed as the percentage relative to the total number of cells in the field of view in the associated brightfield image.

Appendix D

Matlab code for quantifying cosine values

```
1 data=dlmread('direct.txt', '\t', 1, 1); % open text file containing ...
    x and y endpoints in um centered on start point of 0,0 and store ...
    in 4 column martrix
2 track=data(:,1); % get track numbers
3 x=data(:,3); % and associated x and y end-point values
4 y=data(:,4); % and create individual column vectors
5
6 euc=hypot(x,y); % find the hypotenuse / cell trajectory length ...
    (Euclidean distance) of each associated x,y cartesian pair
7 dire=x./euc; % compute cosine theta by taking the quotient of the ...
    adjacent (x) value and the associated hypotenuse value
8 %cosine values range from -1 to 1
9 euc_log=(euc >= 20); % set threshold for eulidean distance and compute ...
    a logical variable
10 dir_slice=euc_log.*dire; % set all directionality values under ...
    threshold to 0
11 dir_s=dir_slice(dir_slice >= 0); % remove 0 values
12
13 dlmwrite('dir_out.txt', dire, 'precision', 5); out % write cosine ...
    values to text file ready for quantitate analysis
14 dlmwrite('dir_out_slice.txt', dir_s, 'precision', 5); % write ...
    thresholded distance cosine values
15 dlmwrite('euclid.txt', euc, 'precision', 5); % write euclidean ...
    distance for each track
```


Bibliography

- Abidine, Y., V. M. Laurent, R. Michel et al. 2015. Local mechanical properties of bladder cancer cells measured by AFM as a signature of metastatic potential. *The European Physical Journal Plus* 130(10):202.
- Adrian, R. H. 1956. The effect of internal and external potassium concentration on the membrane potential of frog muscle. *The Journal of Physiology* 133(3):631–658.
- Ahmed, Nuzhat and Kaye L. Stenvers. 2013. Getting to Know Ovarian Cancer Ascites: Opportunities for Targeted Therapy-Based Translational Research. *Frontiers in Oncology* 3:256.
- Akopian, Armen. 2016. Role of TRP ion channels in physiology and pathology. *Seminars in Immunopathology* 38(3):275–276.
- Al-Hajj, Muhammad, Max S. Wicha, Adalberto Benito-Hernandez et al. 2003. Prospective identification of tumorigenic breast cancer cells. *Proceedings of the National Academy of Sciences of the United States of America* 100(7):3983–3988.
- Allen, Greg M., Alex Mogilner et al. 2013. Electrophoresis of Cellular Membrane Components Creates the Directional Cue Guiding Keratocyte Galvanotaxis. *Current Biology* 23(7):560–568.
- Althaus, Mike, Roman Bogdan, Wolfgang G. Clauss et al. 2007. Mechano-sensitivity of epithelial sodium channels (ENaCs): laminar shear stress increases ion channel open probability. *The FASEB Journal* 21(10):2389–2399.
- Altizer, Alicia M., Sarah G. Stewart, Brian K. Albertson et al. 2002. Skin flaps inhibit both the current of injury at the amputation surface and regeneration of that limb in newts. *Journal of Experimental Zoology* 293(5):467–477.
- Aoki, Koji and Makoto M. Taketo. 2007. Adenomatous polyposis coli (APC): a multi-functional tumor suppressor gene. *Journal of Cell Science* 120(19):3327–3335.
- Archampong, E. Q. and C. J. Edmonds. 1972. Effect of luminal ions on the transepithelial electrical potential difference of human rectum. *Gut* 13(7):559–565.

- Armstrong, E. F. 1933. Enzymes: A discovery and its consequences. *Nature* 131(3311):535–537.
- Asher, Carol, Indranil Sinha et al. 2003. Characterization of the interactions between Nedd4-2, ENaC, and sgk-1 using surface plasmon resonance. *Biochimica et Biophysica Acta - Biomembranes* 1612(1):59–64.
- Asher, Viren, Averil Warren, Robert Shaw et al. 2011. The role of Eag and HERG channels in cell proliferation and apoptotic cell death in SK-OV-3 ovarian cancer cell line. *Cancer cell international* 11(1):1–7.
- Avraham-Chakim, Liron, David Elad, Uri Zaretsky et al. 2013. Fluid-Flow Induced Wall Shear Stress and Epithelial Ovarian Cancer Peritoneal Spreading. *PLoS ONE* 8(4):e60965.
- Azadi, Shohreh, Mohammad Tafazzoli-Shadpour, Masoud Soleimani et al. 2019. Modulating cancer cell mechanics and actin cytoskeleton structure by chemical and mechanical stimulations. *Journal of Biomedical Materials Research - Part A* 107(8):1569–1581.
- Baartscheer, Antonius, Cees A. Schumacher, Ruben Coronel et al. 2011. The Driving Force of the Na⁺/Ca²⁺-Exchanger during Metabolic Inhibition. *Frontiers in Physiology* 2(1).
- Balkay, László, Teréz Márián, Zoltán Krasznai Miklós Emri et al. 1997. Flow cytometric determination of intracellular free potassium concentration. *Cytometry* 28(1):42–49.
- Bangerter, Neal K., Grayson J. Tarbox, Meredith D. Taylor et al. 2016. Quantitative sodium magnetic resonance imaging of cartilage, muscle, and tendon. *Quantitative Imaging in Medicine and Surgery* 6(6):699–714.
- Bansal, S., K. Kaur et al. 1998. Diagnosing ascitic etiology on a biochemical basis. *Hepato-Gastroenterology* 45(23):1673–1677.
- Barrett, Tristan, Frank Riemer, Mary A. McLean et al. 2018. Quantification of Total and Intracellular Sodium Concentration in Primary Prostate Cancer and Adjacent Normal Prostate Tissue With Magnetic Resonance Imaging. *Investigative Radiology* 53(8):450–456.
- Bautista, Wendy, Victor Perez-Alvarez, Frank Burczynski et al. 2014. Membrane potential differences and GABA A receptor expression in hepatic tumor and non-tumor stem cells. *Canadian Journal of Physiology and Pharmacology* 92(1):85–91.
- Baxter, Deborah F., Martin Kirk, Amy F. Garcia et al. 2002. A Novel Membrane Potential-Sensitive Fluorescent Dye Improves Cell-Based Assays for Ion Channels. *Journal of Biomolecular Screening* 7(1):79–85.

- Behrends, Jan C. 2012. Evolution of the Ion Channel Concept: The Historical Perspective. *Chemical Reviews* 112(12):6218–6226.
- Benavides-Serrato, Angelica, Jacquelyn T. Saunders, Brent Holmes et al. 2020. Repurposing Potential of Riluzole as an ITAF Inhibitor in mTOR Therapy Resistant Glioblastoma. *International journal of molecular sciences* 21(1):344.
- Benoit, Evelyne and Denis Escande. 1991. Riluzole specifically blocks inactivated Na channels in myelinated nerve fibre. *Pflügers Archiv European Journal of Physiology* 419(6):603–609.
- Berdiev, Bakhram K., Adriana G. Prat, Horacio F. Cantiello et al. 1996. Regulation of epithelial sodium channels by short actin filaments. *Journal of Biological Chemistry* 271(30):17704–17710.
- Berdiev, Bakhrom K, Jiazeng Xia, Lee Anne McLean et al. 2003. Acid-sensing ion channels in malignant gliomas. *Journal of Biological Chemistry* 278(17):15023–15034.
- Besson, Pierre, Virginie Driffort, Émeline Bon et al. 2015. How do voltage-gated sodium channels enhance migration and invasiveness in cancer cells? *Biochimica et Biophysica Acta (BBA) - Biomembranes* 1848(10):2493–2501.
- Bhalla, Vivek and Kenneth R. Hallows. 2008. Mechanisms of ENaC Regulation and Clinical Implications. *Journal of the American Society of Nephrology* 19(10):1845–1854.
- Binggeli, Richard and Ivan L Cameron. 1980. Cellular potentials of normal and cancerous fibroblasts and hepatocytes. *Cancer Research* 40(6):1830–1835.
- Binggeli, Richard and Roy C. Weinstein. 1986. Membrane potentials and sodium channels: Hypotheses for growth regulation and cancer formation based on changes in sodium channels and gap junctions. *Journal of Theoretical Biology* 123(4):377–401.
- Binnie, C. D. and P. F. Prior. 1994. Electroencephalography. *Journal of Neurology, Neurosurgery & Psychiatry* 57(11):1308–1319.
- Birkeland, Eivind Salmorin, Lisa Maria Koch et al. 2020. Another Consequence of the Warburg Effect? Metabolic Regulation of Na⁺/H⁺ Exchangers May Link Aerobic Glycolysis to Cell Growth. *Frontiers in Oncology* 10(1561).
- Blackiston, Douglas, Dany S. Adams, Joan M. Lemire et al. 2011. Transmembrane potential of GlyCl-expressing instructor cells induces a neoplastic-like conversion of melanocytes via a serotonergic pathway. *Disease Models & Mechanisms* 4(1):67–85.
- Blackiston, Douglas J, Kelly A McLaughlin et al. 2009. Bioelectric controls of cell proliferation: Ion channels, membrane voltage and the cell cycle. *Cell Cycle* 8(21):3527–3536.

- Bondarava, Maryna, Tongju Li, Elmar Endl et al. 2009. α -ENaC is a functional element of the hypertonicity-induced cation channel in HepG2 cells and it mediates proliferation. *Pflügers Archiv - European Journal of Physiology* 458(4):675–687.
- Bondarenko, Alexander. 2004. Sodium-calcium exchanger contributes to membrane hyperpolarization of intact endothelial cells from rat aorta during acetylcholine stimulation. *British Journal of Pharmacology* 143(1):9–18.
- Boonstra, Johannes, Christine L. Mummery, Leon G J Tertoolen et al. 1981. Cation transport and growth regulation in neuroblastoma cells. Modulations of K⁺ transport and electrical membrane properties during the cell cycle. *Journal of Cellular Physiology* 107(1):75–83.
- Borgens, R. B., J. W. Venable et al. 1977. Bioelectricity and regeneration: large currents leave the stumps of regenerating newt limbs. *Proceedings of the National Academy of Sciences* 74(10):4528–4532.
- Boron, Walter F., Matthias A. Hediger, Emile L. Boulpaep et al. 1997. The renal electrogenic Na⁺:HCO₃⁻ cotransporter. *Journal of Experimental Biology* 200(2):263–268.
- Bortner, Carl D and John A Cidlowski. 2003. Uncoupling cell shrinkage from apoptosis reveals that Na⁺ influx is required for volume loss during programmed cell death. *Journal of Biological Chemistry* 278(40):39176–39184.
- Borys, Przemysław. 2013. The role of passive calcium influx through the cell membrane in galvanotaxis. *Cellular and Molecular Biology Letters* 18(2):187–199.
- Boscardin, Emilie, Omar Alijevic, Edith Hummler et al. 2016. The function and regulation of acid-sensing ion channels (ASICs) and the epithelial Na⁺ channel (ENaC): IUPHAR Review 19. *British Journal of Pharmacology* 173(18):2671–2701.
- Brackenbury, William J., Athina Myrto Chioni, James K J Diss et al. 2007. The neonatal splice variant of Nav1.5 potentiates in vitro invasive behaviour of MDA-MB-231 human breast cancer cells. *Breast Cancer Research and Treatment* 101(2):149–160.
- Bregestovski, P, I Medina et al. 1992. Regulation of potassium conductance in the cellular membrane at early embryogenesis. *Journal of Physiology-Paris* 86(1-3):109–115.
- Brevet, Marie, Ahmed Ahidouch, Henri Sevestre et al. 2008. Expression of K⁺ channels in normal and cancerous human breast. *Histology and Histopathology* 23(8):965–972.
- Brevet, Marie, David Fucks, Denis Chatelain et al. 2009. Deregulation of 2 Potassium Channels in Pancreas Adenocarcinomas. *Pancreas* 38(6):649–654.

- Brisson, L., L. Gillet, S. Calaghan et al. 2011. Na^v 1.5 enhances breast cancer cell invasiveness by increasing NHE1-dependent H⁺ efflux in caveolae. *Oncogene* 30(17):2070–2076.
- Burleson, Kathryn M., Linda K. Hansen et al. 2005. Ovarian carcinoma spheroids disaggregate on type I collagen and invade live human mesothelial cell monolayers. *Clinical and Experimental Metastasis* 21(8):685–697.
- Butcher, Darci T, Tamara Alliston et al. 2009. A tense situation: forcing tumour progression. *Nature reviews. Cancer* 9(2):108–22.
- Butterworth, Michael B. 2010. Regulation of the epithelial sodium channel (ENaC) by membrane trafficking. *Biochimica et biophysica acta* 1802(12):1166–77.
- Butterworth, Michael B., Robert S. Edinger, John P. Johnson et al. 2005. Acute ENaC stimulation by cAMP in a kidney cell line is mediated by exocytic insertion from a recycling channel pool. *Journal of General Physiology* 125(1):81–101.
- Cai, Q., L. Yan et al. 2015. Anoikis resistance is a critical feature of highly aggressive ovarian cancer cells. *Oncogene* 34(25):3315–3324.
- Caldwell, Ray A., Richard C. Boucher et al. 2004. Serine protease activation of near-silent epithelial Na⁺ channels. *American Journal of Physiology-Cell Physiology* 286(1):C190–C194.
- Callies, Chiara, Johannes Fels, Ivan Liashkovich et al. 2011. Membrane potential depolarization decreases the stiffness of vascular endothelial cells. *Journal of Cell Science* 124(11):1936–1942.
- Cameron, I L and N K Smith. 1980. Energy dispersive x-ray microanalysis of the concentration of elements in relation to cell reproduction in normal and in cancer cells. *Scanning electron microscopy (Pt 2)*:463–74.
- Cameron, I L, N. K.R. Smith, T. B. Pool et al. 1980. Intracellular concentration of sodium and other elements as related to mitogenesis and oncogenesis in vivo. *Cancer research* 40(5):1493–500.
- Campbell, Richard D. 1983. Mitotic Index. In *Hydra: Research Methods*. Boston, MA: Springer US chapter 22, pp. 165–168.
- Campbell, Thomas M., Martin J. Main et al. 2013. Functional expression of the voltage-gated Na⁺-channel Nav1.7 is necessary for EGF-Mediated invasion in human non-Small cell lung cancer cells. *Journal of Cell Science* 126(21):4939–4949.
- Canady, Karen S., Francis Ali-Osman et al. 1990. Extracellular potassium influences DNA and protein syntheses and glial fibrillary acidic protein expression in cultured glial cells. *Glia* 3(5):368–374.

- Cancer Genome Atlas Research Network. 2011. Integrated genomic analyses of ovarian carcinoma. *Nature* 474(7353):609–615.
- Canessa, C. M., A. M. Merillat et al. 1994. Membrane topology of the epithelial sodium channel in intact cells. *American Journal of Physiology-Cell Physiology* 267(6):C1682–C1690.
- Canessa, Cecilia M., Laurent Schild, Gary Buell et al. 1994. Amiloride-sensitive epithelial Na⁺ channel is made of three homologous subunits. *Nature* 367(6462):463–467.
- Cassel, Dan, Miriam Rotman, Edward J. Cragoe et al. 1988. Preparation of 6-125I-labeled amiloride derivatives. *Analytical Biochemistry* 170(1):63–67.
- Charras, Guillaume and Erik Sahai. 2014. Physical influences of the extracellular environment on cell migration. *Nature Reviews Molecular Cell Biology* 15(12):813–824.
- Chen, Yih-Fung, Peng-Chan Lin, Yu-Min Yeh et al. 2019. Store-Operated Ca²⁺ Entry in Tumor Progression: From Molecular Mechanisms to Clinical Implications. *Cancers* 11(7):899.
- Chen, Yih Fung, Wen Tai Chiu, Ying Ting Chen et al. 2011. Calcium store sensor stromal-interaction molecule 1-dependent signaling plays an important role in cervical cancer growth, migration, and angiogenesis. *Proceedings of the National Academy of Sciences of the United States of America* 108(37):15225–15230.
- Chen, Zaixing, Runzhen Zhao, Meimi Zhao et al. 2014. Regulation of epithelial sodium channels in urokinase plasminogen activator deficiency. *American Journal of Physiology-Lung Cellular and Molecular Physiology* 307(8):L609–L617.
- Chernet, Brook T. and Michael Levin. 2014. Transmembrane voltage potential of somatic cells controls oncogene-mediated tumorigenesis at long-range. *Oncotarget* 5(10):3287–3306.
- Coleman, Nichole, Brandon M Brown, Aida Oliván-Viguera et al. 2014. New positive Ca²⁺-activated K⁺ channel gating modulators with selectivity for KCa3.1. *Molecular Pharmacology* 86(3):342–357.
- Collins, Anne T., Paul A. Berry, Catherine Hyde et al. 2005. Prospective identification of tumorigenic prostate cancer stem cells. *Cancer Research* 65(23):10946–10951.
- Comolli, R., C. Rossetti et al. 1991. Intracellular Na⁺, K⁺, H⁺ and Cl Activities and Membrane Potentials during the 4-Dimethylaminoazobenzene-Induced Rat Hepatocarcinogenesis. In *Chemical Carcinogenesis 2*. Boston, MA: Springer US pp. 213–217.
- Cone, C. and C. Cone. 1976. Induction of mitosis in mature neurons in central nervous system by sustained depolarization. *Science* 192(4235):155–158.

- Cone, Clarence D. 1971. Unified theory on the basic mechanism of normal mitotic control and oncogenesis. *Journal of Theoretical Biology* 30(1):151–181.
- Cone, Clarence D. and Max Tongier. 1973. Contact inhibition of division: Involvement of the electrical transmembrane potential. *Journal of Cellular Physiology* 82(3):373–386.
- Corradi, Anna and Mark A. Wallert. 2020. Investigating the Potential of NHE1 Inhibitors as Potential Adjuvant Therapies in the Treatment of Ovarian Cancer. *The FASEB Journal* 34(S1):1–1.
- Cortese, Barbara, Ilaria Elena Palamà, Stefania D’Amone et al. 2014. Influence of electrotaxis on cell behaviour. *Integr. Biol.* 6(9):817–830.
- Cramer, Louise P. 2010. Forming the cell rear first: breaking cell symmetry to trigger directed cell migration. *Nature Cell Biology* 12(7):628–632.
- Cummings, Kirstie A. and Gabriela K. Popescu. 2015. Glycine-dependent activation of NMDA receptors. *Journal of General Physiology* 145(6):513–527.
- Cuzick, Jack, Roland Holland, Volker Barth et al. 1998. Electropotential measurements as a new diagnostic modality for breast cancer. *Lancet* 352(9125):359–363.
- de la Rosa, Diego Alvarez, Juan F. Navarro-Gonzalez et al. 2016. ENaC Modulators and Renal Disease. *Current Molecular Pharmacology* 6(1):35–43.
- Deen, Surrin S., Frank Riemer, Mary A. McLean et al. 2019. Sodium MRI with 3D-cones as a measure of tumour cellularity in high grade serous ovarian cancer. *European Journal of Radiology Open* 6:156–162.
- Del Mónaco, Silvana M, Gabriela I Marino, Yanina A Assef et al. 2009. Cell migration in BeWo cells and the role of epithelial sodium channels. *The Journal of membrane biology* 232(1-3):1–13.
- Diaz, Daniel, Dulce Maria Delgadillo, Elizabeth Hernández-Gallegos et al. 2007. Functional expression of voltage-gated sodium channels in primary cultures of human cervical cancer. *Journal of Cellular Physiology* 210(2):469–478.
- Disis, Mary L., Matthew H. Taylor, Karen Kelly et al. 2019. Efficacy and Safety of Avelumab for Patients With Recurrent or Refractory Ovarian Cancer. *JAMA Oncology* 5(3):393.
- Diss, James K.J., Simon N. Archer, Joe Hirano et al. 2001. Expression profiles of voltage-gated Na⁺ channel α -subunit genes in rat and human prostate cancer cell lines. *Prostate* 48(3):165–178.

- Djamgoz, MBA, M Mycielska, Z Madeja et al. 2001. Directional movement of rat prostate cancer cells in direct-current electric field: involvement of voltage-gated Na⁺ channel activity. *Journal of cell science* 114(Pt 14):2697–705.
- Dominical, Venina, Leigh Samsel et al. 2017. Masks in imaging flow cytometry. *Methods* 112:9–17.
- Drummond, Gordon B. and Brian D.M. Tom. 2012. Presenting data: can you follow a recipe? *British journal of pharmacology* 165(4):777–81.
- Dunn, Olive Jean. 1964. Multiple Comparisons Using Rank Sums. *Technometrics* 6(3):241–252.
- Edinger, Robert S., Carol A. Bertrand, Christine Rondandino et al. 2012. The Epithelial Sodium Channel (ENaC) Establishes a Trafficking Vesicle Pool Responsible for Its Regulation. *PLoS ONE* 7(9):e46593.
- Elmore, Susan. 2007. Apoptosis: a review of programmed cell death. *Toxicologic pathology* 35(4):495–516.
- Emon, Bashar, Jessica Bauer, Yasna Jain et al. 2018. Biophysics of Tumor Microenvironment and Cancer Metastasis - A Mini Review. *Computational and Structural Biotechnology Journal* 16:279–287.
- Enkvetchakul, D. and C.G. Nichols. 2003. Gating Mechanism of KATP Channels. *Journal of General Physiology* 122(5):471–480.
- Ergonul, Zuhul, Gustavo Frindt et al. 2006. Regulation of maturation and processing of ENaC subunits in the rat kidney. *American Journal of Physiology-Renal Physiology* 291(3):F683–F693.
- Fang, K. S., B. Farboud, R. Nuccitelli et al. 1998. Migration of human keratinocytes in electric fields requires growth factors and extracellular calcium. *Journal of Investigative Dermatology* 111(5):751–756.
- Faouzi, Malika, Frederic Hague, Dirk Geerts et al. 2016. Functional cooperation between KCa3.1 and TRPC1 channels in human breast cancer: Role in cell proliferation and patient prognosis. *Oncotarget* 7(24):36419–36435.
- Farman, N., C. R. Talbot, R. Boucher et al. 1997. Noncoordinated expression of alpha-, beta-, and gamma-subunit mRNAs of epithelial Na⁺ channel along rat respiratory tract. *American Journal of Physiology-Cell Physiology* 272(1):C131–C141.
- Fausto, Nelson. 2004. Liver regeneration and repair: Hepatocytes, progenitor cells, and stem cells. *Hepatology* 39(6):1477–1487.

- Feki, Anis, Philip Berardi, Geoff Bellingan et al. 2009. Dissemination of intraperitoneal ovarian cancer: Discussion of mechanisms and demonstration of lymphatic spreading in ovarian cancer model. *Critical Reviews in Oncology/Hematology* 72(1):1–9.
- Feng, Mingye, Desma M. Grice, Helen M. Faddy et al. 2010. Store-Independent Activation of Orail by SPCA2 in Mammary Tumors. *Cell* 143(1):84–98.
- Fenwick, Elizabeth M., A. Marty et al. 1982. Sodium and calcium channels in bovine chromaffin cells. *The Journal of Physiology* 331(1):599–635.
- Feraille, Eric and Eva Dizin. 2016. Coordinated Control of ENaC and Na⁺,K⁺-ATPase in Renal Collecting Duct. *Journal of the American Society of Nephrology* 27(9):2554–2563.
- Fort, Aurélie, Magali Cordaillat, Catherine Thollon et al. 2009. New Insights in the Contribution of Voltage-Gated Nav Channels to Rat Aorta Contraction. *PLoS ONE* 4(10):e7360.
- Fraser, S. P., James K J Diss, Athina-Myrto Chioni et al. 2005. Voltage-Gated Sodium Channel Expression and Potentiation of Human Breast Cancer Metastasis. *Clinical Cancer Research* 11(15):5381–5389.
- Fraser, Scott P., Iley Ozerlat-Gunduz, William J. Brackenbury et al. 2014. “Regulation of voltage-gated sodium channel expression in cancer: Hormones, growth factors and auto-regulation.”.
- Freedman, B D, M A Price et al. 1992. Evidence for voltage modulation of IL-2 production in mitogen-stimulated human peripheral blood lymphocytes. *Journal of immunology* 149(12):3784–3794.
- Fulgenzi, Gianluca, Laura Graciotti, Monica Faronato et al. 2006. Human neoplastic mesothelial cells express voltage-gated sodium channels involved in cell motility. *The International Journal of Biochemistry & Cell Biology* 38(7):1146–1159.
- Funk, Richard H. W. 2015. Endogenous electric fields as guiding cue for cell migration. *Frontiers in Physiology* 6:143.
- Gao, Qinglei, Zongyuan Yang, Sen Xu et al. 2019. Heterotypic CAF-tumor spheroids promote early peritoneal metastasis of ovarian cancer. *Journal of Experimental Medicine* 216(3):688–703.
- Gao, Rui, Yi Shen, Jing Cai et al. 2010. Expression of voltage-gated sodium channel α subunit in human ovarian cancer. *Oncology Reports* 23(5):1293–1299.
- Gao, Run-chi, Xiao-dong Zhang, Yao-hui Sun et al. 2011. Different Roles of Membrane Potentials in Electrotaxis and Chemotaxis of Dictyostelium Cells. *Eukaryotic Cell* 10(9):1251–1256.

- Gao, Yan, Rosemary Foster, Xiaoqian Yang et al. 2015. Up-regulation of CD44 in the development of metastasis, recurrence and drug resistance of ovarian cancer. *Oncotarget* 6(11):9313–9326.
- Garty, H and L G Palmer. 1997. Epithelial sodium channels: function, structure, and regulation. *Physiological reviews* 77(2):359–96.
- Gazitt, Yair, Arline D. Deitch, Paul A. Marks et al. 1978. Cell volume changes in relation to the cell cycle of differentiating erythroleukemic cells. *Experimental Cell Research* 117(2):413–420.
- Geddes, L. A. and H. E. Hoff. 1971. The discovery of bioelectricity and current electricity The Galvani-Volta controversy. *IEEE Spectrum* 8(12):38–46.
- Gees, Maarten, Barbara Colsool et al. 2010. The role of transient receptor potential cation channels in Ca²⁺ signaling. *Cold Spring Harbor perspectives in biology* 2(10).
- Gerkau, Niklas J., Cordula Rakers, Simone Durry et al. 2018. Reverse NCX attenuates cellular sodium loading in metabolically compromised cortex. *Cerebral Cortex* 28(12):4264–4280.
- Geselowitz, D.B. 1989. On the theory of the electrocardiogram. *Proceedings of the IEEE* 77(6):857–876.
- Ghezzi, Chiara, Donald D. F. Loo et al. 2018. Physiology of renal glucose handling via SGLT1, SGLT2 and GLUT2. *Diabetologia* 61(10):2087–2097.
- Gilly, William F., Rhanor Gillette et al. 1997. Fast and Slow Activation Kinetics of Voltage-Gated Sodium Channels in Molluscan Neurons. *Journal of Neurophysiology* 77(5):2373–2384.
- Girardier, L., J. Seydoux et al. 1968. Membrane potential of brown adipose tissue. A suggested mechanism for the regulation of thermogenesis. *The Journal of general physiology* 52(6):925–940.
- Goldman, David E. 1943. POTENTIAL, IMPEDANCE, AND RECTIFICATION IN MEMBRANES. *The Journal of general physiology* 27(1):37–60.
- Goñi, Félix M. 2014. The basic structure and dynamics of cell membranes: An update of the Singer–Nicolson model. *Biochimica et Biophysica Acta (BBA) - Biomembranes* 1838(6):1467–1476.
- Gorbatenko, Andrej, Christina W. Olesen, Ebbe Boedtkjer et al. 2014. Regulation and roles of bicarbonate transporters in cancer. *Frontiers in Physiology* 5(130).
- Gründer, S, D Firsov, S S Chang et al. 1997. A mutation causing pseudohypoaldosteronism type 1 identifies a conserved glycine that is involved in the gating of the epithelial sodium channel. *The EMBO journal* 16(5):899–907.

- Gründer, Stefan and Xuanmao Chen. 2010. Structure, function, and pharmacology of acid-sensing ion channels (ASICs): focus on ASIC1a. *International journal of physiology, pathophysiology and pharmacology* 2(2):73–94.
- Guo, Aihua, Bing Song, Brian Reid et al. 2010. Effects of Physiological Electric Fields on Migration of Human Dermal Fibroblasts. *Journal of Investigative Dermatology* 130(9):2320–2327.
- Guo, Xiaowei, Xupin Jiang, Xi Ren et al. 2015. The Galvanotactic Migration of Keratinocytes is Enhanced by Hypoxic Preconditioning. *Scientific Reports* 5(1):10289.
- Habela, Christa W. and Harald Sontheimer. 2007. Cytoplasmic volume condensation is an integral part of mitosis. *Cell Cycle* 6(13):1613–1620.
- Habela, Christa W., Michelle L. Olsen et al. 2008. ClC3 Is a Critical Regulator of the Cell Cycle in Normal and Malignant Glial Cells. *Journal of Neuroscience* 28(37):9205–9217.
- Hallas-Potts, Amelia, John C. Dawson et al. 2019. Ovarian cancer cell lines derived from non-serous carcinomas migrate and invade more aggressively than those derived from high-grade serous carcinomas. *Scientific Reports* 9(1):5515.
- Hanahan, Douglas and Robert A. Weinberg. 2000. The Hallmarks of Cancer. *Cell* 100(1):57–70.
- Hanahan, Douglas and Robert A. Weinberg. 2011. Hallmarks of Cancer: The Next Generation. *Cell* 144(5):646–674.
- Harayama, Takeshi and Howard Riezman. 2018. Understanding the diversity of membrane lipid composition. *Nature Reviews Molecular Cell Biology* 19(5):281–296.
- Hernandez-Plata, Everardo, Cindy S. Ortiz, Brenda Marquina-Castillo et al. 2012. Overexpression of Na V1.6 channels is associated with the invasion capacity of human cervical cancer. *International Journal of Cancer* 130(9):2013–2023.
- Hirsh, Andrew J, Juan R Sabater, Andra Zamurs et al. 2004. Evaluation of second generation amiloride analogs as therapy for cystic fibrosis lung disease. *Journal of Pharmacology and Experimental Therapeutics* 311(3):929–938.
- Hodgkin, A L and B Katz. 1949. The effect of sodium ions on the electrical activity of giant axon of the squid. *The Journal of physiology* 108(1):37–77.
- Hodgkin, A. L. and P. Horowicz. 1959. The influence of potassium and chloride ions on the membrane potential of single muscle fibres. *The Journal of Physiology* 148(1):127–160.
- Hodgson, Anjelica and Gulisa Turashvili. 2020. Pathology of Hereditary Breast and Ovarian Cancer. *Frontiers in Oncology* 10:531790.

- Hoeijmakers, Jan H. J. 2001. Genome maintenance mechanisms for preventing cancer. *Nature* 411(6835):366–374.
- Hofmann, Ulrich G., Christian Rotsch, Wolfgang J. Parak et al. 1997. Investigating the cytoskeleton of chicken cardiocytes with the atomic force microscope. *Journal of Structural Biology* 119(2):84–91.
- Hosogi, Shigekuni, Hiroaki Miyazaki, Ken Ichi Nakajima et al. 2012. An inhibitor of Na⁺/H⁺ exchanger (NHE), ethyl-isopropyl amiloride (EIPA), diminishes proliferation of MKN28 human gastric cancer cells by decreasing the cytosolic Cl⁻ concentration via DIDS-sensitive pathways. *Cellular Physiology and Biochemistry* 30(5):1241–1253.
- Hou, Hsien San, Hsieh Fu Tsai, Hsien Tai Chiu et al. 2014. Simultaneous chemical and electrical stimulation on lung cancer cells using a multichannel-dual-electric-field chip. *Biomicrofluidics* 8(5):052007.
- Huang, Yu-Ja, Gwendolyn Hoffmann, Benjamin Wheeler et al. 2016. Cellular microenvironment modulates the galvanotaxis of brain tumor initiating cells. *Scientific Reports* 6(1):21583.
- Hulspas, Ruud, Maurice R.G. O’Gorman, Brent L. Wood et al. 2009. Considerations for the control of background fluorescence in clinical flow cytometry. *Cytometry Part B: Clinical Cytometry* 76B(6):355–364.
- Hummler, Edith, Pierre Barker, John Galzy et al. 1996. Early death due to defective neonatal lung liquid clearance in α ENaC-deficient mice. *Nature Genetics* 12(3):325–328.
- Ilatovskaya, Daria V., Tengis S. Pavlov, Vladislav Levchenko et al. 2011. Cortical actin binding protein cortactin mediates ENaC activity via Arp2/3 complex. *FASEB Journal* 25(8):2688–2699.
- Ince, C., E. van Bavel, B. van Duijn et al. 1986. Intracellular microelectrode measurements in small cells evaluated with the patch clamp technique. *Biophysical Journal* 50(6):1203–1209.
- Ip, Carman K. M., Shan-Shan Li, Matthew Y. H. Tang et al. 2016. Stemness and chemoresistance in epithelial ovarian carcinoma cells under shear stress. *Scientific reports* 6(1):26788.
- Ishibashi, Hitoshi, Andrew J. Moorhouse et al. 2012. Perforated Whole-Cell Patch-Clamp Technique: A User’s Guide. In *Patch Clamp Techniques*, ed. Yasunobu Okada. 1 ed. Tokyo: Springer chapter 4, pp. 71–83.
- Ishii, Kuniaki, Mirei Nagai, Masahiro Takahashi et al. 2003. Dissociation of E-4031 from the HERG channel caused by mutations of an amino acid results in greater block at high stimulation frequency. *Cardiovascular Research* 57(3):651–659.

- Iwanicki, Marcin P., Rachel A. Davidowitz, Mei Rosa Ng et al. 2011. Ovarian cancer spheroids use myosin-generated force to clear the mesothelium. *Cancer Discovery* 1(2):144–157.
- Jacobs, Michael A., Ronald Ouwerkerk, Antonio C. Wolff et al. 2004. Multiparametric and multinuclear magnetic resonance imaging of human breast cancer: Current applications. *Technology in Cancer Research and Treatment* 3(6):543–550.
- Jakic, Bojana, Maja Buszko, Giuseppe Cappellano et al. 2017. Elevated sodium leads to the increased expression of HSP60 and induces apoptosis in HUVECs. *PLoS ONE* 12(6):e0179383.
- Jakobsson, E. 1980. Interactions of cell volume, membrane potential, and membrane transport parameters. *American Journal of Physiology-Cell Physiology* 238(5):C196–C206.
- Jamamosmanovic, A. and W R Loewenstein. 1968. Intercellular communication and tissue growth. *Journal of Cell Biology* 38(3):556–561.
- Jayson, Gordon C., Elise C. Kohn, Henry C. Kitchener et al. 2014. Ovarian cancer. *The Lancet* 384(9951):1376–1388.
- Jernigan, Nikki L. and Heather A. Drummond. 2006. Myogenic vasoconstriction in mouse renal interlobar arteries: Role of endogenous β and γ ENaC. *American Journal of Physiology - Renal Physiology* 291(6):F1184–F1191.
- Jorgensen, Peter L., Kjell O. Håkansson et al. 2003. Structure and Mechanism of Na,K-ATPase: Functional Sites and Their Interactions. *Annual Review of Physiology* 65(1):817–849.
- Justet, Cristian, Frances Evans, Elena Vasilskis et al. 2013. ENaC contribution to epithelial wound healing is independent of the healing mode and of any increased expression in the channel. *Cell and Tissue Research* 353(1):53–64.
- Kapoor, Niren, William Lee, Edlira Clark et al. 2011. Interaction of ASIC1 and ENaC subunits in human glioma cells and rat astrocytes. *American journal of physiology. Cell physiology* 300(6):C1246–59.
- Kasas, S., X. Wang, H. Hirling et al. 2005. Superficial and deep changes of cellular mechanical properties following cytoskeleton disassembly. *Cell Motility and the Cytoskeleton* 62(2):124–132.
- Kay, Alan R and Mordecai P Blaustein. 2019. Evolution of our understanding of cell volume regulation by the pump-leak mechanism. *Journal of General Physiology* 151(4):407–416.

- Kellenberger, Stephan and Laurent Schild. 2002. Epithelial Sodium Channel/Degenerin Family of Ion Channels: A Variety of Functions for a Shared Structure. *Physiological Reviews* 82(3):735–767.
- Keller, Ray. 2005. Cell migration during gastrulation. *Current Opinion in Cell Biology* 17(5):533–541.
- Ketene, Alperen N., Eva M. Schmelz, Paul C. Roberts et al. 2012. The effects of cancer progression on the viscoelasticity of ovarian cell cytoskeleton structures. *Nanomedicine: Nanotechnology, Biology and Medicine* 8(1):93–102.
- Khan, Zeina S., Julianna M. Santos et al. 2018. Aggressive prostate cancer cell nuclei have reduced stiffness. *Biomicrofluidics* 12(1):014102.
- Kis-Toth, Katalin, Peter Hajdu, Ildiko Bacskai et al. 2011. Voltage-Gated Sodium Channel Nav1.7 Maintains the Membrane Potential and Regulates the Activation and Chemokine-Induced Migration of a Monocyte-Derived Dendritic Cell Subset. *The Journal of Immunology* 187(3):1273–1280.
- Kleyman, Thomas R., Marcelo D. Carattino et al. 2009. ENaC at the Cutting Edge: Regulation of Epithelial Sodium Channels by Proteases. *Journal of Biological Chemistry* 284(31):20447–20451.
- Koch, K S and H L Leffert. 1979. Increased sodium ion influx is necessary to initiate rat hepatocyte proliferation. *Cell* 18(1):153–63.
- Koester, Sielgelbaum, Stephen. 2013. Membrane Potential and the Passive Electrical Properties of the Neuron. In *Principles of neural science*, ed. Eric R. Kandel. 5th ed. New York: McGraw-Hill Medical chapter 6, p. 1709.
- Kontomaris, Stylianos-Vasileios. 2018. The Hertz Model in AFM Nanoindentation Experiments: Applications in Biological Samples and Biomaterials. *Micro and Nanosystems* 10(1):11–22.
- Kosari, F, S Sheng, J Li et al. 1998. Subunit stoichiometry of the epithelial sodium channel. *The Journal of biological chemistry* 273(22):13469–74.
- Križanac, Dragana Karan, Antonela Krsić Arapović, Siniša Skočibušić et al. 2018. CD44 Immunoexpression is Unfavorable Predictor in Ovarian Serous Cancer. *Applied Immunohistochemistry and Molecular Morphology* 26(6):398–402.
- Kubista, Mikael, José Manuel Andrade, Martin Bengtsson et al. 2006. The real-time polymerase chain reaction. *Molecular Aspects of Medicine* 27(2-3):95–125.
- Kwon, Taeyun, Sundaram Gunasekaran et al. 2019. Atomic force microscopy-based cancer diagnosis by detecting cancer-specific biomolecules and cells. *Biochimica et Biophysica Acta (BBA) - Reviews on Cancer* 1871(2):367–378.

- Lammert, P. E., J. Prost et al. 1996. Ion drive for vesicles and cells. *Journal of Theoretical Biology* 178(4):387–391.
- Lang, Florian, Markus Ritter, Nikita Gamper et al. 2000. Cell Volume in the Regulation of Cell Proliferation and Apoptotic Cell Death. *Cellular Physiology and Biochemistry* 10(5-6):417–428.
- Lara Rodriguez, Laura and Ian C. Schneider. 2013. Directed cell migration in multi-cue environments. *Integrative Biology* 5(11):1306–1323.
- Ledermann, J.A. 2016. PARP inhibitors in ovarian cancer. *Annals of Oncology* 27:i40–i44.
- Lee, Chong Hyun and Peter C. Ruben. 2008. Interaction between voltage-gated sodium channels and the neurotoxin, tetrodotoxin. *Channels* 2(6):407–412.
- Lee, Dongchul C and Warren M Grill. 2005. Polarization of a spherical cell in a nonuniform extracellular electric field. *Annals of Biomedical Engineering* 33(5):603–615.
- Lekka, Małgorzata. 2016. Discrimination Between Normal and Cancerous Cells Using AFM. *BioNanoScience* 6(1):65–80.
- Lemmon, Mark A. and Joseph Schlessinger. 2010. Cell Signaling by Receptor Tyrosine Kinases. *Cell* 141(7):1117–1134.
- Lengyel, Ernst. 2010. Ovarian Cancer Development and Metastasis. *The American Journal of Pathology* 177(3):1053–1064.
- L’Espérance, Sylvain, Magdalena Bachvarova, Bernard Tetu et al. 2008. Global gene expression analysis of early response to chemotherapy treatment in ovarian cancer spheroids. *BMC Genomics* 9(1):99.
- Levchenko, Vladislav, Nadezhda N. Zheleznova, Tengis S. Pavlov et al. 2010. EGF and its related growth factors mediate sodium transport in mpkCCD c14 cells via ErbB2 (neu/HER-2) receptor. *Journal of Cellular Physiology* 223(1):252–259.
- Levin, Michael. 2011. The wisdom of the body: future techniques and approaches to morphogenetic fields in regenerative medicine, developmental biology and cancer. *Regenerative Medicine* 6(6):667–673.
- Levin, Michael. 2014. Endogenous bioelectrical networks store non-genetic patterning information during development and regeneration. *The Journal of Physiology* 592(11):2295–2305.
- Lévy, R. and M. Maaloum. 2002. Measuring the spring constant of atomic force microscope cantilevers: thermal fluctuations and other methods. *Nanotechnology* 13(1):33–37.

- Li, F K, C H To, J K Leung et al. 2001. Electrophysiology and glucose transport of human peritoneal mesothelial cells: implications for peritoneal dialysis. *Peritoneal dialysis international : journal of the International Society for Peritoneal Dialysis* 21(2):115–121.
- Li, Fei, Tunan Chen, Shengli Hu et al. 2013. Superoxide Mediates Direct Current Electric Field-Induced Directional Migration of Glioma Cells through the Activation of AKT and ERK. *PLoS ONE* 8(4):e61195.
- Li, Hongyi, Yang Yang, Weiqi Hong et al. 2020. Applications of genome editing technology in the targeted therapy of human diseases: mechanisms, advances and prospects. *Signal Transduction and Targeted Therapy* 5(1):1.
- Li, Shujun, Pengtao Bao, Zhikui Li et al. 2009. Inhibition of proliferation and apoptosis induced by a Na⁺/H⁺ exchanger-1 (NHE-1) antisense gene on drug-resistant human small cell lung cancer cells. *Oncology Reports* 21(5):1243–1249.
- Li, Wei, Shu Lan Zhang, Ning Wang et al. 2011. Blockade of T-type Ca²⁺ channels inhibits human ovarian cancer cell proliferation. *Cancer Investigation* 29(5):339–346.
- Li, Yaping, Tao Xu, Xiaomei Chen et al. 2017. Effects of direct current electric fields on lung cancer cell electrotaxis in a PMMA-based microfluidic device. *Analytical and Bioanalytical Chemistry* 409(8):2163–2178.
- Liang, Chun Chi, Ann Y Park et al. 2007. In vitro scratch assay: A convenient and inexpensive method for analysis of cell migration in vitro. *Nature Protocols* 2(2):329–333.
- Liberti, Maria V. and Jason W. Locasale. 2016. The Warburg Effect: How Does it Benefit Cancer Cells? *Trends in Biochemical Sciences* 41(3):211–218.
- Lin, Chia Wei, Feifei Yan, Satoko Shimamura et al. 2005. Membrane phosphoinositides control insulin secretion through their effects on ATP-sensitive K⁺ channel activity. *Diabetes* 54(10):2852–2858.
- Lingueglia, Eric, Emmanuel Deval et al. 2006. FMRFamide-gated sodium channel and ASIC channels: A new class of ionotropic receptors for FMRFamide and related peptides. *Peptides* 27(5):1138–1152.
- Lingueglia, Eric, Stéphane Renard, Rainer Waldmann et al. 1994. Different homologous subunits of the amiloride-sensitive Na⁺ channel are differently regulated by aldosterone. *Journal of Biological Chemistry* 269(19):13736–13739.
- Liu, Cui, Li-Li Zhu, Si-Guang Xu et al. 2016. ENaC/DEG in Tumor Development and Progression. *Journal of Cancer* 7(13):1888–1891.

- Liu, Lian, Billie Jeanne Duke, Bela Malik et al. 2009. Biphasic regulation of ENaC by TGF- α and EGF in renal epithelial cells. *American Journal of Physiology - Renal Physiology* 296(6):F1417–F1427.
- Liu, Yongge, Wei Dong Gao, Brian O'Rourke et al. 1997. Priming effect of adenosine on K(ATP) currents in intact ventricular myocytes: Implications for preconditioning. *American Journal of Physiology - Heart and Circulatory Physiology* 273(4 42-4):1637–1643.
- Livak, Kenneth J., Susan J.A. Flood, Jeffrey Marmaro et al. 1995. Oligonucleotides with fluorescent dyes at opposite ends provide a quenched probe system useful for detecting PCR product and nucleic acid hybridization. *Genome Research* 4(6):357–362.
- Livak, Kenneth J. and Thomas D. Schmittgen. 2001. Analysis of relative gene expression data using real-time quantitative PCR and the 2- $\Delta\Delta$ CT method. *Methods* 25(4):402–408.
- Lobikin, Maria, Brook Chernet, Daniel Lobo et al. 2012. Resting potential, oncogene-induced tumorigenesis, and metastasis: the bioelectric basis of cancer in vivo. *Physical Biology* 9(6):065002.
- Lock, Jeffrey T., Ian Parker et al. 2015. A comparison of fluorescent Ca²⁺ indicators for imaging local Ca²⁺ signals in cultured cells. *Cell Calcium* 58(6):638–648.
- Long, Zhou, Bai Jun Chen, Qian Liu et al. 2016. The reverse-mode NCX1 activity inhibitor KB-R7943 promotes prostate cancer cell death by activating the JNK pathway and blocking autophagic flux. *Oncotarget* 7(27):42059–42070.
- Loof, Arnold De. 1986. The Electrical Dimension of Cells: The Cell as a Miniature Electrophoresis Chamber. In *International Review of Cytology*. Vol. 104 pp. 251–352.
- Lu, Chen, Sandra Pribanic, Anne Debonneville et al. 2007. The PY motif of ENaC, mutated in liddle syndrome, regulates channel internalization, sorting and mobilization from subapical pool. *Traffic* 8(9):1246–1264.
- Lu, Min, Fernando Echeverri, Dalia Kalabat et al. 2008. Small Molecule Activator of the Human Epithelial Sodium Channel. *Journal of Biological Chemistry* 283(18):11981–11994.
- Lupia, Michela and Ugo Cavallaro. 2017. Ovarian cancer stem cells: still an elusive entity? *Molecular Cancer* 16(1):64.
- Ma, Shijun, Afu Fu, Geraldine Giap Ying Chiew et al. 2017. Hemodynamic shear stress stimulates migration and extravasation of tumor cells by elevating cellular oxidative level. *Cancer letters* 388:239–248.

- Mackay, I.M. 2004. Real-time PCR in the microbiology laboratory. *Clinical Microbiology and Infection* 10(3):190–212.
- Maecker, Holden T. and Joseph Trotter. 2006. Flow cytometry controls, instrument setup, and the determination of positivity. *Cytometry Part A* 69A(9):1037–1042.
- Malumbres, Marcos and Mariano Barbacid. 2005. Mammalian cyclin-dependent kinases. *Trends in Biochemical Sciences* 30(11):630–641.
- Mamelak, Adam N. and Douglas B. Jacoby. 2007. Targeted delivery of antitumoral therapy to glioma and other malignancies with synthetic chlorotoxin (TM-601). *Expert Opinion on Drug Delivery* 4(2):175–186.
- Marban, Eduardo, Toshio Yamagishi et al. 1998. Structure and function of voltage-gated sodium channels. *The Journal of Physiology* 508(3):647–657.
- Marino, Andrew A., Ilko G. Iliev, Michael A. Schwalke et al. 1994. Association between Cell Membrane Potential and Breast Cancer. *Tumor Biology* 15(2):82–89.
- Marino, G I, Y A Assef et al. 2013. The migratory capacity of human trophoblastic BeWo cells: effects of aldosterone and the epithelial sodium channel. *The Journal of membrane biology* 246(3):243–55.
- Markadieu, Nicolas, Raphaël Crutzen, Daniel Blero et al. 2005. Hydrogen peroxide and epidermal growth factor activate phosphatidylinositol 3-kinase and increase sodium transport in A6 cell monolayers. *American Journal of Physiology-Renal Physiology* 288(6):F1201–F1212.
- Masereel, B. 2003. An overview of inhibitors of Na⁺/H⁺ exchanger. *European Journal of Medicinal Chemistry* 38(6):547–554.
- Matalon, Sadis, Rafal Bartoszewski et al. 2015. Role of epithelial sodium channels in the regulation of lung fluid homeostasis. *American Journal of Physiology - Lung Cellular and Molecular Physiology* 309(11):L1229–L1238.
- Matthews, Hayden, Marie Ranson et al. 2011. Anti-tumour/metastasis effects of the potassium-sparing diuretic amiloride: An orally active anti-cancer drug waiting for its call-of-duty? *International Journal of Cancer* 129(9):2051–2061.
- Matulonis, U. A., R. Shapira-Frommer, A. D. Santin et al. 2019. Antitumor activity and safety of pembrolizumab in patients with advanced recurrent ovarian cancer: results from the phase II KEYNOTE-100 study. *Annals of Oncology* 30(7):1080–1087.
- Mazzochi, Christopher, James K Buben, Peter R Smith et al. 2006. The carboxyl terminus of the alpha-subunit of the amiloride-sensitive epithelial sodium channel binds to F-actin. *The Journal of biological chemistry* 281(10):6528–38.

- McCaig, C. D., B. Song et al. 2009. Electrical dimensions in cell science. *Journal of Cell Science* 122(23):4267–4276.
- McCaig, Colin D., Ann M. Rajnicek, Bing Song et al. 2005. Controlling Cell Behavior Electrically: Current Views and Future Potential. *Physiological Reviews* 85(3):943–978.
- McCaig, Colin D. and Min Zhao. 1997. Physiological electrical fields modify cell behaviour. *BioEssays* 19(9):819–826.
- McLaughlin, S. and M. M. Poo. 1981. The role of electro-osmosis in the electric-field-induced movement of charged macromolecules on the surfaces of cells. *Biophysical Journal* 34(1):85–93.
- McNicholas, C M and C M Canessa. 1997. Diversity of channels generated by different combinations of epithelial sodium channel subunits. *The Journal of general physiology* 109(6):681–92.
- Mirshahi, M, S Mirshahi, N Golestaneh et al. 2000. Demonstration of the mineralocorticoid hormone receptor and action in human leukemic cell lines. *Leukemia* 14:1097–1104.
- Mizumoto, Kazuhiro, Ronald J. Rothman et al. 1994. Programmed cell death (apoptosis) of mouse fibroblasts is induced by the topoisomerase II inhibitor etoposide. *Molecular Pharmacology* 46(5):890–895.
- Motiani, Rajender K., María C. Hyzinski-García, Xuexin Zhang et al. 2013. STIM1 and Orai1 mediate CRAC channel activity and are essential for human glioblastoma invasion. *Pflugers Archiv European Journal of Physiology* 465(9):1249–1260.
- Motohara, Takeshi, Kenta Masuda, Matteo Morotti et al. 2019. An evolving story of the metastatic voyage of ovarian cancer cells: cellular and molecular orchestration of the adipose-rich metastatic microenvironment. *Oncogene* 38(16):2885–2898.
- Munaron, Luca, S. Antoniotti et al. 2004. Intracellular calcium signals and control of cell proliferation: how many mechanisms? *Journal of Cellular and Molecular Medicine* 8(2):161–168.
- Mycielska, Maria E and Mustafa B A Djamgoz. 2004. Cellular mechanisms of direct-current electric field effects: galvanotaxis and metastatic disease. *Journal of cell science* 117(Pt 9):1631–9.
- Nagy, I. Z, G Lustyik, V Z Nagy et al. 1981. Intracellular Na⁺:K⁺ ratios in human cancer cells as revealed by energy dispersive X-ray microanalysis. *Journal of Cell Biology* 90(3):769–777.

- Nakajima, Ken-ichi, Kan Zhu, Yao-Hui Sun et al. 2015. KCNJ15/Kir4.2 couples with polyamines to sense weak extracellular electric fields in galvanotaxis. *Nature Communications* 6(1):8532.
- Naora, Honami and Denise J. Montell. 2005. Ovarian Cancer Metastasis: Integrating insights from disparate model organisms. *Nature Reviews Cancer* 5(5):355–366.
- Natarajan, Suchitra, Kaitlyn M. Foreman, Michaela I. Soriano et al. 2019. Collagen remodeling in the hypoxic tumor- mesothelial niche promotes ovarian cancer metastasis. *Cancer Research* 79(9):2271–2284.
- Neher, Erwin. 1992a. Correction for liquid junction potentials in patch clamp experiments. *Methods in Enzymology* 207(C):123–131.
- Neher, Erwin. 1992b. Ion Channels for Communication Between and Within Cells (Nobel Lecture). *Angewandte Chemie International Edition in English* 31(7):824–829.
- Nelson, Michaela, Ming Yang, Rebecca Millican-Slater et al. 2015. Na v 1.5 regulates breast tumor growth and metastatic dissemination in vivo. *Oncotarget* 6(32):32914–32929.
- Nesterov, Viatcheslav, Anke Dahlmann, Marko Bertog et al. 2008. Trypsin can activate the epithelial sodium channel (ENaC) in microdissected mouse distal nephron. *American Journal of Physiology - Renal Physiology* 295(4):1052–1062.
- Nguyen, Phu Hung, Julie Giraud, Lucie Chambonnier et al. 2017. Characterization of Biomarkers of tumorigenic and chemoresistant cancer stem cells in human gastric carcinoma. *Clinical Cancer Research* 23(6):1586–1597.
- Nicco, Carole, Monika Wittner, Antonio DiStefano et al. 2001. Chronic exposure to vasopressin upregulates ENaC and sodium transport in the rat renal collecting duct and lung. *Hypertension* 38(5):1143–1149.
- Nilius, Bernd and Guy Droogmans. 1995. Ion Channels in Nonexcitable Cells. In *Cell Physiology Source Book*, ed. Nicholas Sperelakis. Academic Press chapter 22, pp. 315–329.
- Noreng, Sigrid, Arpita Bharadwaj, Richard Posert et al. 2018. Structure of the human epithelial sodium channel by cryo-electron microscopy. *eLife* 7:e39340.
- North, William, Fuli Liu, Liz Lin et al. 2017. NMDA receptors are important regulators of pancreatic cancer and are potential targets for treatment. *Clinical Pharmacology: Advances and Applications* 9:79–86.
- Northcott, Josette M, Ivory S Dean, Janna K Mouw et al. 2018. Feeling Stress: The Mechanics of Cancer Progression and Aggression. *Frontiers in Cell and Developmental Biology* 6:17.

- Nourshargh, Sussan and Ronen Alon. 2014. Leukocyte migration into inflamed tissues. *Immunity* 41(5):694–707.
- Nuccitelli, Richard. 1992. Endogenous ionic currents and DC electric fields in multicellular animal tissues. *Bioelectromagnetics* 13(S1):147–157.
- Nuccitelli, Richard. 2003. A role for endogenous electric fields in wound healing. *Current topics in developmental biology* 58:1–26.
- Nunes Neto, Lucidio P., Guillaume Madelin, Terlika Pandit Sood et al. 2018. Quantitative sodium imaging and gliomas: a feasibility study. *Neuroradiology* 60(8):795–802.
- Oberleithner, H., C. Callies, K. Kusche-Vihrog et al. 2009. Potassium softens vascular endothelium and increases nitric oxide release. *Proceedings of the National Academy of Sciences of the United States of America* 106(8):2829–2834.
- O’Brien, Catherine A., Aaron Pollett, Steven Gallinger et al. 2007. A human colon cancer cell capable of initiating tumour growth in immunodeficient mice. *Nature* 445(7123):106–110.
- Ochs, Hermann R., David J. Greenblatt, Gunther Bodem et al. 1978. Spironolactone. *American Heart Journal* 96(3):389–400.
- Oda, Tomohiro, Sho Ogata, Saki Kawaguchi et al. 2016. Immunocytochemical utility of claudin-4 versus those of Ber-EP4 and MOC-31 in effusion cytology. *Diagnostic Cytopathology* 44(6):499–504.
- Odgen, David. 1994. Microelectrode electronics. In *Microelectrode Techniques: The Plymouth Workshop Handbook*, ed. David Odgen. 2 ed. Cambridge: The Company of Biologists Ltd chapter 16, pp. 407 – 437.
- O’Donnell, Martha E. and Mitchel L. Villereal. 1982. Membrane potential and sodium flux in neuroblastoma X glioma hybrid cells: Effects of amiloride and serum. *Journal of Cellular Physiology* 113(3):405–412.
- Olsen, M. L., S. Schade, S. A. Lyons et al. 2003. Expression of voltage-gated chloride channels in human glioma cells. *Journal of Neuroscience* 23(13):5572–5582.
- Onkal, Rustem, Joanna H. Mattis, Scott P. Fraser et al. 2008. Alternative splicing of Nav1.5: An electrophysiological comparison of ‘neonatal’ and ‘adult’ isoforms and critical involvement of a lysine residue. *Journal of Cellular Physiology* 216(3):716–726.
- Orr, C. W., M. Yoshikawa-Fukada et al. 1972. Potassium: effect on DNA synthesis and multiplication of baby-hamster kidney cells: (cell cycle-membrane potential-synchronization-transformation). *Proceedings of the National Academy of Sciences of the United States of America* 69(1):243–7.

- Ouadid-Ahidouch, Halima, Morad Roudbaraki, Philippe Delcourt et al. 2004. Functional and molecular identification of intermediate-conductance Ca^{2+} -activated K^{+} channels in breast cancer cells: association with cell cycle progression. *American Journal of Physiology-Cell Physiology* 287(1):C125–C134.
- Ousingsawat, Jiraporn, Melanie Spitzner, Rainer Schreiber et al. 2008. Upregulation of colonic ion channels in APC Min/+ mice. *Pflügers Archiv - European Journal of Physiology* 456(5):847–855.
- Ouwerkerk, Ronald, Karen B. Bleich, Joseph S. Gillen et al. 2003. Tissue sodium concentration in human brain tumors as measured with ^{23}Na MR imaging. *Radiology* 227(2):529–537.
- Ouwerkerk, Ronald, Michael A. Jacobs, Katarzyna J. MacUra et al. 2007. Elevated tissue sodium concentration in malignant breast lesions detected with non-invasive ^{23}Na MRI. *Breast Cancer Research and Treatment* 106(2):151–160.
- Ovarian cancer statistics | Cancer Research UK*. 2019.
- Palmer, Biff F. 2015. Regulation of Potassium Homeostasis. *Clinical Journal of the American Society of Nephrology* 10(6):1050–1060.
- Palmer, Lawrence G. 2017. Epithelial transport in The Journal of General Physiology. *Journal of General Physiology* 149(10):897–909.
- Pannu, Harpreet K. and Michael Oliphant. 2015. The subperitoneal space and peritoneal cavity: basic concepts. *Abdominal Imaging* 40(7):2710–2722.
- Pappalardo, Laura W., Omar A. Samad, Joel A. Black et al. 2014. Voltage-gated sodium channel Nav1.5 contributes to astrogliosis in an in vitro model of glial injury via reverse $\text{Na}^{+}/\text{Ca}^{2+}$ exchange. *Glia* 62(7):1162–1175.
- Paszek, Matthew J., Nastaran Zahir, Kandice R. Johnson et al. 2005. Tensional homeostasis and the malignant phenotype. *Cancer Cell* 8(3):241–254.
- Pedersen, Stine F., Else K. Hoffmann et al. 2013. Cell volume regulation in epithelial physiology and cancer. *Frontiers in Physiology* 4:233.
- Pegoraro, Adrian F., Paul Janmey et al. 2017. Mechanical Properties of the Cytoskeleton and Cells. *Cold Spring Harbor Perspectives in Biology* 9(11):a022038.
- Pei, Lin, Ofer Wiser, Anthony Slavin et al. 2003. Oncogenic potential of TASK3 (Kcnk9) depends on K^{+} channel function. *Proceedings of the National Academy of Sciences of the United States of America* 100(13):7803–7807.
- Pelzl, Lisann, Zohreh Hosseinzadeh, Kousi Alzoubi et al. 2015. Impact of $\text{Na}^{+}/\text{Ca}^{2+}$ Exchangers on Therapy Resistance of Ovary Carcinoma Cells. *Cellular Physiology and Biochemistry* 37(5):1857–1868.

- Perfetto, Stephen P., Pratip K. Chattopadhyay, Laurie Lamoreaux et al. 2010. Amine-reactive dyes for dead cell discrimination in fixed samples. *Current protocols in cytometry* Chapter 9(1):Unit 9.34.
- Petrik, David, Michael H Myoga, Sofia Grade et al. 2018. Epithelial Sodium Channel Regulates Adult Neural Stem Cell Proliferation in a Flow-Dependent Manner. *Cell Stem Cell* 22(6):865–878.e8.
- Pillozzi, Serena, Massimo D’Amico, Gianluca Bartoli et al. 2018. The combined activation of K_{Ca} 3.1 and inhibition of K_v 11.1/hERG1 currents contribute to overcome Cisplatin resistance in colorectal cancer cells. *British Journal of Cancer* 118(2):200–212.
- Planes, Carole, Nadia H. Randrianarison, Roch Philippe Charles et al. 2010. ENaC-mediated alveolar fluid clearance and lung fluid balance depend on the channel-activating protease 1. *EMBO Molecular Medicine* 2(1):26–37.
- Plodinec, Marija, Marko Loparic, Christophe A. Monnier et al. 2012. The nanomechanical signature of breast cancer. *Nature Nanotechnology* 7(11):757–765.
- Plummer, Howard K, Qiang Yu, Yavuz Cakir et al. 2004. Expression of inwardly rectifying potassium channels (GIRKs) and beta-adrenergic regulation of breast cancer cell lines. *BMC Cancer* 4(1):93.
- Poku, Linda Osei, M Phil, Yongna Cheng et al. 2020. “²³Na-MRI as a Noninvasive Biomarker for Cancer Diagnosis and Prognosis.”
- Poo, M. 1981. In situ electrophoresis of membrane components. *Annual review of biophysics and bioengineering* 10(1):245–76.
- Porcel, José M., Aureli Esquerda, Silvia Bielsa et al. 2019. Epithelial cell adhesion molecule (EpCAM) from pleural fluid cell lysates is a highly accurate diagnostic biomarker of adenocarcinomatous effusions. *Respirology* 24(8):799–804.
- Potier, Marie, Virginie Joulin, Sébastien Roger et al. 2006. Identification of SK3 channel as a new mediator of breast cancer cell migration. *Molecular Cancer Therapeutics* 5(11):2946–2953.
- Prat, Jaime, H. Belhadj, J. Berek et al. 2015. Figo’s staging classification for cancer of the ovary, fallopian tube, and peritoneum: Abridged republication. *Journal of Gynecologic Oncology* 26(2):87–89.
- Prevarskaya, Natalia, Lei Zhang et al. 2007. TRP channels in cancer. *Biochimica et Biophysica Acta (BBA) - Molecular Basis of Disease* 1772(8):937–946.
- Prevarskaya, Natalia, Roman Skryma et al. 2010. Ion channels and the hallmarks of cancer. *Trends in Molecular Medicine* 16(3):107–121.

- Prince, Lawrence S. and Michael J. Welsh. 1998. Cell surface expression and biosynthesis of epithelial Na⁺ channels. *Biochemical Journal* 336(3):705–710.
- Pu, Jin, Lin Cao et al. 2015. Physiological extracellular electrical signals guide and orient the polarity of gut epithelial cells. *Tissue Barriers* 3(3):1–7.
- Pusch, Michael and Erwin Neher. 1988. Rates of diffusional exchange between small cells and a measuring patch pipette. *Pflügers Archiv European Journal of Physiology* 411(2):204–211.
- Qadri, Yawar J, Arun K Rooj et al. 2012. ENaCs and ASICs as therapeutic targets. *American Journal of Physiology-Cell Physiology* 302(7):C943–C965.
- Qian, Yun, Chi Chun Wong, Jiaying Xu et al. 2017. Sodium Channel Subunit SCNN1B Suppresses Gastric Cancer Growth and Metastasis via GRP78 Degradation. *Cancer Research* 77(8):1968–1982.
- Rajendran, Vijayalakshmi and Mayur Vilas Jain. 2018. In Vitro Tumorigenic Assay: Colony Forming Assay for Cancer Stem Cells. In *Methods in Molecular Biology*. Vol. 1692 Humana Press Inc. pp. 89–95.
- Ransom, B R and S Goldring. 1973. Ionic determinants of membrane potential of cells presumed to be glia in cerebral cortex of cat. *Journal of Neurophysiology* 36(5):855–868.
- Redmann, K, V Müller, S Tanneberger et al. 1972. The membrane potential of primary ovarian tumor cells in vitro and its dependence on the cell cycle. *Acta biologica et medica Germanica* 28(5):853–6.
- Reid, Brian, Richard Nuccitelli et al. 2007. Non-invasive measurement of bioelectric currents with a vibrating probe. *Nature Protocols* 2(3):661–669.
- Renard, Stéphane, Nicolas Voilley, Frédéric Bassilana et al. 1995. Localization and regulation by steroids of the α , β and γ subunits of the amiloride-sensitive Na⁺ channel in colon, lung and kidney. *Pflügers Archiv European Journal of Physiology* 430(3):299–307.
- Ricci-Vitiani, Lucia, Dario G Lombardi, Emanuela Pillozzi et al. 2007. Identification and expansion of human colon-cancer-initiating cells. *Nature* 445(7123):111–115.
- Robles-Martínez, L., E. Garay, M. G. Martel-Gallegos et al. 2017. Kca3.1 Activation Via P2y2 Purinergic Receptors Promotes Human Ovarian Cancer Cell (Skov-3) Migration. *Scientific Reports* 7(1):4340.
- Rodrigues, Melanie, Nina Kosaric, Clark A. Bonham et al. 2019. Wound Healing: A Cellular Perspective. *Physiological Reviews* 99(1):665–706.

- Rodrigues, Tiago, Gabriela Nohemi Nunez Estevez et al. 2019. Na⁺/Ca²⁺ exchangers: Unexploited opportunities for cancer therapy? *Biochemical Pharmacology* 163:357–361.
- Roger, Sébastien, Jérôme Rollin, Aurélia Barascu et al. 2007. Voltage-gated sodium channels potentiate the invasive capacities of human non-small-cell lung cancer cell lines. *International Journal of Biochemistry and Cell Biology* 39(4):774–786.
- Roger, Sébastien, Ludovic Gillet, Jean-Yves Le Guennec et al. 2015. Voltage-gated sodium channels and cancer: is excitability their primary role? *Frontiers in pharmacology* 6:152.
- Rojas, Elizabeth A., Luis Antonio Corchete, Laura San-Segundo et al. 2017. Amiloride, An Old Diuretic Drug, Is a Potential Therapeutic Agent for Multiple Myeloma. *Clinical Cancer Research* 23(21):6602–6615.
- Rooj, Arun K, Carmel M McNicholas, Rafal Bartoszewski et al. 2011. Glioma-specific Cation Conductance Regulates Migration and Cell Cycle Progression * S.
- Rooj, Arun K., Carmel M. McNicholas, Rafal Bartoszewski et al. 2012. Glioma-specific Cation Conductance Regulates Migration and Cell Cycle Progression. *Journal of Biological Chemistry* 287(6):4053–4065.
- Ross, Sandra B., Catherine M. Fuller, James K. Bubien et al. 2007. Amiloride-sensitive Na⁺ channels contribute to regulatory volume increases in human glioma cells. *American Journal of Physiology-Cell Physiology* 293(3):1181–1185.
- Rossi, Luigi, Monica Verrico, Eleonora Zaccarelli et al. 2017. Bevacizumab in ovarian cancer: A critical review of phase III studies. *Oncotarget* 8(7):12389–12405.
- Rossier, Bernard C. and M. Jackson Stutts. 2009. Activation of the epithelial sodium channel (ENaC) by serine proteases. *Annual review of physiology* 71(1):361–79.
- Rother, Jan, Helen Nöding, Ingo Mey et al. 2014. Atomic force microscopy-based microrheology reveals significant differences in the viscoelastic response between malign and benign cell lines. *Open biology* 4(5):140046.
- Rotsch, C. and M. Radmacher. 2000. Drug-induced changes of cytoskeletal structure and mechanics in fibroblasts: An atomic force microscopy study. *Biophysical Journal* 78(1):520–535.
- Rouzaire-Dubois, B and J M Dubois. 1998. K⁺ channel block-induced mammalian neuroblastoma cell swelling: A possible mechanism to influence proliferation. *Journal of Physiology* 510(1):93–102.
- Rouzaire-Dubois, B., J.B. Milandri, S. Bostel et al. 2000. Control of cell proliferation by cell volume alterations in rat C6 glioma cells. *Pflügers Archiv - European Journal of Physiology* 440(6):881–888.

- Runyon, Bruce A. 1994. Care of Patients with Ascites. *New England Journal of Medicine* 330(5):337–342.
- Sachs, H.G., P.J. Stambrook et al. 1974. Changes in membrane potential during the cell cycle. *Experimental Cell Research* 83(2):362–366.
- Sander, Hannah, Samantha Wallace, Rachel Plouse et al. 2019. Ponceau S waste: Ponceau S staining for total protein normalization. *Analytical Biochemistry* 575:44–53.
- Sarkar, Anyesha, Brian M. Kobylkevich, David M. Graham et al. 2019. Electromigration of cell surface macromolecules in DC electric fields during cell polarization and galvanotaxis. *Journal of theoretical biology* 478:58–73.
- Satlin, Lisa M., Shaohu Sheng, Craig B. Woda et al. 2001. Epithelial Na⁺ channels are regulated by flow. *American Journal of Physiology-Renal Physiology* 280(6):F1010–F1018.
- Sauer, H., J. Hescheler, D. Reis et al. 1997. DC electrical field-induced c-fos expression and growth stimulation in multicellular prostate cancer spheroids. *British Journal of Cancer* 75(10):1481–1488.
- Sawyer, Jemima E. R., James E. Hennebry, Alexander Reville et al. 2017. The critical role of logarithmic transformation in Nernstian equilibrium potential calculations. *Advances in Physiology Education* 41(2):231–238.
- Scafoglio, Claudio, Bruce A. Hirayama, Vladimir Kepe et al. 2015. Functional expression of sodium-glucose transporters in cancer. *Proceedings of the National Academy of Sciences of the United States of America* 112(30):E4111–E4119.
- Schaefer, A E, H G Hempling, E E Handler et al. 1972. Measurement of the electrical potential difference and the distribution of ions in the Shay chloroleukemic tumor cell. *Cancer research* 32(6):1170–6.
- Schild, Laurent and Stephan Kellenberger. 2001. Structure function relationships of ENaC and its role in sodium handling. In *Advances in Experimental Medicine and Biology*. Vol. 502 pp. 305–314.
- Schindelin, Johannes, Ignacio Arganda-Carreras, Erwin Frise et al. 2012. Fiji: an open-source platform for biological-image analysis. *Nature Methods* 9(7):676–682.
- Schoenmakers, T. J.M., G. J. Visser, G. Flik et al. 1992. CHELATOR: an improved method for computing metal ion concentrations in physiological solutions. *BioTechniques* 12(6):870–4, 876–9.
- Schumacher, Thekla B., Heinz Beck, Christian Steinhäuser et al. 1998. Effects of phenytoin, carbamazepine, and gabapentin on calcium channels in hippocampal granule cells from patients with temporal lobe epilepsy. *Epilepsia* 39(4):355–363.

- Schutte, B., R. Nuydens, H. Geerts et al. 1998. Annexin V binding assay as a tool to measure apoptosis in differentiated neuronal cells. *Journal of Neuroscience Methods* 86(1):63–69.
- Schwab, Albrecht, Andrea Wulf, Christoph Schulz et al. 2006. Subcellular distribution of calcium-sensitive potassium channels (IK1) in migrating cells. *Journal of Cellular Physiology* 206(1):86–94.
- Sennoune, S. R., J. M. Santos, F. Hussain et al. 2015. Sodium calcium exchanger operates in the reverse mode in metastatic human melanoma cells. *Cellular and Molecular Biology* 61(7):40–49.
- Serrano-Novillo, Clara, Jesusa Capera, Magalí Colomer-Molera et al. 2019. Implication of Voltage-Gated Potassium Channels in Neoplastic Cell Proliferation. *Cancers* 11(3):287.
- Sever, Richard and Joan S. Brugge. 2015. Signal transduction in cancer. *Cold Spring Harbor Perspectives in Medicine* 5(4).
- Sheetz, M P, D Felsenfeld, C G Galbraith et al. 1999. Cell migration as a five-step cycle. *Biochemical Society symposium* 65:233–43.
- Shehadul Islam, Mohammed, Aditya Aryasomayajula et al. 2017. A Review on Macroscale and Microscale Cell Lysis Methods. *Micromachines* 8(3):83.
- Shen, Chang-Hui. 2019. Amplification of Nucleic Acids. In *Diagnostic Molecular Biology*. Elsevier chapter 9, pp. 215–247.
- Shen, S S, S T Hamamoto, H A Bern et al. 1978. Alteration of sodium transport in mouse mammary epithelium associated with neoplastic transformation. *Cancer research* 38(5):1356–61.
- Sheng, Shaohu, Clint J. Perry, Ossama B. Kashlan et al. 2005. Side chain orientation of residues lining the selectivity filter of epithelial Na⁺ channels. *Journal of Biological Chemistry* 280(9):8513–8522.
- Sherley, J. L., P. B. Stadler et al. 1995. A quantitative method for the analysis of mammalian cell proliferation in culture in terms of dividing and non-dividing cells. *Cell Proliferation* 28(3):137–144.
- Shi, Riyi and Richard B. Borgens. 1995. Three-dimensional gradients of voltage during development of the nervous system as invisible coordinates for the establishment of embryonic pattern. *Developmental Dynamics* 202(2):101–114.
- Shigaev, Alexander, Carol Asher, Hedva Latter et al. 2000. Regulation of sgk by aldosterone and its effects on the epithelial Na⁺ channel. *American Journal of Physiology-Renal Physiology* 278(4):F613–F619.

- Sigma-Aldrich. 1998. RPMI-1640 medium with L-glutamine and without sodium bicarbonate hybri-max product number R5382. Technical report Dorset: .
- Slade, Dea. 2020. PARP and PARG inhibitors in cancer treatment. *Genes and Development* 34(5):360–394.
- SMITH, DAVID E., GAIL OTULAKOWSKI, HERMAN YEGER et al. 2000. Epithelial Na + Channel (ENaC) Expression in the Developing Normal and Abnormal Human Perinatal Lung. *American Journal of Respiratory and Critical Care Medicine* 161(4):1322–1331.
- Smith, N K, S B Stabler, I L Cameron et al. 1981. X-ray microanalysis of electrolyte content of normal, preneoplastic, and neoplastic mouse mammary tissue. *Cancer research* 41(10):3877–80.
- Smith, Nancy R, Rodney L Sparks, Thomas B Pool et al. 1978. Differences in the Intracellular Concentration of Elements in Normal and Cancerous Liver Cells as Determined by X-ray Microanalysis. *Cancer Research* 38(7):1952–1959.
- Snyderman, R and E. Goetzl. 1981. Molecular and cellular mechanisms of leukocyte chemotaxis. *Science* 213(4510):830–837.
- Song, Bing, Yu Gu, Jin Pu et al. 2007. Application of direct current electric fields to cells and tissues in vitro and modulation of wound electric field in vivo. *Nature Protocols* 2(6):1479–1489.
- Sparks, R L, T B Pool, N K Smith et al. 1983. Effects of amiloride on tumor growth and intracellular element content of tumor cells in vivo. *Cancer research* 43(1):73–7.
- Sperelakis, Nicholas. 1995. Gibbs-Donnan Potentials. In *Electrogenesis of Biopotentials in the Cardiovascular System*. Boston, MA: Springer Boston pp. 278–285.
- Spizzo, Gilbert, Dominic Fong, Martin Wurm et al. 2011. EpCAM expression in primary tumour tissues and metastases: An immunohistochemical analysis. *Journal of Clinical Pathology* 64(5):415–420.
- Staub, Olivier, Hugues Abriel, Pamela Plant et al. 2000. Regulation of the epithelial Na+ channel by Nedd4 and ubiquitination. *Kidney International* 57(3):809–815.
- Sullivan, W. J. 1968. Electrical potential differences across distal renal tubules of Amphiuma. *The American journal of physiology* 214(5):1096–1103.
- Sun, Hui Qiao, Masaya Yamamoto, Marisan Mejillano et al. 1999. Gelsolin, a Multifunctional Actin Regulatory Protein. *Journal of Biological Chemistry* 274(47):33179–33182.

- Sundelacruz, Sarah, Michael Levin et al. 2009. Role of membrane potential in the regulation of cell proliferation and differentiation. *Stem Cell Reviews and Reports* 5(3):231–246.
- Swaminathan, Vinay, Karthikeyan Mythreye, E. Tim O’Brien et al. 2011. Mechanical Stiffness grades metastatic potential in patient tumor cells and in cancer cell lines. *Cancer Research* 71(15):5075–5080.
- Szatkowski, M, M Mycielska, R Knowles et al. 2001. Electrophysiological recordings from the rat prostate gland in vitro: identified single-cell and transepithelial (lumen) potentials. *BJU International* 86(9):1068–1075.
- Tai, Guangping, Michael Tai et al. 2018. Electrically stimulated cell migration and its contribution to wound healing. *Burns & Trauma* 6(1):20.
- Taki, Masayasu, Hiroaki Ogasawara, Hiroshi Osaki et al. 2015. A red-emitting ratio-metric fluorescent probe based on a benzophosphole P-oxide scaffold for the detection of intracellular sodium ions. *Chemical Communications* 51(59):11880–11883.
- Tan, David SP, Roshan Agarwal et al. 2006. Mechanisms of transcoelomic metastasis in ovarian cancer. *The Lancet Oncology* 7(11):925–934.
- Tan, Siun Chee and Beow Chin Yiap. 2009. DNA, RNA, and protein extraction: the past and the present. *Journal of biomedicine & biotechnology* 2009:574398.
- Tannous, Bakhos A., Adam P. Christensen, Lisa Pike et al. 2009. Mutant sodium channel for tumor therapy. *Molecular Therapy* 17(5):810–819.
- Tarin, David, Janet E. Price, Michael G.W. Kettlewell et al. 1984. Mechanisms of Human Tumor Metastasis Studied in Patients with Peritoneovenous Shunts. *Cancer Research* 44(8):3584–3592.
- Teiwe, Justin and Robert D Toto. 2007. Epithelial sodium channel inhibition in cardiovascular disease. A potential role for amiloride. *American journal of hypertension* 20(1):109–117.
- Todorovic, Slobodan M., Edward Perez-Reyes et al. 2000. Anticonvulsants but not general anesthetics have differential blocking effects on different T-type current variants. *Molecular Pharmacology* 58(1):98–108.
- Tsai, Hsieh Fu, Ching Wen Huang, Hui Fang Chang et al. 2013. Evaluation of EGFR and RTK Signaling in the Electrotaxis of Lung Adenocarcinoma Cells under Direct-Current Electric Field Stimulation. *PLoS ONE* 8(8):e73418.
- Vargha, András, Harold D. Delaney et al. 1998. The Kruskal-Wallis Test and Stochastic Homogeneity. *Journal of Educational and Behavioral Statistics* 23(2):170.

- Varghese, Elizabeth, Samson Mathews Samuel, Zuhair Sadiq et al. 2019. Anti-cancer agents in proliferation and cell death: The calcium connection. *International Journal of Molecular Sciences* 20(12).
- Vembadi, Abhishek, Anoop Menachery et al. 2019. Cell Cytometry: Review and Perspective on Biotechnological Advances. *Frontiers in Bioengineering and Biotechnology* 7(JUN):147.
- Verrey, François. 1999. Early aldosterone action: toward filling the gap between transcription and transport. *American Journal of Physiology-Renal Physiology* 277(3):F319–F327.
- Voloshyna, Iryna, Alessandra Besana, Mireia Castillo et al. 2008. TREK-1 is a novel molecular target in prostate cancer. *Cancer Research* 68(4):1197–1203.
- Vuagniaux, Gregoire, Veronique Vallet, Nicole Fowler Jaeger et al. 2002. Synergistic Activation of ENaC by Three Membrane-bound Channel-activating Serine Proteases (mCAP1, mCAP2, and mCAP3) and Serum- and Glucocorticoid-regulated Kinase (Sgk1) in *Xenopus* Oocytes. *Journal of General Physiology* 120(2):191–201.
- Walker, John M. 1994. The Bicinchoninic Acid (BCA) Assay for Protein Quantitation. In *Protein Protocols Handbook, The*. Vol. 32 New Jersey: Humana Press pp. 11–14.
- Wang, Haixia, Xingtao Long, Dong Wang et al. 2018. Increased expression of Na⁺/H⁺ exchanger isoform 1 predicts tumor aggressiveness and unfavorable prognosis in epithelial ovarian cancer. *Oncology letters* 16(5):6713–6720.
- Wang, Luyun, Yang Liu, Huamin Wang et al. 2014. Epoxyeicosatrienoic Acids Attenuating Hypotonic-Induced Apoptosis of IMCD Cells via γ -ENaC Inhibition. *PLoS ONE* 9(4):e94400.
- Wartenberg, M, J Hescheler et al. 1997. Electrical fields enhance growth of cancer spheroids by reactive oxygen species and intracellular Ca²⁺. *The American journal of physiology* 272(5 Pt 2):R1677–R1683.
- Washington, Christina R., Debra L. Richardson et al. 2019. Olaparib in the treatment of ovarian cancer. *Future Oncology* 15(30):3435–3449.
- Waxman, Stephen G. 2012. Sodium channels, the electrogenosome and the electrogenostat: lessons and questions from the clinic. *The Journal of Physiology* 590(11):2601–2612.
- Weder, Gilles, Mariëlle C. Hendriks-Balk, Rita Smajda et al. 2014. Increased plasticity of the stiffness of melanoma cells correlates with their acquisition of metastatic properties. *Nanomedicine: Nanotechnology, Biology and Medicine* 10(1):141–148.

- Wei, Chaoliang, Xianhua Wang, Ming Zheng et al. 2012. Calcium gradients underlying cell migration. *Current Opinion in Cell Biology* 24(2):254–261.
- Weidle, Ulrich H, Fabian Birzele, Gwendlyn Kollmorgen et al. 2016. Mechanisms and Targets Involved in Dissemination of Ovarian Cancer. *Cancer genomics & proteomics* 13(6):407–423.
- Wellings, S. R. and H. M. Jensen. 1973. On the origin and progression of ductal carcinoma in the human breast. *Journal of the National Cancer Institute* 50(5):1111–8.
- WHO, International Agency for Research on Cancer (Iarc). 2012. GLOBOCAN 2012: Estimated Cancer Incidence, Mortality and Prevalence Worldwide in 2012. Technical report.
- Wible, Barbara A., Liming Wang, Yuri A. Kuryshev et al. 2002. Increased K⁺ Efflux and Apoptosis Induced by the Potassium Channel Modulatory Protein KChAP/PIAS3 β in Prostate Cancer Cells. *Journal of Biological Chemistry* 277(20):17852–17862.
- Wicha, Max S, Suling Liu et al. 2006. Cancer Stem Cells: An Old Idea—A Paradigm Shift. *Cancer Research* 66(4):1883–1890.
- Wintzell, My, Elisabet Hjerpe, Elisabeth Åvall Lundqvist et al. 2012. Protein markers of cancer-associated fibroblasts and tumor-initiating cells reveal subpopulations in freshly isolated ovarian cancer ascites. *BMC Cancer* 12(1):359.
- Witsch, Esther, Michael Sela et al. 2010. Roles for Growth Factors in Cancer Progression. *Physiology* 25(2):85–101.
- Wolf, Katarina and Peter Friedl. 2011. Extracellular matrix determinants of proteolytic and non-proteolytic cell migration. *Trends in Cell Biology* 21(12):736–744.
- Wolf, Katarina, Stephanie Alexander, Vivien Schacht et al. 2009. Collagen-based cell migration models in vitro and in vivo. *Seminars in Cell & Developmental Biology* 20(8):931–941.
- Wolff, Christian, Bruno Fuks et al. 2003. Comparative study of membrane potential-sensitive fluorescent probes and their use in ion channel screening assays. *Journal of Biomolecular Screening* 8(5):533–543.
- Wonderlin, W F, K A Woodfork et al. 1995. Changes in membrane potential during the progression of MCF-7 human mammary tumor cells through the cell cycle. *Journal of cellular physiology* 165(1):177–85.
- Wright, Stephen H. 2004. Generation of resting membrane potential. *Advances in Physiology Education* 28(4):139–142.

- Wu, William Ka Kei, Gui Rong Li, Helen Pui Shan Wong et al. 2006. Involvement of Kv1.1 and Nav1.5 in proliferation of gastric epithelial cells. *Journal of Cellular Physiology* 207(2):437–444.
- Wu, Yan, Juan Zhou, Huan Wang et al. 2016. The activation of p38 MAPK limits the abnormal proliferation of vascular smooth muscle cells induced by high sodium concentrations. *International journal of molecular medicine* 37(1):74–82.
- Wullkopf, Lena, Ann Katrine V. West, Natascha Leijnse et al. 2018. Cancer cells' ability to mechanically adjust to extracellular matrix stiffness correlates with their invasive potential. *Molecular Biology of the Cell* 29(20):2378–2385.
- xin Zhuang, Ying, Ted Shaikewitz, Luis Glaser et al. 1984. Characterization of Potent Na⁺/H⁺ Exchange Inhibitors from the Amiloride Series in A431 Cells1. *Biochemistry* 23(19):4481–4488.
- Xu, Siguang, Cui Liu, Yana Ma et al. 2016. Potential Roles of Amiloride-Sensitive Sodium Channels in Cancer Development. *BioMed research international* 2016:2190216.
- Xu, Wenwei, Roman Mezencev, Byungkyu Kim et al. 2012. Cell Stiffness Is a Biomarker of the Metastatic Potential of Ovarian Cancer Cells. *PLoS ONE* 7(10):e46609.
- Yaari, Yoel, Michael E. Selzer et al. 1986. Phenytoin: Mechanisms of its anticonvulsant action. *Annals of Neurology* 20(2):171–184.
- Yan, Xiaolong, Jing Han, Zhipei Zhang et al. 2009. Lung cancer A549 cells migrate directionally in DC electric fields with polarized and activated EGFRs. *Bioelectromagnetics* 30(1):29–35.
- Yang, H.-y., R.-P. Charles, E. Hummler et al. 2013. The epithelial sodium channel mediates the directionality of galvanotaxis in human keratinocytes. *Journal of Cell Science* 126(9):1942–1951.
- Yang, Ming, Andrew D. James, Rakesh Suman et al. 2020a. Voltage-dependent activation of Rac1 by Nav1.5 channels promotes cell migration. *Journal of Cellular Physiology* 235(4):3950–3972.
- Yang, Ming, Andrew D. James, Rakesh Suman et al. 2020b. Voltage-dependent activation of Rac1 by Na^v 1.5 channels promotes cell migration. *Journal of Cellular Physiology* 235(4):3950–3972.
- Yang, Ming and William J Brackenbury. 2013. Membrane potential and cancer progression. *Frontiers in physiology* 4:185.
- Yang, Ning, Ying Tang, Fang Wang et al. 2013. Blockade of store-operated Ca²⁺ entry inhibits hepatocarcinoma cell migration and invasion by regulating focal adhesion turnover. *Cancer Letters* 330(2):163–169.

- Yang, S. L., Q. Cao, K. C. Zhou et al. 2009. Transient receptor potential channel C3 contributes to the progression of human ovarian cancer. *Oncogene* 28(10):1320–1328.
- Yao, Lina, Peidong Fan, Zhan Jiang et al. 2011. Na^v 1.5-dependent persistent Na⁺ influx activates CaMKII in rat ventricular myocytes and N 1325 S mice. *American Journal of Physiology-Cell Physiology* 301(3):C577–C586.
- Yeung, Tsz-Lun, Cecilia S. Leung, Kay-Pong Yip et al. 2015. Cellular and molecular processes in ovarian cancer metastasis. A Review in the Theme: Cell and Molecular Processes in Cancer Metastasis. *American Journal of Physiology - Cell Physiology* 309(7).
- Yin, H L, J H Hartwig, K Maruyama et al. 1981. Ca²⁺ control of actin filament length. Effects of macrophage gelsolin on actin polymerization. *The Journal of biological chemistry* 256(18):9693–7.
- Yu, Frank H and William A Catterall. 2003. Overview of the voltage-gated sodium channel family. *Genome biology* 4(3):207.
- Yue Loo, Ser, Michelle Ker Xing Chang, Charis Sui Huay Chua et al. 2012. NHE-1: A Promising Target for Novel Anti-cancer Therapeutics. *Current Pharmaceutical Design* 18(10):1372–1382.
- Zhang, Shu, Curt Balch, Michael W Chan et al. 2008. Identification and Characterization of Ovarian Cancer-Initiating Cells from Primary Human Tumors. *Cancer Res* 68(11):4311–4320.
- Zhang, Xue, Yamei Ge, Ashfaq-Ahmad-Shah Bukhari et al. 2019. Estrogen negatively regulates the renal epithelial sodium channel (ENaC) by promoting Derlin-1 expression and AMPK activation. *Experimental & Molecular Medicine* 51(5):1–12.
- Zhang, Yuan, Junhong Zhang, Dongsheng Jiang et al. 2012. Inhibition of T-type Ca²⁺ channels by endostatin attenuates human glioblastoma cell proliferation and migration. *British Journal of Pharmacology* 166(4):1247–1260.
- Zhao, Min. 2009. Electrical fields in wound healing-An overriding signal that directs cell migration. *Seminars in Cell and Developmental Biology* 20(6):674–682.
- Zhao, Min, A Agius-Fernandez, J V Forrester et al. 1996. Orientation and directed migration of cultured corneal epithelial cells in small electric fields are serum dependent. *Journal of cell science* 109(6):1405–1414.
- Zhao, Min, Bing Song, Jin Pu et al. 2006. Electrical signals control wound healing through phosphatidylinositol-3-OH kinase- γ and PTEN. *Nature* 442(7101):457–460.
- Zheng, Jingying, Shuhua Zhao, Xiaolin Yu et al. 2017. Simultaneous targeting of CD44 and EpCAM with a bispecific aptamer effectively inhibits intraperitoneal ovarian cancer growth. *Theranostics* 7(5):1373–1388.

Zs.-Nagy, I., L. Tóth, Z. Szállási et al. 1987. Energy-dispersive, bulk specimen X-ray microanalytical measurement of the intracellular Na⁺/K⁺ ratio in human laryngeal tumors. *Journal of Cancer Research and Clinical Oncology* 113(2):197–202.

Zs.-Nagy, Imre, Gyorgy Lustyik, Valeria Zs.-Nagy et al. 1983. Correlation of Malignancy with the Intracellular Na⁺:K⁺ Ratio in Human Thyroid Tumors. *Cancer Research* 43(11):5395–5402.

Zuckerman, Jonathan B., Xiyin Chen, Joely D. Jacobs et al. 1999. Association of the epithelial sodium channel with Apx and α -spectrin in A6 renal epithelial cells. *Journal of Biological Chemistry* 274(33):23286–23295.